NMR ASSISTED INVESTIGATIONS OF MOLECULAR MOBILITY IN POLYMERIC GELS

A THESIS
SUBMITTED TO THE

UNIVERSITY OF PUNE

FOR THE DEGREE OF

DOCTOR OF PHILOSOPHY
(IN CHEMISTRY)

by

APPAJI BABURAO MANDHARE
(M. Sc.)

NATIONAL CHEMICAL LABORATORY
PUNE 411008 (INDIA)

SEPTEMBER 1998

Dedicated to dear Mahesh

CERTIFICATE

Certified that the work incorporated in the thesis entitled **"NMR Assisted Investigations of Molecular Mobility In Polymeric Gels"** submitted by Mr. A. B. Mandhare, was carried out under my supervision. Such material as has been obtained from other sources has been duly acknowledged in the thesis.

National Chemical Laboratory
Pune 411 008

Dr. R.A. Mashelkar
(Research Guide)

ACKNOWLEDGMENTS

I am very much indebted to my research guide, **Dr. R.A. Mashelkar (FRS), Director General, CSIR** for his excellent guidance, deep interest, and incessant encouragement. He introduces me to variety of interesting research problems. Most of the work done in this thesis has come out from Dr. Mashelkar's original ideas. Frequent discussions with him helped in enriching my scientific awareness. He also contributed significantly in formatting this thesis to the present shape. I am also inspired by his commitment and dedication to the science.

I am very much grateful to **Dr. S. Ganapathy** for sharing his rich knowledge in the theoretical and experimental aspects of solid state NMR, giving enough freedom to use MSL-300 extensively, valuable guidance and for his consistent help at various levels. He also made it possible to perform some novel experiments mentioned in this thesis. Without his constant help it would have been very difficult to bring all this work into the thesis form.

I am indebted to **Dr. P.R. Rajamohanan**, for his most valuable and helpful suggestions and never failing deep interest throughout the progress of this work. Most of the experimental data in this thesis would not been possible without his help.

I thank ***Mr. P.M. Suryavanshi*** for his technical assistance, suggestions and useful advice.

I have benefited greatly from the discussion with *Dr. M.G. Kulkarni, Dr. M.V. Badiger, Dr. R. Vetrivel and Dr. A.K. Lele.*

I am grateful to *Mr. R.R. Hirwani, Dr. (Mrs.) Mayadevi, Mr. Venugopal and Mr. Prabhakaran* for their help and cooperation.

I thank *S.S. Patil, M.J. Thakar, I. Devotta, B.S. Lele, Vivek Joshi, Rohini Patwardharn, Alankar, Badrivishnanth, Prakash, Patrick, Mandar Deshmukh, Damodharan, Wafia, Jyoti, Mr. Jagtap and Gulab,* for their cheerful company and warm friendship.

I am thankful to *Dr. C. Dutt, Dr. S.S. Nadkarni* and *Dr. U. Zope* and my all colleagues at TRC, for their help and cooperation.

I wish to acknowledge with great pleasure the help rendered by *Dr. Ferzaan Engineer, Mrs. and Dr. Jain and Mr. and Mrs. Naveenbhai Patel.*

I am deeply indebted to my family, especially my *Aai, Bhau, Aba* for their moral support and patience. I am also thankful to my *brother, sisters*, and *all my relatives* for their support.

I am especially very grateful to *Onkar, Pradeep and Rushikesh* for their unstinted support, patience and inspiration during this work.

I am thankful to **Director, NCL,** for giving me an opportunity to work in NCL and providing all facilities and permitting me to submit this work in the form of thesis.

A.B. Mandhare

CONTENTS

Chapter III

NMR and Mobility Transition in Polymers

Chapter IV

Magic Angle Spinning and Two-Dimensional NMR Spectroscopy in Polymeric Gels

Part A: Homonuclear ^{1}H-^{1}H 2-D NOESY Experiment

Part B: Heteronuclear ^{13}C-^{1}H 2-D Separation Technique

Chapter V

Molecular Modeling Studies on Water-Macromolecular Interactions

Chapter VI

Proton Magnetic Resonance Imaging and Volume Phase Transition in Poly(*N*-Isopropylacrylamide) Hydrogel

Chapter VII

PREFACE

Macromolecular hydration has been a subject of considerable interest for many years. The amount and nature of water and its interactions with macromolecules play a crucial role in determining many of the properties of the macromolecules including the volume phase transition exhibited by stimuli responsive polymers. Despite the multitude of experimental techniques used to study macromolecular hydration, the precise details of water-macromolecular interactions in the functional environment are not well understood.

This thesis contains studies on dynamic response of macromolecules to hydration probed through solid state NMR spectroscopy and molecular modeling techniques. A wide range of NMR Spectroscopic techniques such as proton wide line, CP/MAS, 2-D homonuclear NOESY and heteronuclear separation NMR and proton micro imaging techniques have been employed to study the hydration induced dynamics of macromolecules, especially which are crosslinked.

Wide line Proton NMR spectroscopic technique has been used to follow the hydration events at earlier stages of hydration in many hydrophilic macromolecules. The proton line width showed a transition when plotted against hydration levels. The transition is termed as "mobility transition". The mobility transition, occurring in the very early levels of hydration, has been detected and demonstrated for the first time in many polymer-water systems. Molecular mobility is shown to occur through an isotropic averaging process for the proton-proton dipolar interactions. The mobility transition depends on the nature of hydrophilic groups present in the polymeric system. The hydration levels at which the mobility transition occurs correspond to the non-freezable bound water content in the systems. The mobility transitions are no way related to the phenomenon of macroscopic volume phase transitions of certain hydrogels.

It is shown that macromolecular hydration can be conveniently studied by MAS based two-dimensional NMR. These studies demonstrate that the 2-D NOESY

experiments can be conducted on hydrogels with relative ease, taking advantage of enhanced spectral resolution obtained by sample rotation at the magic angle. The resulting data contain valuable information about the spin connectivity established by dipolar relaxation interactions in the mobile phase of the polymer gel. This technique is potentially useful in unraveling the motional pathways in polymers, which readily respond to hydration. The importance of dipolar relaxation interactions between the water of hydration and the polymer system is also revealed from these studies. The heteronuclear ^{13}C - ^{1}H separation spectroscopy was employed to locate and separate local dynamics at specific hydration sites in a polymeric gel. Further, the 2-D separation experiment provides dynamical insights in thermally collapsible gels that expel water while undergoing a volume phase transition.

Mobility transition demonstrated in macromolecule-water systems was further studied by using the molecular modeling and molecular dynamics (MD) techniques. These calculations for a linear polymer indicate the influence of water molecules on the single chain conformation of the polymer. The conformational changes of the polymer chains allow further uptake of the water into the polymer network. Thus the close relation between the single chain conformation and the orientation of water molecules around it are brought out by these studies and the mechanism of the water uptake is also revealed. The average distance between the water of hydration and the polymer functional group has been reported. The MD calculations below and above LCST of polymer-water system and the quantitative analysis of hydrogen bonds support the predictions of the LFHB theory.

It has also been shown that the proton imaging experiments are viable in studying the stimuli response of polymeric gels. This has been demonstrated in the LCST polymer PNIPAm for the first time. The microscopic differences in the motional state of the polymer and water components are used to bring in image contrast through appropriate relaxation and diffusion weighting.

List of Figures

Chapter II

Chapter III

Chapter IV

Chapter V

Chapter VI

List of Tables

Chapter I

Chapter II

Chapter III

Chapter V

Chapter I

Introduction to Polymeric Gels and Gel State NMR Spectroscopy

Gels are swollen polymeric networks. They possess the cohesive properties of solids and the diffusive transport properties of liquids. The combination of elastic properties and osmotic reactivity make them very special. In world wide, gels are being looked at as the most exciting materials of the 21st Century. Among other things, this is certainly due to the 'smartness' or 'intelligence' that these gels exhibit. A combination of many analytical techniques are required for the proper understanding of their interesting properties. Among the analytical techniques Nuclear Magnetic Resonance (NMR) Spectroscopy has emerged as a powerful tool which can furnish very useful information at molecular level. This chapter provides an introduction to the science of polymeric gels and their properties such as volume phase transition and some relevant theoretical aspects of solid state NMR spectroscopy.

Part A: Polymeric Gels and their properties

1.1 Introduction to Polymers and their Dynamical Properties

Polymers are complex and giant molecules that possess high molecular weight. They are made up of small repeating units called monomers linked together by the process of polymerization. Polymer is a generic name given to a number of materials of high molecular weights. These materials exist in countless forms and numbers because of a very large number and types of atoms present. Polymers which possess different chemical structures, physical properties, mechanical behavior, thermal characteristics, etc. are classified in different ways, such as, natural and synthetic polymers, depending upon their origin, organic and inorganic polymers, depending upon the nature of the backbone. Polymers are also classified as thermoplastic and thermosetting polymer depending on their thermal properties. Finally, depending on the ultimate form and use, they can be classified as plastics, elastomers, fibres or resins. A linear, branched and crosslinked or network polymers are well known.

Thermal properties of polymers are very well studied and documented (Flory 1953). Due to the amorphous nature of polymers there is a temperature boundary for almost all polymers. Above this temperature, known as glass transition temperature (T_g), they remains soft, flexible and rubbery, while below this temperature they become hard, brittle and glassy. On heating further, the polymer becomes a highly viscous and starts to flow like a liquid. This state is termed as viscofluid state.

At room temperature most of the polymers are solids, exhibiting all characteristics of a low molecular weight substances. At higher temperature, however, the characteristic difference between high and low molecular weight substances can be seen. Depending on the temperature, the molecules of a low molecular weight substance either move apart as a whole or do not move at all, *i.e.* there is a definite temperature (T_m) below which the molecules do not move and above which they move. On the other hand, with polymers, as we increase the temperature, localized units (chain segments) within the long chain molecules are first mobilised before the whole molecule starts moving. Further, polymers often exhibit localised motions that are confined to localised molecular segment.

In polymers, there is an intermediate stage where the localized mobility is activated but the overall mobility is not. The local segments, where mobility is already activated, correspond to the liquid state, while the molecule as a whole, where mobility is forbidden, is in the solid state. This state, which is really a combination of liquid and solid, is called the rubbery state. In this rubbery state, the polymeric materials behave as liquid with superimposed solids at fixed points or as solids with localized segments of a liquid nature. Under the influence of an applied stress, it exhibits properties of a viscous fluid as well as an elastic solid (Ferry 1980) and undergoes a visco-elastic deformation.

When a polymer passes from one state to another, there is a gradual change in many of its physical properties. Among them, specific volume is perhaps the most significant property, which reveals changes during the transition and it frequently utilized to determine the glass transition temperature of the polymer.

The presence or absence of segmental and molecular motions decides whether a polymer is in a solid, rubbery or molten state. The nature and magnitude of these motions depends on the size and geometry of the polymeric chain, flexibility of the chain segments and the type of molecular aggregates formed. Flexibility of the chain segments is determined by the degree of freedom with which different segments along with the chain backbone can rotate around the covalent bonds. The higher the freedom to rotate, the more flexible are the chain segments and hence, the higher their segmental mobility. The segmental and molecular motions, determines the T_g as well as the T_m of the polymer (Roe 1985). T_g depends on the molecular weight and it is observed that T_g value will be lower for low molecular weight polymers (Cowie 1973). The range of T_g also depends on the degree of polydispersity, and broader the molecular distribution, wider is the T_g range.

Low molecular weights non-volatile substances, known as plasticisers, when added to a polymer to improve its flexibility, processibility and hence it's end use as a commercial product. The plasticiser substantially reduces the brittleness of many amorphous polymers because its addition even in small quantities markedly reduces the T_g of the polymer. This effect is due to a reduction in cohesive forces of attraction between polymer chains, plasticiser molecules penetrate into the polymer matrix and establish polar attractive forces between them and the chain segments. These attractive forces reduce the cohesive forces between the polymeric chains and increase the segmental mobility, thereby reducing the T_g value. The presence of solvents (Tan & Challa 1976, Rault *et al* 1995) also modifies the T_g in a similar manner. T_g is an important parameter of a polymeric material. It is used as a measure for evaluating the flexibility of a polymer molecule and the type of response the polymeric material would exhibit to mechanical stress.

1.1.1 Polymeric Gels

Gels are crosslinked networks of polymers swollen in a liquid. They also represent a semi-rigid phase, much like rubbery materials, and exhibit enhanced motional properties. As practically useful materials, they cover a wide range of applications such as, 1) personal care products (diapers, feminine care products and incontinence products); 2) materials in industrial separations (sewage treatment, membrane process and bio-separation) (Badiger *et al* 1992 & Cussler *et al* 1984); 3) pharmaceuticals (controlled-release technology, bioadhesives, and enteric dosage forms) (Bae *et al* 1987 & Kulkarni *et al* 1992) and 4) agriculture (retainers of water and solutes) (Kazanski & Dubrovski 1992). Developing these applications of gels require a fundamental understanding of the relationships between synthesis, characterization, and end-use performance. Gels can be characterized by their equilibrium, dynamic and kinetic properties. These properties depend on the gel state represented by osmotic pressure, temperature, solvent composition and degree of swelling.

A schematic representation for a polymeric gel is shown in Figure 1.1. The interstitial space provided the polymer networks provide a molecular storage for solvent. The phase transitions and critical phenomena in polymer gels are governed by details of polymer-solvent interactions. They provide unique opportunities to explore the fundamentals underlying the molecular interactions and recognition in natural and synthetic polymers.

1.1.2 Thermodynamics of swelling gels

The theory of swelling of non-ionic crosslinked polymeric network was first proposed by Flory (1953), who subsequently modified it to take into account the effect of ionic substituents. Flory proposed an analogy between the swelling equilibrium and the osmotic pressure equilibrium. The total osmotic pressure (π) acting on the gel comprises

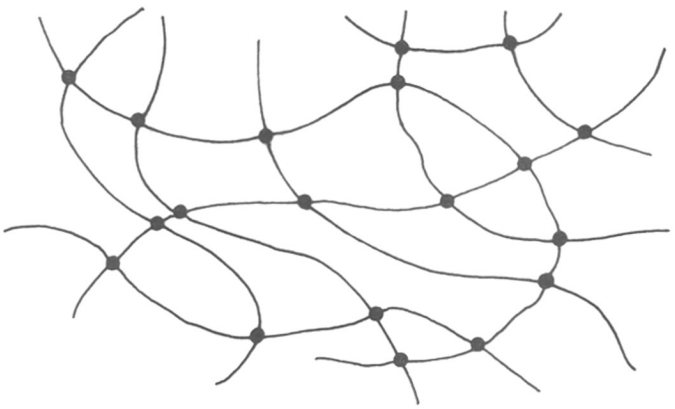

Figure 1.1: Schematic representation of the crosslinked, network structure of polymeric gel.

the forces arising from polymer-polymer affinity and rubber elasticity. It can be given as,

$$\pi = \mu_1 - \mu_1^{\circ} = RT \left\{ ln\,(1- V_2) + V_2 + \chi\, V^2_2 + V_1\,(V_e / V_0)\,(V_2^{1/3} - (V_2/2)) \right\} \qquad (1.1)$$

Here, μ_1 and μ_1° are chemical potentials of solvent within the gel and outside the gel, respectively. V_2 is the volume fraction of the network, χ, the interaction parameter between the polymer and solvent, R, the gas constant, T, the absolute temperature, V_1, the molar volume of the solvent and the term (V_e/V_0), the deformation factor, which arise

due to the elasticity of the network. At equilibrium swelling, $\pi = 0$. With some rearrangement, Equation (1.1) can be written as,

$$-\left[ln\,(1-V_2) + V_2 + \chi\, V_2^2\right] = (V_1/\bar{v}M_c)\left[1 - 2M_c\right](V_2^{1/3} - (V_2/2)) \qquad (1.2)$$

Here, M_c is the molecular weight between crosslinks and M_n, the number average molecular weights. The term $(1\text{-}2\ M_c/M_n)$ in the above equation is the correction factor for network imperfections resulting from the chain ends. Equation (1.2) can be simplified using suitable approximations as follows,

$$q^{5/3} = (\bar{v}M_c/V_1)\,(1 - 2\,M_c/M_n)\,(1/2 - \chi) \qquad (1.3)$$

Equation 1.3 shows that how the swelling ratio (q), which is the volume of the swollen gel divided by the volume of the unswollen gel, changes as a function of the extent of crosslinking and also the thermodynamic quality of the solvent. This equation has been experimentally confirmed for a number of systems.

The extend of swelling attainable in ordinary network systems is rather limited and the swelling ratios usually approach about 10. Some superswelling gels (*e.g.* Hydrolysed starch-*g*-poly(acrylonitrile) (HSPAN), which are essentially ionic networks, attain q values of 100 to 1000. This is because, in the case of networks contain ionizable groups, the swelling forces may be greatly increased as a result of the localization of the charges on the polymer chains. In studying the gel behavior, one has to concern with the amount of swelling as it determines the amount of the gel required carrying out the specific application. It is well known that the gel swelling is inversely proportional to the degree of crosslinking. This reduces gel's elasticity, thereby reducing the swollen volume. Gehrke *et al* (1986) have shown that the gel volume to the (-2/3) power is proportional to the degree of crosslinking as well as the amount of added acid. This is good agreement with the theoretical predictions that describe gel swelling as a function of gel elasticity (related to the degree of cross - linking) and gels ionization (related to the

amount of added acid). As the crosslink density decreases, the polymer chain length between cross-links increases, yielding a looser structure in which more solvent can easily penetrate. This was predicted by Gehrke *et al* (1986) using the Flory's excluded volume theory.

Electrostatic repulsion between like groups set up considerable expansion of the networks. The equilibrium between the swollen ionic gel and its surrounding can be considered by recognizing that the osmotic pressure will arise from a difference in mobile ion concentrations. Using suitable approximations, two asymptotic limits can be calculated. The first one related to the case when the electrolyte concentration outside the gel is negligible. We then have,

$$q^{5/3} = \left[iq/V_m \rho_p + (0.5 - \chi)/ \rho_p V_1 \right] M_c/(1 - 2M_c/M_n) \qquad (1.4)$$

In the presence of significant electrolyte concentration on outside, the expression reduces to

$$q^{5/3} = \left[i^2 / 4V_m^2 I_o + (0.5 - \chi) / \rho_p V_1 \right] M_c / (1 - 2M_c/M_n) \qquad (1.5)$$

Here, i, is the degree of ionization, I_o, the ionic strength of the solvent present outside, V_m, the molar volume of the structural repeat unit of the network and ρ_p, the density of the polymeric network. Badiger *et al* (1992) have validated equation (1.4) and shown that it is capable of quantitatively predicting the extent of swelling in ionic networks.

1.1.3 Hydrogels

Water swollen crosslinked polymers are usually called hydrogels. The fundamental building block of a hydrogel is the water-soluble monomer. There are two

kind of hydrogels, *viz.* naturally occurring (*e.g.* agarose, polysacchrides, gum arabic, gelatin, etc.) and synthetic (*e.g.* poly(ethylene oxide), poly(vinyl alcohol), as poly(*N*-isopropylacrylamide) (PNIPAm), poly(acrylamide), poly(2-hydroxylethyl methacrylate) (PHEMA), etc,). Hydrogels swell to equilibrium in water but preserve their shape. Softness, biocompatibility, hydrophilicity, permeability to metabolites, etc. are the general properties of the hydrogels (Ratner and Hoffman, 1976, Hoffman *et al* 1986). They occupy an important place in the field of gel science and technology. The area of hydrogels is ever growing. The amount of water that they can take up depends on the hydrophilic nature of the polymers in the network and the degree of crosslinking. The extent of swelling attainable determines their end use.

1.1.4 State of Water in the polymeric Gels

The interaction of water with polymers has been an area of great research interest. Water is known to act as a diluent and can depress the glass transition temperature of a glassy polymer. It plasticises or lubricates the chain segments to enhance the segmental mobilities. In general, increasing the water content tends to increase the mobility. An important aspect of the work presented in Chapter III (Section 3.2) and Chapter IV (Section 4.1.6 and 4.2.4) is based on an inspection of the mobility at very early stages of hydration. This has led to our observation of the 'mobility transition' in the hitherto unexplored region of polymer hydration.

Water is known to exists in different state *viz.* bound, interfacial and free in the macromolecules (Foster *et al* 1976, Wöessner and Snowden 1970 & Galin and Galin 1993). However, water exists in two distinctly different physical states in a crosslinked hydrophilic polymeric gel (Hatakeyema *et al* 1984). In the swollen state of the gel, most of the water is in a "free" state and can be classified as freezable water, which becomes ice at 0^0C. Some water molecules, which are associated with the polymeric chains of the gel-network cannot freeze at the usual freezing point. This water is called "non-freezable" or "bound water". It is essential to know the extent of free and bound water

content since they give useful physical insight into the mechanism of water transport within the system. An understanding of the state of the water absorbed by polymeric gels is not only important *per se* but it also provides valuable guidelines for the design of better polymeric gels and also to refute the doubts concerning the usage of such products. The macroscopic property of polymeric gel networks depends upon the state of water. For example, in the case of reverse osmosis membranes, the permeability of water through the membranes depends on the relative population of bound water fractions (Chang *et al* 1974). The activity of biological systems such as proteins and enzymes depends upon how the water associates with these biomolecules in bringing out specific conformations.

The significance of the terms 'bound' and 'free' depends upon the characterization technique. For example, NMR would detect the time scales associated with motion of the water molecule while the DSC measurements signify the heat exchange accompanying a thermal transition and provide an estimate of the bound water unavailable for forming ice-like structures. The average properties of water are known to vary depending upon the degree of binding with the substrate, *e.g.*, water does not crystallize when it is present in the biopolymer as well as in the synthetic polymer at concentration less than 0.30 g water/g polymer (England, 1974 and Dong & Hoffman 1990) whereas at higher water content crystallization takes place and the heat of fusion is almost identical to that of pure water. Secondly, while the water sorbed in the polymer could be distinguished as bound and free water on the basis of the DSC analysis. Important dynamical information is provided by direct NMR observation of the water and polymer protons. The experimental results, presented in Chapter IV (Section 4.1.6 and 4.2.4), provide substantial evidence for increased water and polymer mobility even at a low degree of hydration.

1.1.5 Stimuli responsive gels

An important aspect of some of the polymeric gels, especially that of hydrogels, is ability to response to external stimuli. Hence, they are known as stimuli-responsive gels. There are many possible environmental changes, which can stimulate interesting responses in water-soluble polymers and their crosslinked hydrogels. The polymer network changes its volume in response to a change in environment, such as temperature (Tanaka 1978), pH (Katchalsky *et al* 1950, Siegel and Firestone, 1988, Ricka and Tanaka, 1984), solvent composition (Tanaka *et al* 1980), ionic strength (Tanaka *et al* 1982), electric field (Osada *et al* 1992), and light (Irie 1986). According to nature of stimuli response they are classified as, thermosensitive, pH sensitive, electric field sensitive, light sensitive hydrogels, etc. Prediction and finding of this phenomenon have opened the door to a wide variety of technological applications in various industrial fields. Since the final properties of gels are determined by a number of factors, such as, variations in the type, degree, and distribution of ionizable and nonionizable functional groups, cross-linkers, reaction conditions, etc., there is a world-wide research effort in the synthesis of novel materials and their physico-chemical characterisation. Parallely, attention has also been focused in developing gels as active elements, potentially useful as stimuli responsive molecular sensors (Kokufuta & Tanaka 1991), switches and actuators (Kwon *et al* 1991), membranes, adsorbents, transducers, dehydrants and matrices for drug delivery systems, etc. Many reviews on stimuli responsive gels have appeared recently (DeRossi *et al* 1991, Dusek 1993 & Mashelkar 1993, 1995).

The volume phase transition exhibited by certain polymeric gels, such as poly(*N*-isopropylacrylamide) studied in this thesis, is an important phenomenon, which has been extensively studied in the literature. The first study of the critical phenomenon of volume phase transitions in gels was started by Tanaka (1978), who used dynamic light scattering measurements. Only recently attention has been focused on the molecular level inspection and understanding of the phenomenon (Badiger *et al* 1991, Ganapathy *et al* 1994, Tokuhiro *et al* 1991).

Gels in dry state are hard with various properties ranging from leathery to glassy. In aqueous medium the polymer network imbibes water and the polymer swells to its equilibrium which is defined as the point at which the swelling pressure is balanced by the reactive force of the network. The swelling pressure is the resultant of the difference in water activity inside and outside the polymer and is analogous to osmotic pressure. The equilibrium water content depends on the hydrophilicity of the polymer and the degree of crosslinking and can be range up to well over 90%. In designing applications of the gels, one must accurately know the swelling behavior. However, gel swelling kinetics is more complex than the gel collapse kinetics, since several factors, can be limiting. Certain gels undergo dramatic changes in swelling due to changes in pH, temperature, solvent composition, pressure, etc., (Tanaka 1992). Some aspects are discussed in the following sections.

1.1.5.1 pH sensitive gels

pH sensitive hydrogels usually contains pendant acidic or basic groups such as carboxylic acids and primary amines or strong acid and bases (sulfonic acid and quaternary ammonium salts), which change ionization in response with pH, thus changing the properties of the gel. The equilibrium degree of swelling of these type of gels is influenced by the charge of the ionic monomer, degree of ionization pk_a of the ionizable group, concentration of the ionizable monomer in the network, pH, ionic strength and composition of the swelling solution. It also depends on the crosslinking density and hydrophilicity/hydrophobicity of the polymeric gel.

Upon immersion of this type of gels in the aqueous alkaline solution, ionization of functional groups takes place. The electrostatic repulsion between the anionic groups within the gel causes it to swell. However, when the swollen gel placed in acidic pH, it collapses because of the protonation of the ionic groups. The mechanisms for swelling and collapse are different. The collapse occurs more quickly than swelling. Ionic gels on protonation collapse as hydrogen ions diffuse into the gel. They rapidly react to convert

ionic groups into neutral groups. Thus, a nonionic shell of collapsing gel will develop around a still-swollen ionized core. The diffusion of ions takes place freely in this nonionic shell, so that the collapse is limited by the Fickian diffusion of water out of the gel. Gehrke *et al* (1989) have confirmed this Fickian behavior by measuring the collapse of cylindrical gel samples of differing radii and ionic compositions. The results also show that diffusional resistance both in and around the gel can affect the swelling rate of these gels.

The volume changes of the gel are often due to changes in the ionic charge within the gel. The volume of a charged gel can also be changed with ionic strength, *i.e.*, when the swollen gel immersed in the aqueous solutions of alkali chlorides. Initially, the ion concentration is higher outside the gel than that inside. To achieve osmotic equilibrium, ions must diffuse into the gel, or water must diffuse out of the gel. The decrease in gel swelling comes from an osmotic effect which is depends only on the osmotic force and independent of the specific alkali metal ion. However, due to ionic interactions, these gels can be used to concentrate small negatively charged solutes, as well as large uncharged solutes. The swelling kinetics of pH sensitive gels depends on the rates of diffusion of ions and that of water in the gel structure.

1.1.5.2 Temperature sensitive gels

The second class of gels that show sudden volume changes with small changes in the temperature is called temperature sensitive gels or thermo-reversible gels. These gels are affected relatively little by changes in pH, ionic strength, etc., and hence are more suitable for chemical separation. The temperature sensitive gels, first found by Ilavsky *et al* (1982), can be synthesized from the number of monomers like, *N, N*-diethylacrylamide or *N*-isopropylacrylamide. At low temperatures, the gel is in its swollen state. As the temperature is increased, the gel undergoes a rapid decrease in volume. For example the volume phase transition observed for poly(*N*-isopropylacrylamide) in water is depicted in Figure 1.2.

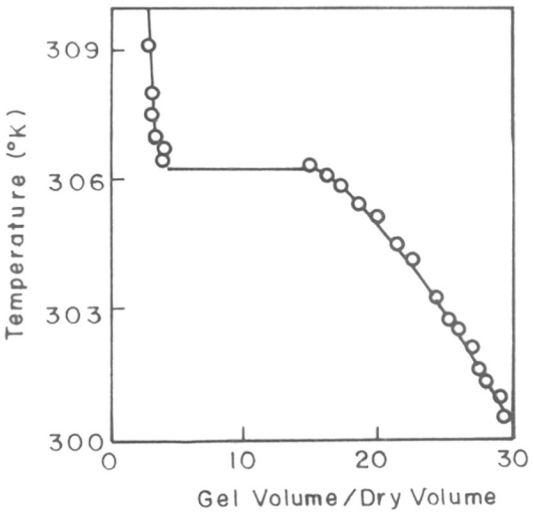

Figure 1.2: Poly(*N*-isopropylacrylamide) gel swelling *vs* temperature.

The volume change in these gels is due to a thermodynamic phenomenon known as lower critical solution temperature (LCST). The polymer, if they are not crosslinked, is completely miscible with water below LCST but above LCST, water-rich and polymer-rich phases are formed. Similarly, in the crosslinked cases, the gel swells to the limit of its cross-links below LCST, and collapse above LCST to form a dense polymer-rich phase. Before a responsive gel can response to the stimuli that stimuli must permeate into the gel itself. In case of temperature sensitive gel the system will not undergo a volume transition in response to a change in its environmental temperature until the temperature within the gel has changed. In other words, the rate of heat transfer may influence the swelling or shrinking rate of such gel. Once the stimulus has altered the gel, then the mass transfer process which allows the movement of solvent into or out of the gel occur.

This could involve the mutual diffusion of the polymer network and the solvent or the rate of the polymer network relaxation to a more expanded or contracted configuration.

Gehrke (1993) has determined the necessary conditions that could cause the rates of ion exchange, heat transfer or solvent mass transfer to influence the rates of gel swelling or shrinking. Increase in temperature of the solution surrounding a thermally responsive gel causes it to shrink, while decrease in temperature causes it to swell. Hence, the rate limiting step in the kinetics of swelling and collapse for the LCST gels could be the rate of water diffusion in the gel, but also by heat transfer or mass transfer rate of the gel. Experimentally, they demonstrated that the rate of heat transfer was very much faster than the rate of mass transfer. Hence, the heat transfer effects can be neglected for such temperature sensitive gels. However, microporous gels may be exceptional for this since in microporous gel mass transfer occurs by a convective process rather than a usual diffusive process.

To predict accurate swelling behavior, Marchetti *et al* (1990) have developed a model for predicting the volume changes in these gels. They have combined the Sanchez and Lacombe (1976 & 1978) theory of mixing and the Flory-Rehner theory of rubber elasticity. They assume that the free energy change is a sum of that due to mixing and that due to elasticity and the mixing contribution includes the usual Flory contribution from the mole fraction and the usual lattice correlation. It also includes the interaction energy per lattice site, which is in turn a function of the polymer-polymer interaction, the polymer-solvent interaction, and the interactions of the polymer and of the solvent with vacant sites. This simple lattice model yields a rich harvest of phase behavior. The model prediction is shown by the solid line in Figure 1.2 for poly(*N*-isopropylacrylamide) gel at 1 atm. In this case, three parameters were adjusted to fit the experimental data namely, the cohesive energy density of the gel, the cross-link density and the interaction energy. Given one set of experimental data for a gel, this model is useful tool for predicting the effect of changing variables such as cross-link density or temperature.

Modeling gel systems which display lower critical solution temperatures is more difficult due to the inability of classical Flory-Huggins polymer-solvent interaction theory to treat this phenomenon and the system-specificity of the interactions which drive many of these transitions. Nonetheless a number of theories are being developed to model this class of gels. The Lattice-Fluid Hydrogen Bond (LFHB) theory employed by Lele *et al* (1995) is capable of explaining the volume phase transition (swelling-collapsing behavior) in LCST polymers.

1.1.5.3 Pressure sensitive gels

Marchetti *et al* (1990) has shown that the lattice model for temperature sensitive gels predicts that the swelling behavior is also a function of pressure as shown in Figure 1.3. At a constant temperature, the gel is expected to swell more as pressure increases. Although this effect may seem counterintuitive, it is the result of minimizing the free energy of the gel-water system by increasing the gel-water interactions. This prediction has been experimentally verified by Lee *et al* (1990), using poly(*N*-isopropylacrylamide) gel as shown in Figure 1.4. The solid line in the figure gives the model prediction based on the same parameters as in Figure 1.2 and is quantitatively consistent with the experimental data. Such a pressure effect could allow cheaper separations than are possible with other gels.

In addition to these, gels sensitive to other stimuli like, electric field (Osada *et al* 1992, Kwon *et al* 1991), light (Mamada *et al* 1990, Suzaki and Tanaka 1990), solvents, stress and specific molecules have also been reported (Tanaka *et al* 1982, Kokufuta *et al* 1991).

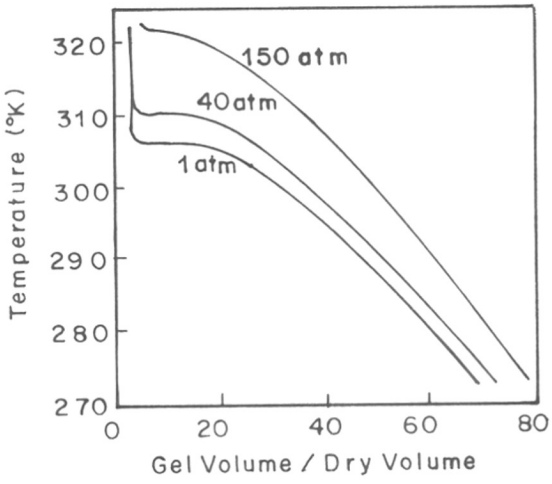

Figure 1.3: Poly(*N*-isopropylacrylamide) gel swelling at various pressures. The model predicts more gradual swelling at higher transition temperature as the pressure increases. Parameter values are the same as Figure 1.2.

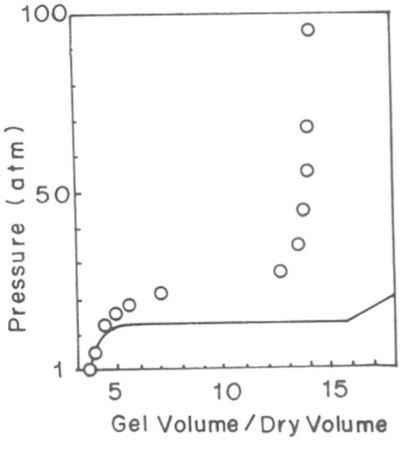

Figure 1.4: Poly(*N*-isopropylacrylamide) gel swelling *vs* pressure. (T=307.5 K). Circles are data points and the solid line is the lattice model prediction with one fitted parameter.

1.1.6 Volume Phase Transitions in Polymeric Gels

Polymeric gels are known to exist in two distinct phases, swollen and collapsed. Volume transition occurs between the phases either continuously or discontinuously in response to chemical and physical stimuli (Tanaka 1992). However, a wide range of synthetic, ionic, non-ionic, (Hirotsu *et al* 1987 & Hirotsu 1993) as well as natural polymeric gels such as gelatin, agarose, DNA etc., (Amiya and Tanaka 1987) (as shown in Figure 1.5) can exhibit either continuous or discontinuous volume phase transitions. For polymeric gel to undergo phase transition, it is necessary that polymers interact with each other through both repulsive and attractive interactions and the balance of these competing interactions has to be modified by various stimuli. The phase behavior of a gel, therefore, crucially depends on the nature of interactions between polymers. Recently, new phases and volume transitions between them have been discovered in some gels (Tanaka 1992). Detailed examination of the gel phase behavior provides a deep insight into the polymer-polymer interactions and configurations of polymers. The knowledge on physical and chemical fundamentals of gel phase transitions and other possible new transitions would play a key role as guiding principles for variety of technological applications of gels. The volume phase transition in polymeric gels and the influence of the various parameter stated above, can be understood in terms of the osmotic pressure of the gel. This consists of three components, namely, the rubber elasticity, the polymer - polymer affinity, and the hydrogen ion pressure.

The interactions between the polymer chains gives rise to polymer-polymer affinity, when the polymer-polymer interaction were favored over the polymer-solvent interaction. The polymer-polymer affinity creates a negative pressure that tends to cause the collapse of the gel. In practice, the gel always attains an equilibrium volume so that its total osmotic pressure is zero. If the pressure is positive, the gel takes up fluid and swells and if pressure is negative it looses fluid and collapses.

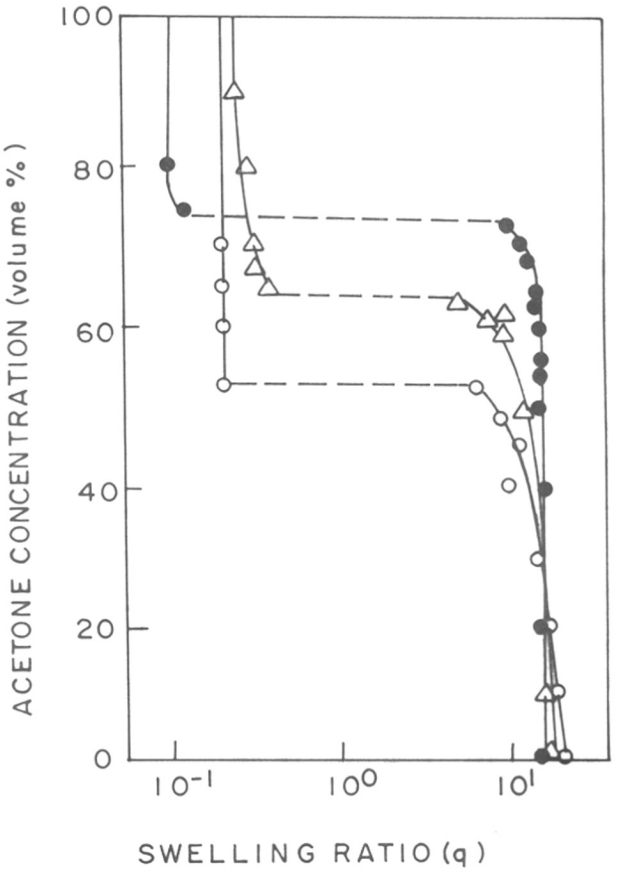

Figure 1.5: Volume phase transition in natural gels
(O) Gelatin, (∇) DNA and (•) Agarose

The continuous variation of the swelling ratio with temperature or solvent composition and the existence of the critical point can be explained on the basis of the phase diagram of the familiar transition in the gas-liquid system (Figure 1.6). The region of negative compressibility in the P-V isotherm has been attributed to the forces arising from the polymer-polymer affinity. Due to the rubber elasticity and hydrogen ion pressure, above the critical point, the osmotic pressure is positive and their magnitude decreases with the gel expansion. Below the critical point (temperature) the net osmotic pressure increases with increasing gel volume. While this explanation is true in principle, the local minimum is not reached in practice. Instead, when the gel reaches the Maxwell line, two domains, namely, swollen and shrunken are formed. Unlike the gas-liquid transition, it is more convenient to discuss the swelling curves for the gels which describes the gel volume at which the total osmotic pressure is zero. It thus, defines the

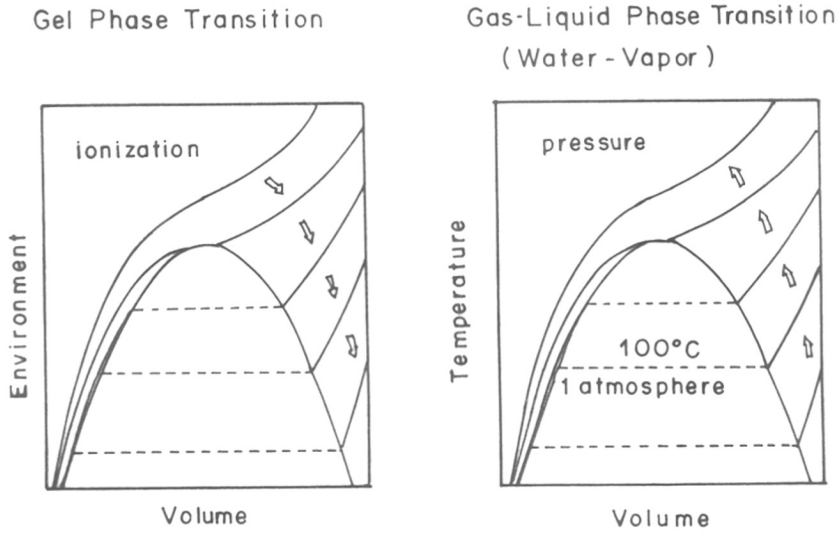

Figure 1.6: Equation of state of a gas-liquid phase and a gel phase systems.

intercepts of all isotherms on zero pressure axes. It is apparent that when the transition temperature is greater than the critical temperature, the volume change is continuous. When it becomes equal to the critical temperature an inflection point reached. As the transition temperature lowered further, the length of the Maxwell line increases and swelling curve exhibits discontinuous transition.

The ionic pressure component of the total osmotic pressure is absent in the case of unionized gels. As the temperature decreases, the force due to polymer-polymer affinity overcomes the force due to rubber elasticity at temperature higher than the critical temperature and the gel collapse in a continuous manner. As the degree of ionization of the network increases, the hydrogen ion pressure also contributes to the total osmotic pressure. As a result, at any temperature or solvent composition the swelling ratio (q) is higher than it would have been in the case of the unionized gel. The negative pressure due to polymer-polymer affinity can then overcome the total positive pressure at temperature below the critical point (temperature). The transition therefore is not only discontinuous but the initial gel volume is higher, as a result the swelling ratio at the transition increases with increasing ionization.

1.1.7 Generalization of volume Phase transitions in polymeric gels

Interactions between macromolecules fall into four categories namely; Ionic, hydrophobic, van der Waals and hydrogen bonding. These four fundamental interactions play an essential role in determining the structures and specific functions of biological macromolecules and their assemblies. The magnitude, temperature dependence, and behavior in aqueous environment are totally different among the fundamental forces, and it is those differences that allow the variety in the biological functions created by these forces. Understanding how these forces determine the phase behaviors of polymers is of fundamental importance. A quantitative approach to elucidate the volume phase transitions in polymers has been given by Tanaka (1978) which is based on a reformulated equation of state of gels, arising out of an extension of Flory's theory of

swelling. Recently, Tanaka (1992) has recognized that these four fundamentally important inter-molecular forces (*viz.* ionic, hydrophobic, van der Waals and hydrogen bonding) contribute to the various types of the phase transition in polymer gels as well. A recent work by Ilmain *et al* (1991) made it possible to classify all gel phase transitions in terms of these four biologically relevant intermolecular forces, each of which may independently be responsible for a discontinuous volume phase transition in polymeric gels.

Gel phase transition is a result of a competitive balance between a repulsive force that acts to expand the polymer network and an attractive force that acts to shrink the network. The most effective repulsive force is the electrostatic interaction between the polymer charges of the same kind, which can be imposed upon a gel by introducing ionization into network. The osmotic pressure by counter ions adds to the expanding pressure. The attractive interactions can be van der Waals, hydrophobic interaction, ion-ion with opposite kinds, and hydrogen bonding. The phase transition was discovered in gels induced by all the fundamental forces are summarized in the following section.

1.1.7.1 van der Waal interaction

Tanaka *et al* (1980) have demonstrated that the partially hydrolyzed poly(acrylamide) gel undergoes phase transition in acetone-water mixture. They observed that the main polymer-polymer affinity is due to the van der Waals interaction. The addition of acetone as a poor solvent to water increases the attraction between the polymer chains to a value sufficiently large enough to induce a transition. They also observed that the transition takes place when the temperature is varied at a constant solvent composition. The gel swells at higher temperatures and shrinks at lower temperatures.

1.1.7.2 Hydrophobic interaction

In polymers with more hydrophobic side groups shows volume phase transition in water. A typical example is the copolymer gels of *N*-Isopropylacrylamide (NIPAm) and sodium acrylate (Hirokawa and Tanaka 1984). It was observed that these gels swells at lower temperature and collapses at higher temperatures. Without ionizable sodium acrylate, the gel undergoes a discontinuous volume change by eight times at 33°C. The transition temperature rises and the volume change becomes larger as the sodium acrylate concentration increases. This clearly indicates that the temperature dependence is due to the hydrophobic interaction between water and gel. In the vicinity of hydrophobic polymer chains the water molecules have more ordered structures, and therefore a lower entropy, than those away from the polymers. However, at higher temperatures the polymer network shrinks and becomes more ordered, but the water molecules excluded from the polymer network become less ordered. More detailed theory and experiments have been found in literature regarding this interaction (Otake *et al* 1988, Inomata *et al* 1990 & Ichita *et al* 1991).

1.1.7.3 Hydrogen bonding

An interpenetrating polymer network (IPN) of poly(acrylic acid/acrylamide) copolymer gel undergoes phase transition in pure water by the influence of cooperative hydrogen bonding (Okano *et al* 1990, Bae *et al* 1988 & 1989). The gel collapses at low temperatures in water and its volume increases as temperature raises. The main driving force for this collapse was found to be hydrogen bonding interactions *i.e.* the so-called "zipper" effect, which described the cooperative nature of the interaction between two polymers. Other systems that showed similar behavior are poly(methacrylic acid) gel and linear poly(ethylene glycol) (Osada and Takeuchi 1983). The thermo-reversible nature of LCST hydrogels was also thought by Walker & Vause (1987) to be due to the breakage of hydrogen bonded associations in the gel-water systems.

Despite the importance of the role played by hydrogen bonding interactions in determining the equilibrium-phase behavior of many gels, only a few theoretical attempts have been made to model hydrogen bonded gel-solvent systems. However, Lattice-Fluid Hydrogen Bond (LFHB) theory was recently extended to hydrogen boned gel-solvent systems by Lele *et al* (1995). They have demonstrated quantitative predictions of equilibrium swelling data of selected gel-solvent systems with the modified theory. More importantly they have shown that the breakage and formation of hydrogen bonds in such systems are responsible for volume phase transitions in PNIPAm (Figure 1.7). These results imply that the LCST is a manifestation of two forces, namely, the hydrogen bonding interactions and the hydrophobic interactions.

1.1.7.4 Electrostatic attraction

Polyampholytes are the polymers having both cationic and anionic groups. These types of polymer networks can have either positive or negative charges due to which they can repel each other over short ranges but attract over long ranges. Myoga and Katayama (1987) studied such type of gels and observed that due to ionic nature of gel, at neutral pH's the gel is indeed shrunken and at both higher and lower pH's it is swollen but the volume change was gradual and continuous. However, Annaka and Tanaka (1992) found a pH-driven phase transition in a polyampholyte gel of copolymer of acrylic acid and methyacrylamidopropylammonium chloride at both higher and lower pH.

The volume phase transitions in gels induced by these four intermolecular forces discussed above has been summarized in Figure 1.8. Figure 1.8a shows how the van der Waals interactions cause phase transitions in hydrophilic gels in a mixed solvent (acrylamide gel in an acetone-water mixture). A non-polar solvent is needed to decrease the dielectric constant of the solvent. Figure 1.8b shows the phenomena for hydrophobic gels, such as, poly(*N*-isopropylacrylamide) undergoing a volume phase transition in pure water, from a swollen state at low temperatures to a collapsed state at high temperatures.

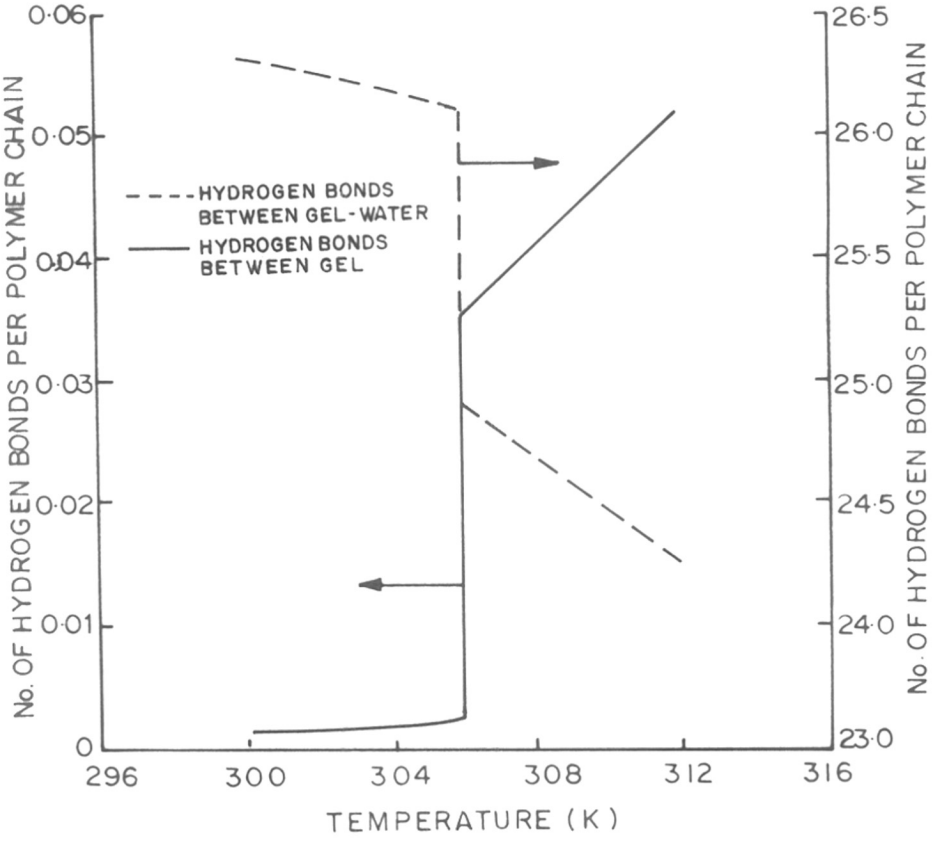

Figure 1.7: Number of interpolymer hydrogen bond per PNIPAm chain (——) and number of hydrogen bonds between one polymer chain of the gel and water molecules (-----) at different temperatures calculated from the modified LFHB theory.

Figure 1.8c shows the gels influenced by cooperative hydrogen bonding. An interpenetrating polymer network (IPN) of acrylic acid/acrylamide gel undergoes volume phase transitions in pure water (the swollen state is the high-temperature state). The repulsive ionic interaction determines the transition temperature and the volume change at the transition. In Figure 1.8d, the role of attractive ionic interaction is shown for pH-driven volume phase transitions. The acrylamide-sodium acrylate/ methacrylamidopropyltrimethylammonium chloride gel system is a typical example of this category.

In many of the systems mentioned so far, a clear understanding of the molecular level interactions that take place during a discontinuous volume phase transition is lacking. In this thesis an attempt has been made to bridge this gap using the thermoreversible poly(*N*-isopropylacrylamide) as a model system. Nuclear Magnetic Resonance (NMR) Spectroscopy has been extensively used for this in the present thesis. In order to put the results obtained in proper perspective a brief introduction to the NMR phenomenon and different NMR techniques, relevant to the context, are presented in the following section.

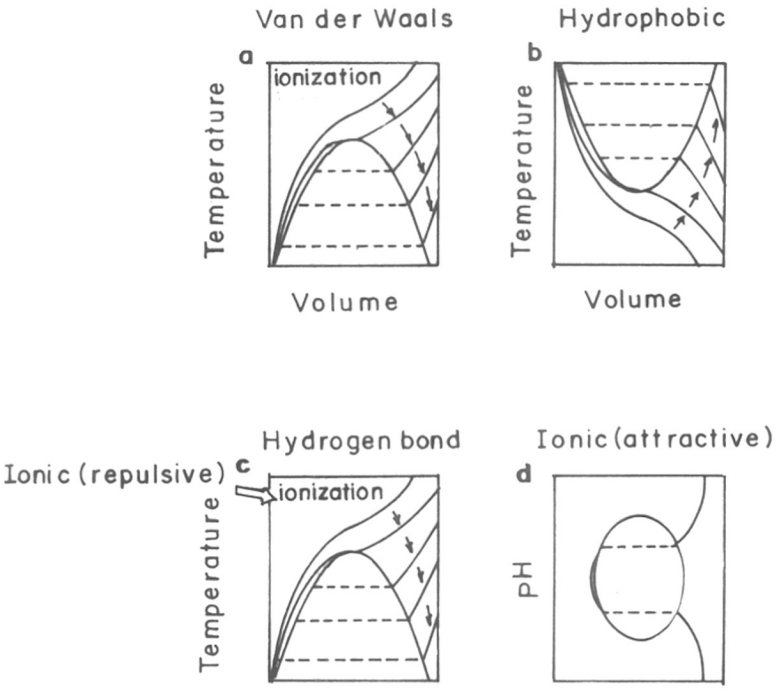

Figure 1.8: Generalization of volume phase transitions in gels induced by the four fundamental forces; (a) van der waals, (b) Hydrophobic, (c) Hydrogen bond and (d) electrostatic forces

Part B: Solid state NMR in Polymer Science

1.2 Introduction

Modern Solid State NMR spectroscopy has developed to become a powerful structural and dynamical characterisation tool for the study of polymeric solids (Schmidt-Rohr & Spiess 1994). Sensitivity-enhancement by cross-polarisation (CP) and resolution enhancement by dipolar-decoupling and Magic Angle Sample Spinning (CP-MAS) have led to a multitude of new 1-D and 2-D experimental schemes to be introduced (Mathias 1991, Saito & Ando 1989, Spiess 1991, Schmidt-Rohr & Spiess 1994) and a wealth of structural and dynamical information to be gathered. Studies on crystallinity (Earl & VanderHart 1979, VanderHart & Khoury 1984, Perez & VanderHart 1987, VanderHart & Perez 1986, Varma *et al* 1997), tacticity (Terao *et al* 1983, Bumm *et al* 1981, 1982) and miscibility in binary blends (Schmidt-Rohr & Spiess 1992, Olabisi *et al* 1979, Paul *et al* 1978, Mirau & Bovey 1990, Miller *et al* 1990) have been reported. Another important development using solid state NMR is the dynamical characterisation of chain motions in rigid polymers by ^{2}H exchange spectroscopy, pioneered by Spiess and his group (Schmidt-Rohr & Spiess 1994, Spiess 1991).

Polymeric gels, which form the subject matter of this thesis, are essentially semi-rigid solids which exhibit enhanced molecular mobility due to the addition of a diluent to the polymer system. Solution state based NMR studies on polymeric gels have been reported in the literature. Doskocilova and Schneider (1981) have studied the high-resolution proton NMR spectra of swollen crosslinked gels such as poly(ethylene oxide), poly(methyl methacrylate) and poly(styrene). The nature of proton line shapes was studied and analyzed in terms of molecular mobility of chains. ^{13}C studies on cross-linked poly(styrene) gels have been reported and an empirical correlation between the ^{13}C line width and cross-link density has been established (Ford and Balkrishnan 1981). Yokoto *et al* (1978) have investigated that the effect of chemical composition, degree of crosslinking and temperature on the molecular mobility of crosslinked hydrogels by ^{13}C

NMR. Basela *et al* (1988) have studied the kinetics of cross-linking in poly(acrylamide) gel by high-resolution proton NMR. Based on these studies, the reactivity ratios of two monomers in copolymerization were estimated.

In the study of polymeric gels, Magic Angle Sample Spinning (MAS) has been popularised in recent years. The NCL group has already contributed a broad knowledge base in this experimentally rewarding area. MAS based 1-D and 2-D experiments have been designed to study local hydration (Rajamohanan *et al* 1991 & 1995), LCST phenomena (Badiger *et al* 1991, Ganapathy *et al* 1994), steady state nuclear Overhauser enhancements (Ganapathy *et al* 1992), chemical exchange and cross-relaxation (Rajamohanan *et al* 1995, Ganapathy *et al* 1995). MAS based proton and carbon experiments are becoming increasingly popular in the area of combinatorial chemistry (Keifer *et al* 1996).

1.2.1 Pulse Fourier-transform NMR

In 1946, the first experiments to detect the nuclear magnetic resonance signals in bulk matter were independently performed by Bloch (Bloch *et al* 1946) and Purcell (Purcell *et al* 1946). Since then NMR spectroscopy has grown enormously, and advancements in theory, experimental methodology and instrumentation have brought NMR into the realms of physics, chemistry, biology and medicine. The phenomenon of NMR was originally discovered as a continuous wave technique (cw), in which either the main magnetic field or the radio frequency is swept through the resonance condition, given by

$$\omega_0 = \gamma H_0 \tag{1.6}$$

The resonance phenomenon carries the signature of various magnetically active nuclei through the magnetogyric ratio γ and the well-known Larmor frequency ω_0 ($= 2\pi\nu_0$), in the externally applied constant magnetic field H_0. By the application of an external radio

frequency, tuned to the Larmor frequency ω_o, the NMR spectrum is recorded in the cw fashion using the absorption (Purcell *et al* 1946) or the induction method (Bloch *et al* 1946). It was soon discovered that the detected resonance frequencies depended on the chemical shift (Proctor & Yu 1950, Dickinson 1950) and this was used to derive the structure of molecules from high-resolution solution state NMR. Subsequently, spin-spin interactions were found, which gave information about the chemical bonding in a molecule and further opened the possibility of double resonance experiments (Hoffman & Forsen 1966, Von Philipsborn 1971). As a result, in the early days, cw NMR in the solution state became one of the most important tools for structural analysis of organic molecules.

The usefulness of Fourier-transform, in extracting the frequency domain spectrum from an observed time domain signal, was pointed out by Ernst and Anderson (1966) and this has lead to explosive developments in NMR methodology, instrumentation and practice (Ernst *et al* 1987, Fukushima & Roeder 1981, Shaw 1984, Chandrakumar & Subramanian 1987). Multi-nuclear multi-dimensional FT-NMR has opened new vistas in scientific and industrial research. Multi-dimensional NMR is today sought for the structure determination of complex biomolecules, such as polypeptides and proteins (Wuthrich 1986).

The pulse FT method involves subjecting the spin system to a short *rf* pulse and observing the subsequent time domain response, followed by Fourier transformation. The basic pulse-FT scheme is pictorially depicted in Figure 1.9. Pulse experiments are more efficient compared to the traditional cw methods since various regions of NMR spectrum are simultaneously excited and detected. More importantly, pulse experiments afford signal averaging of N transients in which the signal to noise (S/N) ratio is improved by a factor $N^{1/2}$. The time domain signal and the frequency domain spectrum are related mathematically by Fourier transform as

$$F(\omega) = \int_{-\infty}^{\infty} S(t)\, e^{-i\omega t}\, dt \qquad (1.7)$$

and the inverse Fourier-transform

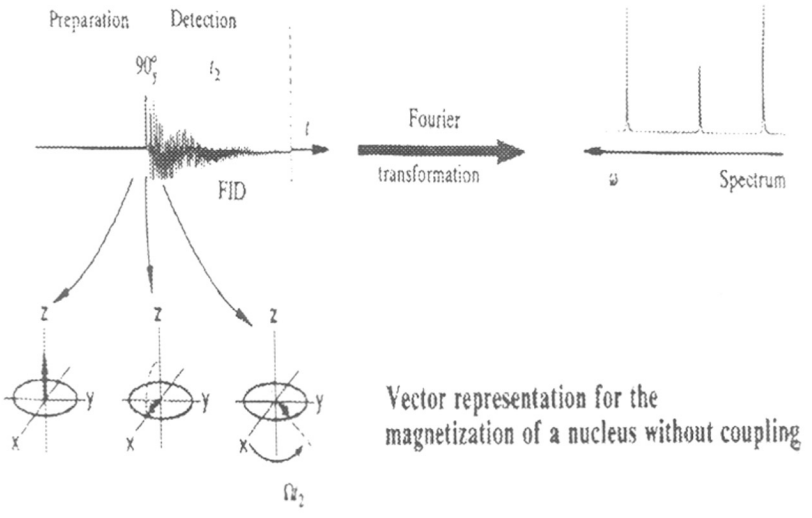

Figure 1.9: The basic principle of FT in one dimension. The initial thermal equilibrium magnetization M_z, aligned parallel to the external static magnetic field H_0, is acted upon by the resonant radio frequency pulse to create transverse magnetisation. A simultaneous quadrature detection of this precessing time domain signal [S(t)] and subsequent complex Fourier transformation (FT) yields a sign discriminated frequency domain spectrum as shown. The evolution of the transverse magnetisation in the vector description is shown below.

$$S(t) = 1/2\pi \int_{-\infty}^{\infty} F(\omega)\, e^{j\omega t}\, d\omega \qquad (1.8)$$

also holds.

The signal representation in the time and frequency domains are tabulated below (Table 1.1) for the FT operations.

Table 1.1

The signal representation in the time and frequency domains

Time domain	FT	Frequency domain
Cos(Ft)	Cos(ωt)	A(ω) + A(-ω)
Cos(Ft)	Sin(ωt)	D(ω) - D(-ω)
Sin(Ft)	Cos(ωt)	D(ω) + D(-ω)
Sin(Ft)	Sin(ωt)	-A(ω) + A(-ω)

By combining the above results properly the results of the Fourier-transform of the time domain signal, embedded in Equation (1.7), can be realised to give

$$S(t) \Rightarrow FT \Rightarrow A(\omega) + iD(\omega) \qquad (1.9)$$

The absorption and dispersion line shapes being given by

$$A(\omega) = T_2/(1+T_2^2\,(\omega-\omega_o)^2) \quad \text{and} \quad D(\omega) = T_2^2(\omega-\omega_o) / (1+(\omega-\omega_o^2)) \qquad (1.10)$$

It is obvious from these expressions that quadrature detection is needed to discriminate between positive and negative resonance frequencies. The process of FT and the resulting line shape is given in Figure 1.10.

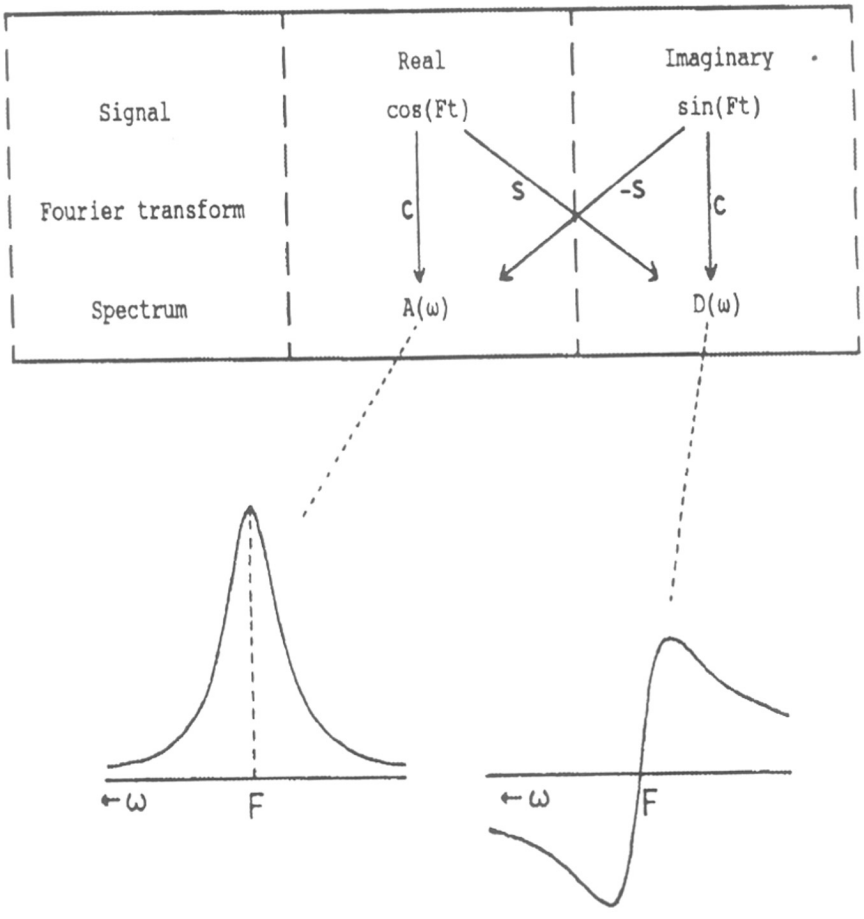

Figure 1.10: Schematic representation of the NMR signal obtained by quadrature detection and the resulting spectrum after Fourier transformation. The *cosine* and *sine* FT are represented by the letters c and s, respectively. The absorption mode spectrum is shown on the left, while the dispersion mode spectrum is shown on the right.

The real part resulting from the FT, which is the spectrum normally displayed, consists of an absorptive Lorentzian line shape, while the imaginary term consists of a dispersive signal.

The time domain signal is initially obtained as an analog signal in a two-channel quadrature detector and is then converted into a digital signal using an analog to digital converter. Fourier transform is carried out numerically on this digital signal using a Cooley-Tukey algorithm (1965) (Fast Fourier Transform or FFT), which requires the data size to be 2^N, where N is the number of complex data points. Since pulsed NMR is amenable for repeated signal averaging of the time domain signal, the method is ideally suited for the NMR spectral observation of rare spins such as ^{13}C, ^{15}N, ^{29}Si, etc. It is therefore not surprising that the pulse Fourier-transform methodology has almost exclusively replaced the traditional cw or the so-called field/frequency sweep method and is by far the method of choice in the realm of modern NMR spectroscopy today.

While pulse FT NMR techniques were continually applied and refined in liquid state NMR studies, the FT methods were mainly used to get undistorted powder patterns in the area of wide-line NMR. The pulse schemes to generate dipolar (Jenner & Broekaert 1967) and quadrupolar echoes (Davis *et al* 1976), were among the very early applications of pulse FT NMR techniques in solid state NMR. However, once line narrowing techniques using MAS were introduced (Andrew *et al* 1958 &1959), the full potential of multi-nuclear multi-dimensional FT NMR in the solid state has been realised.

It is therefore not surprising that the initial development of solid state NMR as a structure-elucidating tool, as good as in liquids, was less successful. The dominance of various spatially dependent interactions and the severe line broadening observed in static spectra could not lead to any chemical information to be discerned. A major step forward in the NMR of solids, even before the advent of FT technique, was the development of resolution enhancement by MAS (Andrew *et al* 1959) and sensitivity enhancement by hetero-nuclear cross-polarisation (CP) (Hartmann & Hahn 1962). Although these

techniques were already available, their combination with pulse FT NMR methodology had to wait for the instrumentation to be developed (Schaefer & Stejskal 1976). Sophistication in instrumentation and methodology has led to the observation of rare spins, such as ^{13}C, ^{15}N, ^{29}Si, etc, and the enormous application potential in material science (Engelhardt 1987) characterisation.

As this thesis is concerned with the use of solid state NMR methods for studying polymeric gels, we will briefly discuss the basic spin interactions and outline their influence in the solid state NMR spectra. This is mainly intended to give an overview of the interactions and techniques. For a more comprehensive treatment of the principles of magnetic resonance, excellent monographs on the subject may be referred (Abragam 1989, Slichter 1990, Mehring 1983, Haeberlen 1976, Gerstein and Dubowsky 1985).

1.2.2 Line Broadening Interactions in Rigid Solids

Polymers in dry state are hard to characterize by the more familiar and highly sensitive proton magnetic resonance owing to the inherent spectral line broadening associated with proton-proton homonuclear dipolar broadening. The removal of homonuclear line broadening can be achieved by the technically demanding multiple-pulse line narrowing techniques (Haeberlen 1976). Fortunately, one does not have to resort to this technique for the polymeric gel state, since the homonuclear dipolar interaction is averaged to a great extent by the enhanced polymeric mobility. MAS only techniques prove to be very useful. In the observation of ^{13}C, line broadening due to heteronuclear ^{13}C-^{1}H dipolar interactions and chemical shielding anisotropies of ^{13}C nuclei contribute to line broadening in rigid polymers. As will be seen, these are less influential in the swollen gel state. For nuclei possessing spin number greater than ½, quadrupolar interactions are the major source of spectral line broadening. However, this will not be discussed further since the nuclei studied in polymeric gels belong to the spin ½ family (^{1}H and ^{13}C).

The interaction Hamiltonian for the spin system is written as the sum of the Zeeman Hamiltonian and the other internal interaction Hamiltonians, namely,

$$H = H_Z + H_Q + H_D + H_\sigma + H_S \qquad (1.11)$$

Where, the subscripts denote the Zeeman (Z), quadrupolar (Q), dipolar (D) and the chemical shielding (S) interactions. H_Z is always much larger than the other interactions, and in NMR experiments the strategy is to selectively study each interaction under conditions which eliminate broadening influences from most other interactions. The above internal interactions, together with their spatial and spin dependencies, are summarised in Table 1.2.

Table 1.2

The NMR interactions arising from local field and their various spacial, spin and field dependencies.

Sr. No.	Interactions	Isotropic average	Spacial Dependence	Spin Dependence	Field Dependence
1.	Chemical Shift	δ_{iso}, σiso	$\Delta\sigma\,[(3\cos^2\theta - 1) + \eta\sigma \sin^2\theta \cos^2\phi]$	S_z	Linear
2.	Homonuclear dipolar	0	$(3R/2)(3\cos^2\theta - 1)$	$3I_zS_z - I.S$	None
3.	Heteronuclear dipolar	0	$R(3\cos^2\theta - 1)$	I_zS_z	None
4.	Indirect Spin-Spin	J_{iso}	$\Delta J\,(3\cos^2\theta - 1)$	$3I_zS_z - I.S$ (homo) I_zS_z (hetero)	None
5.	Quadrupolar	0	$[\chi/(2I-1)]\,[(3\cos^2\theta - 1) - \eta_Q \sin^2\theta \cos^2\phi]$	$3S_z^2 - S^2 + (S_x^2 - S_y^2)$	None

1.2.2.1 Dipolar Interactions

Homonuclear and heteronuclear dipole-dipole interactions are two major sources of line broadening in rigid polymers. The dipolar interactions Hamiltonian for the nuclear pair i, j can be expressed as

$$H_D = [\gamma_i \gamma_j \hbar^2 (1/r_{ij}^3) (\vec{I}_i \cdot \vec{I}_j - 3I_{iz}I_{jz}) (3\cos^2\theta_{ij} - 1)] \quad (1.12)$$

where γ_i and γ_j are the nuclear magnetogyric ratio of the designated spins, r_{ij} is the internuclear distance, θ_{ij} is the angle between static Zeeman field H_o directed along the z-axis in the laboratory frame, and $(\vec{I}_i.\vec{I}_j - 3I_{iz}I_{jz})$ is the spin operator function. The dependence of dipolar interaction on the magnetogyric ratio has important consequences for abundant spins (*e.g.* ^1H, ^{19}F). Homonuclear dipolar interactions render proton spectra to be broad and featureless. For the less abundant or dilute spins (*e.g.* ^{13}C, ^{15}N) of low γ, heteronuclear interactions with the abundant spins, mainly ^1H, broaden the line. The dependence of this interaction on the internuclear vector (r_{ij}) and orientation (θ_{ij}), implies that one can derive structural information (in terms of bond lengths and bond angles) from the dipolar interaction. However, in powdered polymer samples, the presence of many pairs of spins with different r_{ij} and θ_{ij} causes a spread of resonance frequencies, leading to broad and featureless lines.

When molecular motions occur, they impart time dependence due to the changing orientations of the I-S inter-nuclear vector with respect to the magnetic field. As a result, there is a decrease in the observed dipolar line width. The observed reduction in line width is however determined by the details of molecular motion. Isotropic motions seldom occur in the rigid or semi-rigid phase of a polymer and, consequently, residual dipolar interactions always remain and they tend to obscure chemical shifts and scalar couplings. This can be easily removed by using Magic Angle Sample Spinning.

1.2.2.2 Chemical Shielding Anisotropy (CSA)

The electron distribution around a nucleus distorts the magnitude and direction of the applied magnetic field, H_0 to produce an effective field, which varies from one chemical environment to another. The Hamiltonian for this chemical shielding interaction is expressed as

$$H = \gamma I . \sigma . H_0 \tag{1.13}$$

where, γ is the magnetogyric ratio of the nucleus. The chemical shielding, denoted as σ, is a symmetric second rank tensor, which gives fundamental information about the electronic shielding. It is completely characterized by the three principal values, namely, σ_{11}, σ_{22} and σ_{33}, which are the diagonal elements of the tensor in the molecule fixed axis system (Principal Axis System or PAS). The chemical shielding interaction is characterised by the isotropic value (σ_{iso}), the asymmetry (η) and the anisotropy ($\Delta\sigma$), given by

$$\sigma_{iso} = (1/3)\, Tr\,(\sigma) = (\sigma_{11} + \sigma_{22} + \sigma_{33}) / 3 \tag{1.14}$$

$$\Delta\sigma = \sigma_{33} - (\sigma_{11} + \sigma_{22}) \tag{1.15}$$

$$\eta = (\sigma_{22} - \sigma_{11}) / (\sigma_{33} - \sigma_{iso}) \tag{1.16}$$

In a single crystal, the chemical shift depends on its orientation with respect to the applied magnetic field. However, in powdered polymer samples, the random orientation of the chemical bonds with respect to the applied static field results in a superposition of all resonance frequencies, given by,

$$\omega\,(\theta,\varphi) = (\Delta\sigma)\,(1/2)\,(3\cos^2\theta - 1 - \eta \sin^2\theta \cos(2\varphi)) \tag{1.17}$$

where, (θ, φ) are the polar angles, defining the orientation of the magnetic field vector in the principal axis system of the chemical shielding tensor and are shown in Figure 1.11.

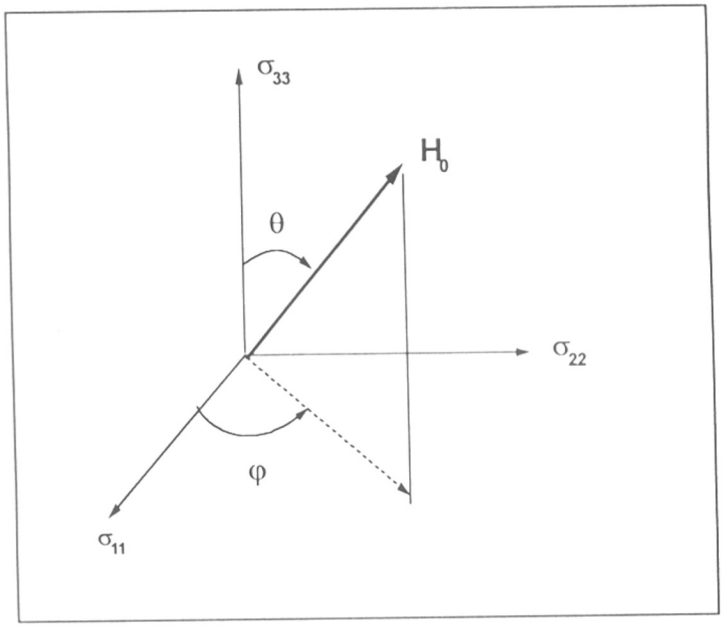

Figure 1.11: The orientation of the static magnetic field defined in the principal axis system (PAS) of the chemical shielding tensor (σ). (θ, ϕ) Corresponds to the polar angles and σ_{11}, σ_{22}, σ_{33} denote the three principal elements of σ.

This gives rise to an asymmetric powder-pattern, the shape and width of which are governed by Eqs. (1.17). Representative CSA powder-patterns are shown in Figure 1.12. As with the dipolar interaction, molecular motions affect the chemical shielding tensor and dynamical information can be obtained by an analysis of the CSA line shapes (Schmidt-Rohr & Spiess 1994). In liquids, the Brownian motion of the molecules lead to an isotropic averaging of the tensor to the scalar value (σ_{iso}, Eq. 1.14), which is the familiar chemical shifts referred to in the solution state NMR.

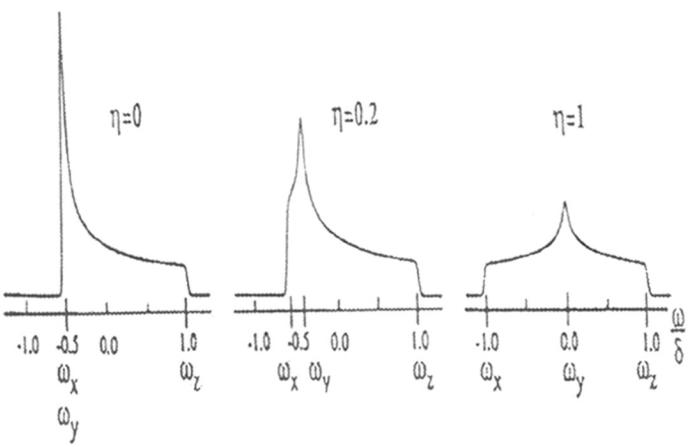

Figure 1.12: Powder pattern representing the anisotropic chemical shielding interaction (CSA) for various values of the asymmetry parameter (η). In this picture, where σ_{iso} is taken as zero. The pattern in the extreme left (η = 0) corresponds to an axially symmetric chemical shielding tensor, while a non-axial tensor is depicted in the pattern shown on extreme right.

1.2.3 Line Narrowing Techniques

1.2.3.1 Magic Angle Sample Spinning (MAS)

The situation in solids contrasts sharply with that of a liquid, where the Brownian tumbling motion of the molecules is isotropic and the motional correlation frequency ($1/\tau_c$) is many orders of magnitude larger than the strength of the dipolar or chemical shielding interaction. This results in a total averaging of the various spatially dependent interactions so that the anisotropic interactions are now replaced by their isotropic values. The dipolar interaction, being traceless, vanishes, while the CSA interaction averages to its scalar value ($1/3$ Tr. $\sigma = \sigma_{iso}$).

The orientational dependence of the dipolar (Eq. 1.12) and CSA (Eq. 1.17) interactions can however be rendered time dependent, by a bodily motion of the sample. This ingenious idea, originally introduced by Andrew *et al* (1959), Lowe (1959) and Kessmeier and Norberg (1967), is depicted in Figure 1.13. Although the interaction vector for the different crystallites make different angles (θ_1, θ_2, θ_3 etc), the 'rotor motion' takes each of these interaction vectors through their respective cones as shown in the figure. By considering that the bodily rotation of the sample projects the various interaction vectors along a common rotational axis, and by considering a cylindrical averaging over one rotor period (0 to $2\pi/\omega_r$), the orientation dependence can be 'magically' removed by choosing the angle between the rotation axis and the magnetic field to be $\cos^{-1}(1/\sqrt{3})$, or the well-known "magic angle". This is mathematically represented by writing the dipolar and CSA interaction, under sample rotation, as

$$\omega^{D}_{spinning} = \tfrac{3}{4}\left(\gamma_1\gamma_2\hbar^2/ r_{12}^3\right)\left[\tfrac{1}{2}\left(3\cos^2\beta - 1\right)\left(3\cos^2\beta'_{12} - 1\right) + \sin^2\beta\sin^2\beta'_{12}\cos\left(2\omega_r t + \varphi\right) + \sin 2\beta \sin 2\beta'_{12}\cos\left(\omega_r t + \varphi\right)\right] \quad (1.18)$$

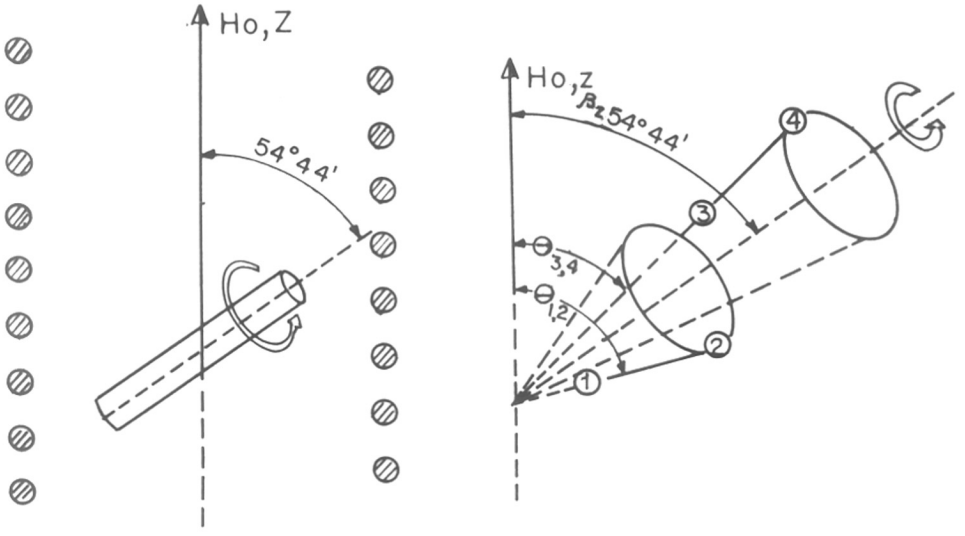

Figure 1.13: Effect of sample rotation on spatially dependent interaction and the effect of sample rotation. The interaction vector is oriented at angles (θ_1, θ_2, θ_3, etc) and the cones traced by these vectors are shown. The effect of sample rotation is to project the time average to lie along the same motional axis for all the interaction vectors. By choosing the rotation axis to be at an angle $\beta = \cos^{-1}(1/\sqrt{3})$, *i.e.*, 54.736^0, the interaction is averaged to its isotropic value.

$$\omega^{CSA}_{spinning} = (1/2)\sin^2\beta\ \mathrm{Tr.}(\bar{\sigma}) + (\tfrac{1}{2})(3\cos^2\beta - 1)\sum_p \sigma_p(\cos^2\chi_p) \qquad (1.19)$$

A geometrical picture, under sample spinning, for the dipolar and chemical shielding interactions are given in Figures 1.14 and 1.15, respectively. Clearly, when one chooses the 'spinner angle' β = "magic angle" = 54.736°, the average over the rotor motion for the CSA interaction is σ_{iso} and that for the dipolar interaction is zero. In addition to the average frequency given by Eq.(1.18) and Eq.(1.19), there are modulation side bands due to the periodicity of the sample rotation at modulo ω_r $2\omega_r$. In the time domain, the spinning side bands manifest as 'rotational echoes' which are separated by the rotor period τ_r (= $1/\nu_r$) (Maricq & Waugh 1979). From the point of view of high resolution this may be considered to be undesirable. However spinning side bands can be minimised by fast sample rotation and eliminated by side band suppression schemes (Dixon 1981 & 1982). When desired, spinning side band intensities may be analysed to deduce CSA interaction parameters (Herzfeld & Berger 1980).

1.2.3.2 Resolution Enhancement by Dipolar Decoupling

Resolution enhancement by MAS is very effective for CSA interaction since this interaction behaves inhomogeneously and such an inhomogeneous broadening can be removed at the 'magic angle' by spinning the sample even at slower spinning speeds. However, since dipolar interactions between homo-spins cause a homogeneous broadening of the proton spectral line, sample rotation at the 'magic angle' must involve spinning speeds that exceed the proton dipolar line widths (*ca.* 50 kHz). Since this is technically not feasible, line-narrowing methods using multiple-pulse sequences have been developed (Waugh *et al* 1968, Mansfield 1971 & Rim *et al* 1973).

In the case of ^{13}C observation, resolution enhancement by MAS tends to remove the CSA broadening only. Since carbon nuclei in polymeric solids are invariably surrounded by protons, ^{13}C-^{1}H dipolar interactions need to be removed.

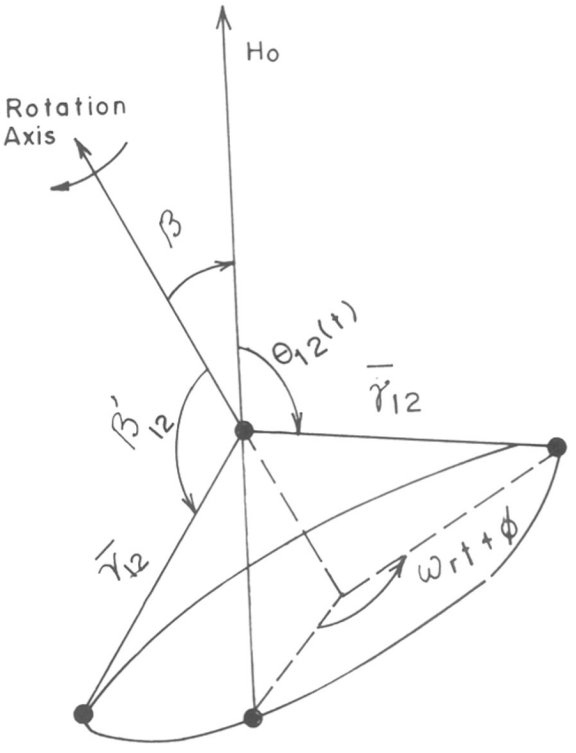

Figure 1.14: Effect of sample rotation on the internuclear vector r_{12} in the dipolar interaction. The angle β between the rotation axis and H is chosen to be the "magic angle" ($(\beta = \cos^{-1}/\sqrt{3}) = 54.736^{\circ}$). The rotational side bands are generated by the modulation terms in Eq. (1.18) due to the periodicity at ω_r and $2\omega_r$.

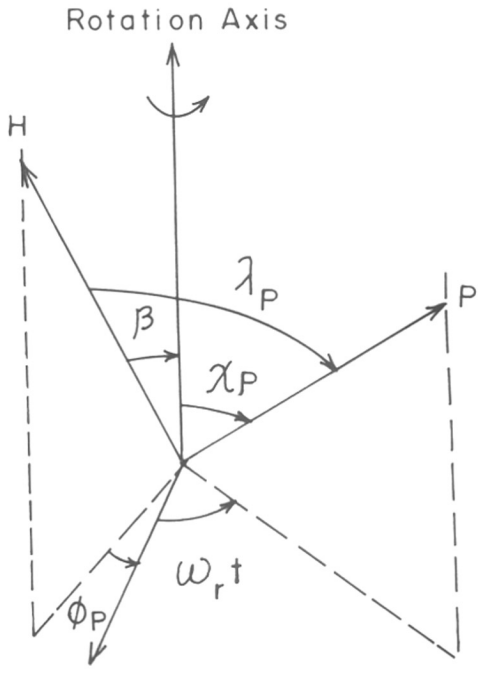

Figure 1.15: Effect of sample rotation on the principal component (P) of the chemical shielding interaction tensor (σ) is shown. The angle β between the rotation axis and H is chosen to be the "magic angle" ($(\beta = \cos^{-1}/\sqrt{3}) = 54.736^{o}$) for line narrowing. The various crystallites of the powdered polymer are oriented at the angle χ_p and the azimuthal angle $\omega_r t$ describes the periodicity of the sample rotation. ϕ_p is initial phase angle.

Because proton spin diffusion is very efficient in rigid polymers, MAS at the usually employed rotor speeds are not effective in removing the C-H dipolar broadening. The dipolar broadening on the observed carbon, due to the directly bonded and/or neighbouring protons, can however be removed by irradiating the protons at their Larmor frequency. This is akin to the broad band proton decoupling in liquids where the scalar coupling (J_{C-H}) is removed by the proton irradiation. This is depicted in Figure 1.16. The r.f field nutates the proton nuclear moment and the average dipolar field seen by the coupled ^{13}C spin vanishes. The strong homonuclear coupling within the proton spin system requires a strong decoupling field strength to be used for an effective removal of the dipolar broadening on the observed ^{13}C. Further, the proton offset frequency must be properly positioned in the spectrum (van der Hart *et al* 1981).

1.2.3.3 Sensitivity Enhancement by Cross-Polarisation (CP) and CP-MAS

The heteronuclear polarisation transfer technique for solids was originally developed by Hartmann and Hahn (1962). In the context of pulsed FT spectroscopy, Pines *et al* (1972 & 1973) developed the cross-polarisation technique for observing solid state NMR spectra of rare spins, especially ^{13}C.

In the laboratory frame, the energy levels of ^{1}H and ^{13}C are mismatched due to a large difference in their respective Larmor frequencies. In a cross-polarization experiment, shown in Figure 1.17, both the spins are placed, maintained, and manipulated in a radio frequency field as though the static field did not exist. This is achieved by initially spin-locking the abundant ^{1}H in a radio frequency field $H_1 << H_0$, followed by contact of the spin in the rotating frame, under Hartmann-Hahn conditions (Hartmann & Hahn 1962) $\gamma_I H_I^{1} = \gamma_S H_S^{1}$. Here I is abundant spin (^{1}H) and S is dilute spin (^{13}C). The magnetization of rare nuclei is then observed either in the presence or absence of ^{1}H decoupling. The effect is more elegantly conceptualized in the thermodynamic picture (Fukushima and Roeder 1981, Mehring 1983). In this picture, the 'hot' rare spins are brought into thermal

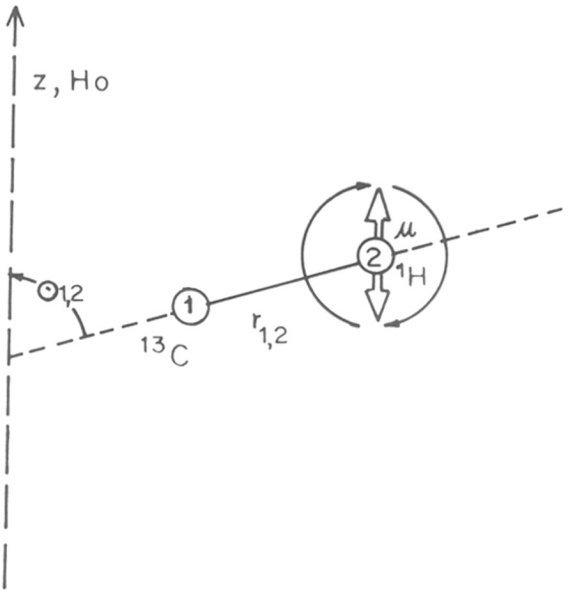

Figure 1.16: The effect of irradiating the proton spins at the proton Larmor frequency and the removal of C-H dipolar broadening on the observed ^{13}C by dipolar decoupling. The proton magnetic moment μ nutated by the resonant proton r.f field so that $\langle\mu\rangle = 0$ and the dipolar field at the observed ^{13}C vanishes.

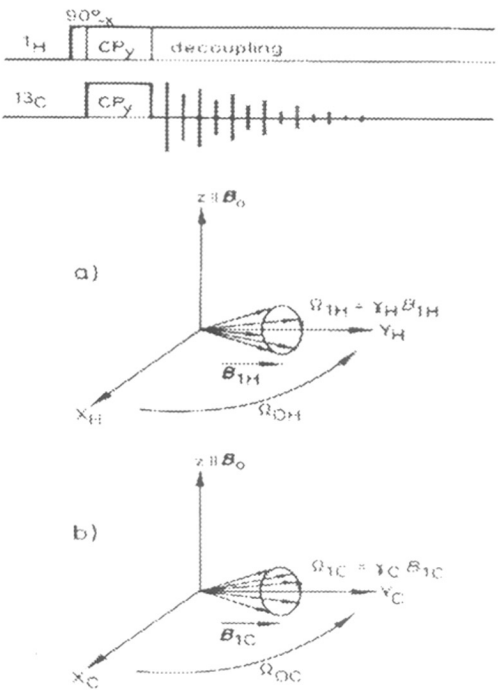

Figure 1.17: The cross-polarisation pulse sequence (top) and the precession of proton and carbon spins about their respective B_1 fields (below). In the double rotating frame, described by Ω_{0H} for ^1H and Ω_{0C} for ^{13}C, the effective precessional frequencies Ω_{1H} and Ω_{1C} are matched to obey the Hartmann-Hahn condition $\Omega_{1H} = \gamma_H B_{1H} = \Omega_{1C} = \gamma_C B_{1C}$ for the cross-polarisation. For the CP-MAS experiment, the sample is rotated at the 'magic angle'.

contact with the 'cold' abundant spins (due to spin locking) so that a magnetisation transfer from the abundant to rare spins occurs. The optimum magnetization enhancement following a single spin lock CP transfer ($\gamma_I = \gamma_S$) is about 4 for ^{13}C. More importantly, since polarisation is transferred from ^{1}H to ^{13}C, the recycle time of the CP experiment is determined by proton T_1, which is always shorter than ^{13}C T_1. Thus, considerable enhancement in ^{13}C detection sensitivity is achieved in a given measure period.

1.2.4 MAS and Solid State NMR of Gels

As mentioned earlier, polymeric gels span a motional regime not covered by the Brownian tumbling in liquids or the restricted mobility in solids. Molecular mobility is enhanced in the gel state but seldom they approach the timescale or the isotropy of the medium. The dipolar interactions are reduced to a great extent, although they are not averaged to zero.

For the ^{1}H observation, the enhanced mobility offers new opportunities to employ MAS only methods to get superior spectral resolution. In the polymeric gels, we are interested to make use of enhanced molecular mobility upon hydration and perform 2-D NMR experiments based on incoherent transfer. The immobilization of the Brownian diffusion and the predominance of local chain motions are conducive for a complete 2-D NOESY study on hydrogels (Chapter IV). The gel state of a macromolecule offers considerable scope from the NMR point of view, since this intermediate-phase regime has not been fully exploited compared to the isotropic liquid phase or the rigid solid phase. Badiger *et al* (1991) have demonstrated the usefulness of the ^{1}H MAS NMR in the study of LCST phenomenon in PNIPAm. The ^{1}H MAS behavior exhibited by the polymeric gel is similar to that observed by Forbes *et al* (1988) in lipids and biological membranes. Even under slow MAS, the proton line breaks into spinning side bands to map the residual dipolar anisotropy. The residual broadening in a static gel would, in principle, have contributions from the chemical shift anisotropy as well. However, since proton chemical shift anisotropies are small (Haeberlen 1976), the broadening is essentially dominated by residual

proton-proton dipolar couplings. While the motional models that apply to lipid systems do not necessarily operate in the polymeric gel, the inhomogeneous nature of proton line broadening is at once revealing, especially through observations of intense side-band formation. The inhomogeneous nature of the proton line shape was demonstrated by Ganapathy *et al* (1989) in hydrolysed starch-*g*-poly(acrylonitrile) gel. The transformation of homogeneous interactions amongst abundant homospins (protons) to an inhomogeneous one leads itself for a physical picture in the following way: A polycrystalline polymeric solid is characterized by a static dipolar Hamiltonian

$$H_{HH}^{D} = \sum_{j>k} D_{jk}(\varphi)\,(3I_{jz}I_{kz} - \bar{I}_j \cdot \bar{I}_k) \qquad (1.20)$$

where, the spin operators have their usual meaning and φ denotes different rotor orientations. Equation 1.20 admits that the spin operators in parentheses for different pairs "ij" and "ik" do not commute and the interaction behaves homogeneously. The condition $\nu_r >> (M_{HH}^2)^{1/2}$, where M_{HH}^2 is the proton second moment, has to be satisfied for line narrowing by MAS to occur. However, in the polymeric gel rapid rotational or reorientational motions of polymer segments reduce the contribution of the intramolecular dipolar interactions to H_{HH}^{D} by a great amount. Intermolecular interactions may not be averaged to that extent since lateral diffusion is absent. Nevertheless, the system can be considered to be "motional averaged" (Abragam 1961) and the condition $M_{HH}^2\tau_v^2 << 1$, where, τ_v is the effective correlation time, will be obeyed, leading to a frequency isolation of coupled protons. The molecular motion projects the various proton-proton interactions along the symmetry axis of the motion. The net result is that the dipolar interaction is scaled by $P_2(\cos\theta)$, where θ is the angle between the symmetry axis and H_o. The resulting "motionally averaged" (Bloom *et al* 1978) dipolar Hamiltonian becomes,

$$\langle H_{HH}^{D} \rangle = \tfrac{1}{2}(3\cos^2\theta - 1)\sum_{j>k} D_{jk}\,(3I_{jz}I_{kz} - \bar{I}_j \cdot \bar{I}_k) \qquad (1.21)$$

This equation admits that the entire dipolar Hamiltonian is multiplied by common factor P_2 (cos θ) and the eigenfunctions of the averaged dipolar Hamiltonian are independent of θ, whereas the eigenvalues are proportional to P_2 (cos θ). In this basis, the spin operators commute and the dipolar interaction H_{HH}^{D} behaves like an inhomogeneous interactions, such as chemical shielding. The resonance frequency under MAS, given by Andrew *et al* (1959), is,

$$\nu(t) = \nu_0 \pm \sum_{i=0}^{2} \nu_i \cos(i\nu_r t) \qquad (1.22)$$

where, the first term on the right is the rotationally invariant part leading to the revelation of individual proton resonances at their isotropic chemical shifts and the terms in the parentheses denote the time-dependent part, modulated at $\pm\nu_r$ and $\pm 2\nu_r$, leading to the formation of spinning side bands on either side of the center band. The side band intensities carry the information about residual dipolar anisotropy through the modulation coefficients ν_i. Equivalently, in the time domain, one observes a train of rotational echoes (Maricq *et al* 1979) the FT of which maps the side-bands pattern.

For the high-resolution observation of ^{13}C in the gel state, the C-H dipolar broadening is removed by dipolar decoupling. However, moderate decoupling field strengths (*ca.* 5-10 kHz) are sufficient to remove motionally averaged residual C-H dipolar broadening in the gel state. For the removal of residual chemical shielding interactions, spinning speeds of 1-2 kHz are sufficient to give spectra which suffer minimally from the interfering effects of spinning side bands.

1.2.5 Two-Dimensional NMR Spectroscopy

One of the most important developments in pulse FT NMR spectroscopy is the introduction of Two Dimensional Fourier Transform NMR (2-D FT NMR) spectroscopy. The concept of 2-D NMR was first put forward in 1971 by Prof. J. Jeener (Jeener 1971)

at the Ampère International School, in Baskopolje, Yugoslavia. Since then 2-D and 3-D NMR spectroscopy have become powerful tools for the structural elucidation of complex molecules, especially proteins (Wuthrich 1986, Oppenheirmer and James 1993).

For 2-D NMR spectroscopy, the 1-D pulse sequence is extended to include a second time dimension. The total experiment is divided into four parts, namely preparation period, evolution period, mixing period and detection period. The basic 2-D NMR experiment is sketched in Figure 1.18. In the case of the preparation period a non-equilibrium state is created by applying proper pulses. The detection period corresponds to the usual time, as in the 1-D experiment, during which the time domain signal is detected with a real electronic detector. FT with respect t_2 therefore provides the ω_2 axis of the 2-D spectrum. For spreading the information along the second dimension, a virtual time variable, evolution time t_1, is introduced as shown in Figure 1.18. During the evolution time, the spin system is allowed to evolve under suitably tailored Hamiltonians. The evolution time is varied in a step-wise fashion, and for each value of incremented t_1, the FID is recorded. In some experiments there is a mixing period consisting of pulses and fixed delays to relate the events that occur during the evolution period t_1 to those occurring during the detection period t_2. Thus, a signal is obtained which is a function of two time variable t_1 and t_2 $S(t_1,t_2)$. FT with respect t_2 of all the FIDs yields ω_2 spectra, the intensities or phase of each signal being modulated according to the different t_1 increments. A second FT along t_1 results in a spectrum as a function of two frequencies ω_2 and ω_1.

An important aspect of 2-D NMR is the way experiments are designed to provide spectral correlation. Experiments based on coherence transfer rely on spin communication through J-couplings or dipolar interactions. This has led to the important class of 2-D experiments called COSY experiments and various other extensions. The other class of a 2-D experiments rely on incoherent transfer, the most extensively used 2-D experiment being the nuclear Overhauser enhancement spectroscopy (NOESY).

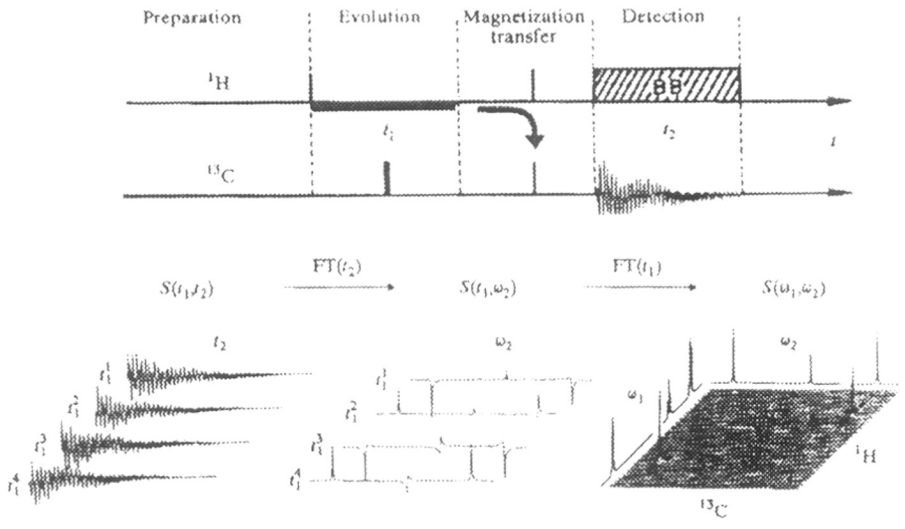

Figure 1.18: Pulse scheme and 2-D Fourier transformation operations, shown for the H-C heteronuclear correlation experiments. The FT with respect to t_2 results in $S(t_1, \omega_2)$ and results in the intensity of the ^{13}C signals to be modulated. The second FT with respect to t_1 reflects the proton evolution along t_1, obtained in the frequency domain as a proton correlated spectrum along ω_1.

1.2.5.1 Line Shapes in 2-D NMR

The signals in t_1 domain are either phase modulated or amplitude modulated. For the phase modulated signal,

$$S(t_1,t_2) = C \exp\{i(F_1t_1 + F_2t_2)\} \tag{1.23}$$

As shown for the 1-D line shape, the FT operations on the complex time domain signal are schematically presented in Figure 1.19. As can be seen, the real part of the resulting spectrum is a superposition of a 2-D absorptive and dispersive line shape. This 'phase twisted' line shape is not desirable from the point of view of 2-D spectral analysis and interpretations. The phasing problem can however be avoided by doing a magnitude calculation. Similarly, by employing amplitude modulation during t_1 and carrying out a real FT on the interferogram, after the imaginary buffer has been blanked, one can obtain a pure 2-D absorption line shape. However, the sign of the F_1 frequency is not determined.

In order to get sign discrimination combined with pure absorption line shape, two methods have been proposed. In the method due to States *et al* (1982), the cosine and sine modulated signals are recorded separately. These two signals are then transformed with respect to t_2.

$$C \text{ Cos } (F_1 t_1) \exp (i F_2 t_2) \xrightarrow{FT} C \text{ Cos } (F_1 t_1 (A_2 (\omega_2) + i D_2 (\omega_2)) \tag{1.24}$$

$$C \text{ Sin } (F_1 t_1) \exp (i F_2 t_2) \xrightarrow{FT} C \text{ Sin } (F_1 t_1 (A_2 (\omega_2) + i D_2 (\omega_2)) \tag{1.25}$$

After a proper phasing of the F_2 spectra, the imaginary parts of these two sets of interferogram are eliminated to produce, after merging real parts of the files,

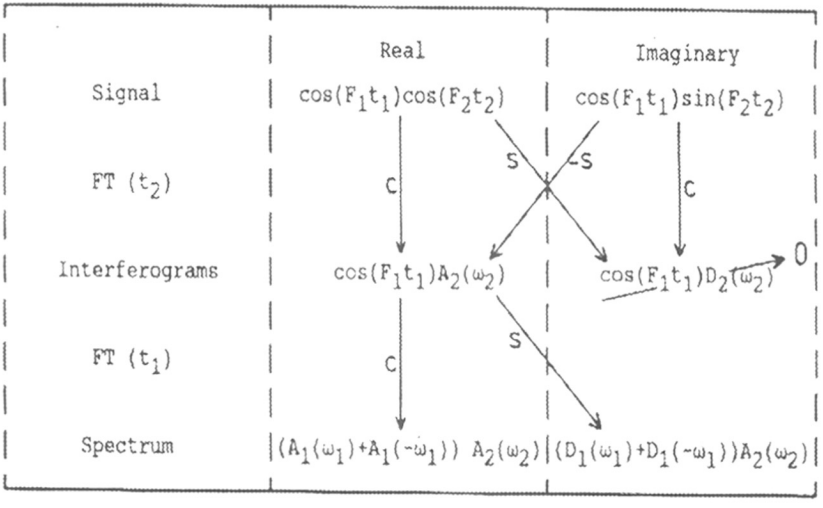

Figure 1.19: Schematic presentation of the processing of a phase modulated signal, which leads to the phase, twisted line shape. A magnitude mode calculation ($\sqrt{R^2 + I^2}$), where R is the real part and I the imaginary part, can be performed to avoid phase problem. The cosine and sine transforms are represented by the symbols **c** and **s**, respectively.

$$S(t_1, \omega_2) = C\ (\text{Cos}\ (F_1\ t_1) + i\ \text{Sin}\ (F_1\ t_1))\ A_2\ (\omega_2) \qquad (1.26)$$

A Fourier transform with respect to t_1 now gives spectrum whose real part has a pure absorption line shape. Further, $S(\omega_1, \omega_2) = A_1\ (\omega_1)\ A_2\ (\omega_2)$, implying that a sign discriminated absorption 2-D line shape has been obtained.

An alternate method, proposed by Morison and Wuthrich (1983), is based on the Time Proportionate Phase Incrementation (TPPI) scheme. This method corresponds to the sequential sampling of 1-D time domain data along t_2 using a single ADC. In the TPPI method, the phase of the signal is shifted $\pi/2$ radians after every second point. This series of sample points are stored in one buffer. With a sampling time τ, the signal can be written as

1^{st} point: $S(t) = C \cos (F\ \tau)$ (1.27a)

2^{nd} point: $S\ (t) = -\ C\ \text{Sin}\ (F_2\ \tau) = C\ \text{Sin}\ ((F + (\pi/2\tau))\ 2\tau)$ (1.27b)

3^{rd} point: $S\ (t) = -\ C\ \text{Cos}\ (F_3\ \tau) = C\ \text{Sin}\ ((F + (\pi/2\tau))\ 3\tau)$ (1.27c)

4^{th} point: $S\ (t) = C\ \text{Sin}\ (F_4\ \tau) = C\ \text{Sin}\ ((F + (\pi/2\tau))\ 4\tau)$ (1.27d)

or generally: $S\ (t) = C\ \text{Sin}\ \{(F + (\pi/2\tau))\ t\}$

As $\pi/2\tau$ is equal to half the spectral width, the spectrum resulting after transformation will be shifted by half the spectral width, thus making it possible to put the transmitter in the middle of spectral width and discriminate between positive and negative F_1 frequencies. This has been accomplished by collecting only one series of data instead of separate real and imaginary signal as is common with quadrature detection. The 2-D generalization of this method means that the phase of the pulse preceding the evolution period is incremented $\pi/2$ radians for every t_1 value to achieve a TPPI for the t_1 amplitude modulation. After FT and elimination of the complex signal, the interferogram is

$$S(t_1, \omega_2) = C\ \text{Sin}\{(F + ((\pi/2\tau))\ t_1\}\ A_2\ (\omega_2) \qquad (1.28)$$

which, is transformed along t_1 using a sine transform to get absorption line shape combined with sign discrimination because of $\pi/2\tau$ resonance offset. The various 2-D line shapes are shown in Figure 1.20. The 2-D spectral presentation is usually shown as a contour plot.

With the above methods of 2-D data collection and data processing, there is no ambiguity on the sign of the cross peaks. This aspect is especially important for the MAS 2-D NMR experiments conducted on gels since the absolute sign of the 2-D cross peaks must be ascertained to identify cross-relaxation *vis a vis* chemical exchange phenomena in the polymeric gels. Phase-sensitive 2-D NOESY experiments in gels were carried out using the TPPI scheme. Further aspects of 2-D pulse experiments specifically employed in this thesis are presented and discussed in Chapter IV.

1.2.6 Magnetic Resonance Imaging

In recent years, magnetic resonance imaging, (MRI) has proved to be extremely useful in chemistry, physics, medicine, material science, etc., due to its noninvasive nature. In conventional NMR spectrometers sample is placed in a homogenous magnetic field, so that all chemically equivalent spins experience the same field and hence precess at the same Larmor angular frequency. However, in NMR imaging involves placing a sample in a deliberately non-uniform magnetic field (Callaghan 1991). The homogeneous field is modified using a system of gradient magnetic coils, which generate linear gradient on the order of a few G/cm.

Magnetic resonance imaging (MRI) has been used to study the transport of liquids in several polymers systems. Blumich & Blumer (1993) has given and excellent review of the use of NMR and MRI in polymer science. This technique has been applied to glassy polymers such as poly(methyl methacrylate) by Weisenberger & Koeing (1989 & 1990), poly(styrene) by Tabak and Carti (1990) and Ilg *et al* (1994) and to rubbery polymers such as nylon (Blackband & Mansfield 1986, Fyfe *et al* 1993).

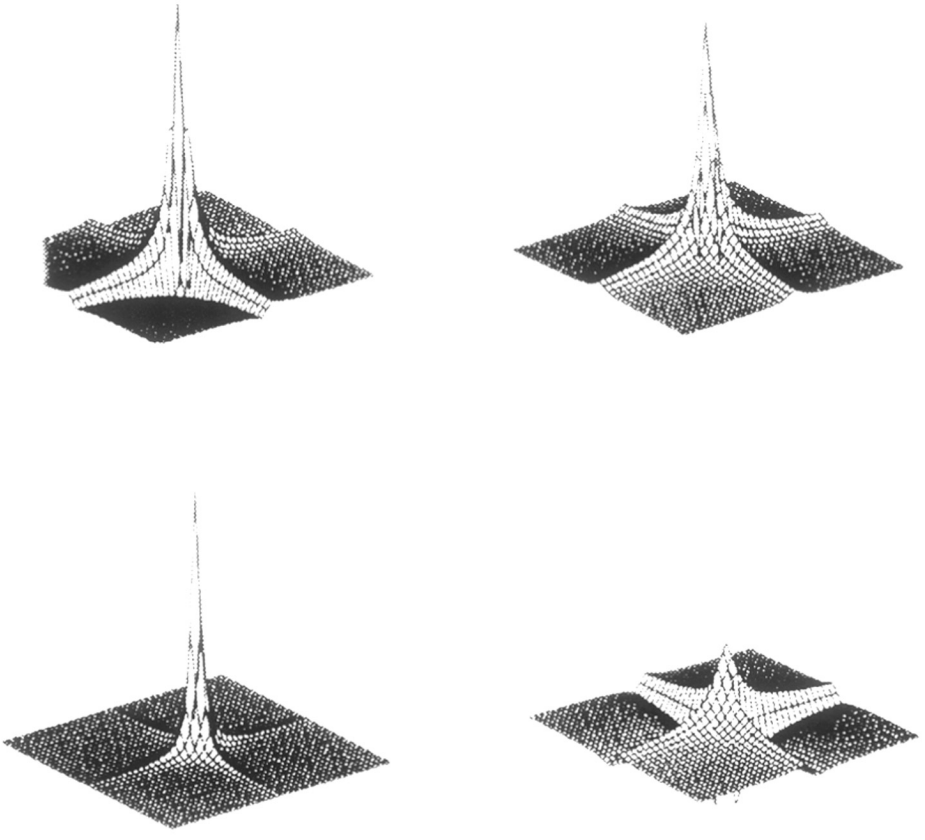

Figure 1.20: 2-D spectral line shapes depicting phase twisted line shape (top left), magnitude mode (top right), absorption (bottom left) and dispersion (bottom right). A F1 sign discriminated pure absorption line shape is obtained along the F1 dimension by States or TPPI method as discussed in the text.

Webb and Hall (1990 & 1991) have used MRI technique to study the vulcanised rubber. More recently, Hyde & Gladden (1995) has used MRI experiments to study the swelling of ultrahigh molecular weight poly(ethylene) by the solvent decalin. Koller *et al* (1991) Rajabi-Siahboomi *et al* (1994) and Hyde *et al* (1995) also used this technique to study hydrophilic polymers for controlled drug release applications.

Polymeric hydrogels under equilibrium swollen conditions do not exhibit macroscopic spatial heterogeneity due to the intricate molecular level mixing of polymer and water domains, and, naturally, they would appear to discount the use of MRI for a study. However, MRI can provide valuable information on gels that respond to stimuli, since the dynamical behavior of polymer and water components occur at different motional timescales. This allows to exploit and use associated dynamical parameters such as spin-lattice (T_1) and spin-spin (T_2) relaxation times and self-diffusion coefficient (D_{self}) for an image weighting. More detailed description of this technique is given in Chapter VI.

1.2.7 Scope of the thesis

Thermo-reversible polymers respond to external stimulus, in the form of temperature, by expelling water from the polymer matrix. Although, the thermodynamic and kinetic aspects of the volume phase transitions in polymeric gels have been extensively studied, little effort have been made to elucidate the state of water in these polymers. Despite the multitude of experimental techniques used to study macromolecular hydration, the precise details of water - macromolecular interactions in the functional environment are not well understood.

In view of the importance of polymeric gels as 'smart materials', a combination of modern solid state NMR spectroscopic and imaging techniques have been used to inspect gels at the microscopic and macroscopic levels. The NMR techniques employed for the studies and the relevant experimental aspects are discussed in Chapter II. An important aspects that has not been well addressed is the dynamical nature of macromolecules at very low levels of hydration. One-dimensional ^{1}H spectroscopy is used to follow the events of hydration at very low levels and to demonstrate the existence of a hitherto unnoticed "mobility transition" in polymeric gels (Chapter III). The nature of water and its interactions with the polymer network essentially characterize hydrogels. Two-dimensional NMR spectroscopic techniques have shown to give unambiguous answers to the nature of water-macromolecular interactions not only in super absorbing gels but also in responsive gels undergoing a discontinuous volume phase transition (Chapter IV). The observations made by means NMR spectroscopic studies are also in good agreement with the molecular modeling studies (Chapter V). The powerful NMR micro imaging technique has not been employed in the study of hydrogels except for the studies related solvent penetration. These have been employed to monitor the thermally induced discontinuous volume phase transition in hydrogels for the first time (Chapter VI).

1.2.8 References

Abragam, A., The Principles of Nuclear Magnetism. **32** of International Series of Monographs on Physics, Clarendon press, Oxford, (1989).

Abragam, A., The Principles of Nuclear Magnetism. Clarendon press, Oxford, 451, (1961).

Amiya, T. and Tanaka, T., Macromolecules, **20**, 1162, (1987).

Andrew, E R., Bradbury, A. and Eades, R. G. Nature, **182**, 1659, (1958).

Andrew, E R., Bradbury, A. and Eades, R. G. Nature, **183**, 1802, (1959).

Annaka, M. and Tanaka, T., Nature, **355**, 430, (1992).

Badiger, M.V., Kulkarni, M.G., Rajamohanan, P.R., Ganapathy, S and Mashelkar, R. A. Macromolecules, **24**, 106, (1991).

Badiger, M.V., Kulkarni, M.G. and Mashelkar, R.A. Chem. Engg. Sci. **47**, 3, (1992).

Bae, Y.H, Okano, T., and Kim, S.W., J. Controlled Release, **9**, 271, (1989).

Bae, Y.H, Okano, T., and Kim, S.W., Makromol. Chem. Rapid Commn., **9**, 185, (1988).

Bae, Y.H., Okano, T., Hsu, E. and Kim, S.W., Makromol. Chem. Rapid. Commun. **8**, 481, (1987).

Basela, J., Liorento, M.A., Nieto, J.L., Fuentes, I.H. and Pierola, I.F., Eur. Polym. Jl. **24**, 161, (1988).

Blackband, S. and Mansfield, P., J. Phys. C, **19**, L49, (1986).

Bloch, F., Hansen, W. W. and Packard, M. Phys. Rev. **69**, 127, (1946).

Bloom, M., Burnell, E. F., Mackay, A.L., Nichol, C.P., Valic, M.I., Weeks, G., Biochemistry, **17**, 5750, (1978).

Blumich, B.; Blumer, P. Makromol. Chem.,**194**, 2133, (1993).

Bumm, A., Cudby, M.E.A., Harris, R.K., Packer, K.J. and Say, B.J., J. Chem. Soc., Chem. Commun., **15**, (1981).

Bumm, A., Cudby, M.E.A., Harris, R.K., Packer, K.J. and Say, B.J., Polymer, **23**, 694, (1982).

Callaghan, P.T., Principles of Nuclear Magnetic Resonance Microscopy, Calrendon Press, Oxford, (1991).

Chandrakumar, N. and Subramanian, S. Modern Techniques in High-Resolution FT-NMR, Springer-Verlag, New York, (1987).

Chang Y.J., Chen, C.T., Toblosky, A.V., J. Polym. Sci., Polym. Phys. Ed. 12, 1, (1974).

Cooley, J. W. and Tukey, J. W. , Math. Comput., **19**, 297, (1965).

Cowie, J.M.G., Polymers: Chemistry and Physics of Modern Materials, Intertext Books, Aylesbury, UK, (1973).

Cussler, E.L., Stokar, M.R. and Vaarberg, J.E., AIChE, J. **30**, 578, (1984).

Davis, J.H., Jeffrey, K.R., Bloom, M., Valic, M.I. and Higgs, T.P., Chem. Phys. Lett., **42**, 390, (1976).

DeRossi, D., Kajiwara, K., Osada, Y., Yamauchi, A. (Eds.) Polymer Gels: Fundamental and Biomedical Applications, Plenum Press, New York, (1991).

Dickinson, W.C., Phys. Res. **80**, 901, (1950).

Dixon, W. T., J. Mag. Reson., **44**, 220, (1981).

Dixon, W.T. J., Chem. Phys. 77, 1800, (1982).

Dong, L.C. and Hoffman, A.S., Proceedings of International Symposium on Controlled Release of Bioactive Materials, Controlled Release Society, Inc., **17**, 116, (1990).

Doskocilova, D. and Schneider, B., Pure and Appl. Chem., **54**, 284, (1981).

Dušek, K. (Ed), In Responsive Gels: Volume Transitions I, Advances In Polymer Science, Springer-Verlag, Berlin, **109**, 2, (1993).

Earl, W.L. and VanderHart, D.L., Macromolecules, **12**, 762, (1979).

Engelhardt, G., High-Resolution Solid-State NMR of Silicates and Zeolites, John Wiley & Sons Ltd., (1987).

England, D. in Water: A Comprehensive Treatise, Edited by Felix Franks, Volume 4 plenum Press, New York, pp305, (1974).

Ernst, R. R. and Anderson, W. A., Rev. Sci. Instrum., **37**, 93, (1966).

Ernst, R. R., Bodenhausen, G. and Wokaun, A. Principles of nuclear Magnetic Resonance in one and two dimensions, Clarendon Press, Oxford, (1987).

Ferry, J.D., In: Viscoelastic Properties of Polymers, 3rd edn., Wiley, New York, (1980).

Flory, P.J., Principles of Polymer Science, Cornell University Press, Ithaca New York, (1953).

Forbes, J., Bowers, J., Shan, X., Moran, L., Oldfield, E. and Mascarello, M.A., J.Chem. Soc., Faraday Trans., I, **84**, 3821, (1988).

Ford, W.T. and Balakrishanan, T., Macromolecules, **14**, 284, (1981).

Foster, K.R., Resing, H.A., Garroway, A.N., Science, **194**, 324, (1976).

Fukushima, E. and Roeder, S. B. W. Experimental Pulse NMR: A Nuts and Bolts Approach, Addition-Wesley Publishing Company, Inc Reading, Massachusetts, USA, Chapter-V 297, (1981).

Fyfe, C.A., Randall, L.H. and Burlinson, N.E., J.Poly.Sci.:Part A: Polym.Chem., **31**, 159, (1993).

Galin, M. and Galin, J.C. , Makcromol.Chemi, **194**, 3479, (1993).

Ganapathy, S., Badiger, M.V., Rajamohanan, P.R. and Mashelkar, R.A. Macromolecules, **22**, 2023, (1989).

Ganapathy, S., Badiger, M.V., Rajamohanan, P.R. and Mashelkar, R.A. Macromolecules, **25**, 4255, (1992).

Ganapathy, S., Rajamohanan, P.R., Ray, S.S., Mandhare, A.B. and Mashelkar, R.A., Macromolecules, **27**, 3432, (1994).

Ganapathy, S., Ray, S.S., Rajamohanan, P.R., Mashelkar, R.A., J. Chem. Phys., **103**, 6783, (1995).

Gehrke, S.H. and Cussler, E.L. Chem. Engg. Sci., **44**, 559, (1989).

Gehrke, S.H., Andrews G.P. and Cussler, E.L. Chem. Engg. Sci. **41**, 2153, (1986).

Gehrke, S.H.; Advance in Polymer Science, **110**, 80, (1993).

Gerstein, B.C. and Dybowski, C.R., Transient Techniques in NMR of Solids: An Introduction to Theory and Practice, Academic, Orlando, (1985).

Haeberlen, U. High Resolution NMR in Solids: Selective Averaging, Advances in Magnetic Resonance, Academic Press, (1976).

Harland, R.S.; Prud'homme, R.K. (Eds.) Polyelectrolyte Gels: Properties, Preparations and Applications, ACS. Symp. Ser., ACS, Washington D.C., 480, (1992).

Hartmann, S.R. and Hahn, E.L., Phys. Rev., **128**, 2042, (1962).

Hatakeyema, T., Tamauchi, A. and Hatakeyema, H., Eur. Polym. J., **20**, 61, (1984).

Herzfeld, J. and Berger, A.E., J. Chem. Phys. **73**, 6021, (1980).

Hirokawa, Y. and Tanaka, T., J. Chem. Phys., **81**, 6379, (1984).

Hirotsu S. In Responsive Gels: Volume Transitions I, Dušek, K. (Ed), Advances In Polymer Science, Springer-Verlag, Berlin, **109**, 2, (1993).

Hirotsu S., Hirokawa, Y. and Tanaka, T., J. Chem. Phys., **87**, 1392, (1987).

Hoffman, A.S., Afrassiabi, A. and Dong, L.C. J. Controlled Release, **4**, 213, (1986).

Hoffman, R.A. and Forsen, S., Progress in NMR Spectroscopy, **1**, 15, (1966).

Hyde, T.M., Gladden, L.F., Mackley, M.R. and Gao, P.J., Polym. Sci. Polym. Chem. Ed., **33**, 1795, (1995).

Hyde, T.M., Gladden, L.F. and Payne, R., J. Controlled Release, **36**, 261, (1995).

Ichita, H., Miyano, Y., Kiyota, Y., and Nakano, Y., Proc. Gel Conference in Tokyo, Polymer Soc., Japan, 92, (1991).

Ilg, M., Pfieiderer, B., Albert, K., Rapp. W., Bayer, E., Macromolecules, **27**, 2778, (1994).

Ilmann, F., Tanaka, T. and Kokufuta, E., Nature, **349**, 400, (1991).

Ilavsky, M., Hrouz, J. Ulbrich, K., Polym. Bull., 7, **107**, (1982).

Inomata, H., Yagi, Y. and Saito, S., Macromolecules, **29**, 4887, (1990).

Irie, M., Macromolecules, **19**, 2890, (1986).

Jeener, J., Ampere International Summer School, Basko Polje, Yugoslavia, (1971).

Jenner, J. and Broekaert, P., Phys. Rev., **157**, 232, (1967).

Katchalsky, A. Kunzle, O. and Kuhn, W., J.Polym. Sci., **5**, 283. (1950).

Kazanski, K.S. and Dubrovski, S.A., Adv. In Polym., Sci., Apringer-Verlay, New York, **104**, 97, (1992).

Keifer, P. A., Baltusis, L., Rice, D.M., Tymiak, A.A., Shoolery, J.N.; J. Magm. Reson. Seri. A, **119**, 65, (1996)

Kessemeier, H., and Norberg, R.E., Phys. Rev. **155**, 321, (1967).

Kokufuta, E. and Tanaka, T., Macromolecules, **24**, 1605, (1991).

Kokufuta, E., Zhang, Y.Q. and Tanaka, T., Nature, **351**, 302, (1991).

Koller, G., Koller, E., Kuhn, W and Moll, F., Pharm. Ind., **53**, 955, (1991).

Komoloski, R.A. High-Resolution NMR Spectroscopy of synthetic Polymers in Bulk, VCH Publisher Inc, (1989).

Kulkarni, M.G., Patil, S.S., Premnath, V. and Mashelkar, R.A. Proc. Royal Soc. Lond. **A439**, 397, (1992).

Kwon, I.C., Bae, Y.H., and Kim, S.W., Nature, **354**, 291, (1991).

Lee, K.K., Cussler, E.L, Marchetti, M. and McHugh, M.A., Chem. Engg. Sci., **45**, 766, (1990)

Lele, A.K., Badiger, M.V., Hirve, M.M. and Mashelkar, R.A., Chem. Engg. Sci., **50**, 3535, (1995).

Lowe, I.J., Phys. Rev. Lett., **2**, 285, (1959).

Mamada, A., Tanaka, T., Kungiwatchkun, O. and Masahiro, I., Macromolecules, **23**, 1517, (1990).

Mansfield, P., J. Phys. **C4**. 1444, (1971).

Marchetti, M., Prager, S. and Cussler, E.L., Macromolecules, **23**, 1760, (1990).

Maricq, M. M. and Waugh, J. S., J. Chem. Phys, **70**, 3300, (1979).

Mashelkar, R.A., Chem. Engg. Sci., **50**, 1, (1995).

Mashelkar, R.A., J. Indian Inst. Sci., **73**, 193, (1993).

Mathias, L.J., Solid State NMR of Polymers, Plenum Press, New York, (1991).

Mehring, M. Principles of High Resolution NMR in Solids, Vol. 12 of NMR-Basic Principles and Progress, Springer-Verlag, New York, 2nd ed., (1983).

Miller, J.B., McGrath, K.J., Roland, C.A., Trask, C.A. and Garroway, A.N., Macromolecules, **23**, 4543, (1990).

Mirau, P.A. and Bovey, F.A., Macromolecules, **23**, 4548, (1990).

Morison, D. and Wuthrich, K., Biochem. Biophys. Res. Comm., **113**, 967, (1983).

Myoga, A. and Katayama, S., Polym. Prep. Japan, **36**, 2852, (1987).

Okano, T., Bae, Y.H., Jacobs, H. and Kim, S.W., J.Controlled Release, **11**, 255, (1990).

Olabisi, O, Robeson, J.W. and Shah, M.T. Polymer-polymer Miscibility. Springer series in Solid-State Science, Academic Press, New York, (1979).

Oppenheimer, N.J. and James, T.L., (Eds.), Methods in Enzymology, **176** and **177**, Academic Press Inc., San Diego, (1993).

Osada, Y. and Takeuchi, Y., Polym. J., **15**, 279, (1983).

Osada, Y., Okuzaki, H. and Hori, H., Nature, **355**, 242, (1992).

Otake, K., Tsuji, T., Konno, M. and Saito, S., J. Chem. Eng. Japan, **21**, 443, (1988).

Perez, E. and VanderHart, D.L., J. Polym. Sci., Polym. Phys., Ed., **25**, 1637, (1987).

Perez, E. and VanderHart, D.L., Macromolecules, **20**, 78, (1987).

Pessen, H. and Kumosinski, T.V., In Methods in Enzymology, Edited by C.H.W. Hirs & S.N. Timasheff, Academic press, New York, **117**, 219, (1985).

Pines, A., Gibby, M.G., and Waugh, J.S., J. Chem. Phys. **56**, 1776, (1972).

Pines, A., Gibby, M.G., and Waugh, J.S., J. Chem. Phys. **59**, 569, (1973).

Proctor, W.G. and Yu, F.C., Phys. Res., **77**, 717, (1950).

Paul, D.R., Barlow, J.W., Bernstein, R.E. and Wahrmuad, D.C., Polym. Engg. Sci., **18**, 1225, (1978).

Purcell, E. M., Torrey, H. C. and Pound, R. V., Phys. Rev. **69**, 37, (1946).

Rajabi-Siahboomi, A.R., Bowtell, R.W., Manfield, P., Henderson, A., Davies, M.C., and Melia, C.D., J. Controlled Release, **31**, 121, (1994).

Rajamohanan, P.R., Badiger, M.V., Ganapathy, S. and Mashelkar R.A., Macromolecules, **24**, 1423, (1991).

Rajamohanan, P.R., Ganapathy, S., Ray, S.S., Badiger, M.V. and Mashelkar, R.A., Macromolecules, **28**, 2533, (1995).

Ratner, B.D. and Hoffman, A.S in " Hydrogels"; Andrade,J.D. (Ed.) ACS Symposium Series, **31**, 1, (1976).

Rault, J., Gref, R., Ping, Z.H., Nguyen, Q.T., Neel, J., Polymer, **36**, 1655, (1995).

Ricka, J. and Tanaka, T., Macromolecules, **17**, 2916, (1984).

Rim, W.K. Elleman, D.D, Vaughan, R.W., J. Chem. Phys., **59**, 3740, (1973).

Roe, Ryong-Joon, Encylcopedia of Polymer Scince and Engineering, 2nd Ed., John, Wiley and Sons, New York, Vol. 7, 531, (1985).

Saito, H and Ando, I., Ann. Reports on NMR Spectroscopy, Academic Press Ltd., **21**, 209, (1989).

Sanchez, I.C. and Lacombe, R.H., J. Chem. Phys., **80**, 2352, (1976).

Sanchez, I.C. and Lacombe, R.H., Macromolecules, **11**, 1145, (1978).

Schefer, J. and Stejakal, E.O., J. Am. Chem. Soc. **98**, 1031, (1976).

Schmidt-Rohr, K. and Spiess, H. W., Multidimensional Solid-State NMR and Polymers, Academic Press, (1994).

Schmidt-Rohr, K., Clauss, J. and Spiess, H. W., Macromolecules, **25**, 3273, (1992).

Shaw, D., Fourier Transform NMR Spectroscopy, 2nd edition, Elsavier, Amsterdam, (1984).

Siegel , R.A. and Firestone, B.A., Macromolecules, **21**, 3254, (1988).

Slichter, C.P. Principle of Magnetic Resonance, Springer, Berlin, 2nd edition. (1990).

Spiess, H. W., Chem. Rev., **91**, 1321, (1991).

States, D.J., Haberkorn, R.A. and Ruben, D.J., J. Magn. Res., **48**, 286, (1982).

Suzaki, A. and Tanaka, T., Nature, **346**, 345, (1990).

Tabak, F. and Corti, M., J. Chem. Phys., **92**, 2673, (1990).

Tan, Y.Y. and Challa, G. Polymer, **17**, 739, (1976).

Tanaka, T., Fillmore, D.J., Sun, S-T, Nishi, I. Swislow, G, Shah, A., Phys. Rev. Lett. **45**, 1636, (1980).

Tanaka, T., In Polyelectrolytes Gels: Properties, Preparation and applications (Eds. Harland, R.S. and Prud'homme, R.K.) ACS Symp. Ser., **480**, 1, (1992).

Tanaka, T., Nishio, I., Sun, S.T. and Uneo-Nishio, S., Science, **218**, 467, (1982).

Tanaka, T., Phys. Rev. Lett., **40**, 820, (1978).

Terao, T, Maeda, S. and Saika, A., Macromolecules, **16**, 1535, (1983).

Tokuhiro, T., Amiya, T., Mamada, A., and Tanaka, T., Macromolecules, **24**, 2936, (1991).

VanderHart, D.L. and Khoury, F., Polymers, **25**, 1589, (1984).

VanderHart, D.L. and Perez, E., Macromolecules, **19**, 1902, (1986).

VanderHart, D.L., Earl, W.L. and Garroway, A.N., J. Magn. Reson., **44**, 361, (1981).

Varma A.J., Chavan V.B, Rajamohanan, P.R. and Ganapathy, S., Polymer Degradation and stability, **58**, 257, (1997).

Von Philipsborn, W., Angew. Chem., Intern. Edn., **10**, 472, (1971).

Walker, J.S. and Vause, C.A., Sci. Am., **256**, 90, (1987).

Waugh, J.S., Huber, J.M. and Haeberlen, U., Phys. Rev. Lett., **20**, 180, (1968).

Webb, A.G. and Hall, L.D., Polym. Cummun., **31**, 422, (1990).

Webb, A.G. and Hall, L.D., Polymer, **32**, 2926, (1991).

Weisenberger, L.A. and Koening, J.L., J. Polym. Sci., Polym. Lett., Ed. **27**, 55, (1989).

Weisenberger, L.A. and Koening, J.L., Macromolecules, **23**, 2445 & 2454, (1990)

Woessner, D.E. and Snowden, B.S. Jr., J. Colloid Interface Sci., **34**, 290, (1970).

Wuthrich, K., NMR of Proteins and Nucleic Acids, Wiley-Interscience, New York, (1986).

Yokoto, K., Abe, A., Hosaka, S., Sakai, I and Saito, H., Macromolecules, **11**, 95, (1978).

Chapter II

Experimental Aspects:

Synthesis of polymers and NMR techniques

In the previous chapter, an introduction to the polymer gel science and the phenomenon of pulse Fourier-Transform NMR has been given and discussed in the context of 1-D and 2-D spectroscopy. Salient features of line broadening mechanisms in solids, their removal by experimental strategies as well as the enhanced mobility in gels have also been dealt with in some detail. In this chapter, the various experimental aspects pertinent to the work described in this thesis will be presented and explained. The chapter is divided into two parts. In part one we have discussed synthesis of the various polymers and in the other part general NMR methodologies employed for the study of polymeric gels.

Part A: Synthesis of various polymers and polymeric gels

2.1 Synthesis of Various Polymers

Acrylamide, acrylonitrile, were obtained from Aldrich Chemical Co., USA and used without further purifying. *N*-isopropyl amine, acrylic acid, benzoyl chloride, hydroquinone, N',N'-methylene-*bis*-acylamide, *N,N,N',N'*-tetramethylethylenediamine (TEMED), potassium persulphate, ceric ammonium nitrate, sodium sulphite, sodium hydroxide, potassium hydroxide, isopropyl alcohol, sulphuric acid, acetone and dimethyl formamide were obtained from local suppliers. All the above chemicals were further purified by using standard procedures given elsewhere (Perrin *et al* 1981).

2.1.1 Synthesis of linear poly(acrylamide)

Linear poly(acrylamide) was prepared by free radical solution polymerization of acrylamide monomer using potassium persulphate as initiator and sodium sulphate as scavenger. Acrylamide monomer 14.0 gm. was dissolved in double distilled water with continuous nitrogen gas bubbling. To this solution 2 ml of isopropyl alcohol was added and the temperature was increased to 60^{O}C. The pH of the solution was adjusted to 3.0 to 3.5 with 2N sulphuric acid, which is followed by the addition of initiator (0.2 g) and 0.025 g scavenger. The reaction was continued for two and half-hours by raising the reaction

temperature to 65^{O}C. The polymer was isolated in the form of powder by precipitation with acetone and was dried at 60^{O}C under vacuum.

Linear poly(acrylamide) with a different molecular weights were synthesized by following the same procedure except for the change of amount of isopropyl alcohol. The molecular weight of the poly(acrylamide) samples was determined by viscometry, using a standard procedure given elsewhere (Klein & Conrad 1980). The detailed description of different molecular weights of the synthesized polymers is given in the Table 2.1.

Table 2.1

Molecular Weights of the Linear poly(acrylamide)

Sr. No.	Intrinsic viscosity [η]	Molecular weight
1.	5.050	19.70 x 10^5
2.	1.435	3.84 x 10^5
3.	0.445	0.84 x 10^5

2.1.2 Hydrolysis of linear poly(acrylamide)

Alkaline hydrolysis of linear poly(acrylamide) was carried out by standard procedure (Kulicke *et al* 1982). A uniform one percent solution (w/v) of the linear poly(acrylamide) (molecular weight 19.7 x 10^5) polymer was prepared in the double distilled water. In to this 300 ml of 2N NaOH solution was added with continuous stirring. The temperature was maintained at 25^{O}C. The hydrolyzed polymer was isolated in the form of a dry powder.

Linear poly(acrylamide) with different extent of hydrolysis was prepared by changing the period of hydrolysis. The detailed description of the alkaline hydrolysis of linear poly(acrylamide) is given in the Table 2.2.

Table 2.2

Alkaline hydrolysis of linear poly(acrylamide)

Sr. No.	Period of hydrolysis (hours)	Percentage of hydrolysis
1	One	10.10
2	Two	26.47
3	Three and half	40.00

The degree of hydrolysis of hydrolysed linear poly(acrylamide) samples was calculated by atomic absorption spectroscopy for sodium as well as potentiometric titration.

2.1.3 Synthesis of crosslinked poly(acrylamide)

Crosslinked poly(acrylamide) was synthesized by a standard procedure (Mathew and Pillai 1992), through the free radical solution polymerization of acrylamide in water using potassium persulphate as an initiator, sodium sulphite as a scavenger and *N,N'* methylene-*bis*-acrylamide as a cross-linker. The percentage of cross-linker was kept 2.0%. The typical synthesis procedure is as follows. 14.0 gm. of acrylamide monomer and 0.6 gm of *N,N'* methylene-*bis*-acrylamide cross-linker was dissolved in the 100 ml of double distilled water. 100 mg of potassium persulphate was added into the mixture with a constant stirring. The temperature of the mixture was increased gradually and maintained at 80°C with stirring until the polymer precipitated. After that 80 ml of double distilled water was added into it and the mixture was again heated at 80°C for 30 minute. The lumps of the polymer were powdered, washed with distilled water, ethanol and methanol repeatedly, in order to wash away residual acrylamide monomer, methylene-*bis*-acrylamide, and potassium persulphate. The cross-linked polymer was obtained in the form of dry powder.

2.1.3.1 Hydrolysis of crosslinked poly(acrylamide)

The 2% crosslinked poly(acrylamide) was subsequently alkaline hydrolyzed by procedure given Tanaka *et al* (1980) and using NaOH. The above gel was placed in a basic solution of pH 12 of 0.4% volume of NaOH solution in water to hydrolyze a portion of the acrylamide groups into the acrylic acid groups ($-CONH_2 \rightarrow -COOH$). The well-established chemistry of the hydrolysis of amide groups in a basic solution was used (Sandler & Karo 1977). More conversion of amide group into carboxylate moieties was achieved by varying the extent of hydrolysis time, such as two, eight and thirty days. The hydrolysed crosslinked poly(acrylamide) samples were isolated in the form of dry powder and dried at 40°C under vacuum.

2.1.4 Synthesis of Hydrolysed starch-*g*-poly(acrylonitrile)

Hydrolysed starch-*g*-poly(acrylonitrile) (HSPAN), samples were synthesized by graft copolymerization of acrylonitrile onto gelatinized starch using ceric ammonium nitrate as a redox initiator by using following procedure. 20 gm of the starch (maize) was weighed and dissolved in 200 ml of double distilled water. This solution was taken into a reactor. The reactor is a three-necked flask fitted with a condenser and half moon shaped stirrer. The reactor was surrounded with a jacket for water circulation. The gelatinization of starch was carried out at 75°C temperature for an hour. The reaction mixture was cooled to 30°C by using the cold water circulation through the reactor jacket. Some portion of the gelatinized starch was isolated in the form of dry powder. Acrylonitrile monomer was grafted on to this gelatinized starch. 33 ml of acrylonitrile monomer was poured into the reactor containing the gelatinized starch. The ceric ammonium nitrate (0.676 gm) catalyst prepared in 15 ml of 0.1N HNO_3 solution was added slowly into the reaction mixture. The reaction conditions like constant stirring and the N_2 gas atmosphere was maintained. The reaction was carried out at 30°C for the four hours.

The synthesized graft copolymer was subsequently hydrolyzed by using potassium hydroxide (21.0 gm). The hydrolysis was carried out for four hours at $90^{O}C$. After the hydrolysis the reaction mixture was neutralized using acetic acid and the product was isolated in the form of a dry powder. The equilibrium water absorbing capacity (swelling ratio) of this polymer was measured and was found to be 170 gm of water per gm of dry polymer. Other samples with different water absorbancy were made, by changing the extent of hydrolysis as shown in the Table 2.3. The grafting was kept constant at 48 %.

Table 2.3

Synthesis and Alkaline Hydrolysis of HSPAN for different Absorbancy [a)]

Sr.No.	Starch	Acrylonitrile	KOH	Time of Hydrolysis (hours)	Absorbancy (g of water/g of dry polymer)
1.	20	33	21.0	4.15	170
2.	20	33	19.5	4.00	160
3.	20	33	17.0	3.00	100
4.	20	33	15.5	2.45	80
5.	20	33	14.0	2.30	50

a) All the quantities are in gm. wt.

The molecular weights of grafted poly(acrylonitride) pendant chain were determined (Ganapathy *et al* 1990) as follows:

The crude graft was thoroughly extracted with pure dimethyl formamide, which dissolves the ungrafted poly(acrylonitrile) homopolymer. The resulting pure graft copolymer was acid hydrolysed to remove the starch backbone. After removing the starch

completely, the grafted poly(acrylonitrile) was recovered and dried. The molecular weight of it was estimated viscometrically using the relationship,

$$[\eta] = kM_n^a \qquad (2.1)$$

where, $[\eta]$ is the intrinsic viscosity measured experimentally at 30°C, M_n is molecular weight, k and a are constants obtained from the literature (k = 3.92 x 10^{-4}, a = 0.75) (Brandrup and Immergut, 1966). The intrinsic viscosity and molecular weights for the different pendant sample capacity are tabulated in Table 2.4.

Table 2.4

Intrinsic viscosity and molecular weights of the grafted polymer in HSPAN

Absorbency (g/g)	Intrinsic viscosity [η]	Molecular weight
170	1.5288	1.04 x10^5
100	1.5008	1.01 x10^5
80	1.4860	1.00 x10^5
50	1.4620	0.98 x10^5

2.1.5 Synthesis of Poly(*N*-isopropylacrylamide) gel

2.1.5.1 Synthesis of *N*-isopropylacrylamide monomer

Acryloyl chloride was prepared by the condensation of acrylic acid and benzoyl chloride using hydroquinone as the inhibitor. The monomer was synthesized in the laboratory by condensation of the acryloyl chloride and isopropyl amine by using a standard procedure (Butler *et al* 1960). A typical procedure was as follows:

12.18 gm. of isopropyl amine and 125 ml. of distilled and dry diethylether were added to a round bottom flask. The temperature was maintained at 0°C. 9.0 gm. of acryloyl chloride was diluted with 25 ml. of diethyl ether and added to the reaction mixture from a dropping funnel in a drop-wise manner over a period of 45 minutes to one hour. The reaction mixture was stirred constantly. After the addition was complete, the reaction mixture was stirred for another 6 hours. The salt was filtered off and the monomer was recovered by distilling off ether at room temperature under vacuum. The solid monomer was re-crystallized from diethyl ether and its, purity was confirmed by TLC and NMR technique.

$$CH_2 = CHCOCl + 2\,(CH_3)_2NH \Rightarrow CH_2 = CHCONHCH(CH_3)_2 + (CH_3)_2NH.HCl$$

The structure of the monomer was confirmed by FT-IR and NMR spectroscopy.

Molecular formula: $C_6H_{11}ON$ (mol. wt. 113)

FT - IR (Neat): 910 and 990 cm^{-1} ($CH_2 = CH$), 1650 cm^{-1} ($O = C - NH$), 3300 cm^{-1} (NH).

^1H NMR ($CDCl_3$): 1.6 δ d (6H $(CH_3)_2$ - CH-), 4.8 δ m ($(CH_3)_2$ - CH-), 6.6 δ dd ($^1H\,HC = CH_2$), 7.3 δ m (2H $CH_2 = C$).

2.1.6 Synthesis of crosslinked Poly(*N*-isopropylacrylamide)

N-isopropylacrylamide was polymerized by the free-radical solution polymerization technique (Notani 1990) at room temperature using water as the solvent as follows:

N- isopropylacrylamide 2.0 gm. was dissolved in 5 ml of double distilled water. 0.0180 gm. of methylene-*bis*-acrylamide as a cross-linker was then added to the monomer solution and dissolved. 0.003 gm. *N,N,N',N'*, tetramethylethylenediamine was added, followed by 0.006 gm. of potassium persulfate as an accelerator and initiator, respectively. The reaction was carried out at 20°C in a 6-mm-diameter glass tube. Nitrogen gas was

bubbled through the reaction mixture, which was then poured in a petridish at room temperature. Polymerization was complete in half an hour. The polymer sheet was kept at room temperature overnight. The polymer discs were obtained by punching the sheet. These were then extracted in water to remove all the unreacted monomer, which was confirmed by spectrophotometric analysis of the extract. Finally, these discs were dried in a vacuum oven at 40°C and then stored in a dessicator. The dried gel was obtained as powder and was slightly opaque at room temperature (22°C). It was found to have equilibrium swelling capacity of 8.0 g of water/ g of the polymer.

2.1.6.1 Swelling Studies for crosslinked poly(*N*-isopropylacrylamide)

Swelling experiments were performed for this polymer both below and above the lower critical solution temperature. The dry polymer disc was weighed and immersed in double distilled water maintained at the temperature of the experiment. The weight of the slab was checked by removing it from water and after blotting it with a tissue paper. This procedure was repeated every 30 minutes till there was no further weight gain. The equilibrium swelling was calculated from the following equation:

$$\% \text{ Swelling} = [(W_s - W_d) / W_s] \times 100 \qquad (2.2)$$

where, W_s denotes the weight of the swollen polymer and W_d denotes the weight of the dry polymer. The calculated equilibrium swelling value of this polymer was 8.0 g/g (water/polymer).

The Lower Critical Solution Temperature (LCST) of this polymer was reported to be 32-33°C (Schild 1992). The LCST of the above polymer was measured and found it to be 30-32°C. This measurement was done by monitoring the volume change of an equilibrium swollen gel as a function of temperature by using a temperature-controlled bath (Julabo, West Germany).

Part B: NMR METHODOLOGY FOR THE STUDY OF POLYMERIC GELS

2.2 NMR of polymeric solids: General aspects

The different types of interactions, which have to be taken into account in NMR spectroscopy have been already discussed in the previous chapter (section 1.2.2) In polymeric solids the important interactions, like H_D and H_{CSA}, which are effectively averaged in solution due to Brownian motion of the molecules, persist. This leads to considerable broadening of the NMR lines, especially in amorphous solids like polymers and crystalline powders. All the contributions to NMR line broadening can be in general classified as homogeneous and inhomogeneous (Fukushima & Roeder 1981). In a homogeneously broadened line all the nuclei in that line make identical contributions with their intrinsic linewidth which is same as the composite. A typical example, being the homonuclear dipolar interactions between the protons in the solids. In an inhomogeneous line separate part of the line can be identified as a separate contribution. A very common example is the *powder pattern* due to chemical shift anisotropy (CSA), as discussed in Chapter I. The heteronuclear dipolar interaction, namely ^{1}H-^{13}C dipolar interaction, is usually considered to be inhomogeneous. However, ^{1}H-^{13}C pairs are not isolated and there is a strong spin-spin interaction between the proton spins within the chain segments (intra) or between the chain segments (inter). As a result, the ^{1}H-^{13}C dipolar interaction becomes homogeneous.

The proton spectrum normally obtained for solids has a typical line width of ~ 50-60 kHz. This is due to the very strong homonuclear dipolar interaction between the protons present in the system, which permits an efficient spin diffusion, and hence a broad Gaussian line. As an example, the ^{1}H spectrum of dry Hydrolyzed starch-*g*-poly(acrylonitrile), HSPAN, is shown in Figure 2.1 (Ganapathy *et al* 1989). It can be seen

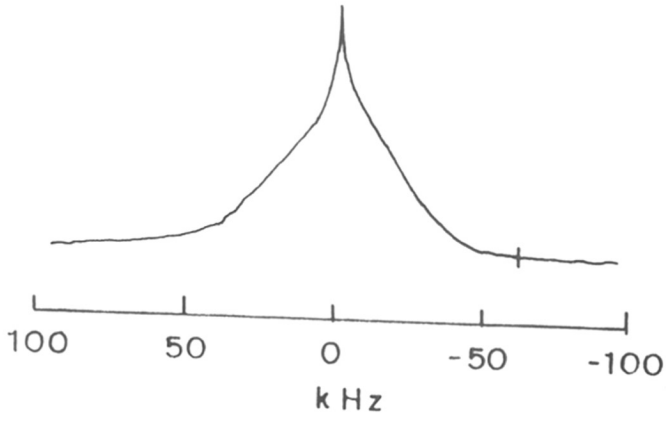

Figure 2.1: Proton static Spectrum of Dry HSPAN

that the spectrum is too broad and featureless to make any assignments. In these circumstances the conventional line narrowing technique such as MAS will not be enough to overcome the strong ^{1}H-^{1}H interactions. Broadening will also be seen for the rare spin ^{13}C spectrum as well, an example is depicted in Figure 2.2a for HSPAN. Here, the dominating interaction is the CSA, as the ^{13}C-^{1}H dipolar interactions are killed by high power decoupling. Such interactions can be narrowed by MAS technique (Figure2.2b) (Ganapathy *et al* 1990) or by solvation (Rajamohanan *et al* 1991). However, in gel, partial or complete averaging of the dipolar and anisotropic interactions will take place due to the enhancement in molecular motions induced by the plasticization by solvents (*e.g.* in present studies water) and leads to narrower lines. A typical example is the ^{1}H (Figure 2.3a) and ^{13}C NMR spectra of HSPAN (Figure 2.3b) obtained in the dry state and in hydrated state.

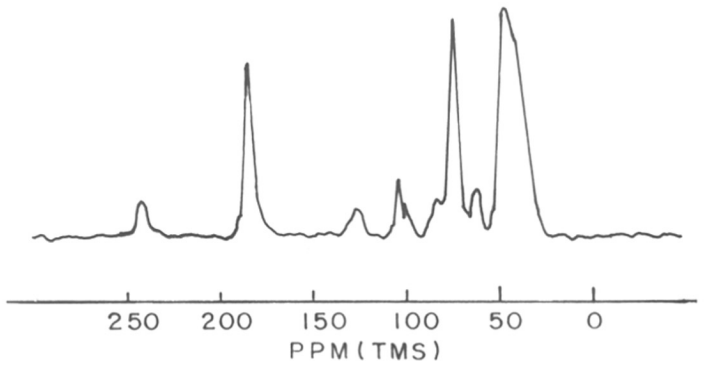

Figure 2.2b: ^{13}C MAS spectrum of dry HSPAN

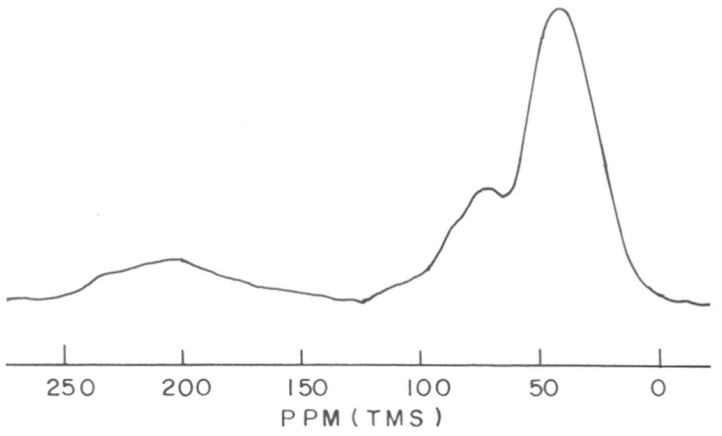

Figure 2.2a: ^{13}C static spectrum of dry HSPAN

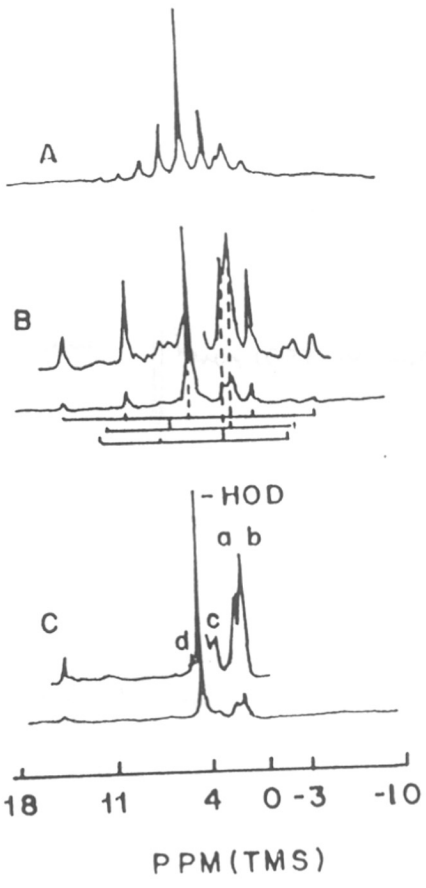

Figure 2.3a: ^{1}H MAS spectra of HSPAN gels: (A) 0.2% saturation, spinning at 450 Hz; (B) 0.2% saturation, spinning at 1.5 kHz and (C) 2% saturation, spinning at 3.1 kHz. The expected positions of first- and second-order spinning side bands are marked by stick diagram below the spectra.

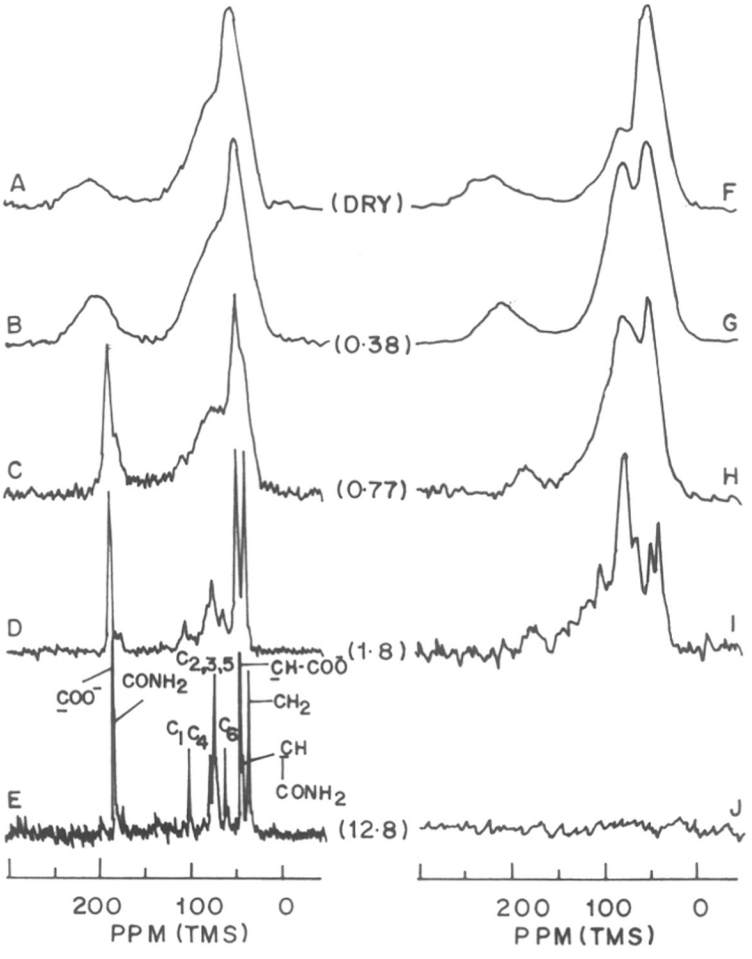

Figure 2.3b: Static dipolar-decoupled ^{13}C Bloch decay spectra of HSPAN as a function of hydration (A-E). All the spectra were taken a 45° flip angle and a recycle time 20s. Number of scans: (A) 2900, (B) 4700, (C) 1600, (D) 1300, (E) 5700. (F-J) Static dipolar-decoupled ^{13}C CP spectra as a function of hydration. All the spectra were obtained by using a CP pulse sequence with an applied radio frequency field of 50 kHz and a mixing time of 1.0 ms. Number of scans: (F) 416, (G) 8100, (H) 16 100, (I) 12 200, (J) 10 200. Hydration levels are indicated in parentheses.

From the experimental point of view, the classification of the interactions as being homogeneous or inhomogeneous has important consequences. The homogeneous proton-proton dipolar interaction, for example, can not be removed by Magic Angle Spinning (MAS), which is introduced earlier. Since the flip-flop process with in the proton spin system occurs in a timescale of about 20 μsec, any experimental methodology chosen to average this interaction must be capable of achieving this with in a cycle time of 20 μsec. Although the orientational dependence of heteronuclear dipolar interaction goes as $P_2(Cos\theta)$ and thus has a 'magic angle', the main bottleneck in using MAS for this situation is the very efficient proton-proton spin communication. Presently, the technically achievable maximum spinning speed is about 25 kHz (rotor period of 40 μsec) and this fails to meet the averaging criterion. Ingenuous averaging schemes using multiple-pulse line narrowing techniques have been developed (Waugh *et al* 1968, Mansfield 1971, Rhim et al 1973, Bronnimann *et al* 1988 and Harris *et al* 1988). In semi-rigid solids, as in the polymeric gels, the beneficial effects of enhanced molecular mobility are indeed very rewarding, since molecular motions scale the dipolar interaction down to the extent that proton-proton spin communication is no more a bottle-neck (Forbes *et al* 1988). MAS based experiments on protons become feasible and can be elegantly combined in various 1-D and 2-D experimental schemes.

The removal of ^{13}C-^{1}H dipolar broadening on the observed ^{13}C resonance by proton decoupling is discussed in Chapter I. Since this interaction is under the influence of a proton dipolar Hamiltonian, one must use an intense r.f field on protons (> 40 kHz) so that the decoupling strength is of the order of the proton dipolar width. Once again, in the experimental implementation for study of gels by solid state NMR, the decoupling requirements become less stringent due to the motional averaging of both the ^{13}C-^{1}H and ^{1}H-^{1}H dipolar interactions.

Therefore, from an experimental angle, different considerations apply for the study of gels by solid state NMR. For proton observation, MAS only methods are sufficient in systems hydrated to a level of 0.8 g/g or greater. For ^{13}C observation, low

decoupling field strength is sufficient for gels hydrated at ~ 0.5 g/g or above. MAS at 2-3 kHz is usually sufficient to remove the residual dipolar and chemical shielding anisotropy broadening in the observation of ^{1}H and ^{13}C spectra of polymeric gels. However, in the case of ^{13}C observation, low power decoupling can be combined with MAS to get the desired signal resolution. The experiments presented in the thesis were carefully implemented by a judicious choice of the MAS speed and the decoupling field strengths, depending on our experience with the way these experimental parameters affect the final spectra of gels hydrated to different extents. These experimental aspects are highlighted in the spectra presented in Figures 2.3a and 2.3b.

In the proton case only a partial averaging of the ^{1}H-^{1}H dipolar interactions by the solvent (water) takes place. Hence MAS has to be employed to get narrower lines (Figure 2.3a). Whereas, in case of ^{13}C spectra (Figure 2.3b), which are taken in the static mode using a simple Bloch decay experiment emphasize the effect of molecular motions on ^{13}C spectra. Hence, the narrowing is arising only from the solvent induced molecular motions.

2.2.1 Experimental and Instrumental Requirements

In general, the requirements for solid state NMR measurement are different to the one used for the liquid state experiments. The demand on the stability of magnet and resolution is not as stringent. Usually a line width of a few Hertz is tolerable. But the demands on the r.f hardware are very high. In order to excite broad spectral lines, the r.f pulse must be very intense (*ca.* 80 kHz) and its duration very short (*ca.* 1 to 2 μs) so that practically no decay of the magnetisation occurs during the pulse. Both these requirements place stringent demands on the spectrometer. The former requirement is met by a optimum design of the transmitting and receiving probe circuit so as to have a very high quality factor (Q). With high power r.f (upto 1 KW) the pulse duration of the 90° flip approaches one microsecond or better and is considered adequate for most demanding experiments. In a high-resolution mode, it is a common practice to delay the data acquisition by tens of microseconds (dead time delay) to avoid the transmitter pulse

breakthrough in to the receiver. For solid state wideline NMR one must have a sufficiently shorter ring down time so that the acquisition of the free induction decay can begin after one or two microseconds after the cessation of the r.f pulse. Or, alternatively, one can resort to the echo techniques developed for solids (Slichter 1989). The conventional solution NMR uses a digitizer, which can digitize at a maximum rate of 125 kHz or less. For wide line solid state measurements the spectral range is large and a fast digitiser must be used. Finally, the NMR probe must be robust and the tuned circuit must withstand high r.f power and maintain the desired detection sensitivity.

2.2.1.1 The Bruker MSL-300 FT-NMR Spectrometer

All the NMR experiments were carried out on a Bruker MSL 300 MHz NMR, which is a central NMR Facility at NCL. A block diagram of the MSL-300 NMR spectrometer is given in Figure 2.4. The heart of the spectrometer is the superconducting magnet, which produces a magnetic field of 7.01 Tesla. The magnet is equipped with cryo-shims as well as room temperature shims. The spectrometer is configured for two channel operation. The observe frequency is sufficiently broad banded, both on the r.f transmitting and receiving side, and nuclei in the range of ^{109}Ag (13.956) to ^{31}P (121.442). The data acquisition and processing (both in 1-D and 2-D) are controlled by the ASPECT-3000 computer. For high speed digitisation, BC-132 fast digitizer board is available on the spectrometer. For high power experiments, such as CP-MAS, the r.f pulses are initially amplified on the low power F1 and F2 transmitters before being fed to high power 1 KW tuned amplifiers. A Bruker BVT-1000 temperature controller is available for variable temperature studies. All the spectrometer operations, such as interface settings, pulse program compilation and execution, data acquisition, data processing and spectral plotting are carried out using the DISMSL software.

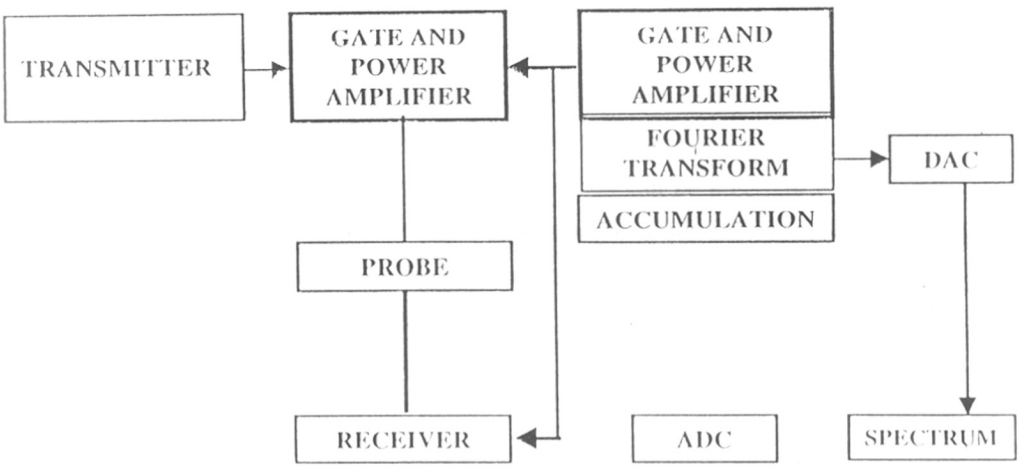

ADC - ANALOG TO DIGITAL CONVERTER

DAC - DIGITAL TO ANALOG CONVERTER

Figure 2.4: Block diagram of the MSL-300 NMR spectrometer

A micro imaging unit is also attached to this spectrometer. The micro imaging unit consists of a selective excitation unit (SEU), a linear r.f power amplifier for protons (5 W), and a gradient drive unit (GDU). The SEU provide the amplitude modulated RF pulses. The gradient cards of the imaging probehead are driven by GDU. The imaging software provided on the MSL-300 has a library of stored waveforms for a standard set of pulse shapes. The shaped pulses are amplified by the linear r.f power amplifier before being fed into the micro imaging probehead. The gradients are generated by the DISMSL software and the current through the gradient coil can be precisely controlled within a given imaging pulse sequence. The imaging probe is actively shielded and provides a very efficient damping of the eddy currents generated after the application of the gradient pulse. Figure 2.5 shows a block diagram of the Bruker micro imaging accessory on the MSL-300 FT NMR spectrometer.

2.2.1.2 Proton Wide-line, CP-MASS and Micro Imaging Probes

For the NMR studies presented in the thesis three kinds of probes were used. (i) Home-built wide line probe for recording broad line proton spectra in mobility transition studies (Chapter III) (ii) Bruker CP-MAS probe for Magic Angle Sample spinning (MAS) and cross polarization (CP-MAS) experiments (Chapter IV) and iii) Bruker micro imaging probe, for imaging experiments (Chapter VI).

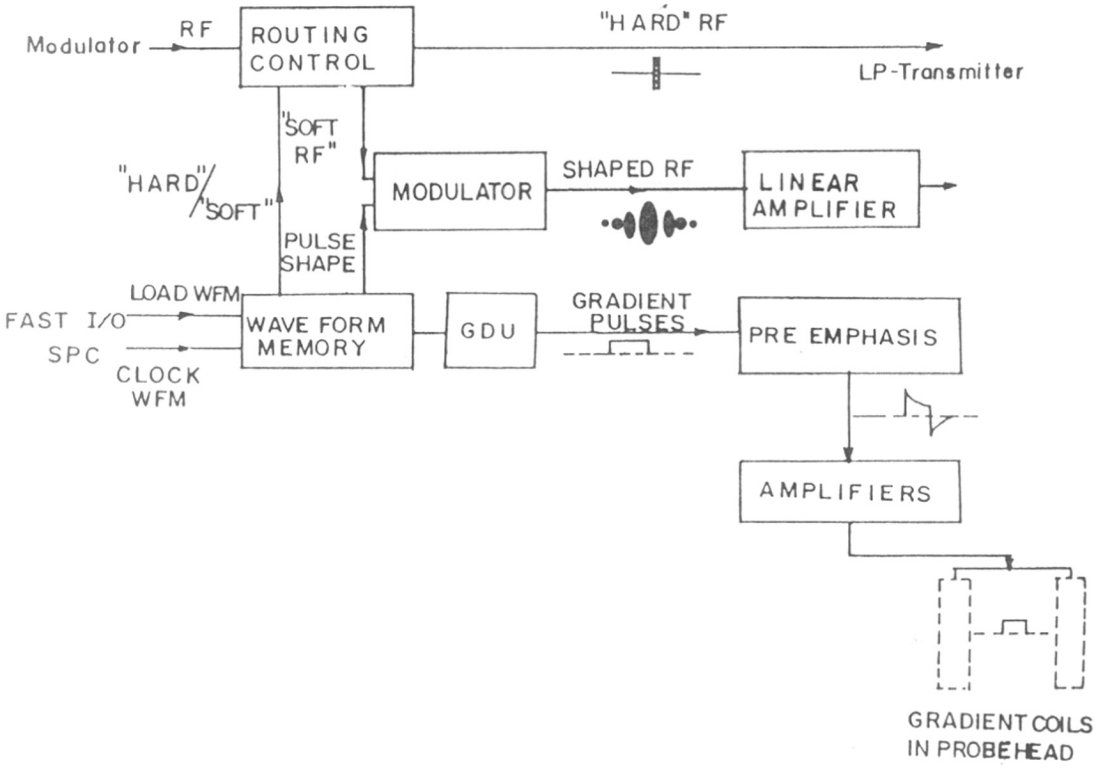

Figure 2.5: Block diagram of the MSL-imaging unit

A home-built probe optimised for measurements on solids with shorter dead time (2-3 μs) and high H_1 field generation was specially fabricated and used for the wide line NMR measurements. An existing probe body was used to mount the tuning and matching capacitors. A 50 ohm semi-rigid co-axial cable was used to feed the r.f to the coil. The solenoidal r.f coil had i.d of 5 mm and was made from a flattened silver-coated copper wire. High Q high voltage VOLTRONICS tunable r.f capacitors were used. The probe circuit was tuned to 300.13 MHz and impedance matched to 50 ohms. The proton background signal from the probe was found to be negligible. This probe was exclusively used to record proton spectra of rigid and hydrated polymers in the study of mobility transitions (Chapter III). The circuit diagram of the home-build wide-line NMR probe is shown in Figure 2.6

MAS experiments were carried out on CP/MAS probe supplied by Bruker. This probe uses 7 mm (o.d.) zirconia rotors, equipped with double air bearings and variable temperature (VT) capability. Rotor loading into the stator is performed with the help of a rotor transfer line. Sample insertion, ejection and spinning are controlled by a pneumatic unit, which also provides an optical detection and indication of the spinning speed. For variable temperature operations, the bearing air is used for the temperature control. This probe uses a single coil doubly tuned resonant circuit (300/288 MHz and 46-85 MHz) with an excellent isolation of the proton decoupler frequency on the observe X channel (better than 30 dB).

The proton imaging experiments (Chapter VI) were performed using a dedicated imaging probehead housing a 15mm imaging insert.

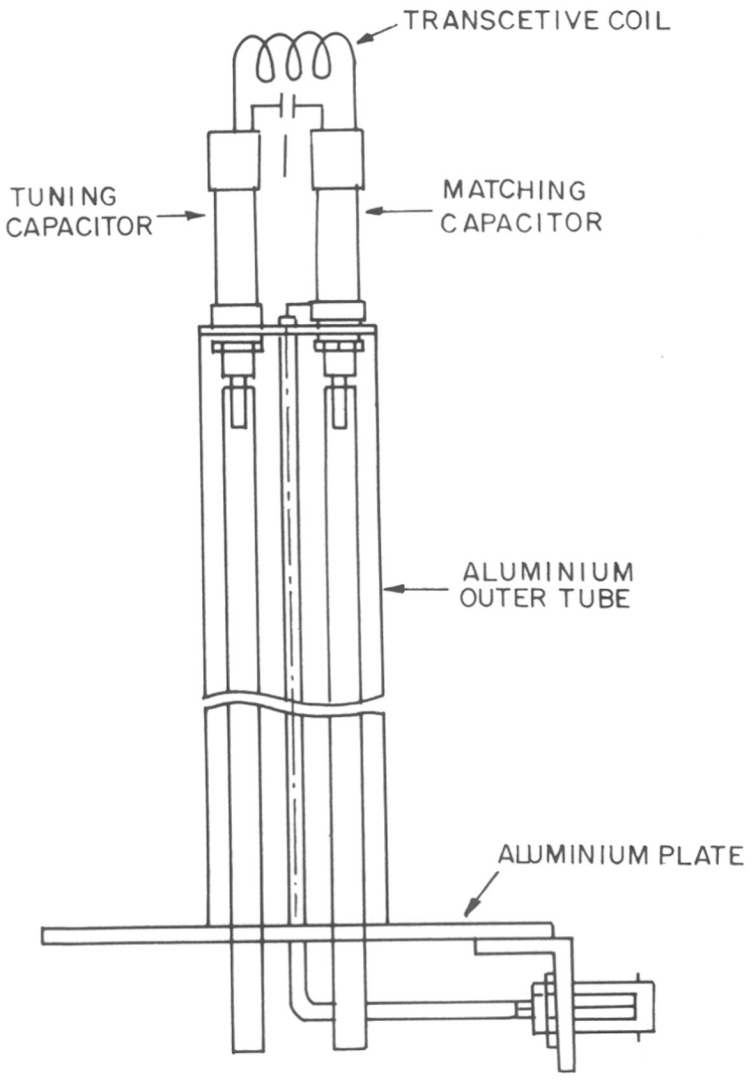

Figure 2.6: The circuit diagram of the home-build wide-line NMR probe

2.2.1.3 Shimming, Pulse Calibration, Data Collection and Referencing

The homogeneity of the magnetic field was adjusted by shimming on FIDs. For ^{1}H water taken in small 5 mm o.d NMR tubes of ~ 4 cm length, was used. The shim controls were adjusted so that the FID envelope was a single exponential with the longest possible decay time. A linewidth of the order of 20 Hz could easily be achieved for water, which was good enough for carrying out wide line experiments. This resolution was further improved in the CP/MAS probe due to sample spinning.

For the home-built probe the proton $\pi/2$ pulse width was calibrated using the high power mode and was found to be 1.9 μs on water. The $\pi/2$ pulse calibration for the ^{1}H and ^{13}C channels on the CP-MAS probe was done directly on the polymer gel and was typically 5 to 6 μs, depending upon the state of hydration of the polymer.

For proton wide line experiments, the FIDs were collected using a spectral width (SW) of either 500 kHz or 1 MHz using 1K real data points. In the 1D pulse sequences, the transmitter r.f and receiver phases were cycled using the CYCLOPS (CYCLically Ordered Phase Sequence) phase cycling scheme to get rid of the artifacts arising from amplitude and phase imbalance in the quadrature receiver and the d.c offset (Hoult 1978 & 1978). The CYCLOPS phase cycling is given below,

Tx ϕ)	+X	-Y	-X	+Y
R(ϕ)	+X	-Y	-X	+Y

The FIDs were zero filled to 2K/4K prior to Fourier transformation. The raw data were exponentially multiplied with varying line broadening (LB) of 5 Hz to 100 Hz, depending on the observed line widths. ^{13}C data were usually collected using a 125 kHz spectral window using 2K real data points. The raw data were exponentially multiplied (LB = 5 to 25 Hz) before Fourier transformation.

For referencing of ^{1}H spectra the proton resonance of water was used and its chemical shift taken as 4.8 ppm. For ^{13}C, chemical shifts were referenced with respect to the CH carbon of adamantine, which was taken as 37.8 ppm (from TMS).

For the imaging probe shimming was done on the water sample taken in a tube of ~ 14 mm diameter placed in the 15mm insert. The height of the tube was adjusted in such a way that the water is at the center of the RF coil.

2.2.2 CP-MAS Experiments: Hartmann-Hahn Matching and Magic Angle Setting

The cross-polarisation experiment was used in the two dimensional ^{13}C-^{1}H separation experiments. The basic ingredient of the CP sequence is,

R.F Channel H H,C H,R

Duration [D11------D5--------AQ-------Relaxation Delay------]$_{NS}$

Phase $\phi1$ $\phi2, \phi3$ $\phi4, \phi5$

Scan	1	2	3	4	5	6	7	8
$\phi1$(H)	+X	-X	+X	-X	+X	-X	+X	-X
$\phi2$(H)	-Y	-Y	-Y	-Y	-Y	-Y	-Y	-Y
$\phi3$(C)	+X	+X	-Y	-Y	-X	-X	+Y	+Y
$\phi4$(H)	-Y	-Y	-Y	-Y	-Y	-Y	-Y	-Y
$\phi5$(C)	+X	-X	-Y	+Y	-X	+X	+Y	-Y

where the 8 scan cycle incorporates the basic CYCLOPS cycle in conjunction with the spin-temperature alternation. The proton 90° pulse (D11) and the contact time (D5) are designated using Bruker MSL convention. The proton and carbon channels are designated by the letters H and C, respectively and R denotes the Receiver. The contact time D5 is optimally chosen to give the maximum CP signal.

Before setting up the 2-D experiment, the CP match conditions had to be established. Further, the magic angle had to be precisely set to get high-resolution spectra. For the ^{13}C cross-polarization experiment, the Hartmann-Hahn match condition (Hartmann-Hahn 1962) was adjusted using a spinning sample of adamantane. The spinning speed was kept ~ 1 kHz and a contact time of 5 msec was employed. The $^{13}C/^{1}H$ power levels were adjusted in such a way that the Hartmann-Hahn match condition was obtained at the r.f field strength of ~ 50 kHz which corresponds to a 90° pulse of 5 μsec. The proton decoupling was also maintained at ~ 50 kHz in most of the cases. The decoupling field strength was changed as per sample requirement. The line width of the admantane signals was found to be ~ 5 Hz. The same match condition was maintained for other solid state ^{13}C measurements. For the gels, especially the one hydrated to larger extent, the ^{1}H and ^{13}C tuning was found to be quite different. In these cases, the match condition was established on the sample itself in the following way. The proton decoupled ^{13}C Bloch-decay signal was directly observed and the power of X channel was adjusted to get a ^{13}C $\pi/2$ pulse of ~ 6 μsec. In a similar way, the power level on the F2 channel was adjusted to get the same $\pi/2$ pulse on protons of the same gel sample. In this case, the F2 channel was usually routed through the preamplifier in order to maintain the observed $\pi/2$ pulse conditions. Subsequent to these adjustments, the Hartmann-Hanh condition was checked using the cross-polarisation pulse sequence and further optimised directly on the gel sample.

Since the removal of chemical shielding anisotropy is important for high resolution ^{13}C observation in the polymer systems studied, the magic angle had to be set precisely and checked periodically. The magic angle (54.7°) could be accurately set by monitoring the rotational echoes of the quadrupolar satellite transitions of ^{79}Br nucleus (I = 3/2) (ν_0= 75.16 MHz) in a spinning sample of KBr (Frye and Macial 1982). The carrier frequency was adjusted to be on-resonance with the central transition and angle was adjusted to get maximum number of rotational echoes.

The samples were packed tightly in 7 mm zirconia rotor and normally spun at a speed of 1.5 to 4 kHz. The data were collected using a 125 kHz spectral window. For the CP-MAS experiments, a relaxation delay of 500 msec to 4 sec was used depending on the nature of the compound. The number of accumulations were usually in the range of 400 to 4000, depending upon the hydration level and the amount of gel that could be packed into the rotor.

2.2.3 Imaging Experiments

The proton imaging experiments were also performed on the Bruker MSL-300 FT NMR spectrometer, using the micro imaging accessory described in section 2.2.1.2. The image acquisition was carried out using the spin-echo technique (Callahan 1991). Further experimental details of the imaging experiments are provided in Chapter VI.

2.2.4 Variable Temperature Experiments

The variable temperature measurements were carried out in the Bruker CP/MAS NMR probe. The temperature was regulated by means of Bruker BVT-1000 unit where the temperature settings can be done in 1 K steps. Heat exchange is effected by gas flow. The temperature is monitored with a copper-constantan thermocouple located very close to the sample tube and is controlled by a regulated heater in the probe arm. For temperatures above room temperature, compressed dry air is used. The air-flow is regulated by means of a flow rate valve located in the BVT 1000 unit. The temperature was varied from 295K to 314K. An independent temperature calibration of the micro imaging probe was carried out using a copper-constantan thermo-couple and temperature measurement directly on the sample.

2.2.5 Deconvolution of 1-D and 2-D NMR Spectra

In the wide-line proton NMR studies, it was necessary to deconvolute the overlapping resonances of the polymer and water. The Bruker utility software LINESIM was used. A Gaussian, Lorentzian or a mixed Gaussian-Lorentzian line shape could be suitably chosen for the deconvolution of various spectra recorded on different polymer-water system at different hydration levels.

2.2.6 TWO-DIMENSIONAL NMR EXPERIMENTS

One of the major developments in field of pulse FT-NMR spectroscopy was the introduction of two dimensional pulse techniques (Ernst *et al* 1987). The 2-D technique involves the detection of the NMR signal as a function of two time variables so that a double Fourier-transform operation spreads the information content of the spectrum in a frequency plane spanned by two orthogonal dimensions. The basic scheme of 2-D NMR is sketched in Figure 2.7. The experimented is segmented by four periods, namely, preparation, evolution, mixing and detection. The evolution and detection periods are conventionally denoted by t_1 and t_2, respectively.

Figure 2.7: Schematic of the basic 2-D NMR scheme

The preparation period generally consists of a relaxation delay to bring the spin system to thermal equilibrium followed by a pulse scheme to take the spin system to some well-defined initial state. This usually corresponds to the creation of transverse magnetization using a non-selective 90° pulse. During the subsequent evolution period the spin system evolves under the desired spin interaction(s), judiciously designed for the requirement. In some experiments there is mixing period consisting of pulses and time delays to relate the evolution to the detection period during which signal is detected. Thus

the experiment is performed for a certain t_1 value and the time domain signal is recorded as a function of t_2. A sequential incrementation of t_1 from experiment to experiment and accumulation of the FID signal at each t_1 generates the 2-D data matrix $S(t_1, t_2)$, which upon double Fourier-transformation leads to a two dimensional frequency spectrum $S(\nu_1, \nu_2)$ which can be obtained through the mathematical relationship

$$S(\nu_1, \nu_2) = \int_0^\infty \int_0^\infty S(t_1, t_2)\, D(\nu_1, \nu_2) e^{-ivt1}\, e^{-iv2t2}\, dt_1 dt_2 \qquad (2.3)$$

In the present thesis, 2-D NMR techniques have been combined with Magic Angle Spinning to study the dynamic response of HSPAN and PNIPAm gels. The high resolution provided by MAS on the proton spectra allowed to combine MAS with 2-D NOESY technique and study of polymer-polymer and polymer-water interactions in HSPAN gels. The ^{13}C CP-MAS experiment was used in a 2-D sense to provide a heteronuclear correlation. Since these experiment were exclusively used for the studies, which are outlined and discussed in Chapter IV, the experimental aspects pertaining to the pulse sequence description and phase-cycling schemes are presented in Chapter IV.

2.2.6.1 2-D Data processing

For the processing of 2-D data in the pure-phase absorption mode, the very first time domain serial file was Fourier transformed and phased to get an pure absorption spectrum after multiplying by proper window functions in both the dimensions. The zero order and first order constants (PH0 and PH1) were memorized. The TPPI data processing scheme takes this phase information while processing of the 2-D data set to give a pure absorption line shape in both the F_1 and F_2 dimensions.

2.2.7 Computational Techniques Used

2.2.7.1 Molecular Modeling and Molecular Dynamics Techniques

Molecular modeling and Molecular Dynamics (MD) technique have been used to study the polymer-water interactions. The software packages like InsightII, Discover, Polymerizer, Builder, etc., (Biosym/MSI, Inc., USA, version 95) were used for these studies. The Molecular Modeling and MD calculations were performed on the Silicon Graphics Indigo^2 Extreme.

2.2.8 References

Brandrup, J. and Immergut, E.H., Polymer Handbook, Interscience Publishers, (1966).

Bronnimann, C.E., Hawkins, B.L., Zhang, M. and Maciel, G.E., Anal. Chem., **60**, 1743, (1988).

Butler, K., Thomas, P.R. and Tyler, G. J., J. Polym. Sci., **48**, 357, (1960)

Callahan, P.T., Principles of Nuclear Magnetic Resonance Microscopy, Oxford University Press, Oxford, (1991).

Ernst, R.R, Bodenhausen, G., and Wokaun, A., Principles of Nuclear Magnetic Resonance in one and two Dimensions, Clarendon, Oxford, (1987).

Forbes, J., Husted , C. and Oldfield, E., J. Am. Chem. Soc., **110**, 1059, (1988).

Frye, J.S. and Macial, G.E., J. Magn. Reson., 48, 125, (1982).

Fukushima, E. and Roeder, S.B.W., Experimental Pulse NMR: A Nuts and Bolts Approach, Addition-Wesley Publishing Company, Inc., Massachusetts, USA, (1981).

Ganapathy, S., Badiger, M.V., Rajamohanan, P.R. and Mashelkar, R.A. Macromolecules, **22**, 2023, (1989).

Ganapathy, S., Rajamohanan, P.R., Badiger, M.V. and Mashelkar, R.A. New Polymeric Materials, **2**, 205, (1990).

Hartmann, S., R., Hahn, E.L., Phys. Rev. **128**, 2042, (1962).

Harris, R.K., Jackson, P., Merwin, L.H., Say, B.J. and Hagde, G., J. Chem. Soc., Faraday 1, **84**, 3649, (1988).

Hoult, D. I., "Nuclear Magnetic Resonance: Specialist Periodical Report", The Chemical Society, Ch. 7, London, (1978).

Hoult, D. I., "Progress in NMR Spectroscopy" **12**, Pergamon, Oxford, (1978).

Klein, J. and Conrad, K.D., Makromol. Chem., **181**, 227, (1980).

Kulicke, W.M., Kniewske, R. and Klein, J., Prog. Polymer Sci., **8**, 373, (1982).

Mansfield, P. J. Phys. C, **4**, 1444, (1971).

Mathew, B. and Pillai, R., Polymer International, **28**, 201, (1992).

Notani, P., M.Sc.Thesis, Pune University, (1990).

Perrin, D.D., Armarego, W.I.F. and Perrin, D.R., Purification of Laboratory Chemicals, 2nd edn., Pergamon Press, London, (1981).

Rajamohanan, P.R., Badiger, M.V., Ganapathy, S. and Mashelkar R.A, Macromolecules, **24**, 1423, (1991).

Rhim, W.K., Elleman, D.D. and Vaughan, R.W., J.Chem. Phys., **59**, 3740, (1973).

Sandler, S.R. and Karo, W., Polymer Synthesis II, Academic, New York, 271, (1977)

Schild, H.G. Prog. Polym. Sci.,**17**, 163, (1992).

Slichter, C.P. Principles of Magnetic Resonance, Springer Series in Solid-State Sciences 1, Ch. 8, pp367, Springer-Verlag (1989).

Tanaka, T., Fillmore, D., Nishio, I., Sun, S-T. Shah, A, and Swislow, G., Phys. Rev. Lett., **45**, 1636, (1980).

Waugh, J.S., Huber, L. and Haeberlen, U., Phys. Rev. Lett., **20**, 180, (1968).

Chapter III

NMR and Mobility Transition in Polymers

3. Introduction

Macromolecular hydration in synthetic and natural macromolecules has been a subject of considerable interest for many years. The amount and nature of water plays a critical role in determining number of the mechanical and chemical properties of synthetic polymers and many biological functions in biologically important macromolecules (Rupley & Careri 1991, Bryant 1988 and Rowland 1980). For example, the nature of water-macromolecule interactions has been recognized as one of the major determinant factors controlling chain folding, conformational stability, substrate binding, enzymatic activity etc., in many biological systems. Water is known to exist in different states *viz.* bound, interfacial and free, in the macromolecule swollen/dissolved in water system (Wǫessner and Snowden 1970 & Foster *et al* 1976). Many of the thermodynamic and chemical properties of the proteins and nucleic acids are known to undergo sudden changes at very low hydration levels. There has been a considerable discussion in literature about many aspects of protein hydration (Rupley & Careri 1991, England 1974 and Berendsen 1975).

The water-macromolecular interaction can be studied by a multitude of experimental techniques (Pessen & Kumosinski 1985). Among the different spectroscopic techniques, NMR has emerged as a powerful tool to study water-polymer interactions (Kuntz *et al* 1969, Fung 1986, Bahneider *et al* 1985). Multi-nuclear and multi-dimensional NMR has provides in depth knowledge about the interactions at the molecular level between water and specific sites in macromolecular systems. Many aspects of macromolecular hydration are not very well understood in spite of a number of studies. Solid state NMR techniques such as ^{13}C CP-MAS can be employed in less hydrated macromolecular systems (Ganapathy *et al* 1990). Though these techniques provide considerable sites specificity it suffers from lack of sensitivity at natural abundance. Proton NMR offers a very high sensitivity though spectral selectivity is less. Due to this unique characteristic, proton NMR spectroscopy has become a powerful tool in the study of hydrated synthetic and biopolymers.

Polymeric materials in solid state are hard to characterize by proton magnetic resonance owing to the inherently large spectral line broadening, which arises from static dipole-dipole interactions among the abundant proton spins as discussed in Chapter I (Section 1.2.2) (also see Abragam 1989 and McBriety 1974). The proton NMR gives a featureless broad line spectrum with a line width of approximately 50-60 kHz. This line broadening is so large that it obsures fine spectral features such as the chemical shifts and coupling constants and renders the study of polymeric system difficult. It is known that macromolecular mobility can cause a motional averaging of static proton dipolar interactions and reduce the observed proton spectral line width (Ganapathy *et al* 1989). The extent of proton line narrowing, however, depends on the exact nature of the polymer mobility. Unless the polymer motions are isotropic, or nearly so, the dipolar couplings can not be averaged to zero, and therefore, fine resolution of polymer structure can not be revealed.

It is also well known that the addition of solvent or plasticiser to a polymer enhances the polymer mobility (Ford & Balakrishanan 1981, Blum *et al* 1984, Jelinski *et al* 1985 and Ganapathy *et al* 1986). The details of the polymer motions and dynamics depend on the specific nature and extent of polymer-solvent interactions and this in essence determines the observed residual proton spectral line width. In cross-linked polymers, the degree of cross-linking determines the equilibrium swelling capacity of the polymer in suitable solvents. The extent of chain mobility depends upon the degree of cross-linking and the type of the solvent used. This has been shown to cause proton line narrowing in cross-linked poly(styrene) by Bahneider *et al* (1985) and Badiger (1988).

Ganapathy *et al* (1989) has demonstrated that the high-resolution solid state NMR can be used to study the proton NMR of superabsorbing hydrogels namely, HSPAN in the gel state. They have shown that even at very low concentration of water (0.2% saturation ~ 0.34g/g), the static proton spectrum at room temperature is quite narrow and exhibits a near super-Lorentzian line shape due to extensive motional averaging of static proton dipolar interactions. They have also shown that the residual line width, approx. 2.1 kHz can be

further narrowed by using magic angle sample spinning (MAS) technique. The process of preferential hydration in the HSPAN hydrogel has been demonstrated by Rajamohanan *et al* (1991) using solid state ^{13}C NMR. They shown that the change in the line shapes occurs when a given site is hydrated and this can be used to study and fit a model for the hydration-induced dynamics.

Polymeric hydrogels are three-dimensional cross-linked networks swollen in water. They possess many interesting properties in the swollen state. Softness, elasticity, and capacity to store varying amounts of water within network make them unique materials. The phenomenon of discontinuous volume phase transition associated with some of these gels is one of the most fascinating and important aspects (Chapter I). The macroscopic volume phase transitions in these systems is brought about by very small change in some external stimuli (Shibayama and Tanaka 1993). The stimuli responsive behavior of these polymers made them an important class of compounds having a variety of technological applications in different fields (De Rossi *et al* 1991, Harland & Purd'homme 1992). The microscopic molecular level interactions associated with some of these macroscopic transitions have been probed recently using different spectroscopic techniques (Ganapathy *et al* 1989 & 1995, Dong and Hoffman 1990, Hoffman 1995 , Tokuhiro *et al* 1991, Badiger *et al* 1991 & Rajamohanan *et al* 1994).

Most of the studies reported indicate that the volume phase transition in responsive gels occurs at the higher level of hydration or in the equillibrium swollen state. There is no report in the literature regarding the phase transition and dynamics of the hydrogel-water systems at very low levels of hydration. However, we report here some unusual microscopic transitions brought about by water itself at levels of hydration far away from the equilibrium swollen state using proton NMR spectroscopy. We proposed to call this "mobility transition" as it is directly related to the motional properties of the polymer network system. This is different from the macroscopic volume phase transitions observed. The mobility transition has been shown to be rather general in nature for different macromolecular systems.

3.1 Experimental work

3.1.1 Synthesis of polymers and polymeric gels

The polymeric systems, like linear poly(acrylamide) (PAM) of different molecular weights and alkaline hydrolysed, crosslinked PAM gels, partially hydrolysed PAM gels, HSPAN, PNIPAm and gelatinized starch were prepared as given in the Chapter II.

3.1.2 Sample Preparation for NMR experiments

The finely powdered polymers were dried at 120°C for two to three hours and stored in a decicator containing P_2O_5. 50 mg of dried sample was weighed accurately and was allowed to hydrate in a 100% relative humidity chamber containing 99.8% D_2O at different length of time. The amount of D_2O taken up by the sample was estimated gravimetrically. The samples of higher hydration levels were made by addition of the required amount of D_2O to 50 mg of dried sample using micropipette. These samples were kept overnight for equilibration, before starting the measurements. The hydrated samples were transferred in to a small glass tube (7 mm, o. d. and 2.5 cm, length).

3.1.3 NMR Measurements

The ^1H static NMR measurements were made on a Bruker MSL-300 FT-NMR spectrometer operating at 300.13 MHz for proton, using a home built probe as discussed in experimental aspects of NMR part of Chapter II section 2.2.1.2 and 2.2.1.3.

3.2 Results and discussion

Although Proton NMR spectroscopy provide very high sensitivity in the study of water - macromolecular systems, at higher levels of hydration the proton NMR is dominated by the bulk water signal which obscure the macromolecular signals. To reduce contribution

from water signal in the observed proton NMR spectrum we used 99.8% D_2O for hydrating the polymer so that we can directly monitor at the polymer proton signal as a function of hydration.

Proton static spectra obtained for linear poly(acrylamide) (PAM) of molecular weight ~ 2×10^6 as a function of hydration is shown in the Figure 3.1 (A-H). The hydration levels (g of water/g of dry polymer) are shown against each spectrum. The expanded spectra of G and H are also shown in the Figure 3.1. The measured ^1H line width data obtained at each hydration level (by deconvoluting the spectra presented in Figure 3.1) are given in the Table 3.1 (Appendix I).

A plot of the line width data given in Table 3.1(Appendix I) against the hydration levels is presented in Figure 3.2. This figure clearly shows three distinct regions:

I) A region spreading from 0.0 g/g to 0.3 g/g levels of hydration where the static proton line widths are not affected much as a function of hydration

II) The region where the proton line widths undergoes a drastic change (0.3 g/g - 0.6 g/g)

and

III) A region (0.6 g/g onwards) where the line widths are practically invariant.

The proton line width of dry polymer powder of the linear PAM is the order of 52 - 55 kHz and this gaussian line is characteristic of dipolar coupled rigid lattice systems. As the polymer is hydrated the line width show a slow and gradual decrease. For example, the line width observed at a hydration of 0.32 g/g is ≈ 40 kHz (region I). Further increase in hydration lead to a sudden narrowing of the line. At a hydration of 0.5 g/g the line width reduced to ≈13.5 kHz and at 0.7 g/g, its reduces further to ≈ 1 kHz (region II). On hydrating further the line width decreases once again very slowly (region III).

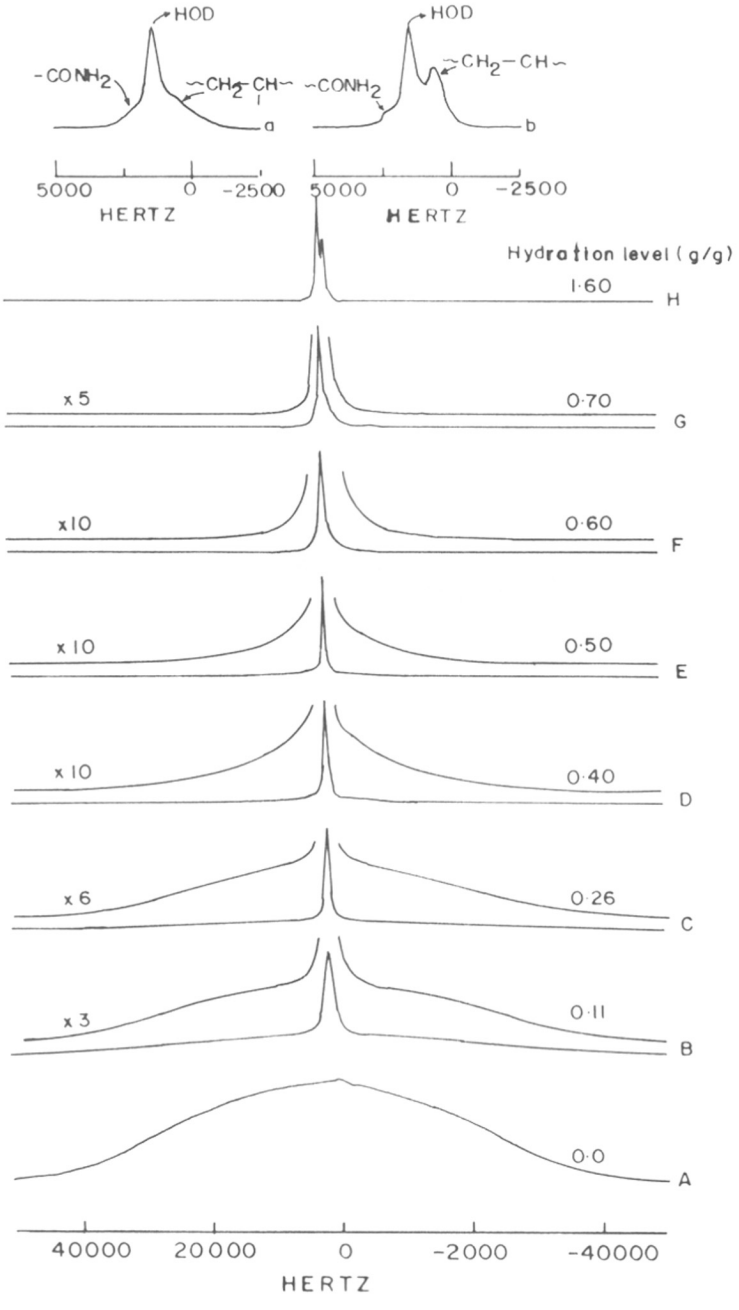

Figure 3.1: Proton static spectra of linear poly(acrylamide) (MW = 2.0 x 10^6) as a function of hydration (A-H). The hydration levels (g of water /g of polymer) are shown against each spectrum. (a) and (b) are the expanded spectra of (G) and (H), respectively.

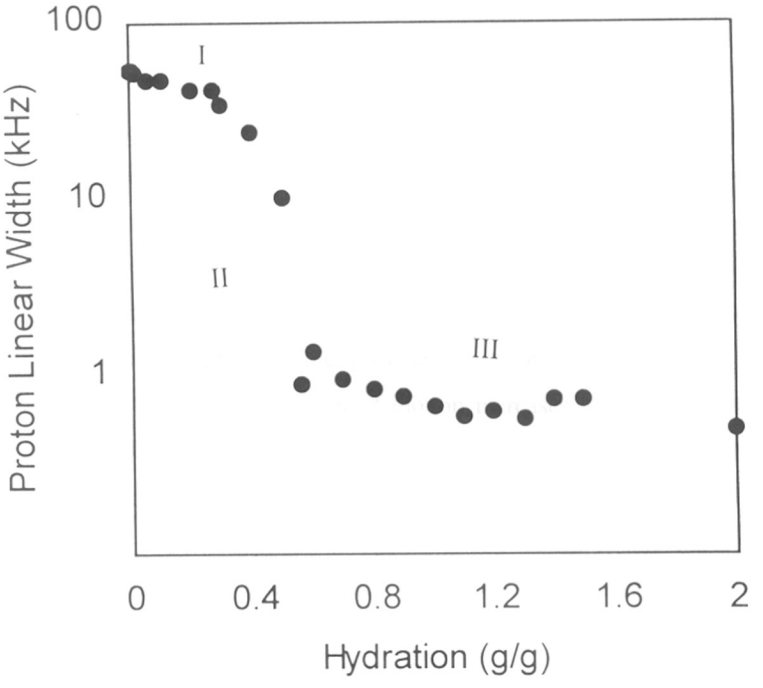

Figure 3.2: Variation in proton line width measured at half intensity points as function of hydration (g/g) for linear PAM (MW = 2.0 x 10^6)

In case of this linear PAM one can envisage the occurrence of the following processes as the rigid dry segments come into contact with water molecules. The initial site of hydration will be the amide functionalities. It is likely that this bonded water will be shared between the neighboring segments. This is the process that takes place in the region- I. It is known that in solutions the amide function can be associated with many water molecules. The oxygen atom of the carbonyl site can act as hydrogen bond donor for at least two water molecules and each proton of the $-NH_2$ group can be an acceptor for the two water molecules. In the initial stages of hydration with which we are concerned, this many water molecules are unlikely to be associated with each of the amide group. It is well known that water plasticizes the polymer segments during the process of hydration. Hence, as more and more water comes in, the polymer segmental motions will be correspondingly enhanced. As the polymer segmental motion increases the static proton - proton dipolar interactions, which governs the line broadening, will be considerably reduced and this leads to the observed narrowing of the polymer lines (Badiger *et al* 1991). The static proton spectra of the polymer seem to undergo a sudden change in line width in the 0.3 - 0.6 g/g hydration levels and the relative change in line width is negligible at higher hydrations. This implies that only a small amount of water (~ 0.5 g/g) is required for the polymer segmental motions which are rapid enough to average the proton-proton dipolar interactions. This amount of water is very close to the, so-called bound water limit. In analogy with the protein hydration, one can consider this as the amount of water, required to form the monolayer coverage of the polymer segments. In proteins it is well known that many thermodynamic parameters show a sudden change at 0.2-0.3 g/g hydration levels where the initial sites of binding is considered as the charged groups followed by other polar groups and weakly polar regions (Rupley & Careri 1991).

Normally the "hydration end points" observed for proteins are less than the one observed for the linear PAM system. The most likely reason for this is the lack of ionic functional groups in PAM case. In order to check the effect of ionic group in the mobility transition we have carried out the static proton NMR line width measurements for alkaline

hydrolyzed poly(acrylamide) system. Increasing amounts of carboxylate moieties have been introduced by varying the extent of hydrolysis period. The results are shown in Figure 3.3. The measured ^1H line widths are given in the Table 3.2 and 3.3 (Appendix I). It has been observed that the mobility transition indeed took place at earlier hydration levels as the extent of hydrolysis increased. For example in case of 40 % alkaline hydrolyzed sample, the mobility transition was found to occur at 0.40 – 0.5 g/g compared to the value of 0.50 – 0.55 g/g for 10% alkaline hydrolyzed sample.

We have also observed the similar kind of the mobility transition in linear PAM with different molecular weights. These results are shown in Figure 3.4 (a, b, c). The measured ^1H line width for the different molecular weights (MW = 3.84×10^5 & 8.4×10^4) of linear PAM and hydration data for each sample are given in the Table 3.4 and 3.5 respectively (Appendix I). Here we have observed that mobility transition is independent of the molecular weight but it depends on the degree of the hydrolysis and more stiffer and took place at earlier hydration levels as the extent of the hydrolysis increased.

As no chemical cross-links are present in this linear polymer, only physical entanglements will impose some restriction to the mobility of polymer chains. The first water (0.0-0.25 g/g) added interacts with the amide functionality of this polymer, hydrating the –C=O and the NH_2 sites. At 0.25 g/g, this corresponds to approximately one water molecule per repeat unit. The precise nature of hydration events that take place at this level is not clear, although it has been suggested by quantum mechanical calculations (Scheiner and Wang 1993) that the carbonyl site is preferred by water compared to amine sites. Further hydration (0.25 - 0.6 g/g) is thought to cause a breakage of physical entanglements, leading to a completion of the first hydration layer.

The hydrated water is considered as the strongly bound non-freezable water, which exhibits anisotropic motional properties (Ganapathy *et al* 1995, Shirley & Bryant 1982). The dynamic properties of the polymer, as sensed by proton line width data, show a dramatic

(a)

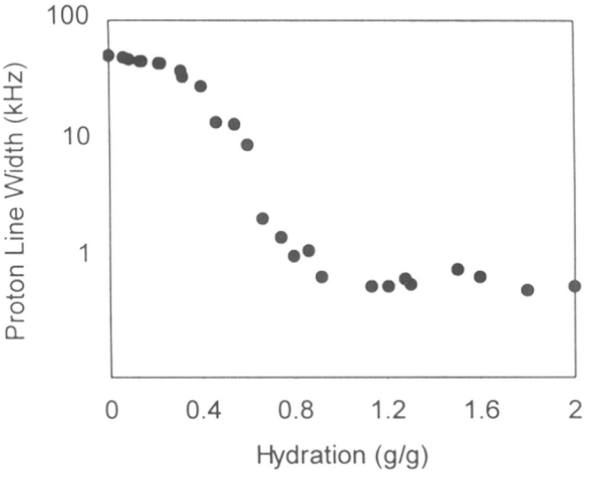

(b)

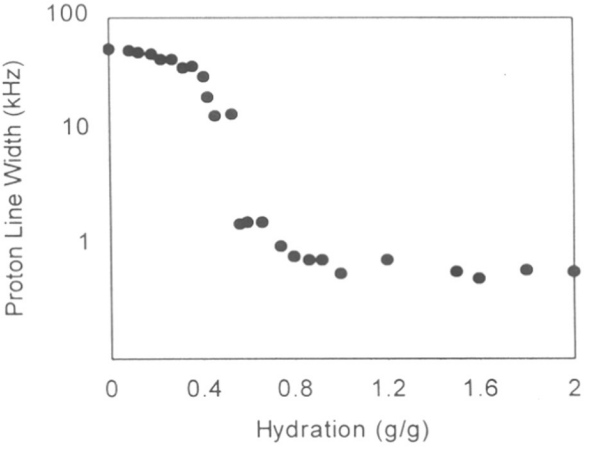

Figure 3.3: Effect of Hydrolysis on mobility transition of linear PAM. Variation in proton line width measured at half intensity points as function of hydration (g/g) for (a) 10% alkaline hydrolysed PAM and (b) 40% alkaline hydrolysed PAM

(a)

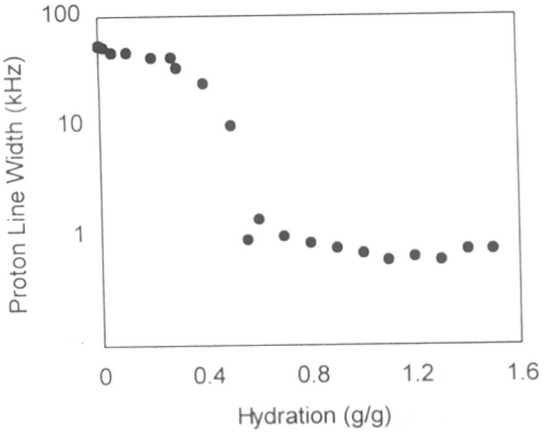

(b)

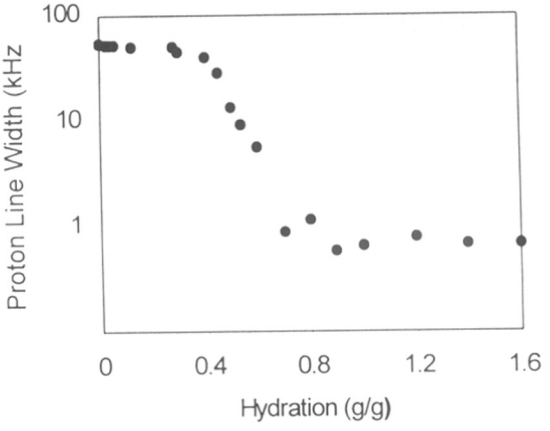

(c)

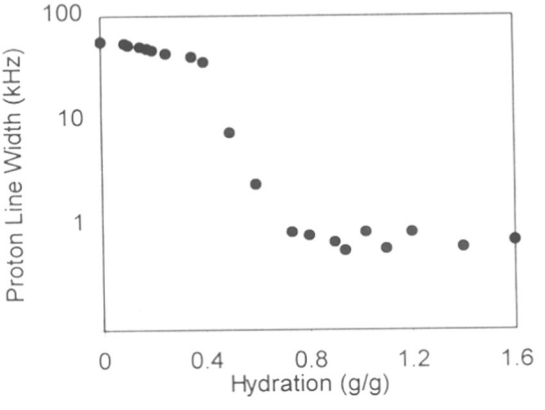

Figure 3.4: Effect of molecular weight on mobility transition of linear PAM.
Variation in proton line width measured at Half intensity points as function of hydration (g/g) for three different weight average molecular weights linear PAM. (a) 2.0×10^6 MW (b) 3.84×10^5 MW (c) 8.4×10^4 MW

change in this region. When hydration is further increased beyond 0.6 g/g, water is loosely bound to the polymer and highly mobile local structures ensue.

Similarly, we have also observed mobility transition in the 2% cross-linked PAM gel. The proton line width change as a function of hydration is shown in Figure 3.5. The measured ^{1}H line width at each hydration level is given in the Table 3.6 (Appendix I). In 2% crosslinked PAM system the proton line width of dry polymer powder of is the order of 60-62 kHz. In order to check the effect of ionic group in the mobility transition we have also carried out the static ^{1}H NMR line width measurements for 2% cross-linked alkaline hydrolyzed PAM system. Increasing amounts of carboxylate moieties have been introduced by varying the extent of hydrolysis. The results are shown in Figure 3.6. The measured ^{1}H line width of corresponds to hydration is given in the Table 3.7, 3.8 and 3.9 (Appendix I). As in the case of linear PAM, the mobility transition is found to be hydrolysis dependent and indeed took place at earlier hydration levels as the extent of hydrolysis increased. For example in case of 30 days alkaline hydrolyzed sample, the mobility transition was found to occur at 0.20 – 0.25 g/g compared to the value of 0.40 – 0.42 g/g for 8 days alkaline hydrolyzed sample.

The mobility transitions were also observed in superabsorbing graft co-polymers *viz.* hydrolyzed starch-g-poly(acrylonitrile), (HSPAN) with various equilibrium swelling capacities (170, 100, 80 and 50 gm of water/gm of dry polymer). The results are summarized in Figure 3.7 (a) and Figure 3.7(b). The hydration and line width data are given in the Table 3.10 to 3.13 (Appendix I). As shown in the figure the proton line widths of dry polymer powders of HSPAN are in the order of 46 to 48 kHz. The line width observed at a hydration of 0.40 g/g is ≈ 25 kHz (region I). At a hydration of 0.5 g/g the line width reduced to ≈10.5 kHz and at 0.8 g/g, its reduces further to ≈ 1 kHz (region II). The mobility transition in HSPAN occur in the hydration range 0.5 to 0.7 g/g. The transition region show only a marginal change with increasing in the extent of hydrolysis.

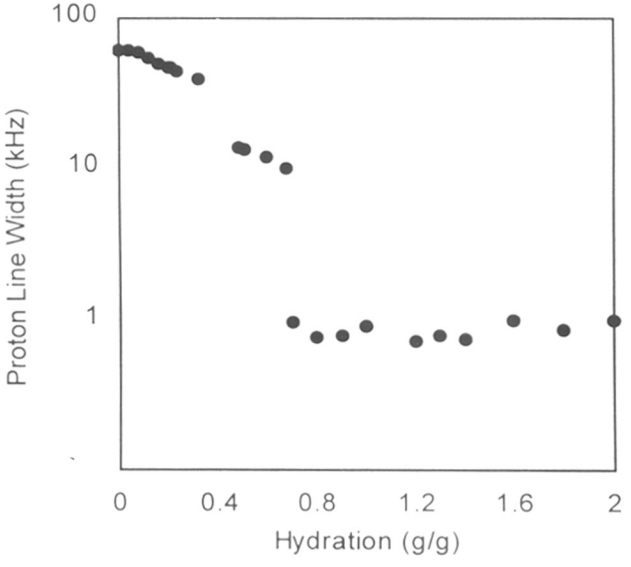

Figure 3.5: Variation in proton line width measured as function of hydration (g/g) for 2% crosslinked PAM

(a)

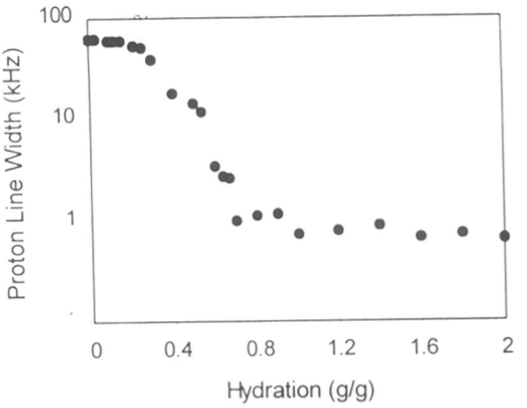

(b)

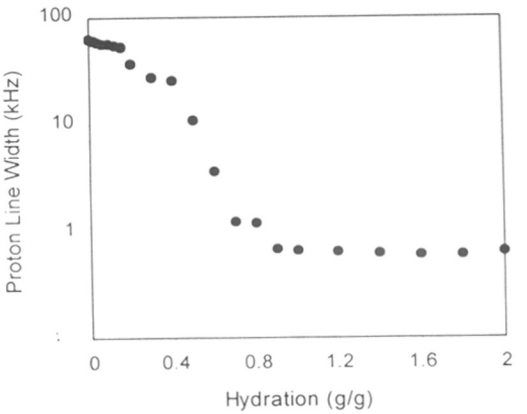

(c)

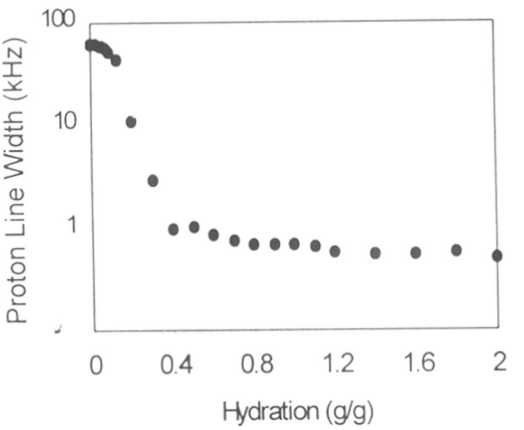

Figure 3.6: Effect of hydrolysis on mobility transition of 2% crosslinked PAM. Variation in proton line width measured as function of hydration (g/g) for (a)Two days (b) Eight Days and (c) Thirty Days alkaline hydrolysed 2% crosslinked PAM.

(a)

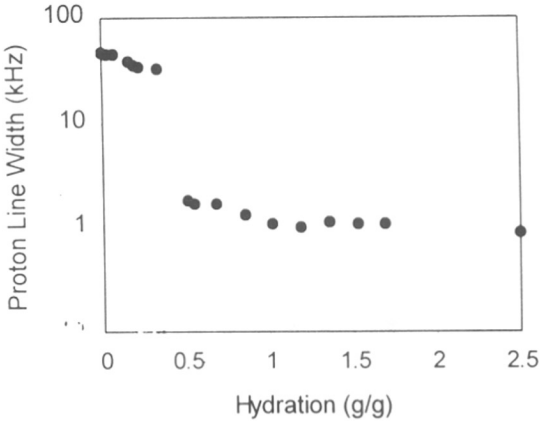

(b)

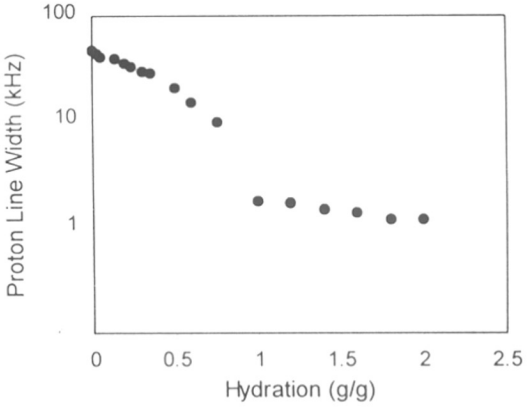

Figure 3.7(a): Mobility transition in superabsorbing HSPAN.
Variation in proton line width measured at half intensity points as function of hydration (g/g) for HSPAN (a) 170 g/g water capacity (b) 100 g/g water capacity

(c)

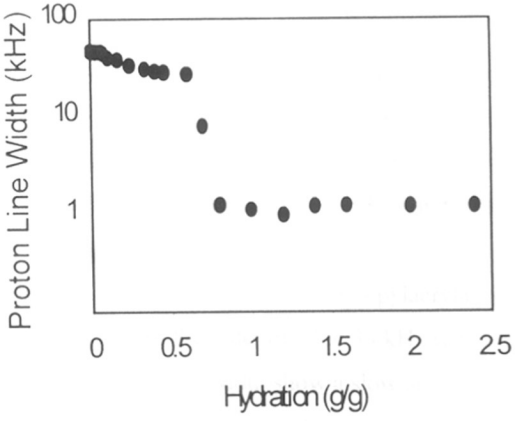

(d)

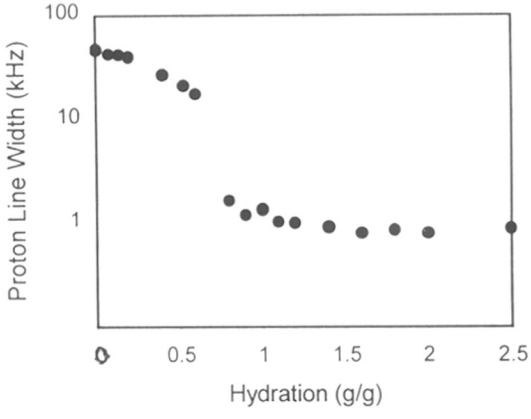

Figure 3.7(b): Mobility transition in superabsorbing HSPAN
Variation in proton line width measured at half intensity points as function of hydration (g/g) for HSPAN
(c) 80 g/g water capacity and (d) 50 g/g water capacity

This is probably due to the fact that the relative amount of the carboxylate units introduced will not be appreciable compared to the total amount of the polar groups present in the system.

Similar observations also seen in other polymeric system such as, thermo-reversible *viz.* poly(*N*-isopropylacrylamide) and commercial superabsorber namely, SANWET. The data is shown in Figure 3.8 and 3.9, respectively. The hydration levels and the corresponding line width data is given in the Table 3.14 and 3.15, respectively (Appendix I).

In case of the LCST polymer, poly(*N*-isopropylacrylamide) the proton line width of dry polymer powder of gel is of the order of 32 to 33 kHz with a gaussian type of line shape. As the polymer is hydrated the line width show a slow and gradual decrease. The line width observed at a hydration of 0.30 g/g is ≈ 3 kHz (region I). At a hydration of 0.4 g/g the line width reduced to ≈1.5 kHz and at and above 0.5 g/g, its reduces further below one kHz (region II). On hydrating further the line width decreases once again very slowly (region III). It is interesting to note that the mobility transition hydration level of ~ 0.4 g/g measured by NMR in the present work corresponds very closely to the bound water content in the collapsed PNIPAm gel as shown by the other research groups (Dong and Hoffman 1990).

We have also carried out hydration dependant studies on maize starch. The maize starch used for the synthesis of HSPAN, being crystalline, could not take up enough water. Hence, the mobility transition could not be demonstrated in this system. It is well known that crystalline starch on gelatinization become more amorphous in nature and can take up more amount of water. We have used dry gelatinized starch to study the effect of hydration and result is shown in Figure 3.10 and Table 3.16 (Appendix I). It is interesting to note that here the mobility transition is seen at a later stage (1.1 g/g).

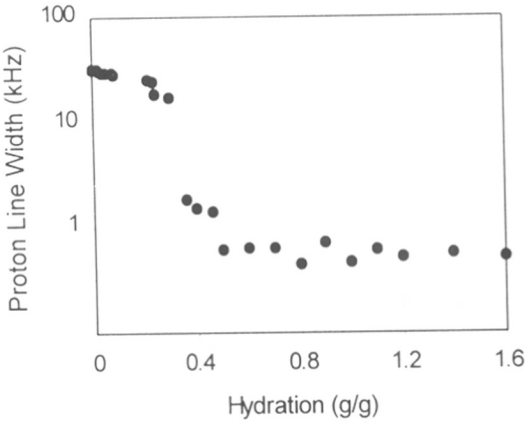

Figure 3.8: Variation in proton line width measured at half intensity points as function of hydration (g/g) for PNIPAm.

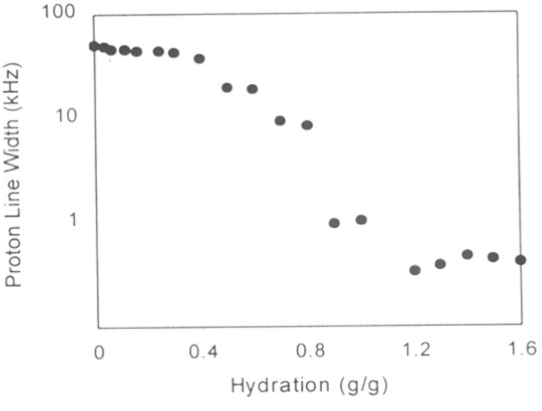

Figure 3.9: Variation in proton line width measured at half intensity points as function of hydration (g/g) for SANWET

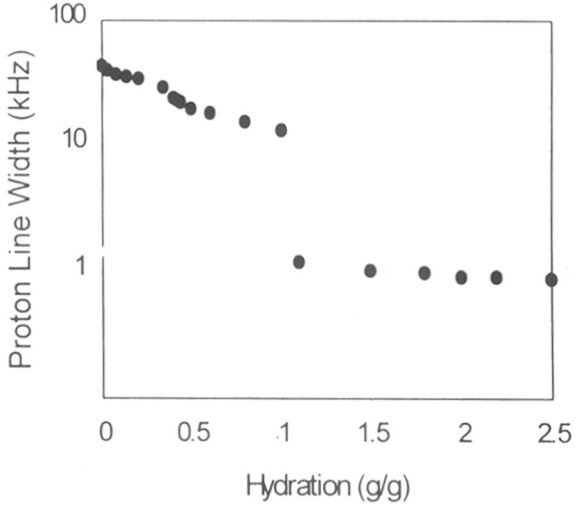

Figure 3.10: Variation in proton line width measured at half intensity points as function on hydration (g/g) for gelatinized starch

The reason for this is most likely the nature of polar groups (-OH) present in this system compared to the $-CONH_2$ and $-COO^-$ groups present in the other polymers studied here. In the HSPAN system studied here contains starch unit as the backbone. The presence of the pendant polyelectrolyte part shifts the mobility transition to the lower levels of hydration.

It is interesting to note in passing that the hydration levels at which the mobility transition observed could be correlated with the non-freezable bound water present in the polymeric systems. In many of the biological systems a universal range of 0.25- 0.4 g/g has been reported wherein many of its properties are changed. This range is normally mentioned as hydration end point and considered as the amount of water, required to form a monolayer type of coverage of macromolecular chains. The universality of this range is due to the similarity of the polar groups present in the systems. This implies that the point at which the mobility transition, take place can be considered as the non-freezable bound water limit in respective systems. At and above the bound water limits the polymer segments achieve a sudden enhancement in the segmental motions leading to an overall cooperative motion of the swollen polymeric system. This leads to an effective averaging of the proton-proton dipolar interactions and hence the line width of the polymer signals. It is important here to note that only small amount of water is sufficient to impart large scale motions at the microscopic segmental levels although the macroscopic manifestations are not large enough.

In nutshell, the following features can be generalized for the systems studied here. The polymer resonance starts off as a featureless Gaussian line at very early levels of hydration (< 0.4 g/g), transforming into super-Lorentzian and Lorentzian line of exceptional sharpness at high hydration levels (> 0.7 g/g). Fine chemical shift resolution is revealed at 1.0 g/g or more. We mainly focus our attention on the restricted hydration range of 0.45-0.65 g/g where strikingly visible line width changes, a transition, occurs. This discontinuous change in the proton line-width in the transition region flanked by limiting plateaus in the low and high hydration range. Despite the increased line narrowing that occurs in the high hydration range (0.65 - 2.0 g/g), the change in line width is not quite as large as in the main

transition region. We can therefore mark two plateau regions between which a "mobility transition" occurs. The plateau values of the line width are ~60-50 and ~1.0 kHz, respectively. A summary of the mobility transition is given in Table 3.17.

Table 3.17

Proton static NMR line width data for Various Polymers.

Sr. No.	POLYMER NAME	LINE WIDTH (kHz) REGION			MOBILITY TRANSITION RANGE (gm/gm)
		I	II	III	
1.	Linear PAM	62.00	13.00	01.00	0.35 – 0.50
2.	Crosslinked PAM	63.00	15.00	01.00	0.40 – 0.50
3.	HSPAN	48.00	14.00	01.00	0.50 – 0.70
4.	PNIPAm	33.00	17.00	01.00	0.30 – 0.35
5.	Gelatinized Starch	42.00	20.00	01.00	0.90 – 1.10
6.	SANWET	47.00	23.00	01.30	0.70 – 0.80

3.2.1 Mobility transition as a glass transition phenomenon

The complex behavior of a macromolecular-water system has at best been discussed only on qualitative terms by several investigators. Semi-empirical relationships have been invariably used to discuss the phenomenon, and no simple mathematical relationships that account for the more general nature of the observed polymer mobility have been used. An adequate description is one in which the addition of water is considered to lower the glass transition temperature (T_g) of the polymer system. The depression of T_g due to diluent addition and the enhancement of chain mobilities have been well documented in various polymer-diluent systems (Kelly & Bueche 1961). The quantity of interest for the local dynamics is the monomeric friction coefficient, which characteristics the resistance

encountered by a monomer unit moving through its surroundings. Initially, in the absence of water, the restriction to polymer mobility is the steric hindrance resulting in strong intramolecular potential barriers, which can be effectively overcome at elevated temperatures. For a dry polymer, such as PAM, these barriers hindering polymer mobility can be effectively overcome only at elevated temperatures (T>165°C). For the room temperature measurement, the polymer system is in the rigid lattice regime, giving rise to a dipolar broadened proton resonance of line width ~50 kHz.

The depression of T_g for a binary polymer-diluent system arises when the polymer and diluent are miscible at the molecular level. This is provided by the local interactions at the hydrophilic sites as discussed in the previous section. This miscible solvent water affects the segmental frictional coefficient, or the intrinsic viscosity of the system. It is appropriate to discuss chain movements in viscous aqueous environment at the polymer-water interface. The effect of water on glass transition temperature of hydrogels and the existence of non-freezable bound water have been reported (Nielson 1962, Willer 1966, Rault *et al* 1995 and Ratto *et al* 1995). The plasticization due to water causes a depression in the glass transition temperature of the binary polymer-water system. This is well documented in a variety of polymer-diluent systems. The effect of diluents on the T_g of the hydrated polymer is expressed by the Fox-Flory equation

$$(1/T_g) = (w_p / T_{gp}) + (w_w / T_{gw}) \qquad (3.1)$$

where, T_g, T_{gp} and T_{gw} are the glass transition temperatures for the polymer-water, polymer and water systems, respectively. w_w is the weight fraction of water and $w_l = 1 - w_p$. Using a value of 138 K for T_{gw} (Johari *et al* 1987) and 438 K for T_{gp} of PAM (Molyneux 1974 and 1984), the T_g of polymer-water system can be evaluated at each hydration level. This is shown in Figure 3.11. A linear variation in T_g, suggested earlier for other model polymers (Tan & Challa 1976, Miyoshi *et al* 1994), is visible only at very low water contents.

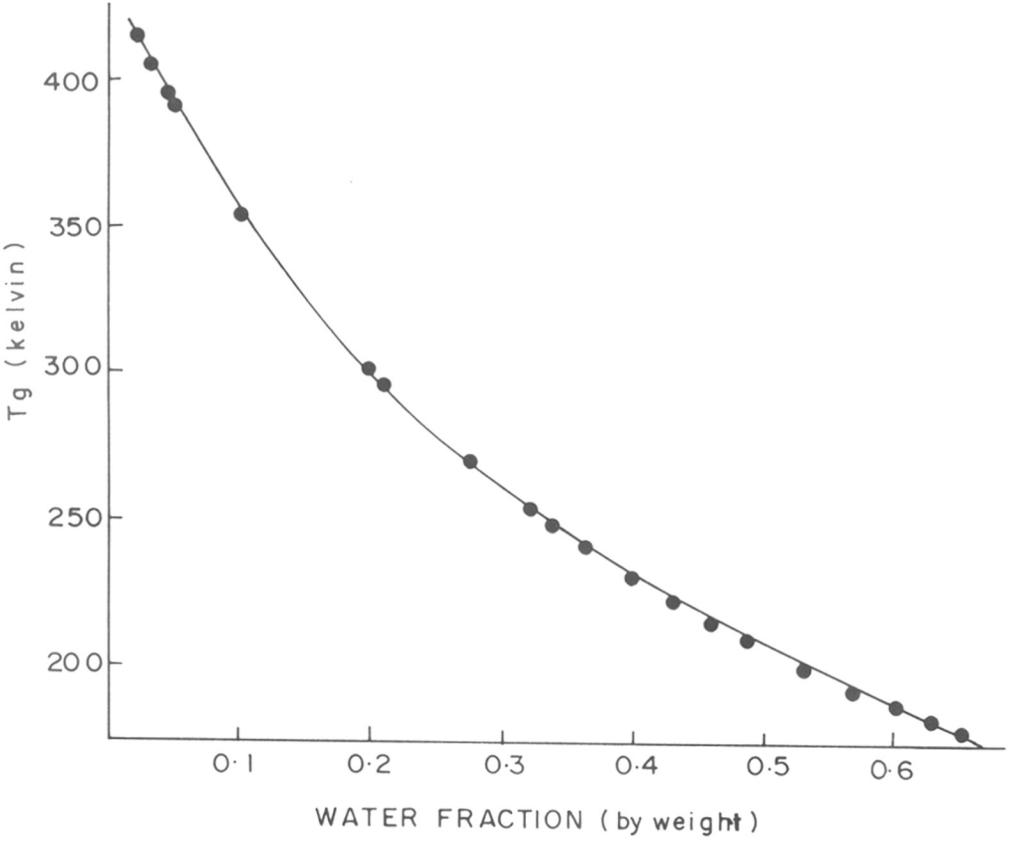

Figure 3.11: Variation in glass transition temperature (T_g) as function of water content of PAM-water system.

The above description therefore transforms the hydration zone spanned by the polymer into an equivalent temperature zone through the depression of T_g. The temperature of NMR measurement (295 K) is much lower than the T_g of the polymer so that the polymer system may consider to be annealed. The polymer segmental mobility is too slow and the validity ($\omega_o \tau_c >> 1$) holds. The cross over of the T_g to the room temperature mark occurs at a hydration level of 0.4 g/g and has a direct bearing on the onset of the mobility transition shown in Figure 3.1. The T_g at 0.6 g/g is 241 K and the polymer-water system has been pushed into the rubbery region where isotropic molecular motions effectively average proton-proton dipolar interactions to a very low value of proton line width of ~0.5 kHz.

Several interesting aspects of the observed mobility transition may be noted. The transition from a rigid lattice to a fluid like behavior occurs all in a very narrow hydration range. The observed phenomenon is also a single step process, which does not go through any intermediate motional modes. The motions are clearly, isotropic as otherwise hindered motions would leave the proton line widths at much larger values (~10-20 kHz) in the second plateau. There is also a correspondence between the mid-point of the transition and the hydration threshold for the bound water limit. For most of the synthetic and biopolymers, the functional groups that attract water have similar hydration numbers for the primary hydration shell and the bound water contents are uniformly similar at around 0.25-0.5 g/g in these systems. We have confirmed this by careful line width measurements as a function of hydration in a variety of polymer-water systems.

3.3 Concluding remarks

Mobility transition occurring in the very early levels of hydration has been detected and demonstrated for the first time in many polymer-water systems. Molecular mobility is shown to occur through an isotropic averaging process for the proton-proton dipolar interactions. The static proton NMR line-width measurement studies in polymers possessing hydrophilic groups such as $-CONH_2$, $-COO^-$, -OH etc, hydrated by 99.8% D_2O, exhibit a

mobility transition at very early levels of hydration (0.25-0.5 g/g). The mobility transition depends on the nature of hydrophilic groups present in the polymeric system. The presence of more polar functional groups shifts the mobility transition to a lower level of hydration. The hydration levels at which the mobility transition is seen corresponds most probably to the non-freezable bound water content in the systems studied. The mobility transitions are no way related to the phenomenon of macroscopic volume phase transitions of certain hydrogels. The present results contradicts with the scaling concepts theories developed for cases of high polymer concentrations and implies that this may not be valid and subtle and profound transitions may be actually taking place at the segmental mobility level. Our findings have implications in the use of such gels as reactive media, where molecular mobility and the amount of water are crucial in enhancing the reaction rates.

3.5 REFERENCES

Abragam, A., The Principles of Nuclear Magnetism, **32**, of International Series of Monographs on Physics, Clarendon Press, Oxford, (1989).

Badiger, M.V., Kulkarni, M.G., Rajamohanan, P.R., Ganapathy, S and Mashelkar, R. A. Macromolecules **24** , 106, (1991).

Badiger M.V., Ph.D. Thesis, Bombay University, (1988).

Bahneider, D., Doskocilova, D., Dybal, J. Polymer, **26**, 253, (1985).

Berendson, H.J.C., in: "Water. A Comprehensive Treatise", Franks, F. (Ed.), Vol.**5**, p.293, Plenum Press, New York (1975).

Blum, F.D., Dickson, J.E., Miller, W.G., J.Poly.Sci. Poly.Phy.Ed., **22**, 211, (1984).

Bryant, R.G., Stud. Phys. Theor. Chem, **38**, 683 (1988).

De Rossi, D., Kajiwara, K., Osada, Y. and Yamudin, A. (Eds.) "Polymer Gels; Fundamental and Biochemical Applications", Plenum Press, New York (1991).

Dong, L.C.; Hoffman, A.S. Proceedings of the International Symposium on Controlled Release of Bioactive Materials, Controlled Release Society, Inc. **17**, 116 (1990).

England, D. in Water : A comprehensive Treatise, Edited by Felix Franks Vol.**4**, Plenum Press, New York, 305, (1974).

Ford W.T. and Balkrishnan, T. Macromolecules, **14**, 284, (1981).

Foster, K.R., Resing, H.A., Garroway, A.N., Science, **194**, 324, (1976).

Fung, B.M., Methods in Enzymology, Parker L. Ed., Academic Press, New York, **127**, 151, (1986).

Ganapathy, S., Rajamohanan, P.R., Badiger, M.V., Mashelkar, R.A. New Polym. Mater., **2**, 205(1990).

Ganapathy, S., Rajamohanan, P.R., Ray, Siddarth S., Mandhare, A.B., Mashelkar, R.A. Macromolecules, **27**, 3432 (1994).

Ganapathy, S.; Badigar, M.V.; Rajamohanan, P.R and Mashelkar, R.A. Macromolecules, **22**, 2023, (1989).

Ganapathy, S., Ray, S.S., Rajamohanan, P.R. and Mashelkar, R.A. J. Chem. Phys., **103**, 6783, (1995) .

Ganapathy, S., Chacko , V.P. and Bryant, R.G., Macromolecules, **19**, 1021, (1986).

Hagler, A.T. in: "The peptides", J. Meienhofer (Ed.), Academic Press, NewYork, p.213 (1985).

Harland. R. S. and Purd'homme, R. K. (Eds.) "Polyelectrolyte Gels; Properties Preparations and Applications", ACS Symp.Ser. 480, Washington DC (1992).

Hoffman A.S., Macromol. Symp., **98**, 645, (1995).

Jelinski, L.W., Dumais, J.J., Cholli, A.L., Ellis, T.S., Sarasz, F.E., Macromolecules, **18**, 1091, (1985).

Johari, G. P., Hall Brucker, A., Mayer, E., Nature **330** 552 (1987).

Kelly, F.N. and Bueche, F., J. Polymer Sci., **50**, 549 (1961).

Kuntz, I.D.,Jr., Brassfield, T.S., Law, G.D., Purcell,G.V., Scicence, **163**, 1329 (1969).

McBriety,V. J. Polymer, **15**, 503, (1974).

Miyoshi, P., Takegoshi, K. and Hikichi, K., Polymer J., **26**, 485 (1994).

Molyneux, P., "Water soluble synthetic polymers" ; Properties and behaviour, " Vol **1** CRC press. p 84 (1984).

Molyneux, P., in: "Water. A Comprehensive Treatise", Franks, F. (Ed.), Vol.**4**, p.569, Plenum Press, New York (1974).

Nielson, L. E., "Mechanical Properties of Polymers " Reinhold NewYork p 21 (1962).

Pessen, H. and Kumosinski,T.V., Methods in Enzymology, Hirs, C.H.W., Timasheff, S.N., Eds. Academic Press, New York, Vol **117, 219** and References therein, (1985).

Rajmohanan, P.R., Badiger, M.V., Ganapathy,S., Mashelkar R.A., Macromolecules, **24**, 1423, (1991).

Rajmohanan, P.R., Badiger, M.V., Ganapathy,S., Mashelkar R.A., Macromolecules, **27**, 3432, (1994).

Ratto, J.A.; Hatakeyamma, T. and Blumstein R.B., Polymer, **36**, 2915 (1995).

Rault, J., Gref, R., Ping, Z.H., Najuyen, G.T. and Neel, J., Polymer, **36**, 1655 (1995).

Rowland, S.P "Water in Polymers", Rowland, S.P. (Ed.) ACS Symp. Series, 127 , American Chemical Society, Washington,D.C (1980).

Rupley, J.A. and Careri, G., Adv. Protein Chem., Anfinsen, C.B., Edsall, J.T., Richards, F.M. and Eisenberg, D.S., (Eds.), 41, 38, Academic Press, New york (1991).

Scheiner, S. and Wang, L., J. Am. Chem. Soc., **115**, 1958, (1993).

Shibayama, M. and Tanaka, T., Advances in Polymer Science, **109**, 1, (1993).

Shirley, W.M. and Bryant, R.G., J. Am. Chem. Soc., **104**, 2910 (1982).

Tan , Y. Y., Challa, G., Polymer **17**, 739 (1976).

Tokuhiro, T., Amiya, T., Mamada, A. and Tanaka, T., Macromolecules **24**, 2936, (1991).

Willer , M. L., "The Structure of Polymers "Reinhold New York p 291 (1966).

Woessner, D.E., ; Snowden, B.S., Jr.J. Colloid Interface Sci., **34**, 290, (1970).

Appendix I

Table 3.1

Polymer proton line width data as a function of hydration for linear poly(acrylamide) (MW ~$2x10^6$)

Sr. No.	Hydration level (g/g)	Proton line width (kHz)
1	0.000	54.50
2	0.009	53.83
3	0.017	52.37
4	0.053	47.18
5	0.106	46.71
6	0.203	42.08
7	0.278	41.06
8	0.300	34.05
9	0.400	23.80
10	0.500	10.16
11	0.557	0.93
12	0.600	1.40
13	0.700	0.98
13	0.800	0.86
14	0.900	0.77
15	1.000	0.69
16	1.100	0.60
17	1.200	0.65
18	1.300	0.59
19	1.400	0.75
20	1.500	0.75
21	2.000	0.51

Table 3.2

Polymer proton line width data as a function of hydration for Alkaline Hydrolyzed (10%) linear poly(acrylamide) (MW~2.0 x10^6)

Sr. No.	Hydration level (g/g)	Proton line width (kHz)
1	0.000	51.50
2	0.064	49.90
3	0.090	48.70
4	0.134	47.00
5	0.146	46.10
6	0.216	44.95
7	0.222	43,89
8	0.308	38.90
9	0.320	34.45
10	0.400	29.19
11	0.460	14.19
12	0.540	13.99
13	0.600	9.05
14	0.660	2.21
15	0.740	1.49
16	0.800	1.05
17	0.860	1.17
18	0.920	0.69
19	1.280	0.68
20	1.134	0.58
21	1.210	0.59
22	1.300	0.61
23	1.500	0.81
24	1.600	0.71

Table 3.3

Polymer proton line width data as a function of hydration for Alkaline Hydrolyzed (40%) linear poly(acrylamide) (MW~2.0 x10^6)

Sr. No.	Hydration level (g/g)	Proton line width (kHz)
1	0.000	53.50
2	0.086	51.08
3	0.128	49.30
4	0.188	48.70
5	0.226	43.34
6	0.272	43.86
7	0.326	36.89
8	0.366	37.92
9	0.410	30.63
10	0.428	20.12
11	0.460	13.68
12	0.536	14.17
13	0.568	1.55
14	0.600	1.62
15	0.660	1.60
16	0.740	0.99
17	0.800	0.79
18	0.860	0.74
19	0.920	0.74
20	1.000	0.56
21	1.200	0.75
22	1.500	0.58
23	1.600	0.52
24	1.800	0.60
25	2.000	0.58

Table 3.4

Polymer proton line width data as a function of hydration for linear poly(acrylamide) (MW ~3.84×10^5)

Sr. No.	Hydration level (g/g)	Proton line width (kHz)
1	0.000	55.08
2	0.026	53.20
3	0.038	52.60
4	0.052	52.37
5	0.120	51.47
6	0.280	51.20
7	0.300	46.06
8	0.400	41.02
9	0.450	29.20
10	0.500	13.48
11	0.540	9.20
12	0.600	5.63
13	0.700	0.88
13	0.800	1.17
14	0.900	0.60
15	1.000	0.67
16	1.200	0.81
17	1.400	0.68
18	1.600	0.68
19	1.800	0.50
20	2.000	0.75

Table 3.5

Polymer proton line width data as a function of hydration for linear poly(acrylamide) (MW ~ 8.4 x10^4)

Sr. No.	Hydration level (g/g)	Proton line width (kHz)
1	0.000	56.98
2	0.092	54.34
3	0.106	53.56
4	0.156	50.37
5	0.176	49.08
5	0.200	47.81
6	0.253	44.13
7	0.350	41.06
8	0.400	36.25
9	0.500	7.65
10	0.600	2.49
11	0.740	0.85
12	0.800	0.81
13	0.900	0.69
13	0.940	0.56
14	1.020	0.85
15	1.100	0.59
16	1.200	0.85
17	1.400	0.62
18	1.600	0.72
19	1.800	0.80
20	2.000	0.70
21	2.000	0.51

Table 3.6

Proton line width data as a function of hydration for 2% cross-linked poly(acrylamide)

Sr.No.	Hydration level (g/g)	Proton line width (kHz)
1	0.000	61.79
2	0.040	60.20
3	0.080	59.85
4	0.120	55.00
5	1.600	50.00
6	0.200	46.80
7	0.212	46.63
8	0.230	44.00
9	0.320	40.00
10	0.480	13.76
11	0.510	13.43
12	0.600	12.00
13	0.680	10.08
14	0.700	0.97
15	0.800	0.76
16	0.900	0.79
17	1.000	0.92
18	1.200	0.72
19	1.300	0.78
20	1.400	0.74
21	1.600	1.00
22	1.800	0.86
23	2.000	1.00
24	2.200	0.58

Table 3.7

Polymer proton line width data as a function of hydration for Two days alkaline hydrolyzed 2% cross linked poly(acrylamide)

Sr. No.	Hydration level (g/g)	Proton line width (kHz)
1	0.000	62.56
2	0.022	62.50
3	0.030	62.39
4	0.092	60.30
5	0.108	60.30
6	0.122	60.20
7	0.156	60.00
8	0.218	54.37
9	0.256	52.50
10	0.300	38.80
11	0.400	18.38
12	0.500	14.12
13	0.544	12.00
14	0.600	3.38
15	0.640	2.67
16	0.674	2.60
17	0.700	1.00
18	0.800	1.10
19	0.900	1.14
20	1.000	0.72
21	1.200	0.77
22	1.400	0.88
23	1.600	0.68
24	1.800	0.72
23	2.000	0.64

Table 3.8

Proton line width data as a function of hydration for Eight days alkaline hydrolyzed 2% crosslinked poly(acrylamide)

Sr. No.	Hydration level (g/g)	Proton line width (kHz)
1	0.000	62.50
2	0.016	60.34
3	0.024	60.24
4	0.042	59.01
5	0.062	58.00
6	0.096	57.80
7	0.122	54.75
8	0.154	53.70
9	0.200	37.99
10	0.300	27.80
11	0.400	25.80
12	0.500	11.08
13	0.600	3.69
14	0.700	1.25
15	0.800	1.20
16	0.900	0.70
17	1.000	0.67
18	1.200	0.65
19	1.400	0.63
20	1.600	0.60
21	1.800	0.60
22	2.000	0.64

Table 3.9

Proton line width data as a function of hydration for Thirty days alkaline hydrolysed poly(acrylamide) gel

Sr. No.	Hydration level (g/g)	Proton line width (kHz)
1	0.000	62.52
2	0.026	61.78
3	0.044	59.84
4	0.056	58.00
5	0.068	57.58
6	0.086	52.00
7	0.124	43.00
8	0.200	11.00
9	0.300	3.00
10	0.400	1.00
11	0.500	1.02
12	0.600	0.85
13	0.700	0.75
14	0.800	0.70
15	0.900	0.70
16	1.000	0.69
17	1.100	0.67
18	1.200	0.59
19	1.400	0.55
20	1.600	0.55
21	1.800	0.57
22	2.000	0.52

Table 3.10

Proton line width data as a function of hydration for HSPAN (170 g/g absorption capacity)

Sr. No.	Hydration level (g/g)	Proton line width (kHz)
1	0.000	47.920
2	0.028	45.350
3	0.074	45.269
4	0.160	39.060
5	0.196	35.860
6	0.226	34.544
7	0.340	32.291
8	0.510	1.834
9	0.550	1.700
10	0.680	1.680
11	0.850	1.297
12	1.020	1.070
13	1.190	0.988
14	1.360	1.112
15	1.530	1.098
16	1.700	1.089
17	2.500	0.875
18	3.400	0.587
19	5.100	0.554
20	8.500	0.533
21	12.000	0.637

Table 3.11

Proton line width data as a function of hydration for HSPAN (100 g/g absorption capacity)

Sr. No.	Hydration level (g/g)	Proton line width (kHz)
1	0.000	47.10
2	0.026	44.60
3	0.050	41.10
4	0.136	39.30
5	0.192	35.90
6	0.200	35.00
7	0.240	33.30
8	0.300	30.09
9	0.352	29.07
10	0.500	20.80
11	0.600	15.06
12	0.750	9.80
13	1.000	1.77
14	1.200	1.68
15	1.400	1.48
16	1.600	1.37
17	1.800	1.20
17	2.000	1.18
19	2.500	1.17

Table 3.12

Proton line width data as a function of hydration for HSPAN (80 g/g absorption capacity)

Sr. No.	Hydration level (g/g)	Proton line width (kHz)
1	0.000	47.19
2	0.030	46.21
3	0.060	46.05
4	0.066	45.95
5	0.080	44.31
6	0.112	40.03
7	0.170	38.42
8	0.240	33.25
9	0.340	30.42
10	0.400	29.00
11	0.456	28.66
12	0.600	27.14
13	0.700	8.00
14	0.800	1.26
15	1.000	1.10
16	1.200	0.98
17	1.400	1.20
18	1.600	1.23
19	2.000	1.20
20	2.400	1.21
21	2.800	1.12
22	3.000	0.98
23	4.000	0.96

Table 3.13

Proton line width data as a function of hydration for HSPAN (50 g/g absorption capacity)

Sr. No.	Hydration level (g/g)	Proton line width (kHz)
1	0.000	47.70
2	0.080	42.70
3	0.140	42.20
4	0.200	40.80
5	0.400	27.30
6	0.526	21.40
7	0.600	17.65
8	0.800	1.66
9	0.900	1.20
10	1.000	1.37
11	1.100	1.04
12	1.200	1.01
13	1.400	0.93
14	1.600	0.80
15	1.800	0.86
16	2.000	0.80
17	2.500	0.89

Table 3.14

Polymer proton line width data as a function of hydration for poly(*N*-Isopropylacrylamide)

Sr. No.	Hydration level (g/g)	Proton line width (kHz)
1	0.000	32.20
2	0.020	31.50
3	0.028	31.05
4	0.040	29.86
5	0.050	29.50
6	0.074	29.08
7	0.084	28.06
8	0.214	25.54
9	0.236	24.30
10	0.240	18.34
11	0.300	17.01
12	0.360	1.80
13	0.400	1.50
13	0.460	1.40
14	0.500	0.62
15	0.600	0.63
16	0.700	0.64
17	0.800	0.45
18	0.900	0.72
19	1.000	0.47
20	1.100	0.60
21	1.200	0.51
22	1.400	0.56
23	1.600	0.52
24	1.800	0.56

Table 3.15

Polymer proton line width data as a function of Hydration for SANWET

Sr. No.	Hydration level (g/g)	Proton line width (kHz)
1	0.000	50.88
2	0.040	48.89
3	0.066	46.50
4	0.114	45.41
5	0.160	44.10
6	0.246	43.66
7	0.300	42.42
8	0.400	37.81
9	0.500	19.60
10	0.600	18.86
11	0.700	9.31
12	0.800	8.43
13	0.900	0.97
13	1.000	1.05
14	1.200	0.34
15	1.300	0.39
16	1.400	0.48
17	1.500	0.45
18	1.600	0.41
19	1.800	0.40
20	2.000	0.42

Table 3.16

Proton line width data as a function of Hydration for Gelatinized starch

Sr.No.	Hydration level (g/g)	Proton line width (kHz)
1	0.000	43.10
2	0.032	40.10
3	0.078	37.90
4	0.134	35.30
5	0.200	35.00
6	0.340	29.30
7	0.400	24.40
8	0.420	23.00
9	0.440	22.00
10	0.500	19.50
11	0.600	18.50
12	0.800	15.80
13	1.000	13.50
14	1.100	1.20
15	1.500	1.02
16	1.800	1.00
17	2.000	0.90
18	2.200	0.92
19	2.500	0.86

Chapter IV

Magic Angle Spinning and Two-Dimensional NMR Spectroscopy in Polymeric Gels

The response of macromolecules to hydration at very low levels has already been described in the previous two chapters. The behavior of macromolecules as well as that of water at higher levels of hydration is also subjects of great importance especially from the polymeric gels as well as biological point of view. These aspects are addressed in this chapter using two-dimensional (2-D) NMR spectroscopy. The chapter is divided into two parts. The first part describes the homonuclear ^{1}H-^{1}H 2-D NOESY experiment and the second part the heteronuclear ^{13}C-^{1}H 2-D Separation technique.

Part A: Homonuclear ^{1}H-^{1}H 2-D NOESY Experiment

4.1 Introduction

The structural organization and local dynamics of polymer segments are of considerable importance in the physico-chemical properties of gels. Superabsorbing polymers, which retain a large amount of water within the polymer networks, find extensive use in agriculture. Similarly, gels, which respond to stimuli, such as temperature, electric field, shear, etc, find use in control release applications (Dong & Hoffman 1991). In all these hydrogels, water plays a pivotal role in dictating the physical, chemical and mechanical properties of the systems. Detailed understanding of the interactions between the polymer and water is therefore considered to be of paramount importance. Water in macromolecules exist in different states (Wǫessner & Snowden 1970, Foster *et al* 1976) namely, bound, interfacial and free and there is substantial evidence for the existence of these organized states from studies of hydration on synthetic (McBrierty *et al* 1992, Ganapathy *et al* 1986) and biopolymers (Otting and Wuthrich 1989, Otting *et al* 1991, Shirley & Bryant 1982, Clore *et al* 1990). Additionally, it is also known that the presence of a solvent causes an enhancement of the molecular motions in the polymer system. Studies about the state of water, dynamics of water and the dynamics of macromolecules are beginning to emerge as an area of great interest and importance (Ganapathy *et al* 1989, Badiger *et al* 1991, Jelinski *et al* 1985, Forbes *et al* 1988, Schmeider *et al* 1985).

The response of macromolecules to hydration at very low levels has been already been described in the previous chapter. The behaviour of macromolecules as well as that of water at higher levels of hydration are also subjects of great importance, since the dynamical aspects of macromolecular hydration have to be looked at in the water-rich regime. These aspects are addressed in this chapter using two-dimensional (2-D) NMR spectroscopy. The 2-D studies are devoted to two polymeric systems, a superabsorber, hydrolysed starch-*g*-poly(acrylonitrile) (HSPAN) and the thermoreversible poly(*N*-isopropylacrylamide) (PNIPAm). This chapter is divided into two parts. The first part describes the homonuclear ^{1}H-^{1}H 2-D NOESY experiment and the second part the heteronuclear ^{13}C-^{1}H Separation technique.

4.1.1. Magic Angle Spinning and 2-D Spectroscopy

Although, conventional one-dimensional (1-D) NMR spectroscopy has made major contributions towards understanding of the nature of macromolecules, only recently, the more elegant multi-dimensional NMR techniques have been applied to the study of macromolecular systems. Our main interest in using solid state NMR spectroscopy is to allow inspection at the molecular level so that the dynamical events can be studied at the segmental level. In view of the significant developments in multi-dimensional NMR (Schmidt-Rohr & Spiess 1994, Ernst *et al* 1987, Macura & Ernst 1980, Gordon & Wuthrich 1978, Bluimich & Spiess 1988), two-dimensional NMR methods are considered to be superior compared to conventional 1-D NMR methods. We have therefore sought to apply the 2-D NMR techniques in the study of polymeric gels.

From the point of view of the motional state of a polymer, the immobilization of the Brownian diffusion and the predominance of local chain motions in the gel state render the application of 2-D methods to gels relatively easy. Further, the gel state of a macromolecule offers considerable scope from the NMR point of view, since this intermediate phase has not been fully exploited compared to the isotropic liquid phase or the rigid solid phase. In the gel state, the various NMR spin interactions that lead to

spectral line broadening are averaged to a great extent by enhanced polymer mobility in the presence of a diluent. Sample rotation at the "magic angle" is sought to remove the residual line broadening and reveal chemically distinct ^{1}H and ^{13}C resonances in the repeat unit. More importantly, MAS of swollen polymers offers increased sensitivity in heteronuclear experiments due to large sample volume and packing density. The ultimate signal resolution achieved in the MAS spectra is quite adequate for identifying the 2-D correlations. The interfering effects of spinning side bands are also minimal.

The two-dimensional NMR experiment has been introduced and discussed in Chapter II. Many homonuclear and heteronuclear versions of the 2-D experiments have been developed (Ernst *et al* 1987, Martin and Zektzer 1988, Sanders & Hunter 1987, Derome 1987). From the point of view of our discussion, the 2-D experiments can be broadly classified into two classes, depending on the nature of information obtained. The spectral correlation through nOe is provided by the 2-D NOESY experiment. The spatially dependent dipolar interaction is provided by the heteronuclear 2-D separation experiment. ^{1}H-^{1}H 2-D NOESY and heteronuclear (^{1}H-^{13}C) 2-D separation experiments have been applied to study both polymer-polymer and polymer-water interactions. This chapter discusses the experimental approaches we have taken, the applicability of these techniques to polymeric gels and the dynamical information gleaned from such studies.

4.1.2 Nuclear Overhauser Enhancement in Gels

Since nuclear Overhauser enhancement (nOe) forms the basis of the 2-D NOESY experiment, the following section is devoted to provide a brief description of the phenomenon. The effect of molecular mobility on the steady state nOe in homonuclear spin system is considered and discussed in the context of restricted molecular mobility in gels.

4.1.2.1 Phenomenon of nOe

In high resolution NMR, as in liquids or in samples spun at the magic angle, one can perturb one resonance by saturation or inversion so that the net intensities of other resonances in the spectrum may change. This phenomenon is called nOe and its importance lies primarily in the fact that the resonance that changes their intensities are due to spins close in space to directly affected by the perturbation. The nOe is the only technique that does not depend on the presence of scalar coupling for its operation. Instead, the interaction involved is the direct magnetic coupling between nuclei (the dipolar coupling), which does not usually have any observable effect on spectra recorded in solution. This situation is also the same in gels spun at the "magic angle", since the sample rotation removes the residual dipolar couplings. Although static dipolar couplings are removed by MAS, the dipolar interactions influence the various relaxation processes in the spin system through a second order effect. This is because there are spin operators in the dipolar Hamiltonian which can couple the corresponding eigen states in a coupled spin system and the internal molecular motions can promote an efficient dipolar relaxation. Since the dipolar coupling is related to the internuclear distances and the molecular motion provides a modulation of this dipolar interaction, nOe is found to be a very useful tool in the structural and dynamical characterization of complex molecules.

The nOe has its origin in the population changes brought about by a particular form of relaxation, namely dipole-dipole cross-relaxation. The phenomenon is more clearly depicted in Figure 4.1 for an isolated two-spin (1/2, 1/2) system (Neuhaus and Williamson 1989).

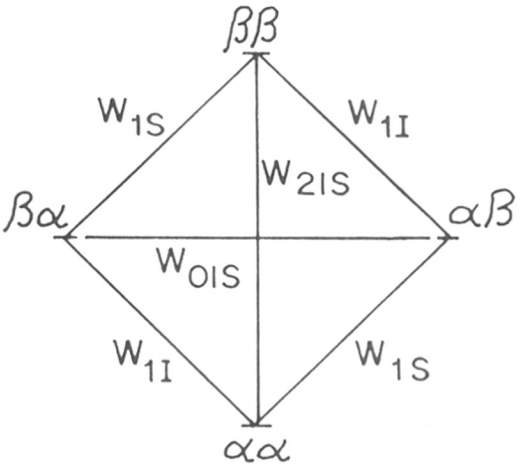

Figure 4.1: Energy level diagram for a two-spin (I= ½) system, showing definition of transition probabilities and spin states. Spin states are written with the state of I first and that of S second, *e.g.* αβ means spin I in state α and spin S in state β.

From the figure it is clear that the intensity of I is proportional to the sum of the population differences ($N_{\alpha\alpha} - N_{\beta\alpha}$) and ($N_{\alpha\beta} - N_{\beta\beta}$), while that of S is proportional to ($N_{\alpha\alpha} - N_{\alpha\beta}$) + ($N_{\beta\alpha} - N_{\beta\beta}$). At thermal equilibrium, for a homonuclear system, the levels are αα, the nearly degenerate levels αβ and βα with essentially identical populations to one another, followed by ββ. The same population difference exists across all four single quantum transitions (αα ↔ βα, αα ↔ αβ, αβ ↔ ββ and βα ↔ ββ), and so the equilibrium intensities I^0 and S^0 are identical as shown in Figure 4.2a. This figure also shows that there are transitions αα ↔ ββ, with transition probability W_{2IS} and αβ ↔ βα, with transition probability W_{0IS}. These two spin transitions are central to the theory of the nOe, because it is precisely these transitions that give rise to nOe enhancements, by allowing saturation of *S* to affect the intensity of *I*. It may also be noted that these transitions are coupled by the double quantum and flip-flop operators of the dipolar Hamiltonian. The selection rules that govern the interaction of the spin system with an

external oscillating field (the r.f field or the NMR signal) are different from the selection rules that apply to interactions of the spins with the lattice *via* energy exchange events.

When the S resonance is saturated, this equalizes the populations of levels $\alpha\alpha$ and $\alpha\beta$, and similarly those of levels $\beta\alpha$ and $\beta\beta$, thereby increasing the populations of levels $\alpha\beta$ and $\beta\beta$ while decreasing the populations of levels $\alpha\alpha$ and $\beta\alpha$ as shown in Figure 4.2b. There is no immediate change in the intensity of I resonance, as the population differences ($N_{\alpha\alpha} - N_{\beta\alpha}$) and ($N_{\alpha\beta} - N_{\beta\beta}$) are, at this stage, is unchanged. It is clear that the W_{1I} and W_{1S} transitions can only produce independent spin-lattice relaxation of I and S, respectively. However, if the transition described by the probability W_{2IS} occurs, it will act to restore the populations of the $\alpha\alpha$ and $\beta\beta$ levels towards their thermal equilibrium values. Saturation of S has caused the population of level $\beta\beta$ to increase, and that of $\alpha\alpha$ to decrease; W_2 relaxation will therefore act to reverse this, leading to a decrease in the population of the $\beta\beta$ level and an increase in the population of the $\alpha\alpha$ level. This necessarily results in an increase in the population differences ($N_{\alpha\alpha} - N_{\beta\alpha}$) and ($N_{\alpha\beta} - N_{\beta\beta}$), in other words, an increase in the intensity of the *I* resonance. Thus, if the W_2 transition occurs, it provides a positive nOe of the *I* signal. By an entirely analogous logic, it should be clear that "flip-flop" relaxation across the W_0 transition leads to negative nOe enhancement *i.e.* decrease in the intensity of I signal on saturating S. When combined with the requirement that saturation of S maintains population equality across the S transitions, these arguments lead to the population distributions shown schematically in Figure 4.2c and 4.2d.

The nOe enhancement, $f_I\{S\}$ is defined as the fractional changes in the intensity of I on saturating S:

$$f_I\{S\} = (I - I^0) / I^0 \qquad (4.1)$$

where, I^0 is the equilibrium intensity of I. From the above definition, the nOe will be positive if the new intensity is greater than the unperturbed intensity and negative if it is less.

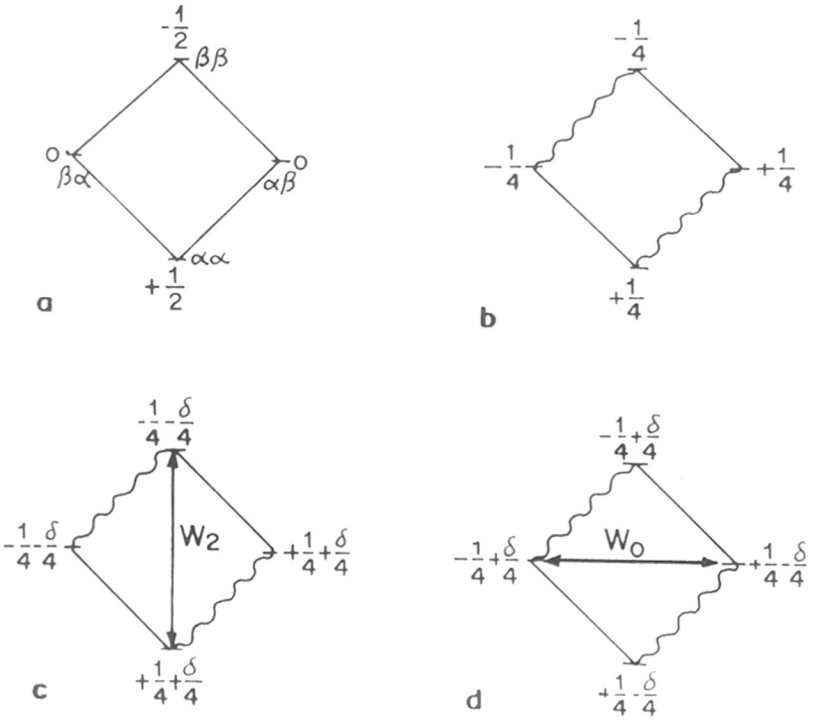

Figure 4.2: Origin of nOe in a homonuclear two-spin (I=1/2) system. The intensity I^0 ($S = S^0$) is here represented by a total population difference of one unit, and for convenience, the populations $N_{\alpha\beta}$ and $N_{\beta\alpha}$ are set to zero. **(a)** represents the situation at equilibrium. **(b)** represents the situation after saturation of the S resonance. Population $N_{\alpha\alpha}$ and $N_{\alpha\beta}$ are equalized, as are $N_{\beta\alpha}$ and $N_{\beta\beta}$; the intensity if I is still one unit, but that of S is now zero. **(c)** Shows the effect of W_2 relaxation during saturation of S. Population ($\delta/2$ units) has been transferred from state $\alpha\alpha$ to state $\beta\beta$, while saturation of S maintains the population equality across the S transitions. This has the effect of increasing the total intensity of I to ($1+\delta$) units, *i.e.* a positive NOE enhancement. **(d)** Shows the effect of W_0 relaxation during saturation of S. Population ($\delta/2$ units) has been transferred from state $\beta\beta$ to $\alpha\alpha$, so changing their populations in the direction of equilibrium. This has the effect of decreasing the total I intensity to ($1-\delta$) units, *i.e.*, a negative NOE enhancement.

4.1.2.2 Steady State nOe and Dependence on Molecular Mobility

The general theory of nOe was originally developed by Solomon (Solomon 1955) and is fully described by Noggle and Schirmer (1971). The observed intensities of I and S are proportional to I_z and S_z, the macroscopic longitudinal magnetization due to I and S, respectively, immediately prior to application of the observe pulse. These vectors I_z and S_z are themselves proportional to the population differences between the states. In terms of the various transition probabilities, one can write for the rate of change of z-magnetization of I signal as

$$dI_z/dt = - (I_z - I^o_z) (W_{0IS} + 2 W_{1I} + W_{2IS}) - (S_z + S^o_z) (W_{2IS} + W_{0IS}) \quad (4.2)$$

This equation, often called the Solomon equation, may be considered to be heart of nOe theory. From it we may very simply derive an expression for the steady-state nOe enhancement of I due to the saturation of S. At steady state, $dI_z/dt = 0$ and $S_z = 0$, so that,

$$0 = - (I_z - I^o_z) (W_{0IS} + 2 W_{1I} + W_{2IS}) + S^o_z (W_{2IS} - W_{0IS}) \quad (4.3)$$

Thus,

$$(I_z - I^o_z) / S^o_z = (W_{2IS} - W_{0IS}) / (W_{0IS} + 2 W_{1I} + W_{2IS}) \quad (4.4)$$

Since $S^o_z = (\gamma_S / \gamma_I) I^o_z$, we have

$$f_I\{S\} = (I_z - I^o_z)/I^o_z = (\gamma_S/\gamma_I) \{(W_{2IS} - W_{0IS}) / (W_{0IS} + 2 W_{1I} + W_{2IS})\} \quad (4.5)$$

The quantity $(W_{2IS} - W_{0IS})$ has the same form as predicted from our quantitative arguments concerning nOe enhancement, *i.e.* W_{2IS} causes a positive nOe enhancement, W_{0IS} a negative one, while W_1 transitions do not contribute. The term $(W_{2IS} - W_{0IS})$ describes the rate of dipole-dipole transitions giving rise to a nOe enhancement. It is

often called the cross-relaxation rate constant and is given by the symbol σ_{IS}. The term $(W_{0IS} + 2W_{1I} + W_{2IS})$ is dipolar longitudinal relaxation rate constant of spin I, and is given by ρ_{IS}. Using these symbols, Equation 4.5 can be written as

$$f_I \{S\} = (\gamma_S / \gamma_I)\, \sigma_{IS}/\rho_{IS} \tag{4.6}$$

The relaxation rates are determined by the details of molecular mobilities present in the system. We consider that the molecular motions are random and isotropic, characterized by the motional correlation time τ_c. The transition probabilities are related to the Fourier-transform of the time varying correlation function which is invariably assumed to be exponential. That is,

$$G(\tau) = \exp(-\tau / \tau_c) \tag{4.7}$$

The spectral density function $J(\omega)$ is therefore Lorentzian, given by,

$$J(\omega) = 2\, \tau_c^2 / (1 + \omega^2\, \tau_c^2) \tag{4.8}$$

From the form of the spectral density function $J(\omega)$, one can work out how the transition probability W depends on τ_c, for a transition whose corresponding frequency is ω_n.

Even for a first-order, isotropically tumbling, rigid systems, the detailed calculations of W_{0IS}, W_{1I}, W_{1S}, and W_{2IS} form the dipolar interaction Hamiltonian are quite involved, being a function of the orientations and separation of the two dipoles. Nonetheless, the results are quite simple, namely

$$W_{0IS} = (1/20)\, K^2\, J(\omega_I - \omega_S) = (1/10)\, K^2\, \tau_c / [1 + (\omega_I - \omega_S)^2\, \tau_c^2\,] \tag{4.9}$$

$$W_{1I} = (3/40)\, K^2\, J(\omega_I) = (3/20)\, K^2\, \tau_c / [1 + \omega_I^2\, \tau_c^2\,] \tag{4.10}$$

$$W_{1S} = (3/40)\, K^2\, J(\omega_S) = (3/20)\, K^2\, \tau_c / [(1 + \omega_S^2\, \tau_c^2)] \tag{4.11}$$

$$W_{2IS} = (3/10)\, K^2\, J(\omega_I + \omega_S) = (3/5)\, K^2\, \tau_c / [1 + (\omega_I + \omega_S)^2\, \tau_c^2\,\} \tag{4.12}$$

where $K = (\mu_O/4\pi)\ (\hbar\ \gamma_I\gamma_S\ r^{-3}_{IS})$ and represents the strength of the dipolar relaxation interaction.

We can now write for σ_{IS} and ρ_{IS} in terms of τ_c as,

$$\sigma_{IS} = W_{2IS} - W_{0IS} = (1/10)\ K^2\tau_c\ [6/\ \{1 + (\omega_I + \omega_S)^2\ \tau_c^2\ \} - 1\ /\ \{1 + (\omega_I - \omega_S)^2\tau_c^2\}] \qquad (4.13)$$

$$\rho_{IS} = W_{0IS} + 2\ W_{1IS} + W_{2IS} = (1/10)\ K^2\tau_c\ [1/\ \{1 + (\omega_I - \omega_S)^2\tau_c^2\ \} + 3\ /\ \{1 + \omega_I{}^2\tau_c^2\} + 6\ /\{1 + (\omega_I + \omega_S)^2\tau_c^2\}] \qquad (4.14)$$

Considering that in this two-spin system, W_{1I} and W_{1IS} are synonymous, the fractional nOe enhancement, $f_1\{S\}$, may now be expressed in terms of τ_c as

$$f_1\{S\} = (\gamma_S/\gamma_I)\ [(6/\ 1 + (\omega_I + \omega_S)^2\tau_c^2\ ) - (1\ /\ 1 + (\omega_I - \omega_S)^2\tau_c^2)]\ /\ [(1/\ 1 + (\omega_I - \omega_S)^2\tau_c^2\ ) + (3\ /\ 1 + \omega_I{}^2\tau_c^2) + (6\ /1 + (\omega_I + \omega_S)^2\tau_c^2)] \qquad (4.15)$$

For the two-spin system relaxing entirely by the dipole-dipole mechanism, $f_1\{S\}$ has the same meaning as η_{max}, the maximum theoretical two-spin enhancement. In the homonuclear case, $\gamma_I = \gamma_S$, and there is only one frequency $\omega_I \cong \omega_S \cong \omega$, so that $(\omega_I - \omega_S)\tau_c$ is always much less than one. Therefore, $f_1\{S\}(\eta_{max})$ simplifies to

$$f_1\{S\} = (\eta_{max}) = 5 + \omega_I{}^2\tau_c^2 - 4\omega_I{}^4\tau_c^4/\ 10 + 23\ \omega_I{}^2\tau_c^2 + 4\ \omega_I{}^2\tau_c^2 \qquad (4.16)$$

This function, shown in Figure 4.3, which summarizes most of what we need to know concerning the variation of homonuclear nOe enhancements with the motional correlation time τ_c. For small molecules with short τ_c, the limiting value for η_{max} is +50%. For large molecules with long τ_c, the limiting value for η_{max} is –100%.

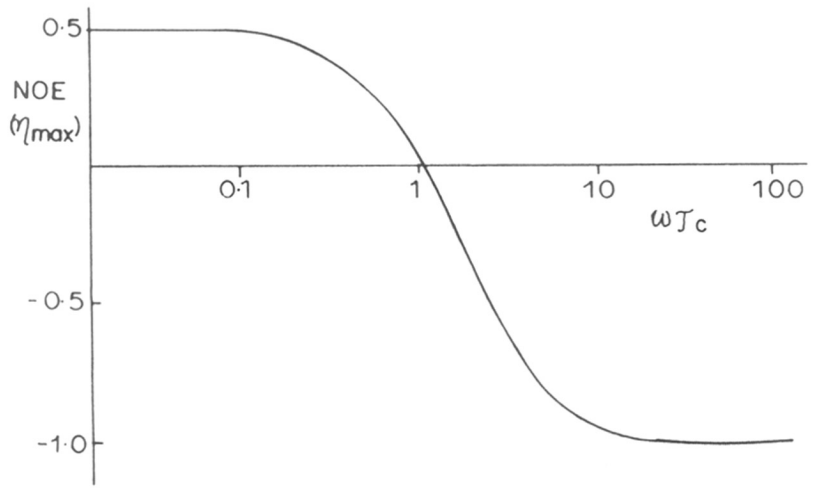

Figure 4.3: Variation of ^1H-^1H steady state nOe with τ_c to show 50% and −100% enhancements in the extreme correlation limits

An important aspect of the steady state nOe for dipolar coupled protons is that the sign of nOe changes while going from one correlation regime to the other. In the phase-sensitive 2-D NOESY experiment this is reflected as change in sign of the cross-peak, from negative ($\omega\ \tau_c << 1$) to positive ($\omega\ \tau_c >> 1$). It may be noted that in chemically exchanging systems magnetization transfer *via* chemical exchange is analogous to nOe transfer and can complicate the interpretation (e.g., protons in amide groups). Fortunately, in the short correlation limit the two proton peaks can be readily distinguished by the opposite sign for the cross-peaks. On the other hand, in the long correlation limit both these mechanisms lead to the same sign for the cross-peaks and one must resort to rotating frame (ROESY) experiments (Rajamohanan *et al* 1995).

4.1.3 ^1H-^1H 2-D NOESY in Hydrogels

The polymer system chosen for the ^1H-^1H 2D NOESY studies is a superabsorbing polymer, hydrolysed starch-*g*-poly(acrylonitrile), (HSPAN) which has applications in diverse areas (Fanta *et al* 1974, Masuda 1983, Tayler *et al* 1977, Freitas *et al* 1987, Ratner *et al* 1976, Hoffman *et al* 1986). Besides, this polymer is known to respond to hydration readily and has also been extensively studied by the NCL group (see Ganapathy *et al* 1989 & 1992, Badiger *et al* 1991, Rajamohanan *et al* 1991).

4.1.4 Synthesis of HSPAN

Hydrolysed starch-*g*-poly(acrylonitrile) (HSPAN) was synthesized using the procedure described in Chapter-II. It was found that the equilibrium water absorption capacity of this polymeric gel was 170g water/g of dry polymer. This corresponds to 100% saturation in water. The percentage of grafting and molecular weight of the grafted polymer were determined to be 48 % and 1.2 x 10^5 respectively. We have chosen three different hydration levels 3.4, 17.0 and 34.0 g/g. These hydrated samples were prepared by adding known amounts of water (99.8 % D_2O, obtained from BARC, Mumbai) directly to the dry polymer. The samples were kept 4-6 days for equilibration. Hydration levels were estimated gravimetrically and are expressed as weight ratios (gm of water / gm of polymer).

4.1.5 ^1H-^1H 2-D NOESY Experimental Details

The pulse sequence for the ^1H-^1H 2D NOESY experiment is the familiar NOESY sequence:

$$(\pi/2)_{\phi 1} - t_1 - (\pi/2)_{\phi 2} - \tau_m - (\pi/2)_{\phi 3} - AQ\ (t_2)_{R\phi} - \text{(relaxation delay)} \qquad (4.17)$$

The first ($\pi/2$) pulse produces transverse magnetization which precesses during the incremented period t_1. During the period t_1, the proton resonances are frequency labeled and this information is subsequently preserved with a longitudinal magnetization storage by the action of the second ($\pi/2$) pulse. The mixing time τ_m allows the longitudinal components to mix when acted upon by cross-relaxation. The last ($\pi/2$) pulse converts the longitudinal magnetization into an observable transverse magnetization. The appearance of cross-peaks in the 2-D plot is indicative of magnetization transfer. Phase cycling was employed to get rid of unwanted magnetisation. In order to observe cross-peaks that develop exclusively through nOe and to allow F_1 quadrature detection, the r.f pulses are phase cycled following the scheme indicated below. Further, axial peak suppression and quadrature cycling (CYCLOPS), to remove d.c offset and quadrature image, are incorporated into the phase cycling. In order to get a pure phase 2-D spectra, the Time Proportionate Phase Incrementation (TPPI) scheme developed by Marion & Wuthrich (1983) is employed. The following phases for the transmitter and receiver (R) were used.

$\phi 1$	+X	-X	+X	-X	+X	-X	+X	-X
	+X	-X	+X	-X	+X	-X	+X	-X
$\phi 2$	+X	+X	+X	+X	+X	+X	+X	+X
	-X	-X	-X	-X	-X	-X	-X	-X
$\phi 3$	+X	+X	-X	-X	+Y	+Y	-Y	-Y
Rϕ	+X	-X	-X	+X	+Y	-Y	-Y	+Y
	-X	+X	+X	-X	-Y	+Y	+Y	-Y

The phase-sensitive homonuclear ^1H-^1H 2-D NOESY experiments were performed on a Bruker MSL-300 FT-NMR spectrometer at the proton resonance frequency of 283.70 MHz and at ambient MAS probe temperature (295 K). At the time this experiment was performed, the MSL-300 NMR spectrometer had a magnet quench and the magnetic field was not completely restored. Since the magnet could not be

recharged to its original field of 7.01 Tesla, the proton resonance was located at 283.70 MHz and the MSL-300 r.f hardware was suitably modified to perform the 2-D NOESY experiment at 283.70 MHz. MAS was kept at 1.8 kHz and a recycle time of 3 secs was used. The total time for 2-D experiment was approximately 2 hrs. The t_1 was incremented in steps of 162 μsec following the TPPI procedure and 16 transients were accumulated in each of the 64 experiments. A sweep width of 3 kHz and 512 real data points were used. The data were apodized with sine-squared bell window function in both F_1 and F_2. The water resonance at 4.8 ppm reflects residual HOD as well as any initial water in this superabsorbing polymer. A 10% random variation of the mixing time was used to suppress J cross-peaks.

4.1.6 Results and Discussion

The 2-D NOESY contour plot of the hydrated polymer (3.4 g/g) in 99.8% D_2O is shown in Figure 4.4. This data was taken at a mixing time of 500 msec. At this hydration level, the integrated area of water (HOD) peak was estimated to be 54% of the total integrated area of the 1-D MAS spectrum. Considering the polymeric composition and molecular weight (1.2×10^5) of the pendant chain we estimate that at this hydration level all the hydrophilic sites in the pendant chain and starch backbone are hydrated. Since the water content is very high, a gel prepared in H_2O would give rise to a strong water peak and would swamp the cross-peaks. The amount of residual water in the 3.4 g/g hydrated sample represents an appropriate dilution of H_2O in D_2O required to hydrate all the sites and yet reveal the polymer-water cross-peaks. The 2-D experiment was conducted in the phase-sensitive mode, rather than in the magnitude mode, to reveal the absolute sign of the resulting cross-peaks, which we found to be positive. The projection of the 2-D NOESY data parallel to the F_2 axis is also shown. The corresponding one-dimensional MAS spectrum (F_2 projection) is also shown in Figure 4.4b, where the distinct proton sites in the pendant chain and starch backbone could be identified and assigned. The proton spectrum of a static gel given in Figure 4.4c is also presented for comparison.

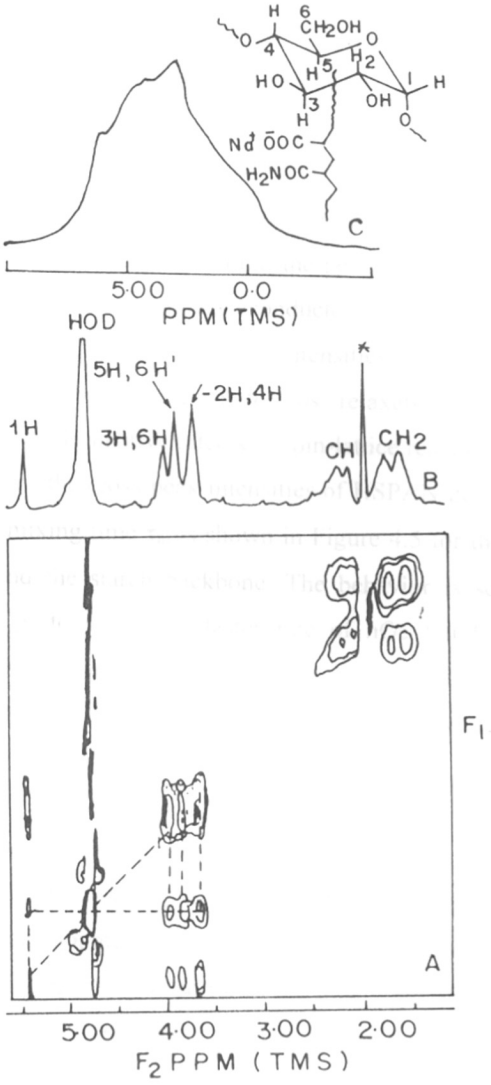

Figure 4.4: 2-D NOESY of 3.4 g/g hydrated HSPAN gel.
(A) Phase-sensitive homonuclear ^{1}H-^{1}H 2-D NOESY contour plots of hydrolysed starch-g-poly(acrylonitrile) gel hydrated to 3.4 g/g (water/polymer) in 99.8 % D_2O. τ_m = 500 msec. (B) Projection of 2-D data in (A) along F_2 axis, showing the 1-D MAS spectrum. The signal marked with asterisk is the impurity signal. (C) Static ^{1}H spectrum of the dry polymer. The strong water signal gives a ridge parallel to the F_1 axis.

It is clear that MAS affords the fine spectral resolution required to carry out the 2-D NOESY experiment.

The 2-D contour plot displays the various NOESY connectivities. It is seen that the 2-D cross peaks develop exclusively within the pendant and starch units due to the grafted nature of the polymer. Experiments conducted at various mixing times in the range 50-1000 msec confirm that cross peak intensities follow a transient response characterized by, (1) an exponential rise due to cross-relaxation between the interacting spins and (2) a decay due to dissipative effects of spin-lattice relaxation (Macura & Ernst 1980). The dependence of the cross-peak intensities of HSPAN gel hydrated to 17.0 g/g (water/polymer) on the mixing time τ_m is shown in Figure 4.5 for the proton resonances of the pendent chain and the starch backbone. The behavior is seen to be markedly different. The pendant protons show a faster rate of nOe build up than the starch backbone. It is further noted that the cross-peaks develop with the same positive sign as the diagonal peaks, showing thereby that the resulting Overhauser enhancements are negative (Ganapathy *et al* 1992).

The above observation clearly shows that the motional dynamics of the polymer system is considerably enhanced in the presence of water. Moreover, since positive cross-peaks develop, the nOe development occurs in the so-called "spin-diffusion" regime, or the long correlation limit ($\omega\tau_c >> 1$), in so far as the time scale of the hydration-induced polymer mobility is concerned (Krishnan *et al* 1989, Majumdar & Hosur 1990, Ad Bax *et al* 1986, Bryant 1988). This is in accordance with earlier ^{13}C nOe experiments (Ganapathy *et al* 1992) conducted as a function of hydration in water swollen HSPAN gel. It was found that the steady state ^{13}C nOe increased with increase in the degree of hydration, but the theoretical maximum ^{13}C nOe of 198.8 % could not be observed even at very high hydration levels. The cross-peaks also distinctly demarcate the intra-molecular dipolar interactions within a given segment (*i.e.* pendant chain or starch backbone). In fact, no starch-pendant group 2-D NOESY connectivity could be established irrespective of the level of hydration of the polymer or the choice of mixing

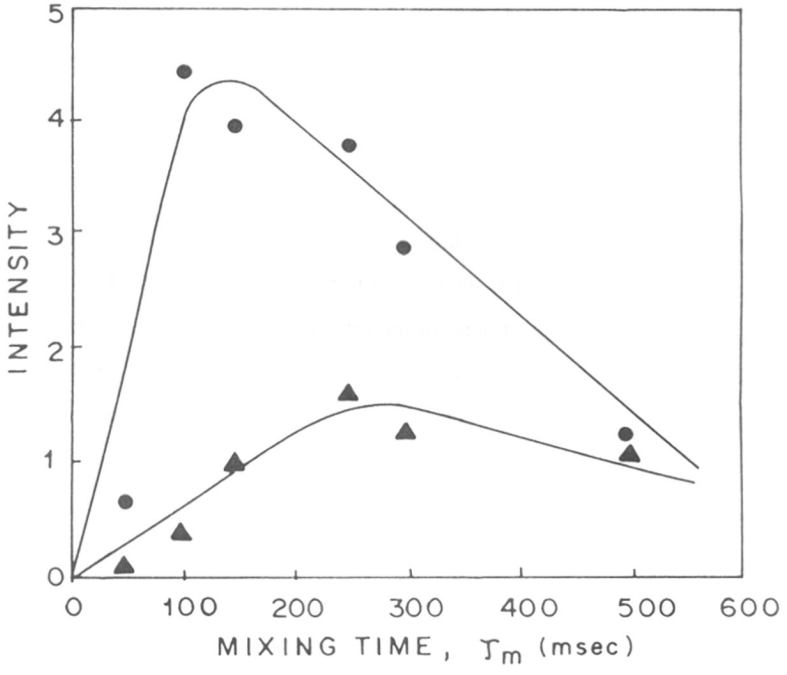

Figure 4.5: Dependence of the cross-peak intensity on the mixing time τ_m for hydrolysed starch-g-poly(acrylonitrile) gel hydrated to 17.0 g/g (water/polymer). Cross-peak intensities measured from experimental 2-D NOSEY data are denoted by •, between pendant CH and CH2 and by ▲, between starch 1H and 2H. The solid line through the data points has been drawn by hand to show the transient response of the cross-relaxation process.

time. This confirms that in this grafted copolymer, the pendant chains are indeed spatially isolated from starch units. The intra-unit connectivity is established primarily by dipolar cross-relaxation interaction within the given segment, modulated by chain motions. These are strongly favored for the CH and CH_2 protons of the pendant chains and the CH_2, anomeric protons of the puckered glucopyranose ring of the starch backbone. The observed difference in the mixing time dependence of the cross-peak intensity for the pendant and starch proton may be attributed to the difference in motional correlation time, molecular geometry or both.

The interaction between the water of hydration and the polymer system is also revealed in the 2-D NOESY experiment (Figure 4.4). It is clear that there is a uniform migration of water magnetization across the entire starch unit, as revealed by enhanced water-polymer cross peaks and a decreased water resonance on the diagonal. However, there is no 2-D connectivity of water with the aliphatic resonances of the pendant unit. As shown previously (Rajamohanan *et al* 1991), water in this polymeric gel is easily accessible to the various hydrophilic groups (COO^-, $CONH_2$ of pendant and OH^- of starch) which act as hydration sites. While the plasticization induced by water to enhance the polymer mobility is revealed by polymer-polymer cross peaks, the association of water with the polymer system is revealed by water-polymer cross peaks. Thus the present 2-D experiment brings about this important feature on the state of water, which has drawn the attention of many researchers (Bryant 1988, Rupley & Careri 1991) in a single run. The absence of cross-peaks with the pendant protons is likely to be caused by the long H-H distance due to hydrogen bonding of water at the carboxylate and amide sites, or due to very short correlation time for water motion, or both.

For the glucose unit, only hydroxyl sites affect hydrogen-bonding capability for water. At low hydration levels, the water molecule is tightly bound; presenting very reduced mobility due to at least two strongly energetic hydrogen bonds with primary absorption sites (Guilbolt *et al* 1985). This would lead to a significant cross-peak development in the "spin diffusion" regime ($\omega\tau_c >> 1$) and this was observed in the 3.4

g/g hydrated polymer (Figure 4.4). On the other hand, increased water mobility at higher hydration levels would attenuate or eliminate cross peaks with starch protons. This is clearly demonstrated in Figure 4.6, where the 2-D NOESY data taken at a constant mixing time of 500 msec on a 34.0 g/g in 99.8% D_2O hydrated polymer are shown for comparison. The importance of cross-relaxation between the starch and water protons via the secular 'flip-flop' process, rather than proton chemical exchange, has been suggested recently by Tanner *et al* (1991). The 2-D NOESY data, presented here, especially for the 3.4 g/g hydrated polymer, lends support to this view.

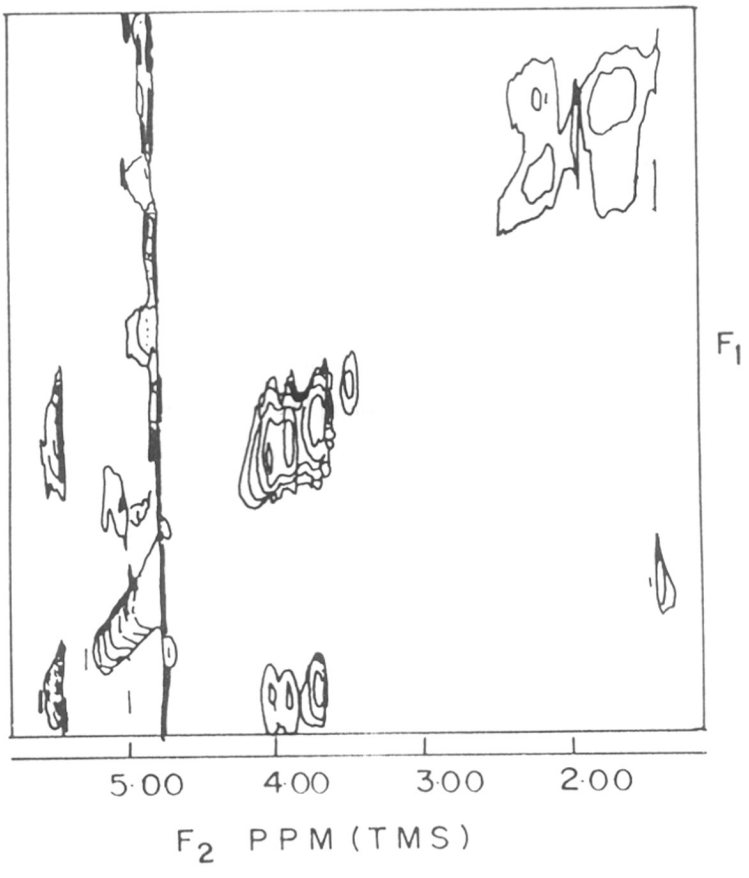

Figure 4.6: 2-D NOESY of 34 g/g hydrated HSPAN gel.
Phase-sensitive ^{1}H-^{1}H 2-D NOESY contour plots of hydrolysed starch-g-poly(acrylonitrile) gel hydrated to 34.0 g/g (water/polymer) in 99.8 % D_2O, at τ_m = 500msec.

Part B: Heteronuclear ^{13}C-^{1}H 2-D Separation Technique

4.2 ^{13}C-^{1}H 2-D Separation and a Study of Hydration in Gels

4.2.1 Introduction

This section describes how the dynamic state of water and of the polymeric gels can be studied by two-dimensional heteronuclear ^{13}C-^{1}H separation solid-state NMR spectroscopy. The technique, known as WISE, was proposed and discussed by Spiess and co-workers (Schmidt-Rohr *et al* 1992). In this 2-D experiment, by allowing proton evolution during incremented evolution period t_1, proton-carbon mixing during the mixing period τ_m, and high-resolution carbon detection during the detection period t_2, a two-dimensional separation of carbon and proton spectral response is obtained. During t_1, a component of the precessing proton transverse magnetization is spin-locked along an applied r.f field, and this modulates the intensity of the ^{13}C resonance, which participates in the magnetization transfer *via* cross-polarisation This leads to an indirect detection of the proton spectrum along the F_1 axis when the time domain data set $S(t_1, t_2)$ is double Fourier-transformed to yield the 2-D frequency domain spectrum $F(\omega_1,\omega_2)$. High-resolution ^{13}C detection is achieved by combining dipolar decoupling and magic angle sample spinning (MAS), while the proton-carbon mixing is established by a matched Hartmann-Hahn (Hartmann & Hahn 1962) cross-polarization scheme. The dynamical state of the polymer and water is directly coded by observing the events during this mixing period. The 2-D separation spectroscopy is used to study the hydration details in the superabsorbing hydrophilic polymer hydrolysed starch-*g*-poly(acrylonitrile) (HSPAN) and the LCST polymer poly(*N*-isopropylacrylamide) (PNIPAm).

4.2.2 Experimental Work

4.2.2.1 Synthesis of HSPAN and PNIPAm

The synthesis of HSPAN is already described in the Chapter II and PNIPAm was synthesized as described in Chapter II. Hydrated HSPAN was prepared by controlled

exposure of the dry polymer to water vapour in a humidity chamber. For the 2-D experiment, a sample of HSPAN having 0.4 g/g hydration level was prepared. Hydrated PNIPAm was prepared by direct addition of a known amount of water to the dry polymer and subsequent equilibration for 4-5 days.

4.2.3 ^{13}C-^{1}H Separation Experimental Details

The 2-D ^{13}C-^{1}H separation experiments were performed on the Bruker MSL-300 FT-NMR spectrometer at the Larmor frequencies of 300.13 MHz and 75.48 MHz for ^{1}H and ^{13}C, respectively. The pulse sequence used in this experiment is:

$$(\pi/2)^{I}_{\phi 1} - (t_1/2) - (\pi)^{S}_{+x} - (t_1/2) - (\tau_m)^{I,S}_{\phi 2,\phi 3} - (t_2)^{I}_{R\phi} - \text{(relaxation delay)} \qquad (4.18)$$

where, I and S denote ^{1}H and ^{13}C irradiation, respectively, ϕ's are the transmitter rf phases, and R_ϕ represents the receiver phase. The transmitter and receiver phases are given below.

ϕ_1	+X	+X	+X	+X	+Y	+Y	+Y	+Y	-X	-X	-X	-X	-Y	-Y	-Y	-Y
ϕ_2	+X	-X	+Y	-Y	+Y	-Y	-X	+X	-X	+X	-Y	+Y	-Y	+Y	+X	-X
ϕ_3	+X	+X	+X	+X	+Y	+Y	+Y	+Y	-X	-X	-X	-X	-Y	-Y	-Y	-Y
Rϕ	+X	-X	+Y	-Y	+Y	-Y	-X	+X	-X	+X	-Y	+Y	-Y	+Y	+X	-X

The π pulse in the middle of the t_1 period is not required when wide-line proton response is obtained. Quadrature detection in t_1 was employed when the desired proton spectral separation displays individual proton resonances at the isotropic chemical shift. Proton spin-temperature alternation and CYCLOPS during t_2 were incorporated in a 16 step phase cycling. For cross-polarisation mixing, a 40 kHz r.f field was used on the ^{1}H and ^{13}C channels. A power mode calculation was employed. The MAS was maintained at around 2.3 kHz. Other relevant 2-D parameters are included in the figure captions. For

the LCST polymer PNIPAm, the 2-D experiment was carried out at temperatures below (298 K) and above (323 K) LCST. The temperature was controlled using the Bruker BVT-1000 temperature controller.

4.2.4 Results and Discussion

The two-dimensional carbon-proton spectral separation for unhydrated dry HSPAN, together with the F_1 and F_2 projections is shown in Figure 4.7(A). This experiment was carried out at 298 K. Due to dipolar decoupling and magic angle spinning, distinct ^{13}C sites in the pendant chains and the starch backbone are resolved and identified in the ^{13}C spectrum. The contours in this figure show the separation of the proton spectrum at each resolved carbon. For this dry polymer sample, cross-sections at each carbon in the repeat unit give rise to identical, in terms of line shape and line width, wide-line proton spectra. The cross-section through each resolved carbon resonance yields identical wide-line proton spectra. These are featureless Gaussians of width 48 kHz in each case. Manifestation of the same broad-line proton spectrum at each carbon site shows that in this rigid phase pure polymer proton "spin diffusion" is very efficient and polarisation is transferred to the individual carbons from polymer protons acting as a single thermodynamic reservoir.

The two-dimensional experiment on a hydrated HSPAN (0.4 g of water/ g of dry polymer) leads to a ^{13}C-^{1}H spectral separation in a similar way. This is shown in Figure 4.7(B), where the two-dimensional data were limited to 28 experiments due to experimental constraints. Unlike the dry polymer, the proton spectra obtained at the distinct carbon sites are clearly seen to be different in this hydrated polymer. A proton line exhibiting a broad and a very narrow component is separated at starch (C_1, $C_{2,3,5}$) and pendant (CH, CH_2) carbon resonance positions. For the carboxylate/amide (COO^-, $CONH_2$) carbons of the pendant chain, the two-dimensional separation essentially leads to a single Lorentzian proton line of width 4.5 kHz. While it is a formidable task to calculate these proton line shapes resulting from multi-spin dipolar interactions in the

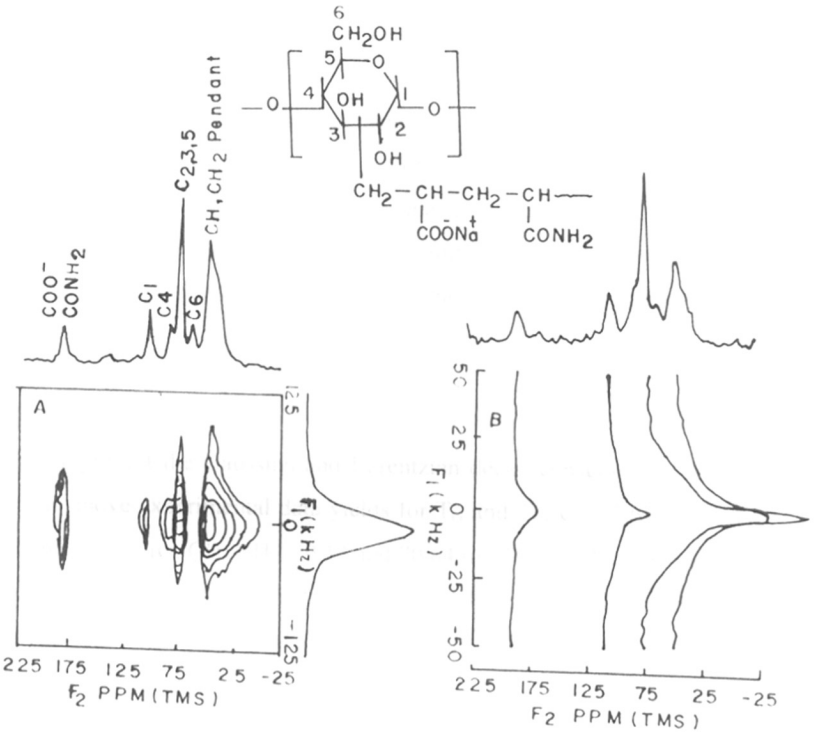

Figure 4.7: (A) Two-dimensional heteronuclear ^{13}C-^{1}H separation for dry hydrolysed starch-*g*-poly(acrylonitrile) (T = 298 K). The contours show the separation of the proton spectrum at each resolved carbon. For the dry polymer, cross-sections at each carbon in the repeat unit give rise to identical (in line shape and line width) wide-line proton spectra. Hence only the F_1 projectioned proton wide-line spectrum is shown. These spectra were obtained by extracting the submatrix column at each carbon site and Fourier-transforming along with F_1. The t_1 increment is 1 μs, and the number of experiments is and 24. The number of scans is 400. The cross-polarization mixing time is 700 μs.

(B) Two-dimensional heteronuclear ^{13}C-^{1}H separation for 0.4 g/g (water/polymer) hydrated hydrolysed starch-*g*-poly(acrylonitrile), (T = 298 K). The contors show the separation of the proton spectrum at each resolved carbon. For this hydrated polymer, the F_1 cross-sections corresponding to different carbon resonances show distinct proton spectra. These spectra were obtained by extracting the submatrix column at each carbon site and Fourier-transforming along with F_1. The t_1 increment is 10 μs, and the number of experiments is and 28. The number of scans is 480. The cross-polarization mixing time is 600 μs.

hydrated state, a characterization of the broad and narrow components in terms of line shape and line width is completely sufficient to unravel hydration details. This is done by an analysis of the t_1 time domain resonance at each carbon, obtained from the 2-D data set S (t_1, t_2) after Fourier-transformation along t_2. The results are shown in Figure 4.8. Considering a composite line shape for the proton line resolved at each carbon site, we may formally associate Gaussian and Lorentzian components to the t_1 time domain response, which can be readily fitted to the sub-matrix data set using the fitting function,

$$I = I_L(0) \exp(-t_1/T_L) + I_G(0) \exp((-t_1/T_G)^2) \qquad (4.19)$$

where, T_G and T_L represent the Gaussian and Lorentzian decay constants, respectively. The analysis of the above experimental data yields for T_G and T_L: C_1, 27.67 and 694.56 μs; $C_{2,3,5}$, 21.21 and 784.31 μs; CH, CH_2, 20.13 and 70.64 μs. These values correspond to line widths for the Guassian (C_1 = 19.2 kHz, $C_{2,3,5}$ = 25.04 kHz; CH, CH_2 = 26.38 kHz) and Lorentzian (C_1 = 458 Hz, $C_{2,3,5}$ = 406 Hz; CH, CH_2 = 4.51 kHz). For the proton response resolved at $COO^-/CONH_2$, analysis yields only a Lorentzian decay with T_L = 59.6 μs ($\Delta\nu$ = 5.34 kHz).

For the starch C_1 and $C_{2,3,5}$ and the pendant CH/CH_2, the broad and narrow components of the 2-D separated proton line shapes are identified with polymer and water protons, respectively (Tanner *et al* 1991). This identification is supported by the present observations that the intensity of the narrow component changes in proportion with the amount of hydration water and with the isotopic dilution with D_2O. Similarly, it is found that under identical experimental conditions the $COO^-/CONH_2$ carbon signal intensity is drastically reduced in the 2-D experiment for a 0.4 g/g D_2O (100%, Aldrich Co., USA) hydrated polymer. Thus for these carbons, the single Lorentzian proton spectrum is mainly due to water, thus envisaging a direct interaction with the hydrated water at these sites.

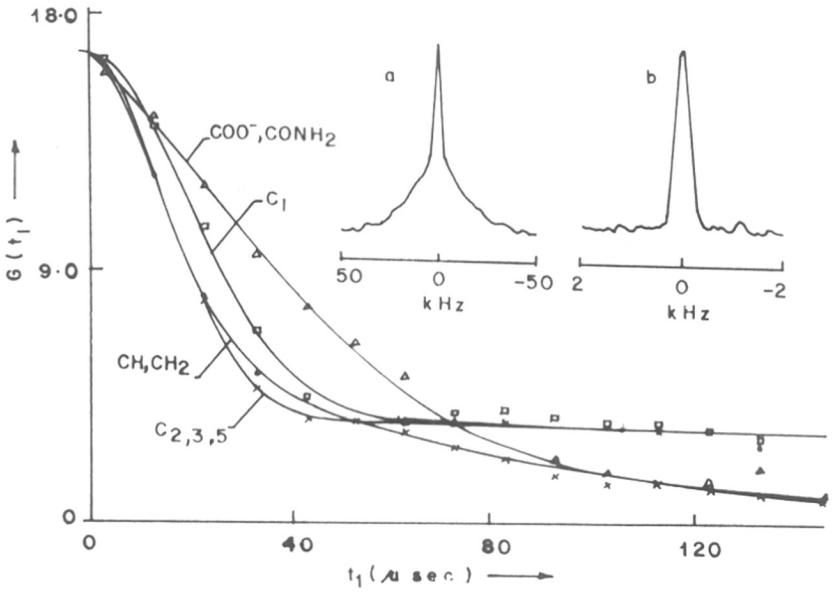

Figure 4.8: Time-domain response obtained from the 2-D data set of 0.4 g/g hydrated hydrolysed starch-g-poly(acrylonitrile), after Fourier transformation along t_2. Various symbols denote experimental data points for the different carbons. The solid line has been calculated by fitting to a Gaussian-Lorentzian function as explained in Section 4.2.4. The insert shows the proton spectra obtained by Fourier-transforming the t_1 domain interferograms of $C_{2,3,5}$: (a) data obtained from 28 experiments using a t_1 increment of 10 μs; (b) data obtained from 24 experiments using a t_1 increment of 125 μs. The narrow proton resonance in b ($\Delta\nu$ = 345 Hz) is due to water (also see text).

In HSPAN, the carboxylate and amide groups of the pendant chains and the hydroxyl groups (OH^-) of the starch backbone act as primarily hydration sites (Rajamohanan *et al* 1991). Moreover, due to grafting, the pendant and starch units are spatially isolated. Consequently, the hydrated water protons at these units are isolated from one another as well. For the starch units there are two main proton types, namely, water protons and the polymer protons (non-exchangeable CH and CH_2 protons and exchangeable OH protons) (Tanner *et al* 1991). The exchangeable hydroxyl protons may not be distinguishable from the hydration water at these sites due to rapid exchange. Similarly, pendant units comprise only two types of protons, namely, hydrogen-bonded water protons at the COO^- and $CONH_2$ sites and the polymer protons (CH, CH_2). We also noted that at the 0.4 g/g hydration level, there is no bulk water phase (Rodehed & Ranby 1986).

The polymer protons and water protons constitute two separate proton pools that interact magnetically (Shirley & Bryant 1982, Wise & Pfeffer 1987, Jelinski *et al* 1980, Edzes & Samulski 1977). The protons in the polymer phase as well as the protons in the water phase have, at any time, a uniform spin temperature. The large dipolar width for the polymer component shows that within the polymer phase spin diffusion among the polymer protons will establish a common spin temperature. In the water phase, this is achieved by rapid chemical exchange, dominant at starch sites or by mutual spin-spin interactions, which may be considered for the hydration water located at the less restricted $-COO^-$ and $-CONH_2$ sites. The longitudinal magnetization in each phase may therefore be considered to be uniform. The slow molecular mobility in the polymer phase and the rapid water motions in the water phase would suggest that the water phase acts as a relaxation sink for the polymer protons. On the basis of earlier studies of biopolymer hydration, the cross-relaxation time for the diffusion for the laboratory-frame magnetization from the polymer to water protons occurs in the tens of the millisecond time scale (Edzes & Samulski 1977). To the best of our knowledge, no literature value of the spin diffusion time for the exchange of spin-locked magnetization between the polymer and water protons in a hydrated macromolecular system is available. In a

separate experiment we have allowed complete dephasing of the rapidly decaying polymer component and spin locked only the water component. Upon 2-D Fourier transformation, we see only the narrow water proton spectrum appearing along F_1. This is demonstrated in Figure 4.8(a) and 4.8(b) for the $C_{2,3,5}$ of the starch backbone. For Figure 4.8(a) the data obtained from 28 experiments using a t_1 increment of 10 μs and for Figure 4.8(b) data obtained from 24 experiments using t_1 increment of 125 μs. This observation, in turn, indicates that the heteronuclear ^1H-^{13}C cross-polarisation process occurs bimodally from each of these distinct proton reservoirs to the nearby carbons.

The polymer protons in the starch backbone and pendant chains experience strong dipole-dipole interactions, occurring in the rigid polymer phase, giving rise to the Gaussian line shape for the broad polymer component ($\Delta\nu \sim 25$ kHz). This width is however reduced from the rigid lattice value of 48 kHz, noticed for the dry polymer, due to enhanced polymer segmental mobility upon hydration. For "bound" water molecules, intramolecular dipole-dipole interactions are averaged by the anisotropic water motions. This gives rise to the Lorentzian line shape for the water component, with a line width that is considerably smaller than that of the polymer component. It has been clearly observed that the water component is narrower at the starch sites ($\Delta\nu \sim 400$ Hz) than at the pendant sites (4-5 kHz), thus showing that water mobility is more restricted at the carboxylate and amide sites. It has been observed here that the line narrowing effects due to MAS ($\nu_r = 2.3$ kHz) are negligible for the broad polymer component. For the more restricted water at $COO^-/CONH_2$ sites, interactions within the tightly bound water molecules impart homogeneous broadening to the residual water line width, making it less amenable for narrowing by MAS. For the less restricted water at the hydroxyl sites, the water line may be considered to be inhomogeneously broadened, and MAS is effective in narrowing the water resonance. These are reflected in the width of water resonance indirectly detected in the 2-D experiment (Yesinowshi *et al* 1988 & Brunner *et al* 1990). This is attributable to difference in the strength of the hydrogen bonds formed by water at these sites (Vinogradov *et al* 1970).

Similar 2-D separation experiment has also been carried out for poly(*N*-isopropylacrylamide), hydrogel. The two-dimensional plot obtained is shown in Figure 4.9. This polymer is known to respond to water readily and undergo a thermo-reversible volume phase transition at 305K due to a lower critical solution temperature (LCST) phenomenon (Schild 1992 and Tokuhiro *et al* 1991). It exists in either of the two hydrated states, namely, an equilibrium-swollen state (below LCST) or a collapsed state (above LCST). For the equilibrium-swollen polymer, the two-dimensional experiment does not lead to wide-line proton separation at the carbon sites. Instead, the cross-sections show isolated C-H correlations (as shown in Figure 4.9A), thus giving a high-resolution polymer proton spectrum along the F_1 axis (a). Noticeably, the dominant water resonance and the amide (-CONH-) peak in the ^{1}H MAS spectrum are not retrieved in the 2-D experiment. The hydration level used here far exceeds the bound-water limit (Dong and Hoffmann 1990) and allows a dominant bulk water phase to dictate the motional dynamics of the system. The polymer mobility has been enhanced to such extent that proton-proton spin interactions within the polymer phase are greatly averaged. As shown elsewhere (Badiger *et al* 1991), the resulting polymer proton line is inhomogeneously broadened, and MAS affords an efficient narrowing to allow proton chemical shift evolution during t_1. The water-induced polymer motions are clearly anisotropic, lest no correlation via cross-polarization would be observed. Water, due to its high dynamic state is totally decoupled from the polymer system and is pre-cluded from participating in the cross-polarization process.

The two-dimensional plot for the collapsed state, (above LCST) of the polymer, however, leads to proton wide-line separation at each of the carbon resonance. This is shown in Figure 4.9B. Importantly, there is no fine chemical shift resolution in the indirectly detected proton spectrum. The proton subspectra at each resolved carbon site are similar, characterized by a single Lorentzian of width ~ 8 kHz. Since at 318 K the polymer is in the collapsed state, a significant amount of free water has been removed from the polymer matrix, as independently verified using the solid state ^{1}H NMR spectral measurements at temperatures above and below the LCST of this polymer (Badiger *et al*

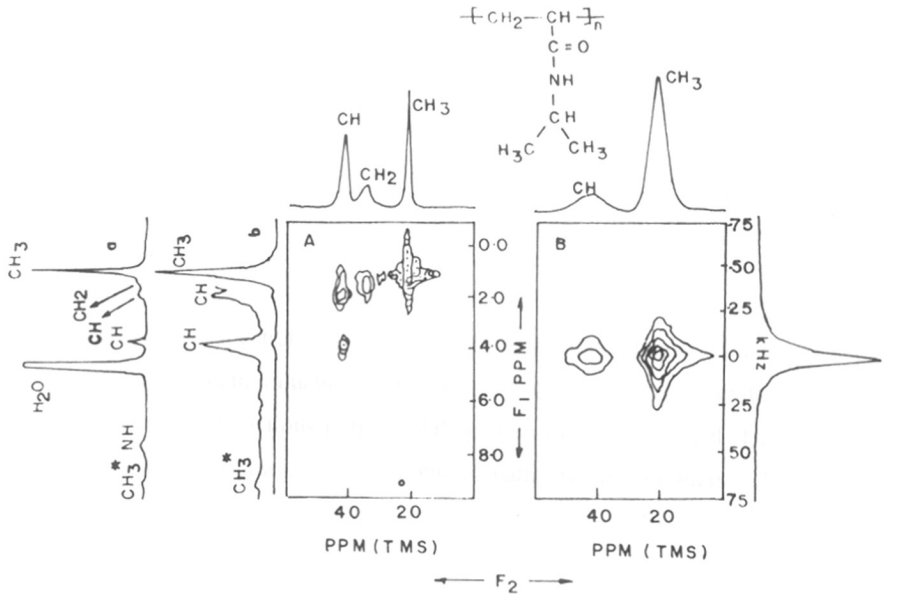

Figure 4.9: (A) Two-dimensional heteronuclear ^{13}C-^{1}H separation for LCST polymer poly(*N* - isopropylacrylamide) at 298 K (below LCST). Contour plots show the proton spectral response at each resolved carbon. At 298 K, cross-sections at the observed carbon positions give rise to distinct high-resolution proton spectra, correlating the carbon resonance with the polymer dipolar coupled proton at the proton chemical shift. The sum of these proton subspectra leads to the F_1 projection, as shown.. The 1-D ^{1}H MAS spectrum is also shown for comparison. The ^{1}H sideband is marked with an asterisk. The absence of the C=O peak is due to motional effects of the polymer. The t_1 increment is 125 μs, and the number of experiments is 90. The number of scans is 880 and the cross-polarization mixing time is 2.5 ms.

(B) Two-dimensional heteronuclear ^{13}C-^{1}H separation for LCST polymer poly(*N* - isopropylacrylamide) at 323 K (above LCST). Contour plots show the proton spectral response at each resolved carbon. At 323 K, cross-sections at the observed carbon positions lead to identical (in line shape and line width) wide-line proton spectra. Hence only the F_1 projected proton spectrum is shown. The absence of the CH_2 peak is due to motional effects of the polymer. The t_1 increment is 3.33 μs and the number of experiments is 64. The number of scans is 400. The cross-polarization mixing time is 450 μs.

1991). This noninteracting bulk water is essentially eliminated in the indirectly detected proton spectrum. A DSC study (Dong & Hoffmann 1990) on this polymer has also shown that above the LCST nearly all the water in the polymer is nonfreezing bound water.

4.2.5 Concluding remarks

In this chapter it is shown that macromolecular hydration can be conveniently studied by MAS based two-dimensional NMR. In these studies we have shown that the 2-D NOESY experiments can be conducted on hydrogels with relative ease, taking advantage of enhanced spectral resolution obtained by sample rotation at the magic angle. The resulting data contain valuable information about the spin connectivity established by dipolar relaxation interactions in the mobile phase of the polymer gel. This technique is potentially useful in unraveling the motional pathways in polymers, which readily respond to hydration. It appears that a common feature of the gel NOESY behavior is that the network is largely dominated by cross-relaxation mechanism in the "spin-diffusion" regime. The importance of dipolar relaxation interactions between the water of hydration and the polymer system is also revealed from these studies. The heteronuclear ^{13}C - ^{1}H separation spectroscopy is a useful technique to separate local dynamics at specific hydration sites in a polymeric gel. Further, the 2-D separation experiment provides dynamical insights in thermally collapsible gels that expel water while undergoing a volume phase transition. These experiments offer considerable scope to delineate dynamic details at an enhanced level of molecular inspection and further pave the way for studies of hydration in biopolymers such as collagen, DNA, etc.

4.2.6 References

Ad Bax, Sklenar, V. and Summers, M. F., J. Magn. Resn., **70**, 327, (1986).

Badiger, M.V., Kulkarni, M.G., Rajamohanan, P.R., Ganapathy, S. and Mashelhar, R.A., Macromolecules, **24**, 106, (1991).

Blümich, B. and Spiess, H.W. Angew.Chem.Intl.Ed.Eng., **27**, 1655, (1988).

Brunner, E., Freude, D., Gerstein, B.C., Pfeifer, H., J. Magn. Reson. **90**, 90, (1990).

Bryant, R.G. Studs. Phys. Theor. Chem. (Chem. Phys. Solvation, Pt. C.) Pagonadza, R.R., Kalman, E. and Karnyshev, A.A. Ulstrup, J.(Eds.), **38**, 683, (1988).

Clore, G.M., Bax, A., Wingfield, P.T., Gronenborn, A. M., Biochemistry, **29**, 5671, (1990).

Derome, A.E., Modern NMR techniques for Chemistry Research, Organic Chemistry Series, Vol. **6**, Pergamon Press, (1987).

Dong, L.C. and Hoffman, A.S. Proceedings of the International Symposium on Controlled Release of Bioactive Materials, Controlled Release Society, Inc., **17**, 116, (1990).

Dong, L.C. and Hoffman, A.S., J. Controlled Release, **15**, 141, (1991).

Edzes, H. T.; Samulski, E.T. Nature, **256**, 521, (1977).

Enest, R.R., Bodenhausen, G. and Wokaun, A., Principles of Nuclear Magnetic Resonance in one and two Dimensions, Clarendon, Oxford, (1987).

Fanta, G.F., Burr,R.C., Doane, W.M. and Russell, C.R., Starke, **30**, 237, (1974).

Forbes, J., Bowers, J., Xi, S., Moran, L., Oldfield, E. and Moscarello, M.A., J.Soc. Faraday Trans.1, **84**, 3821, (1988).

Foster, K.R., Resing, H.A., Garroway, A.N., Science, **194**, 324, (1976).

Freitas, R.F.S. and Cussler, E.L., Sep. Sci. Technol., **22**, 911, (1987).

Ganapathy, S., Badiger, M.V., Rajamohanan, P.R. and Mashelkar, R.A., Macromolecules, **25**, 4255, (1992).

Ganapathy, S., Badiger, M.V., Rajamohanan, P.R. and Mashelkar, R.A., Macromolecules, **22**, 2023, (1989).

Ganapathy, S., Chacko, V.P., Bryant, R.G., Macromolecules, **19**, 1021, (1986).

Ganapathy, S., Rajamohanan, P.R., Badiger, M.V. and Mashelkar, R.A., New Polymeric Materials, **2**, 205, (1990).

Gordon, S.l. and Wüthrich, K. J. Am. Chem. Soc., **100**, 7094, (1978).

Guilbolt, A. and Mercier, C. in "The Polysaccharides" Aspinall, G. O. (Editor), Academic Press (London), **3**, 209, (1985).

Hartmann, S.R.; Hahn, E.L. Phys. Rev., **128**, 2042, (1962).

Hoffman, A.S., Afrassiabi, A. and Dong, L.C. J. Controlled Release, **4**, 213, (1986).

Jelinski, L. W.; Sullivan, C.E.; Torchia, D.A., J. Magn. Reson., **19**, 133, (1980).

Jelinski, L.W., Dumais, J.J., Cholo, A.L., Ellis, T.S. and Karasz, F.E. , Macromolecules, **18**, 1091, (1985).

Krishnan, V.V., Murali, N. and Kumar A., J. Magn. Reson., **84**, 255, (1989).

Macura, S. and Ernst, R.R., Molecular Physics, **41**, 95, (1980).

Majumdar, A. and Hosur, R.V., J. Magn. Resn., **88**, 284, (1990).

Marion, D. and Wüthrich, K., Biochem. Biophys. Res. Commun,. **113**, 967, (1983).

Martin, G. E., and Zektzer, A.S., 2-D NMR Methods for Establishing Molecular Connectivity, VCH Publishers, New York, (1988).

Masuda, F., Chem.Econ.Eng.Rev., **15**, 19, (1983).

McBrierty, V. J., Quinn, F.X., Keeli, C., Wilson, A.C., Friends, G.D., Macromolecules, **25**, 4281, (1992).

Neuhaus, D. and Williamson, M., The Nuclear Overhauser Effect, In structural and Conformational Analysis, Chapter 1 & 2 VCH, Publishers, (1989).

Noggle, J.H. and Schirmer, R.E., The Nuclear Overhauser Effect-chemical Applications, Academic Press, (1971).

Otting, G. and Wuthrich, K., J.Am. Chem. Soc., **111**, 1871, (1989).

Otting, G., Liepinsh, E., Wuthrich, K., Science, **254**, 974, (1991).

Rajamohanan, P.R., Badiger, M.V., Ganapathy, S. and Mashelkar R. A., Macromolecules, **24**, 1423, (1991).

Rajamohanan, P.R., Ganapathy, S., Badiger, M.V. and Mashelkar R.A., Macromolecules, **28**, 14936 (1995).

Ratner, B.D. and Hoffman, A.S in "Hydrogels", Andrade, J.D. (Ed.) ACS Symposium Series, **31**, 1, (1976).

Rodehed, C.; Ranby, B., J. Appl. Polym. Sci., **32**, 3309, (1986).

Rupley, J.A. and Careri, G. in "Advances in Protein Chemistry," **41**, 38, (1991) and references therein.

Sanders, J.K.M. and Hunter, B.K., Modern NMR Spectroscopy, A Guide for Chemists, Oxford University Press, (1993)

Schild, H.G., Prog. Polym. Sci., **17**, 163, (1992).

Schmeider, B., Doskocilova, D. and Dybal, J. Polymer, **26**, 253, (1985)

Schmidt-Rohr, K. and Spiess, H.W., Multidimensional Solid State NMR and Polymers, Academic Press, (1994).

Schmidt-Rohr, K., Clauss, J., Spiess, H.W. , Macromolecules, **25**, 3273, (1992).

Shirley, W.M., Bryant, R.G., J. Am. Chem. Soc., **104**, 2910, (1982).

Solomon, I,. Phys. Rev., **99**, 559, (1955).

Tanner, S.F., Hills, B.P. and Parker, R., J. Chem.Soc. Faraday Trans., **87**, 2613, (1991).

Tayler, N.W. and Bagley, E.B. J. Appl. Polym. Sci., **21**, 113, (1977).

Tokuhiro, T., Amiya, T., Mamada, A. and Tanaka, T. Macromolecules, **24**, 2936, (1991).

Vinogradov, S.N., Linnell, R.H., Hydrogen Bonding; Van Nostrand Reinhold Co.; New York, 121, (1970).

Wise, W.B., Pfeffer, P.E., Macromolecules, **20**, 1550, (1987).

Woessner, D.E., Snowden, B.S. Jr., J. Colloid Interface Sci., **34**, 290, (1970).

Yesinowshi, J.P., Echert, H., Rossman, G.R., J.Am. Chem. Soc., **110**, 1367, (1988).

Chapter V

Molecular Modeling Studies on Water-Macromolecular Interactions

In Chapter III, we have shown that the step-wise addition of water to polymers and polymeric gels, such as poly(acrylamide), (PAM) and poly (*N*-isopropylacrylamide), (PNIPAm), undergoes a "mobility transition" that occurs at very early levels of hydration. This occurs earlier than those are normally associated with volume phase transitions that occur in responsive gels. However, the mobility transition is further studied by using molecular modeling approach to give more insight into the water-macromolecular interactions is presented in this Chapter. The main aim is to use energy minimized conformations of the polymer single chain is derived from energy minimization, further the molecular dynamic technique was applied to probe the mobility of hydrated polymer and the structure of water molecules around the polymer chains. Molecular modeling and molecular dynamic aspects related to polymer-water interactions will be discussed in this chapter.

5. Introduction

Smart polymeric gels have been extensively investigated today due to their potential applications in various fields (Dagani 1997). These gel-based systems undergo reversible and discontinuous macroscopic volume changes in response to various external stimuli as discussed in the Chapter I and III. The existence of molecular level transitions accompanying macroscopically observable transitions in volume has been extensively probed recently (Schild 1992, Ohta *et al* 1991, Katayama *et al* 1992, Tokuhiro *et al* 1991) These properties were closely related to the structure and conformations of these polymeric gels. It is well known that the specific conformation of many enzymes and proteins were responsible for the specific activity and regulate the specific functions (Rupley & Careri 1991). In these applications these systems undergoes some unusual structural and conformational changes. The amount of water also play crucial role in the enzymatic activity of a certain proteins and enzymes (Zaks & Klibanov 1984).

Water plays an extremely important role in determining the macroscopic properties of many of the macromolecules (Molyneux 1974 & 1984, Rowland 1980 and Bryant, 1988). Hydrophilic hydration and hydrophobic effects have a crucial role in determining the

conformations of biologically important macromolecules and many of their functions (Berendson 1975, Rupley & Careri 1991). Studies on the hydration of macromolecules have been a subject of great interest especially from the dynamic point of view of the macromolecule and water. Protein hydration is an important subject of interest as its folding conformations get affected due to the state of water. These water-macromolecular interactions can be studied by the 1-D/2-D NMR techniques. The 2-D NMR offers unique opportunity to probe the localized polymer-water interactions through the heteronuclear Overhauser enhancement (nOe), ^{13}C-{^{1}H} HOESY. Recently, Ganapathy *et al* (1995) has studied polymer-water interactions in case of cross-linked PAM gel using this 2-D NMR spectroscopy. They observed that for C=O, ^{13}C nOe develops exclusively through interactions with hydrated water. They have shown that in view of the inverse sixth power distance on the cross-relaxation rate σ_{CH}, a precise estimate of water-carbonyl distance can be measured by using, ^{13}C -{^{1}H} HOESY experimental data. Through a water selective transient Overhauser experiment, the cross-relaxation rate was estimated to be 1.546×10^{-4} sec^{-1} by an analysis of transient nOe data. The geometrical part of the σ_{CH} was evaluated by separating the dynamical part through temperature dependent ^{17}O spin-lattice relaxation time measurements. The NMR data analysis carried out by them finally yields a value of 3.45Å for the carbonyl-water interaction.

It is well known that the first-order thermo-reversible volume phase transition in the crosslinked PNIPAm gel occurs near the LCST of the linear polymer solution (Marchelli *et al* 1990). At temperature well below the critical temperature of the solvent the LCST phenomenon occurs due to specific molecular interactions in the mixture. Various theoretical developments have been proposed to model the volume transitions in PNIPAm gels (Otake *et al* 1989, Marchetti *et al* 1990 and Prange *et al* 1989). Recently, Lele *et al* (1995) have proposed an extended lattice-fluid-hydrogen-bond (LFHB) theory to model the swelling behavior of hydrogen-bonded gel-solvent systems such as poly(ethylene oxide) and PNIPAm gels. The extended LFHB model is obtained by adding the free energy of offine deformation of an elastic network to the free energy of the mixture given by the LFHB model of Panayiotou and Sanchez (1991). Besides, quantitatively fitting the experimental data, the theory predicts that at the transition temperature for PNIPAm gel there is a sharp

rearrangement of hydrogen bonds in the mixture. The theory also predicts that the hydrophobicity of PNIPAm should increase with temperature for the discontinuous volume phase transition to occur. The theory suggests that the hydrogen bonding interactions as well as the hydrophobic interactions are crucial for obtaining volume transitions. More important is that theory is also able to relate macroscopic observations to volume transition to molecular interactions in the gel phase. This has immense significance in terms of the ability of the theory to eventually design "tailed" gel having controlled transition. Lele *et al* (1995) had shown that the breakage and formation of hydrogen bonds in PNIPAm system are responsible for volume phase transition. At the LCST, there is a rapid increase in the number of hydrogen bonds formed between PNIPAm molecules of the gels and simultaneously there is a rapid decrease in the number of hydrogen bond formed between polymer segments and water molecules above the LCST.

Molecular modeling has become a well-established research technique during the last decade due to advances in computer hardware and software technology. Recently, Biosym/Molecular Simulation Inc., USA, has developed various software packages, which are able to handle the systems from the small molecules to the large molecules like, enzymes/proteins, polymers, receptors, networks, transition metals etc. Molecular modeling systems provide powerful tools for building, visualizing, analyzing, and storing models of complex molecular systems that can help to interpret various interactions within a molecules or interactions between binary systems. It also helps to study various structural related physico-chemical properties, possible different conformations, transition states, as well as the structure-property relationships (Hansch and Klein 1994).

Recently, molecular dynamics (MD) simulations have been carried out by Tamai *et al* (1996) for the hydrogel models of poly(vinyl alcohol), PVA, poly(vinyl methyl ether), PVME and poly(*N*-isopropylacrylamide), PNIPAm to elucidate the structure and dynamics between water and polymers. However, their focus was mostly on the motions of the water molecules and its properties in the hydrogels. They analyzed the dynamics of hydrogen bonds, using trajectories of MD simulations. The translational and rotational motions of water molecules are investigated and related to the hydrogen-bond dynamics and to the

equilibrium solvation structures. They have also shown that the mobility of water molecules is lowered around polymer chains for both translational and rotational motions.

5.1 Methods

In the last ten years, the static views of the molecules have been considerably enlarged to include new perspectives introduced by molecular dynamics. X-ray crystal structures represent a time - averaged structure of a continuously moving system, while molecular dynamics simulates the actual, instantaneous motion of the system. Here, each atom is treated as a particle responding to Newton's equations of motion. The successive integration of these equations leads to the positions and velocities. Analyses are made through periods of typically 1000 -100000 *fs* as many interesting wide range motions are fully developed within 100000 *fs* or less. Molecular dynamics is useful in order to identify preferred motions of synthesized small polymers (Tamai *et al* 1996) and bio-polymers (Olson & Zhang 1994, Rupley & Careri 1991).

NMR technique has been used to predict structural information for small proteins and macromolecules. Computational experiments have confirmed the validity of this technique by demonstrating appropriate agreement between NMR-determined structures and x-ray diffraction determined structures. Although traditional structure prediction and the studies of macromolecule-solvent interactions and its dynamics techniques using distance geometry computations alone, or in conjunction with molecular mechanics minimization have been successful with small proteins, peptides and other macromolecules. However, they have many disadvantages, like the number of 3-D conformations, computational space, number of possible local minima increase and the process can become trapped in local minima which increases exponentially with the size of the molecules being studied. One can overcome these problems by using expanding the molecular mechanics energy expression to include terms to describe dihedral angle energies, torsional relationships, van der Waals attractions, electrostatic interactions, and hydrogen bonding interactions, greatly reduces the allowable conformational space accessible to macromolecules. This more complete energy expression enhances the correctness of the calculations and the results.

The problem of large structures getting trapped in local minima can be obviated to some extent in molecular calculations by using molecular dynamics. Chemical systems being simulated by molecular dynamics evolve over time. These systems are simulated at finite temperatures, meaning that atoms have kinetic energy and corresponding velocities. These velocities allow atoms or groups of atoms to propagate over conformational energy barriers and into new conformational states. Potentially, these new states are lower energy states. Over time, molecular dynamics simulations tend to drift toward lower energy conformations, and therefore drift toward structures, which are more likely to be the correct 3-D structure of the system. During the process of increasing the temperature (heating) and annealing, molecular dynamics technique saves the snapshots of the molecule's trajectory for later animation and analysis of the macromolecular-solvent interactions.

In this study we have chosen two polymers, namely, PAM and PNIPAm which are interesting polymers with wide applications (Kulicke *et al* 1982, Hoffman *et al* 1986 & Dong *et al* 1987). They possess very interesting dynamic properties, which are exhibited by the hydrophilic and hydrophobic nature of these polymers, when they are exposed to water. The single chain configuration of the polymer will be affected by the water molecules leading to changes in their conformations. This effect, in-turn will allow further uptake of water into the polymer network. Thus, we believe that studies on the single chain conformation of the polymer and the nature of interaction of water will provide the basic model for understanding of the water-polymer interactions.

The insight here is given for the observation of microscopic transition caused by water in the molecular mobility of PAM and PNIPAm polymeric systems. Since the mobility transition is water induced, the water-macromolecule interactions are very important. Hence, the relation between such mobility transition and the variation in single chain conformation and polymer-water interactions are brought out by the molecular modeling studies. We used the molecular modeling and molecular dynamics (MD) techniques to examine the single chain configuration of PAM and PNIPAm and its interaction with water molecules, respectively. The dynamics of polymer-water system is

studied in order to understand the water-macromolecule interactions in the discontinuity in the mobility of polymer chain and probable location of the water molecules in the polymeric systems as observed by NMR studies. Molecular modeling also used for the study of the breaking and forming of the hydrogen bonds below and above the LCST of the PNIPAm.

5.2 Computational Details

5.2.1 Computational Method

The conformation of PAM and PNIPAm chain with different number of monomers varying from 10 to few hundreds were determined using the molecular force field method. The total energy of the system is expressed as in the following equation:

$$E_{total} = E_{bonded} + E_{non\text{-}bonded}$$

where,

$$E_{bonded} = E_{bond\ length} + E_{bond\ angle} + E_{dihedral}$$

and

$$E_{non\text{-}bonded} = E_{electrostatic} + E_{van\ der\ Waals}$$

Central Valance Force Field (CVFF) (Ermer 1976 & Hagler 1985) in the DISCOVER package supplied by Biosym/Molecular Simulations Inc., USA was used for the energy calculations. Molecular modeling of the polymer-water systems was carried out on Silicon Graphics Indigo^2 workstation.

The single chains of PAM and PNIPAm polymers with different number of monomers were constructed using INSIGHT II (1994) (Biosym/MSI, USA) as the computer graphics models. Further, their total energy values were minimized first by the Steepest Descent method to eliminate initial bad contacts and later by more accurate methods such as Conjugate Gradient and Newton-Raphson methods (Discover User Guide, 1994). Molecular dynamics (MD) simulations (Allen & Tildesley 1987) were carried out at micro-canonical ensemble level at 300K. Verlet algorithm (Verlet 1967) was used to solve the equations of

motion. Typical time step used in the MD simulations was 1fs (10^{-15} sec) and the calculations were carried out for 10,000 time steps. Thus the duration of the simulation is 10 ps (10x 10^{-12} sec).

Molecular modeling and molecular dynamics techniques are used to study the nature of the water-polymer interactions below and above the LCST in PNIPAm. Molecular dynamics (MD) simulations for PNIPAm was carried out at micro-canonical ensemble level at temperatures of 298K (below LCST) and 313K (above LCST) and same time step was used as that of PAM. The number of hydrogen bonds formed between polymer and water has been measured below and above the LCST.

5.3. Results and Discussion

Several interesting aspects of the observed mobility transition has been noted and discussed in Chapter III. The transition from a rigid lattice to a fluid like behavior occurs in a very narrow hydration range. The observed phenomenon is also a single step process, which does not go through any intermediate motional modes. The motions are clearly isotropic in nature, as otherwise hindered motions would leave the proton line widths at much larger values (~10-20 kHz) in the transition region. There is also a correspondence between the mid-point of the transition and the hydration threshold for the bound water limit. For most of the synthetic and bio-polymers, the functional groups that attract water have similar hydration numbers for the primary hydration shell and the bound water contents are uniformly similar at around 0.5-0.6 g/g in these systems which are discussed in Chapter III.

5.3.1 Modeling and Molecular Dynamics (MD) Calculations

5.3.1.1 PAM and PNIPAm models.

The vinyl amide and *N*-isopropylacryamide monomer units, which were used to build the PAM and PNIPAm polymers, are shown in Figure 5.1. Atactic (with 0.07% of

meso) single chain homopolymer (Miyoshi *et al* 1994) containing different number of monomers were built as computer graphics models. The initial orientation of the monomers were head to tail with a regular dihedral angle of 180 degrees. The conformations of these chains with different number of monomers, at their minimum energy values are shown in Figure 5.2a. The chain with 11 monomers is almost linear. However, the polymer chains with larger number of monomers clearly indicated a helical conformation for PAM (Figure 5.2a) and PNIPAm (Figure 5.2b and Figure 5.2c). In fact, the model with 11 monomers (Figure 5.2a(i)) is the linear part of the helix. A model with 51 monomers (Figure 5.2a(ii)) is typically a repeating unit in the helix. Since this model contains all the distinct features of an infinitely long single chain of PAM and PNIPAm, we have considered this model for the further studies to understand the interaction with water molecules. The validity of the choice of this model is further confirmed by building models with higher number of 101 and 151 monomers as shown in the (Figures 5.2a(iii) and 5.2a(iv) respectively) and by obtaining their energy minimized configurations.

5.3.3 PAM-Water and PNIPAm-water Interactions

The interaction of water with the model containing 51 monomer units for both the polymers was studied in detail. The polymer chain was soaked with different levels of water and the location and orientation of the water molecules were the equilibrium configuration derived from earlier MD simulations for liquid water, corresponding to 1g of water in a box with 1 cm^3 volume. A rectangular box was simulated which exactly fits the polymer chain model. Then the dimension of the box was extended in all directions by several and the extended volumes were soaked with liquid water. The thickness of water layer and the actual number of water molecules and the number of water molecules per monomer, from which g/g of solvent to polymer ratio could be calculated for PAM-water system and PNIAPm-water system are given in Table 5.1 and 5.2, respectively.

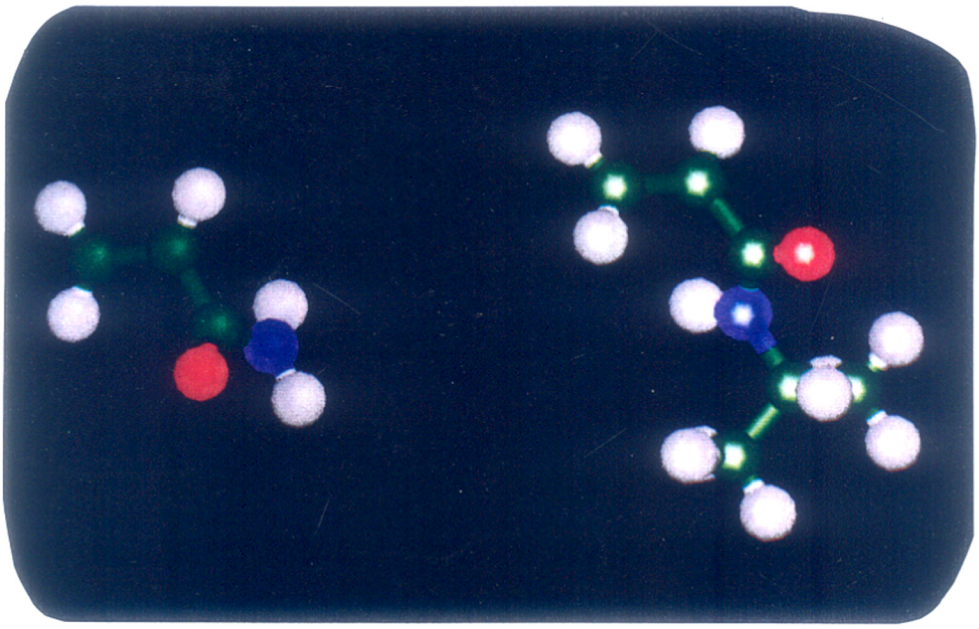

Figure 5.1: Minimum energy configuration of the monomer units for PAM and PNIPAm. (white - hydrogen; green - carbon; blue - nitrogen; red - oxygen).

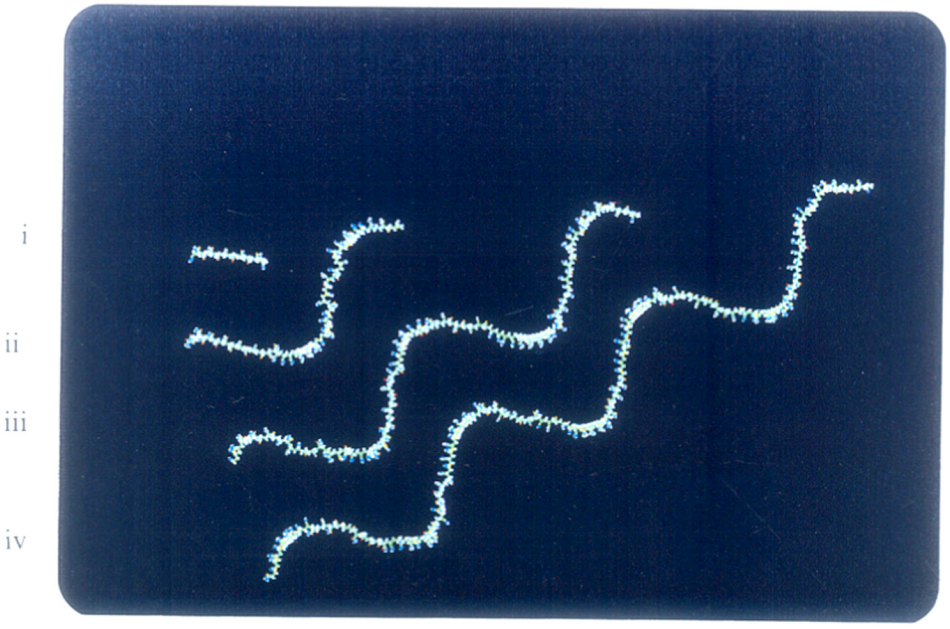

Figure 5.2a: Minimum energy conformation of PAM single chains containing (i) 11 monomers (ii) 51 monomers (iii) 101 monomers (iv) 151 monomers

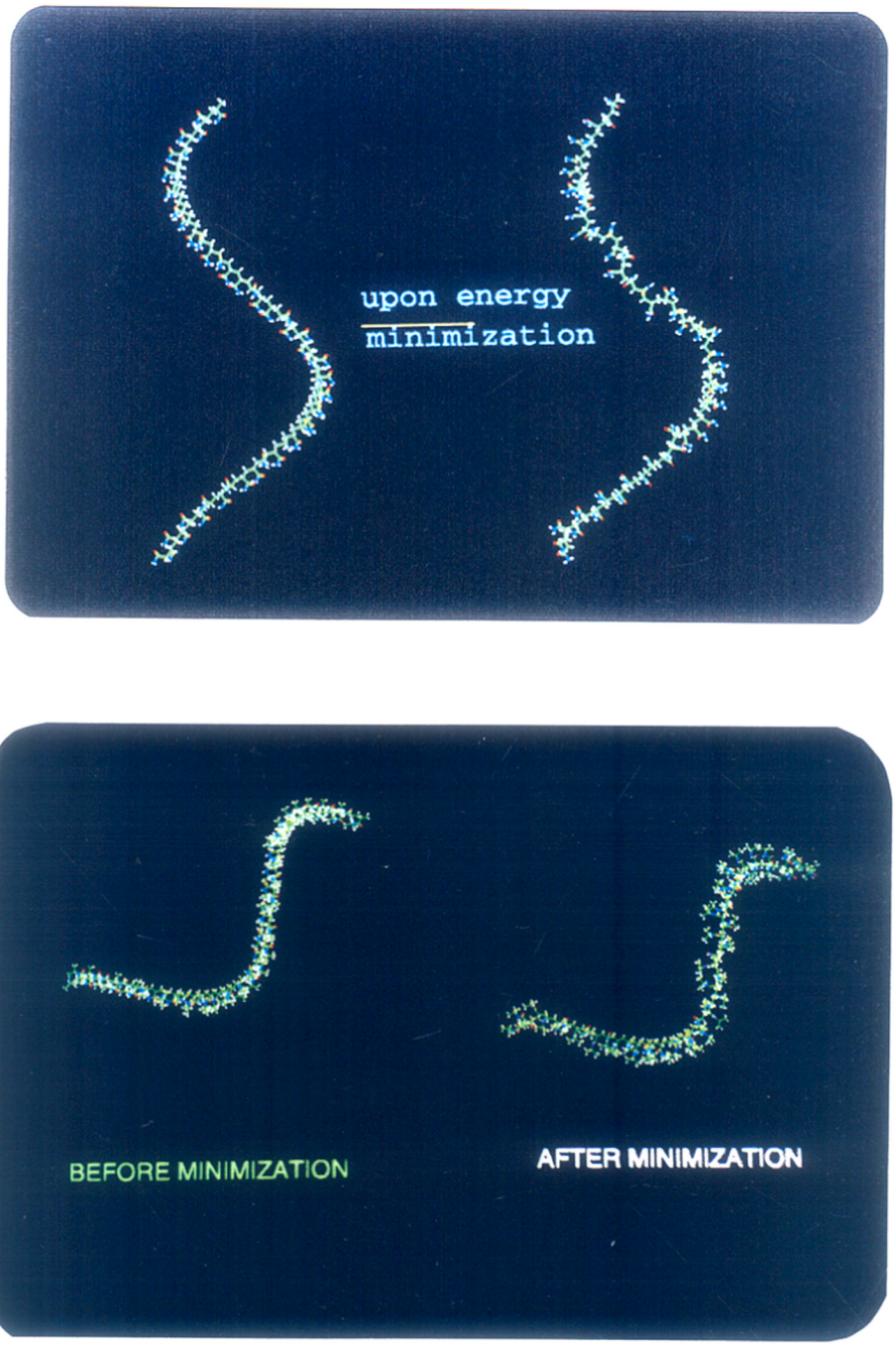

Figure 5.2b: Minimum energy conformation of PAM (above) and PNIPAm (below) single chains containing 51 monomers used in the molecular modeling and modeling dynamic studies.

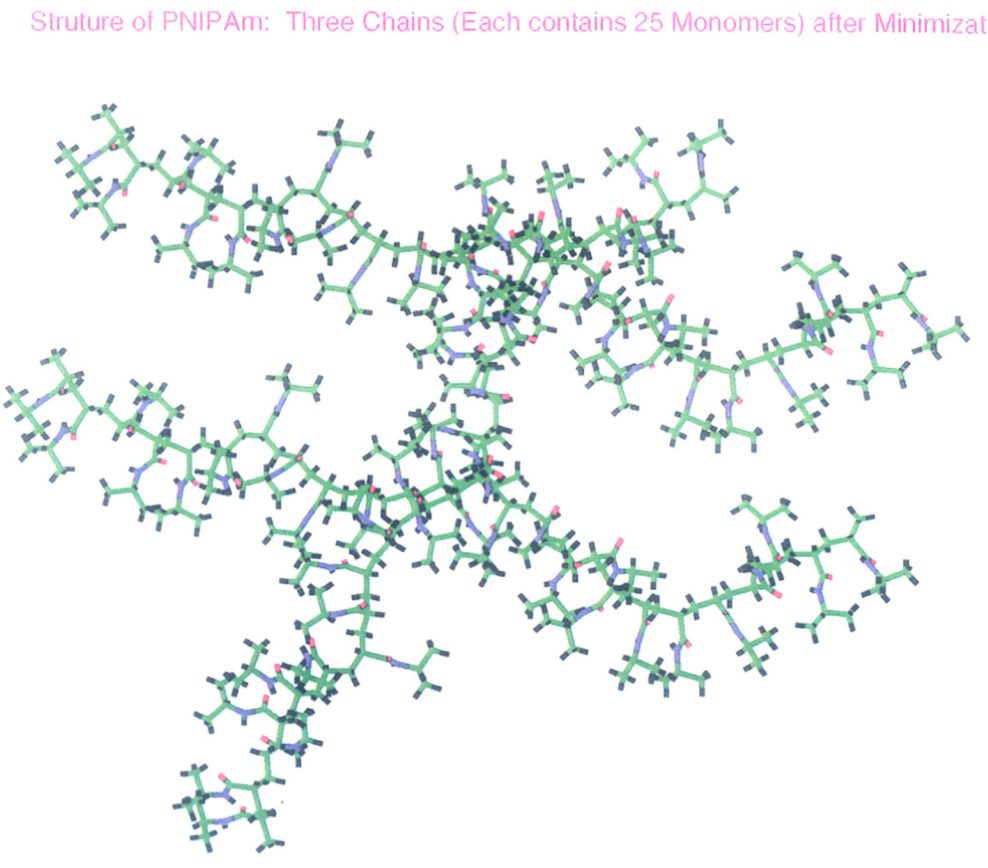

Figure 5.2c: Minimum energy conformation of PNIPAm three chains each containing 25 monomers used in the molecular modeling and modeling dynamic studies.

Table 5.1

The Results of PAM-Water Molecule Interaction Studies.

The Single chain Model of PAM (51 monomer residues)

Thickness of Water layer (A°) surrounding polymer where liquid water is included	Nil	1.50	2.00	3.00	4.00	5.00	6.00
Number of water Molecules	0	33	85	242	407	533	652
Water molecules per monomer	-	0.65	1.67	4.75	7.98	10.45	12.78
Energy for the favourable configuration (kcal/mol)	-739.00	-1047.61	-1565.58	-2515.19	-4171.57	-5495.36	-6671.92

Table 5.2

Results of PNIPAm-Water Interactions Studies.

The single chain Model of PNIPAm contains 51 monomers.

Thickness of water layer (A°) surrounding polymer where liquid water is included	Nil	Nil	2.00	2.00	3.00	3.00	5.00	5.00
Temperature of MD simulation (K)	298 (Below LCST)	313 (Above LCST)	298 (Below LCST)	313 (Above LCST)	298 (Below LCST)	313 (Above LCST)	298 (Below LCST)	313 (Above LCST)
Number of water molecules	0	0	121	121	297	297	781	781
Water molecules per monomer	-	-	2.37	2.37	5.82	5.82	15.31	15.31
Energy for the favorable configuration (kcal/mol)	-1873.56	-1764.46	-3815.58	-3450.59	-5076.78	-4722.26	-7559.30	-7423.94

Static energy minimization calculations were performed to locate the favorable positions for water molecules. The calculated energy is also tabulated in Table 5.1 and 5.2. It is clearly seen that the potential energy is increasing as a function of number of water molecules, as expected. However, the correlation of energy with the number of water molecules is featureless. Nevertheless, the positions of water molecules as observed from the molecular graphics pictures shown in Figure 5.3 (for PAM-water) at different levels of water concentration has brought out certain subtle changes in the polymer conformation and its volume.

In case of PNIPAm-water system we have also carried out the molecular modeling studies at different temperatures (e.g. 298K, 305K, 309K and 313K) on chain containing 51 monomers and 5 Å *i.e* 781 water molecules. The results are shown in the Table 5.3.

Table 5.3

Results of PNIPAm-Water Interactions Studies.

The single chain Model of PNIPAm contains 51 monomers and 781 water molecules at different temperatures

Temperature of MD simulation (K)	298	305	309	313
Number of water molecules	781	781	781	781
Energy for the favorable configuration (kcal/mol)	-7559.30	-7492.28	-7478.48	-7423.94

On the basis of molecular modeling and molecular dynamics studies on PAM and PNIPAm polymers following observations were made.

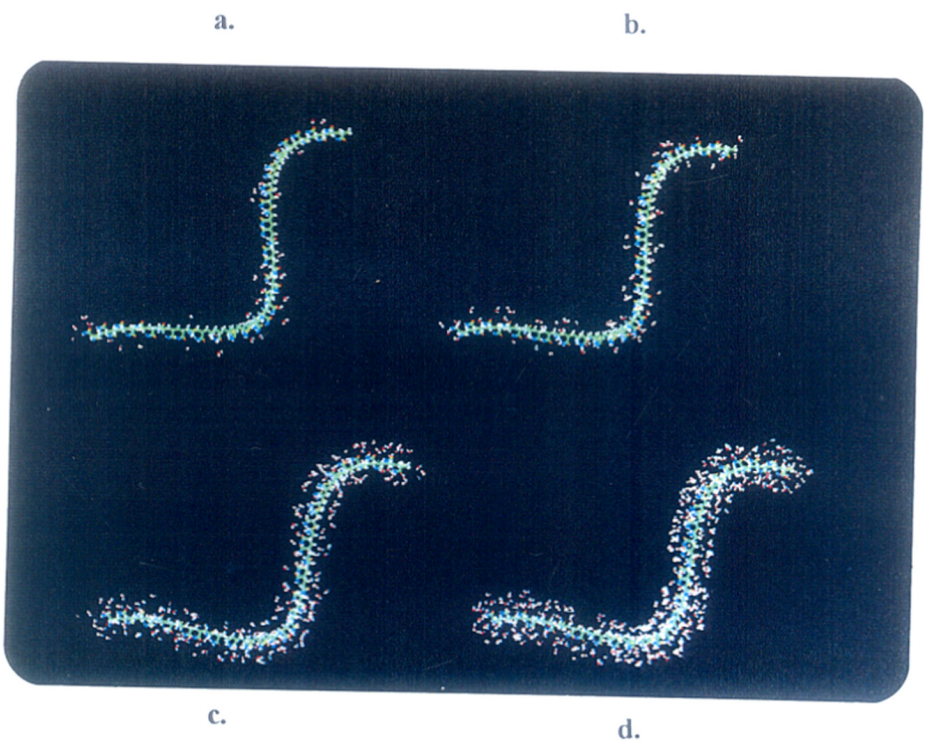

Figure 5.3: A single chain of PAM with 51 monomers soaked with different amount of water molecules. There is a clear distinction in the location of water molecules as well as the polymer chain conformation as the number of water molecules varied from 33(a), 85(b), 242(c) and 407(d).

1. Most of the bound water molecules were hydrogen bonded to the polar carbonyl and amine groups of both the polymer chains. In the helical conformation of the polymer chains, there were regions of 'linear' and the 'chain-turns', as can be seen from Figure 5.2. The hydrogen-bonded, bound water molecules were mostly on the chain-turns rather than the linear region of the chains.

2. When the number of water molecules increased from 33 (Figure 5.3a) to 85 (Figure 5.3b), in case of PAM polymer, the water molecules started to bound to the linear region of the molecules. The water bound to the linear region is found to cause distortion in the linearity of the chain, thus causing changes in the single chain conformation of the polymers. The consequent changes in the dynamics of both the polymer chains are discussed in the latter section.

3. The average distance between the carbonyl group of both the polymers and the water was measured. The distances were in the range of 2.5 to 4.5Å. The average distance was calculated and found to be 3.5 Å in the case of the PAM soaked with 85 and 242 water molecules. This distance between water and carbonyl group of PAM predicted by modeling was compared with the distance value (≈3.45Å) determined recently by Ganapathy, *et al* (1995) using Heteronuclear Overhauser NMR spectroscopy (HOESY). The model of PAM chosen for MD calculations is validated by the excellent agreement in PAM-water distances derived from modeling and HOESY technique. The location of water close to amide carbonyl was also seen by the analysis of the trajectory of the PAM-water system. This close location and interactions between amide carbonyl observed by us is also supported by recent quantum chemical calculations on amide-water systems (Scheiner & Wang 1993).

4. However, the average distance between carbonyl group of PNIPAm polymer and water was calculated and found to be 3.95 Å. This distance is slightly higher than that of PAM-water system. The possible reason may be the chemical nature of the polymers.

Here the PAM is more hydrophilic in nature while PNIPAm is more hydrophobic in nature.

5. From the MD calculations, it was observed that the above LCST the number of the hydrogen bonds formed between PNIPAm and water system are less as compared with the below LCST. At higher temperatures the polymer chain changes its conformation as well as the molecular motions in terms of the kinetic energy, which are responsible for the breaking of the hydrogen bonds between the polymer chain and water. At higher temperature polymer-water system would be in the high dynamic state. The molecular motions will be higher at higher temperature. This may cause the breaking of some hydrogen bonds between polymer-water system. This observation is well agreed with the results predicted by Lele *et al* (1995 & 1997) using the Lattice fluid hydrogen bond (LFHB) theory.

Molecular modeling studies show that water imposes constraints to the preferred conformations of the polymer chain. For a single chain, used in the present computational study, the bound water molecules show a regular orientation, while the farther water molecules are free from the interactions with the polymer. While the modeling of the single chain-water system do show that water organizes and folds the polymer main chain, the random orientation for distant water molecules may not be considered realistic. In an actual case, one must consider more than one chain, although the molecular modeling becomes too tedious. One might naively expect that these distant water molecules would see other polymer chains running by and would therefore interact with them to orientationally fold them in a manner we notice with the bound water here. It is therefore conceivable that a total picture of water interaction in linear PAM and PNIPAm systems is one in which all the water put into the system would interact with the polymer chains and reorient the chains.

5.3.4 Molecular Dynamics Studies of PAM-Water System

The four static model where the interaction of water with PAM studied (as shown in Figure 5.3). Among them two static models containing 85 and 282 water molecules was

further analyzed by MD simulations. The variation of total energy, potential energy and kinetic energy as a function of time was simulated. A visual analysis of a "movie" representing the MD trajectories of the polymer-water systems indicated random motions of water molecules. The dynamics of water molecules as well as polymer chain during the various steps of simulations are shown in Figures 5.4 and 5.5 for the PAM chain soaked with 85 and 242 water molecules, respectively. It can be observed from these, that with the progress of MD simulation, the PAM chain is getting more distortions leading to more number of "chain- turns" in a given chain.

As it has been observed earlier (Figure 5.3), the more number of chain turns will lead to higher amounts of bound water molecules. Thus, the concentration of water and the conformation of polymer chain have a symbiotic relation in causing a drastic increase in bound water. When the bound water/free water ratio increases, there is a dramatic increase in the rotational freedom of the amine group of the pendant. This was observed by the increase in the root mean square displacement of the hydrogens of the amino group. The volume of the PAM chain itself was decreasing (as shown in Table 5.4) with the progress of the MD simulation, while the volume of polymer-water system was increasing. Thus the MD simulations revealed quite drastic differences between the systems with less and more amounts of water.

5.3.5 Molecular Dynamics Studies of PNIPAm-Water System

Three static models at two different temperatures, i.e., at 298K (below LCST) and at 313K (above LCST) where the interaction of water with PNIPAm on single chain containing 51 monomers and three chains containing 25 monomers each, were studied (as shown in the Figure 5.6a and Figure 5.6b) and further analyzed by MD simulations. A visual analysis of a "movie" representing the MD trajectories (at two different temperature i.e. below LCST (298K) and above LCST (313K) temperature of PNIPAm) of the polymer-water systems indicated random motions of water molecules.

Table 5.4

Volume analysis of the PAM-Water system

(Volume x 10^5 Å) at different soaking level

Frame No.	33 water molecules	85 water molecules	188 water molecules	242 water molecules	313 water molecules
1	1.41	1.47	1.46	1.39	1.44
101	1.33	1.35	1.46	1.30	1.43
201	1.32	1.29	1.42	1.08	1.42
301	1.17	1.16	1.33	1.04	1.40
401	1.04	1.13	1.29	0.97	1.34
501	0.90	1.05	1.26	0.94	1.29
601	0.80	1.03	1.23	0.86	1.24
701	0.74	0.95	1.18	0.80	1.19
801	0.72	0.79	1.12	0.77	1.15
901	0.72	0.72	1.10	0.76	1.12
1001	0.71	0.69	1.10	0.72	1.11
1011	0.71	0.66	1.09	0.66	1.10

The dynamics of water molecules as well as polymer chain during the various steps of simulations are shown in Figures 5.7 and 5.8 for the PNIPAm chain soaked with 297 and 781 water molecules, respectively. It can be observed from these figures that with the progress of MD simulation, the PNIPAm chain is getting more distortions leading to more number of "chain- turns" in a given chain. The water molecules those bounded to the polymer chain show a regular orientation. However, at the higher temperature the water molecules goes away from the polymer chain are free from the interactions with the polymer and other water molecules are located around the pendant isopropyl groups of the PNIPAm polymer.

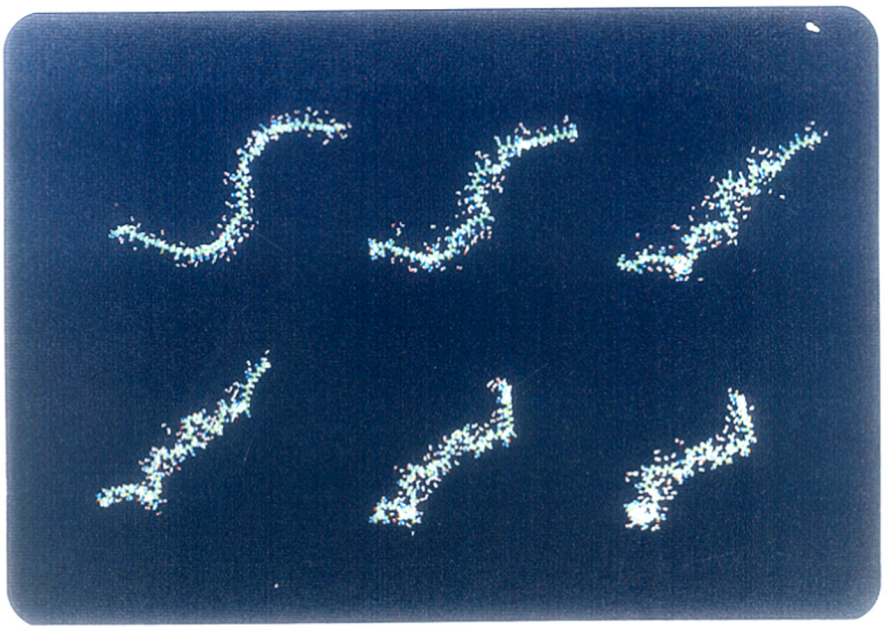

Figure 5.4: The snap shot pictures derived during the dynamics of PAM and 85 water molecules. The conformation of the single chain of polymer with 51 monomers and the structure of water molecules during the MD simulation after 0 step (a), 2000 steps (b), 4000 steps (c), 6000 steps (d), 8000 steps (e) and 10000 steps (f) are shown.

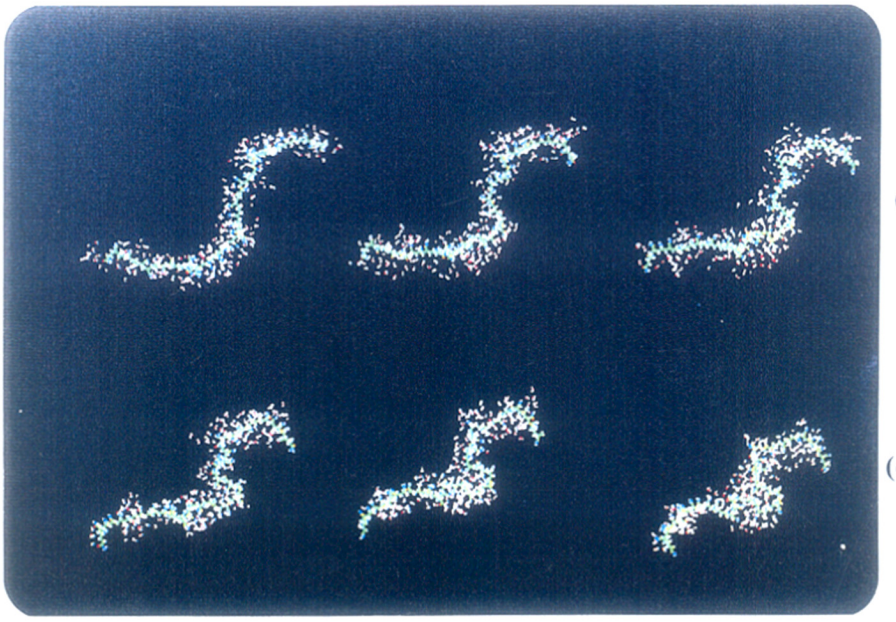

Figure 5.5: The snap shot pictures derived during the dynamics of PAM and 242 water molecules. The conformation of the single chain of polymer with 51 monomers and the structure of water molecules during the MD simulation after 0 step (a), 2000 steps (b), 4000 steps (c), 6000 steps (d), 8000 steps (e) and 10000 steps (f) are shown.

We have analyzed MD trajectories of the single and three chains of PNIPAm polymer at both the temperatures (*i.e.* below and above the LCST) for further understanding the polymer-water interactions. The results of the three chains each containing 25 monomer units and 1048 water molecules are shown in the Figure 5.9 and the corresponding energy changes are given in the Table 5.5. It can be observed from MD simulation studies that the polymeric chain are getting more distortions and undergoes the conformation changes at different temperatures. It is also observed that the length of the helical chain of both the polymers get further affected by the temperature. We also carried out calculations on the number of hydrogen bonds between polymer chain and water at above and below LCST. Here we found that above the LCST the number of hydrogen bond is less as compared with the number of hydrogen bond at below the LCST. The hydrogen bonding data between the water molecules and PNIPAm polymer has been summarized in Table 5.6. The present MD calculations of hydrogen bonding below and above LCST of PNIPAm polymer well agreed with the LFHB theory (Lele *et al* 1995).

Table 5.5

Results of PNIPAm-Water Interactions Studies.
Three chain Model of PNIPAm (Each Chain Contains 25 monomers).

Thickness of water layer (A^0) surrounding polymer where liquid water is included	Nil	Nil	5.00	5.00
Temperature of MD Simulation (K)	298	298	298	313
Number of water molecules	0	0	1048	1048
Water molecules per monomer	-	-	15.31	15.31
Energy for the favorable configuration (kcal/mol)	-1739.00	-1682.82	-5155.47	-4428.56

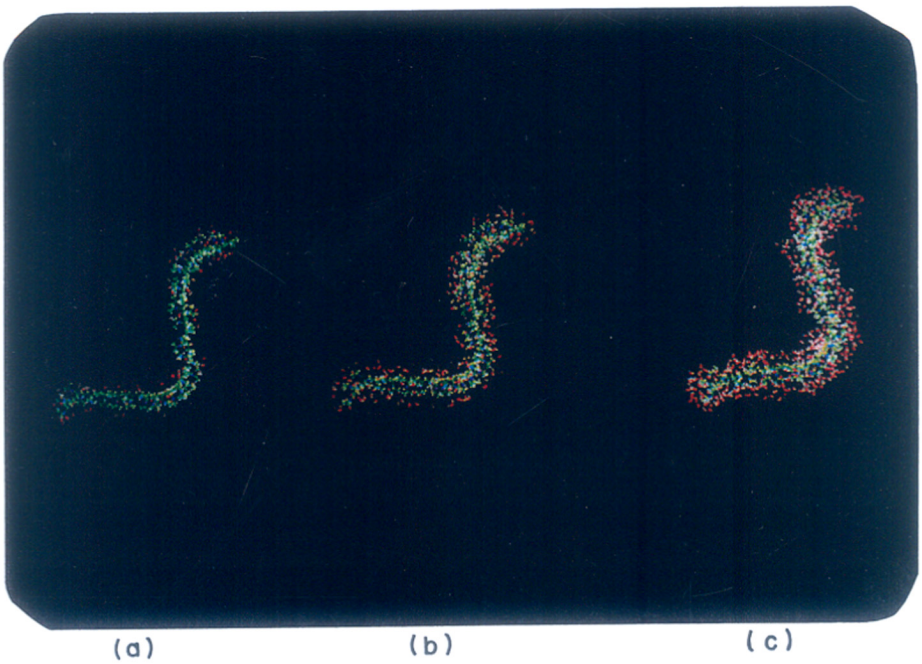

Figure 5.6a: A single chain of PNIAPm with 51 monomers soaked with different amount of water molecules. There is a clear distinction in the location of water molecules as well as the polymer chain conformation as the number of water molecules varied from (a) 121, (b) 297 and (c) 781.

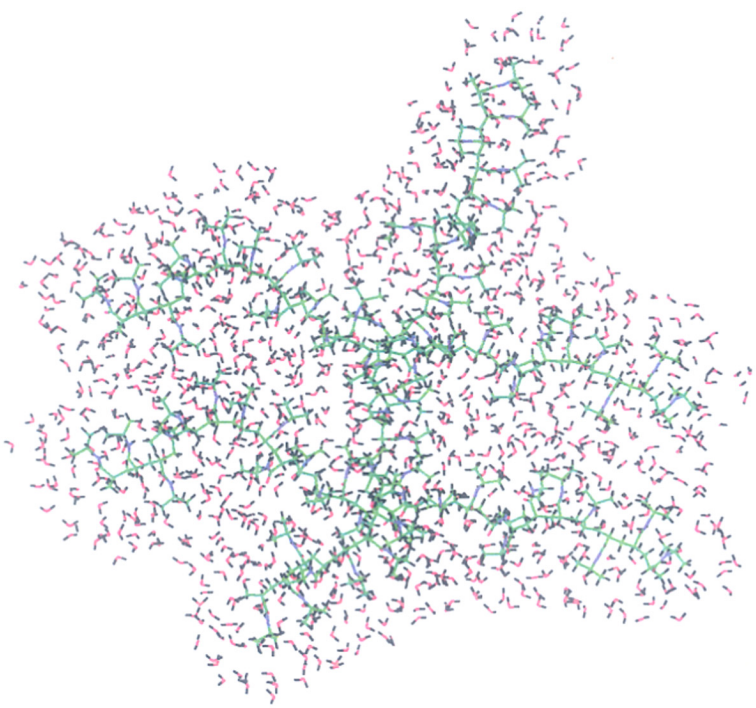

Figure 5.6b: Three chains of PNIPAm with (each chain contains) 25 monomers soaked with 1048 water molecules.

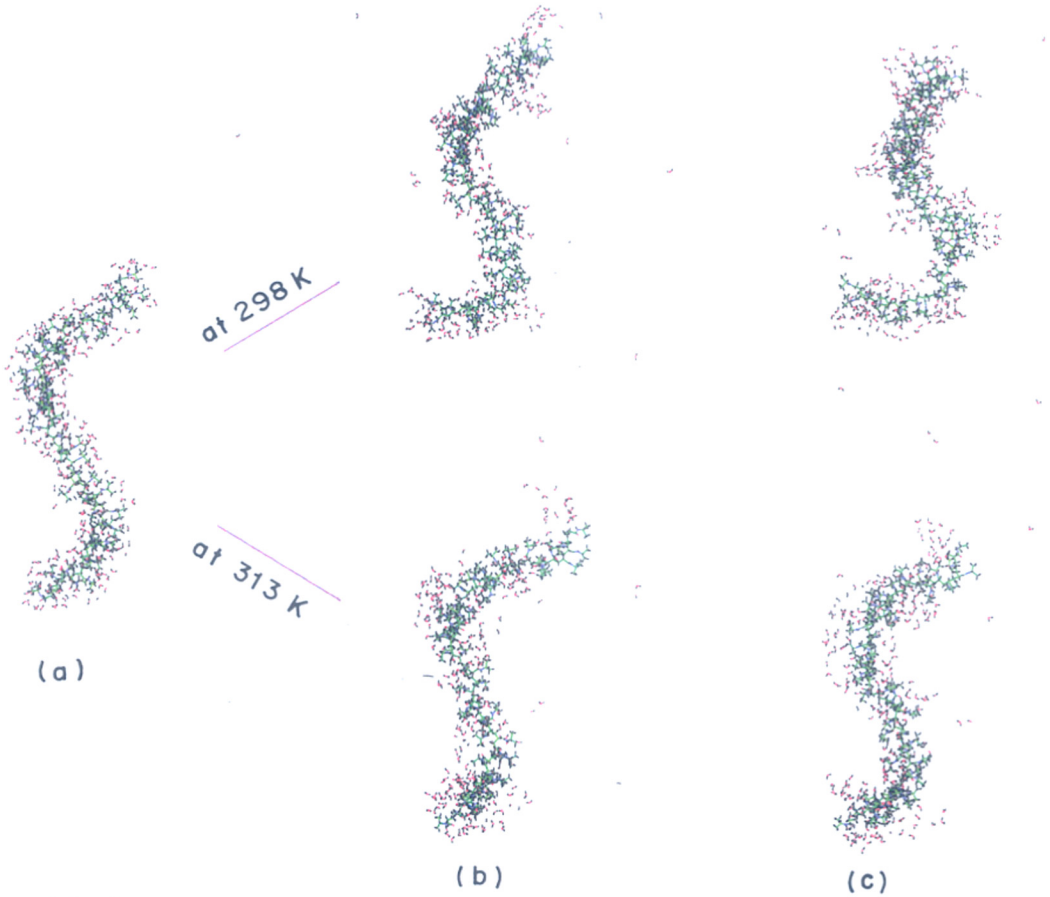

Figure 5.7: The snap shot pictures derived during dynamics of PNIPAm and 297 water molecules. The conformation of single chain of PNIPAm with 51 monomers and structure of water molecules during the MD simulation at 298K (Below LCST) and at 313K (Above LCST) after (a) 0 steps, (b) 5000 steps and (c) 10,000 steps are shown.

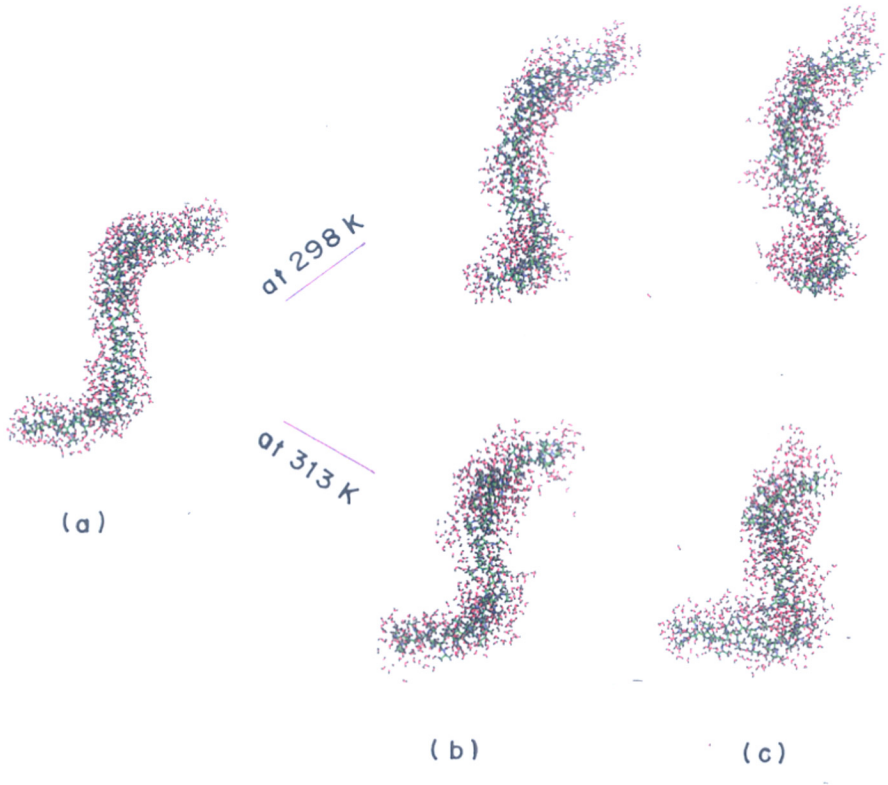

Figure 5.8: The snap shot pictures derived during dynamics of PNIPAm and 781 water molecules. The conformation of single chain of PNIPAm with 51 monomers and structure of water molecules during the MD simulation at 298K (Below LCST) and at 313K (Above LCST) after (a) 0 steps, (b) 5000 steps and (c) 10,000 steps are shown.

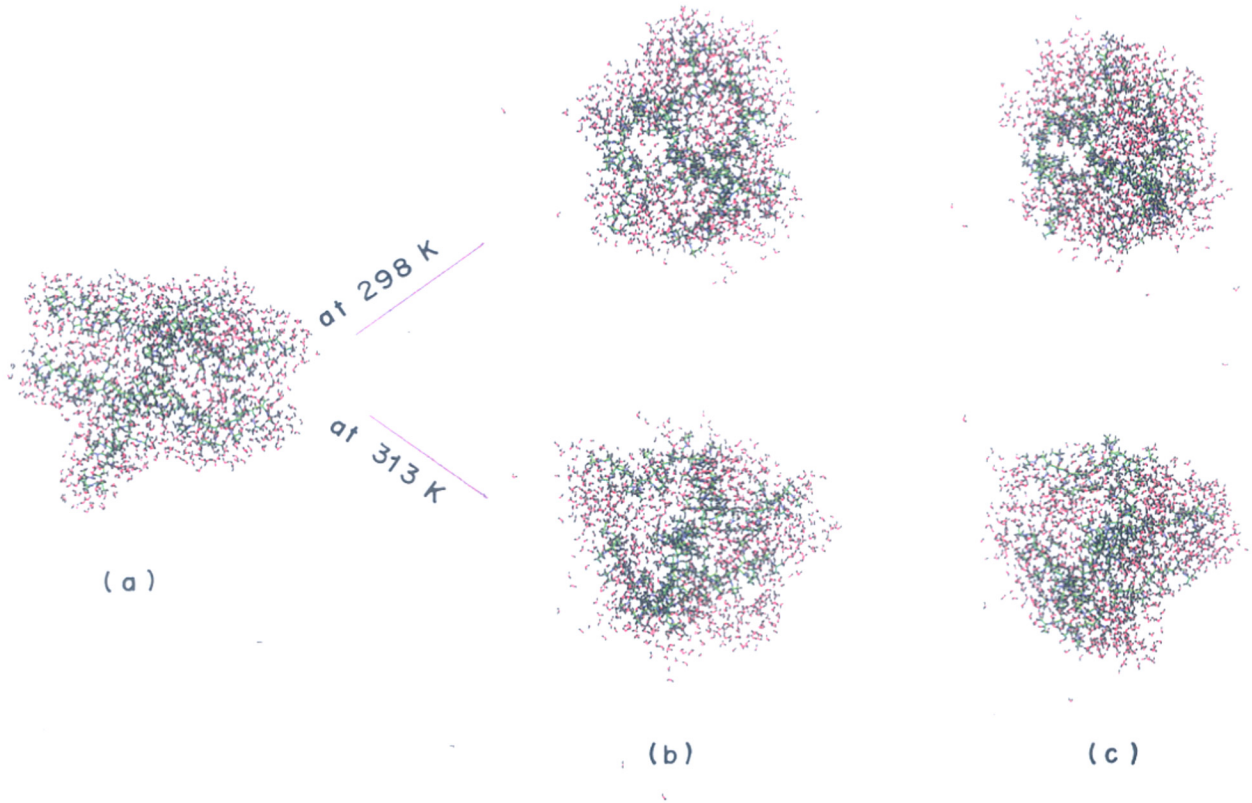

Figure 5.9: The snap shot pictures derived during dynamics of PNIPAm and 1048 water molecules. The conformation of three chains of PNIPAm with 25 monomers each and structure of water molecules during MD simulation at (A) 298K (Below LCST) and at (B) 313K (Above LCST) during the MD calculations after (a) 0 steps, (b) 5000 steps and (c) 10.000 steps.

Table 5.6

Hydrogen bond calculations between Water and PNIPAm below and above LCST

Sr. No.	Name of the Theory	Molecular Weight	No. of Hydrogen bonds between Water and polymer	
			Below LCST	Above LCST
1	**LFHB**	10,000 (6000)	140 84	100 60
2	**Molecular Dynamics** a) Single chain containing 51 Monomers b) Three chains containing 25 Monomers	6000 5177	77 80	59 64

5.4. Concluding remarks

Mobility transition occurring in the very early levels of hydration has been detected and demonstrated for the first time in PAM and PNIPAm-water systems. Molecular mobility is shown to occur through an isotropic averaging process for the proton-proton dipolar interactions. The molecular modeling and molecular dynamics calculations for a linear polymer indicate the influence of water molecules on the single chain conformation of the polymer. The interaction of water with the single chains of these two polymers is maximum at the chain-turns and the interactions with linear region lead to distortion of the chains. These conformational changes of the polymer chains allow further uptake of the water into the polymer network. Thus the close relation between the single chain conformation and the orientation of water molecules around it are brought out by these studies and the mechanism of the water uptake is also revealed. The existence of similar mechanism is expected in the cross-linked polymer, which can also be studied using these techniques. The average distance of 3.5 Å between the carbonyl group of PAM and water

bound to that, predicted by MD studies are in good agreement with that reported by earlier NMR studies. The average distance between carbonyl group of PNIPAm and water bound to it was calculated and found to 3.95Å. Our MD calculation below and above LCST of PNIPAm-water system and the quantitative analysis of hydrogen bonds support the predictions of the LFHB theory.

5.5. References

Allen, M.P. and Tildesley, D.J., in: "Computer Simulation of Liquids", Clarendon Press, Oxford Science Publications, Oxford., (1987).

Berendson, H.J.C., in: "Water. A Comprehensive Treatise", Franks, F. (Ed.), Vol.**5**, p.293, Plenum Press, New York (1975).

Bryant, R.G., Stud. Phys. Theor. Chem., **38**, 683, (1988).

Dagani, R. Chemical and Engineering News, **75**, 26, (1997).

Discover User Guide, version 2.9.5/94.0. San Diego: Biosym Technologies, (1994).

Dong, L.C. and Hoffman , A.S., Reversible Polymeric Gels and Related Systems, P.S. Russo (Ed.) ACS Symp. Series, **350**, 236, ACS, Washington DC, (1987).

Ermer, O., Structure and Bonding, **27**, 161, (1976).

Ganapathy, S., Ray, S.S., Rajmohanan, P.R. and Mashelkar, R.A., J. Chem. phys., **103**, 6783, (1995).

Hagler, A.T. in: "The peptides", J. Meienhofer (Ed.), Academic Press, New York, 213 (1985).

Hansch, C. and Klein, T.E., Methods in Enzymology, Langone, J.J. (Ed.), **202**, 512, (1994).

Hoffman A.S., Afrassiabi, A. and Dong, L.C., J. Controlled Release, **4**, 213, (1986).

Insight II User Guide, version 2.3.0. San Diego: Biosym Technologies, (1994).

Katayama, S., Kazama., S. and Yoshioka, H., J. Phys. Chem. **96**, 2023, (1992).

Kulicke, W.M., Kniewske, R. and Klein, J., Prog. Polymer Sci., **8**, 373, (1982).

Lele A.K., Badger M.V., Hirve, M. M. and Mashelkar, R.A., Chem.Engg.Sci., **50**, 3545, (1995).

Lele A.K., Devotta, I. and Mashelkar, R.A., J. Chem Phys. **106**, 4668, ((1997).

Marchelli M., Prager,S. and Cussler, E.L., Macromolecules, **23**, 1760, (1990).

Marchelli M., Prager,S. and Cussler, E.L., Macromolecules, **23**, 3445, (1990)

Miyoshi, P., Takegoshi, K. and Hikichi, K., Polymer J., **26**, 485, (1994).

Molyneux, P., "Water soluble synthetic polymers" ; Properties and behaviour, vol **1** CRC press. p 84, (1984).

Molyneux, P., in: "Water. A Comprehensive Treatise", Franks, F. (Ed.), 1974, Vol.**4**, p.569, Plenum Press, New York (1974).

Ohta, H., Ando, I., Fugishige, S., and Kubota, K. J. Mol. Struct. **245**, 391, (1991).

Olson, W.K. and Zhang, P., "Methods in Enzymology", Langone, J.J. (Ed.), **203**, 403, (1995).

Otake, K., Inomata, H., Konno, M and Saito, S., J. Chem. Phys., **91**, 1345, (1989).

Panayiotou , C.G. and Sanchez, I.C. J. Phys. Chem., **95**, 10090, (1991).

Prange M.M., Hopper, H.H. and Prausnitr, J.M., AIChE, J., **35**, 803, (1989).

Rowland, S.P. (Ed.) "Water in Polymers," ACS Symp. Series, 127, American Chemical Society Washington, D.C. (1980).

Rupley, J.A. and Careri, G., Adv. Protein Chem., Anfinsen, C.B., Edsall, J.T., Richards, F.M. and Eisenberg, D.S., (Eds.), **41**, 38, Academic Press, New York, (1991).

Scheiner, S. and Wang, L., J. Am. Chem. Soc., **115**, 1958, (1993).

Schild. H.G. and Tirrel, D. A., Macromolecules **25**, 4553, (1992).

Schild. H.G., Progress in Polymer Science, **17**, 163, (1992).

Tamai, Y., Tanaka, H. and Nakanishi, K., Macromolecules, **29**, 6750, (1996).

Tokuhiro, T., Amiya, T., Mamada, A. & Tanaka, T., Macromolecules **24**, 2936 (1991).

Verlet, L. Phys. Rev., **159**, 98, (1967).

Zaks, Aleksey and Klibanov, Alexander M. Science, 149, (1984).

Polymeric gels that respond to stimuli, such as temperature, electric field, pH, solvent composition, etc., have been studied by one or two-dimensional NMR spectroscopic techniques. The elementary application of proton line width measurements to depict the mobility transitions at early levels of hydration has been introduced and discussed in Chapter III. The application of 2-D NMR spectroscopy for studying the state of water and the motionally averaged polymer has been demonstrated and fully discussed in Chapter IV. Water-polymer interactions and probable location of water in the polymer have been studied by molecular modeling and molecular dynamics technique and discussed in Chapter V. This chapter is devoted to the application of Magnetic Resonance Imaging (MRI) technique to study the stimuli response in a hydrogel. Specifically, the imaging technique has been used in the study of volume phase transition, induced by temperature, in the LCST polymer PNIPAm.

6. Introduction

Although, modern NMR spectroscopic methods have been used in the studies on gels by the NCL group (Ganapathy *et al* 1990, Rajamohanan *et al* 1995, Ganapathy *et al* 1992), as well as other groups (Cohen Addad 1993, Yokota *et al* 1978, Yasunaga *et al* 1997, Pop *et al* 1996 and Gladden 1994), including the LCST phenomenon in PNIPAm (Badiger *et al* 1991, Ganapathy *et al* 1994, Tokuhiro *et al* 1991), Magnetic Resonance Imaging (MRI) experiments to study the LCST phenomenon in a polymer gel have not been conducted so far. Imaging experiments have been used earlier to monitor the solvent penetration profiles in rubbery and glassy polymers (Yasunaga *et al* 1997, Koening 1991, Blumich & Blumer 1993, Parker & Koening 1996, Webb & Hall 1991, Hyde & Gladden 1995 & 1998) and in the study of strained elastomers (Blumer & Blumich 1997). Polymeric gels under equilibrium swollen conditions do not exhibit macroscopic spatial heterogeneity due to the intricate molecular level mixing of polymer and water domains, and, naturally, they would appear to discount the use of MRI for a study. However, as we show in the present study, MRI can provide valuable information

on gels that respond to stimuli, since the dynamical behavior of polymer and water components occur at different motional timescales. This allows us to exploit and use associated dynamical parameters such as spin-lattice (T_1) and spin-spin (T_2) relaxation times and self-diffusion coefficient (D_{self}) for an image weighting. Experimental demonstration of the applicability of proton imaging to study volume phase transition in the LCST polymer PNIPAm is provided and discussed.

6.1. Basic Principles of Magnetic Resonance Imaging

NMR spectroscopy deals with experiments conducted in a highly homogeneous static magnetic filed. In a well shimmed magnet, identical nuclei (e.g., protons) in identical environments (e.g., water) experience the same magnetic field B_0 and hence the same Larmor frequency, given by

$$\omega_o = 2\pi\nu_o = \gamma B_o \qquad (6.1)$$

where, γ is the magnetogyric ratio of the nucleus. However, when nuclei experience different environments, the magnetic field is not of the same value at each chemically distinct environment. This manifests itself as discrete signals at various chemical shifts. This is the basis for elucidating the molecular structure and hence the homogeneity of the magnetic field is of paramount importance. Since the magnetic field is very homogeneous, signature about the spatial localisation of the observed spins in a macroscopic object is not carried.

The spatial localization of the nuclei can not be obtained in a homogeneous static magnetic field B_o, since the resonance frequency is the same, being independent of the position (x, y, z). Here, x, y, z correspond to the spatial coordinates which describe the location of the point in the object with reference to a cartesian frame. It was discovered at the beginning of the 1970's that spatially resolved NMR can be realised when a time dependent linear magnetic field gradient $\mathbf{G}(\mathbf{r}, t)$ is superimposed on $\mathbf{B}_o$, *i.e.*

$$\mathbf{B}(\mathbf{r}, t) = \mathbf{B}_o + \mathbf{G}(\mathbf{r}, t) \tag{6.2}$$

Since the applied gradient is linear in the coordinate variable x, y, z, it implies that the field gradient $\mathbf{G}(\mathbf{r}, t)$ has a linear dependence on the position. Since the resonance frequency is proportional to the magnetic field, a linear relationship between the resonance frequency and the spatial position $\mathbf{r}$ can be established through the relation

$$\nu(\mathbf{r}, t) = (\gamma/2\pi)\, \mathbf{B}(\mathbf{r}, t) \tag{6.3}$$

The contribution made by each component of the gradient field $\mathbf{B}_o + \mathbf{G}(\mathbf{r}, t)$ is determined by the spatial derivative of the gradient field. The field gradient has a tensorial representation having nine components, as given below

$$\text{Grad } \mathbf{G}(\mathbf{r}, t) = \begin{pmatrix} \partial Bx/\partial x & \partial Bx/\partial y & \partial Bx/\partial z \\ \partial By/\partial x & \partial By/\partial y & \partial By/\partial z \\ \partial Bz/\partial x & \partial Bz/\partial y & \partial Bz/\partial z \end{pmatrix} \tag{6.4}$$

Since $\mathbf{B}_o$ is usually much larger (7 T), while the gradients are much smaller (*ca.* 1 mT), components perpendicular to $\mathbf{B}_0$ may be neglected, so that components parallel to $\mathbf{B}_0$ are to be considered for the spatial dependence of the resonance frequency. This allows us to write for the tensor components that have an influence on the resonance frequency as

$$g_x = (\partial Bz/\partial x) \tag{6.5}$$

$$g_y = (\partial Bz/\partial y) \tag{6.6}$$

$$g_z = (\partial Bz/\partial z) \tag{6.7}$$

An inspection of Equations (6.5 – 6.7) at once suggests that these are nothing but the cartesian components of the field gradient vector **g**.

The positional dependence of the Larmor frequency may be written as

$$\mathbf{B}(x, y, z) = \mathbf{B}_o + \mathbf{G}(x, y, z) \tag{6.8}$$

$$\mathbf{B}(x, y, z) = \mathbf{B}_o + \mathbf{g}\,\mathbf{r} \tag{6.9}$$

The spatial dependence of the resonance frequency is given by

$$\omega(\mathbf{r}) = \omega_0 + \gamma\,\mathbf{g}\,\mathbf{r} \tag{6.10}$$

which leads to the spread of frequencies as

$$\Delta\omega = \gamma\,\mathbf{g}\,\Delta\mathbf{r} \tag{6.11}$$

The distribution of the gradient field and their effect on the nuclear resonance is shown in Figure 6.1.

It may be noted from Equation (6.11), that the spatial resolution one can obtain in an imaging experiment is directly proportional to the magnitude of the applied gradient $|g|$ and the dimensions of the object $\Delta\mathbf{r} = (\Delta x, \Delta y, \Delta z)$. Thus, conducting pulse NMR experiments in the presence of linearly varying static field gradients, suitably applied during the pulse sequence, constitutes the basic experimental scheme for the imaging of a macroscopic object.

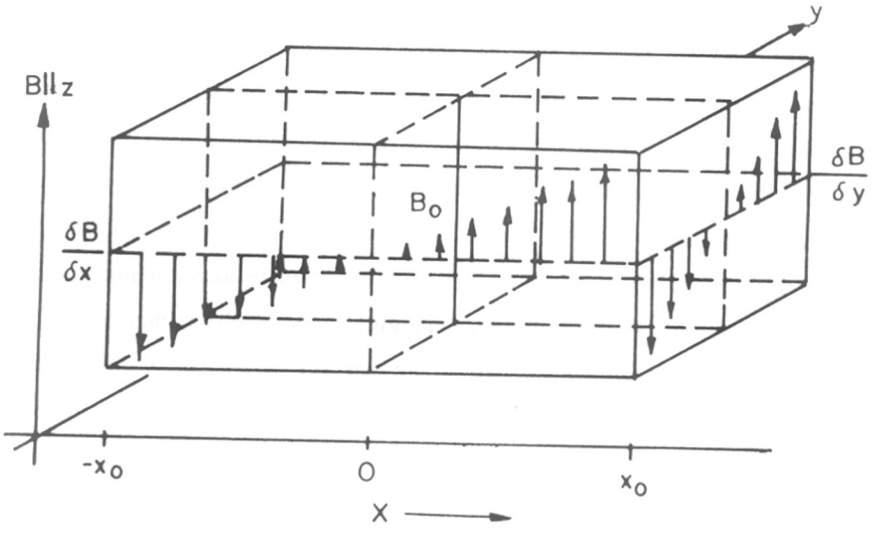

Figure 6.1: A schematic representation of the three-dimensional distribution of the gradient field $\mathbf{G}(r)$ ($= \mathbf{g}\,\mathbf{r}$). The gradient fields change linearly over the sample volume. For $-x_0,-y_0,-z_0 < x,y,z < 0$, the magnetic field B_0 is reduced due to the gradient field $\mathbf{G}(r)$ and for $0 < x,y,z < -x_0,-y_0,-z_0$, the magnetic field is strengthened. With respect to the Larmor frequency (ω_0) resonance condition, the resonance frequency in the left half of the cube volume is lower, while in the right half it is higher.

6.1.1 Spin-echo Imaging Sequence

The pulse sequence employed in the imaging experiment is based on the Hahn spin-echo pulse sequence in the presence of x, y, z gradients, as shown in Figure 6.2. The 90^{o} transmitter pulse at the very beginning of the sequence excites all the spins within the object contained in the r.f coil. The transverse magnetization so created then precesses under the influence of the applied gradients G_x and G_y. G_x and G_y have an exactly defined amplitude and duration. G_y is the incremented phase-encoding gradient and occurs simultaneously with the other in-plane gradient G_x. The amplitude of G_y is changed from experiment to experiment during the 2-D run and the spatial information in the first dimension is encoded by the application of the read-gradient in the x-direction. This gradient rephases the magnetization dephased by the initial dephasing x-gradient so that a spin-echo is formed in the middle of the acquisition window. In the 2-D imaging experiment, slice selection is achieved by a resonant r.f pulse having a flip angle of 180^{0} and a defined bandwidth $\Delta\omega$ in the presence of the z-gradient, which is normal to the selected slice. Using a *sin (x)/x* modulation for the r.f (sinc shape), a slice of thickness $\Delta z = \Delta\omega / (\gamma g_z)$ can be selectively excited.

6.2. Experimental Details

The proton imaging experiments were performed on a Bruker MSL-300 FT-NMR spectrometer operating at the proton Larmor frequency of 300.13 MHz. The spectrometer is equipped with a Bruker Micro-imaging unit (40 Gauss/cm) and a dedicated imaging probehead. A salient hardware feature of the micro imaging unit is already given in Chapter II. An imaging insert of 15mm was used. The image acquisition was carried out using the spin-echo technique (Callahan 1991) discussed in the previous section. A sinc shaped r.f pulse in the presence of z-gradient was used for slice (1 mm) selection. For the acquisition of one-dimensional proton spin density profiles of a chosen slice, the phase encoding was switched off and the spin-echo experiment conducted by varying the read gradient only.

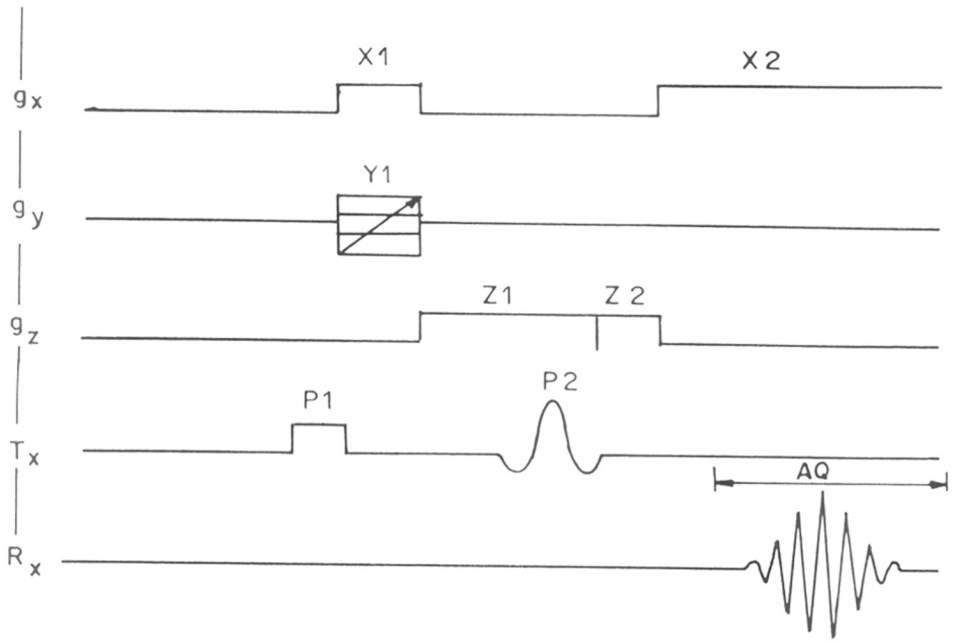

Figure 6.2: The spin-echo imaging sequence with x, y and z gradients, which is used for the proton imaging of PNIPAm gel. P1 is the 90^0 degree broad band pulse, while P2 pulse is a sinc shaped slice-selective 180^0 pulse. The amplitude of the gradient Z1 and the bandwidth of the *r.f* pulse determine the thickness of the selected slice. The amplitude of gradient X2 determines the in-plane resolution. The amplitude of Y1 changes in the course of a two-dimensional imaging sequence by the increment ΔY1. T_X represents the transmitter channel (proton) and R_X represents the receiver channel. The P1 pulse is phase cycled +X, -X to compensate the receiver d.c offset.

The spin system was preconditioned for relaxation (T_1, T_2) and diffusion (D_{self}) weighting by incorporating the appropriate pulse schemes, prior to slice selection (as shown in the Figure 6.3, Figure 6.4 and Figure 6.5). The temperature of the gel was precisely controlled using a Bruker BVT-1000 controller. PNIPAm was synthesized by polymerizing *N*-isopropylacrylamide monomer using ethylene glycol dimethacrylate as a cross-linking agent and azo-*bis*-isobutyronitrile as an initiator (Ray *et al* 1998) and its equilibrium swelling capability and LCST temperature were measured as discussed in Chapter III. It was found to have 8 g/g (gram of water per gram of dry polymer) swelling capacity and 32°C LCST temperature.

6.3. Results and Discussion

We show in Figure 6.6 the comparison of planar proton images of PNIPAm gel in its equilibrium swollen state (22°C, below LCST,) and collapsed state (40°C, above LCST). These images, as well as others, were obtained on a swollen gel cast as a uniform cylinder of diameter 12 mm and positioned centrally in a glass tube (15 mm outer diameter) containing water. The collapse of the gel is noticed as decreased circular cross-sectional area (Figure 6.6). The LCST transition is more precisely depicted through one-dimensional image profiles, as demonstrated in Figure 6.6. Since the applied gradient varies linearly, the one-dimensional projection of proton spin density from the excited slice of a cylindrical gel is semi-circular (Figure 6.7 A, left). However, to distinctly monitor the LCST transition of PNIPAm gel, we have used a T_2 weighting scheme at the beginning of the pulse sequence to distinguish the one-dimensional image profile due to polymeric gel in the middle (Figure 6.7 A, right) from the overall profile (Figure 6.7 A, right). This aid in the clear depiction of the volume phase transition in PNIPAm (Figure 6.7 B).

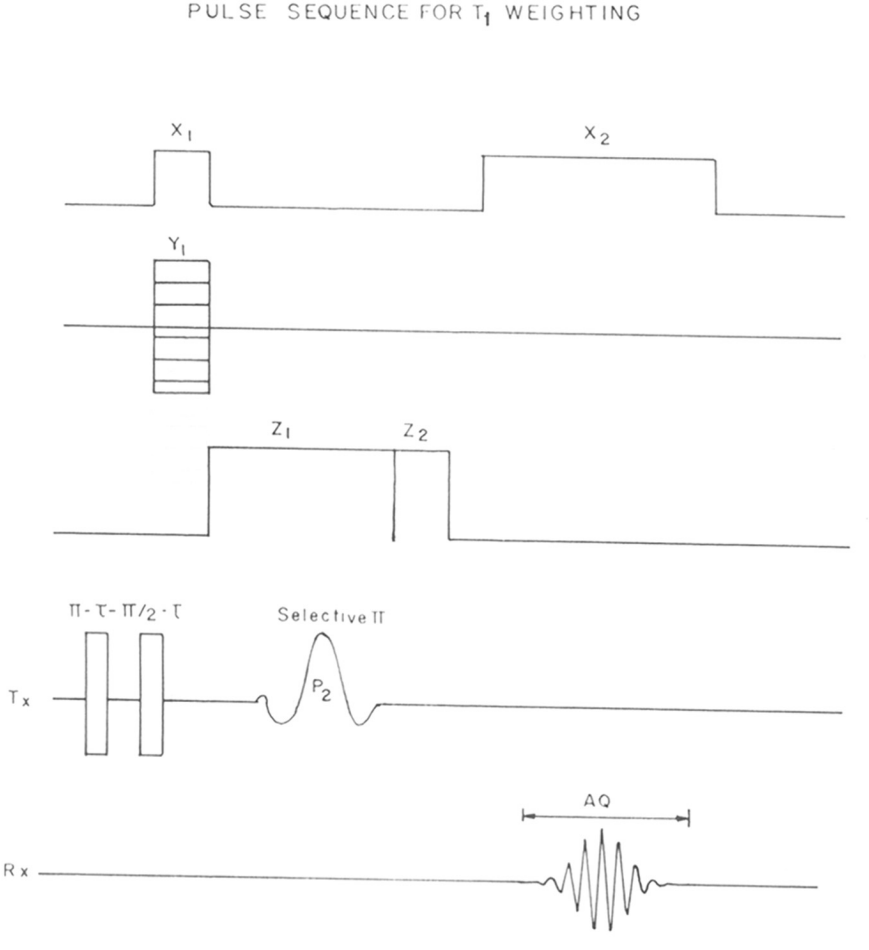

Figure 6.3: T_1 weighted single slice image pulse sequence obtained by pluging in the standard inversion recovery pulse sequence prior to the slice selection, to the single slice imaging sequence given in Figure 6.2. The τ_{null} of water was estimated separately by the inversion recovery T_1 measurement at a set temperature. This value of τ_{null} was employed in the pulse sequence (see text).

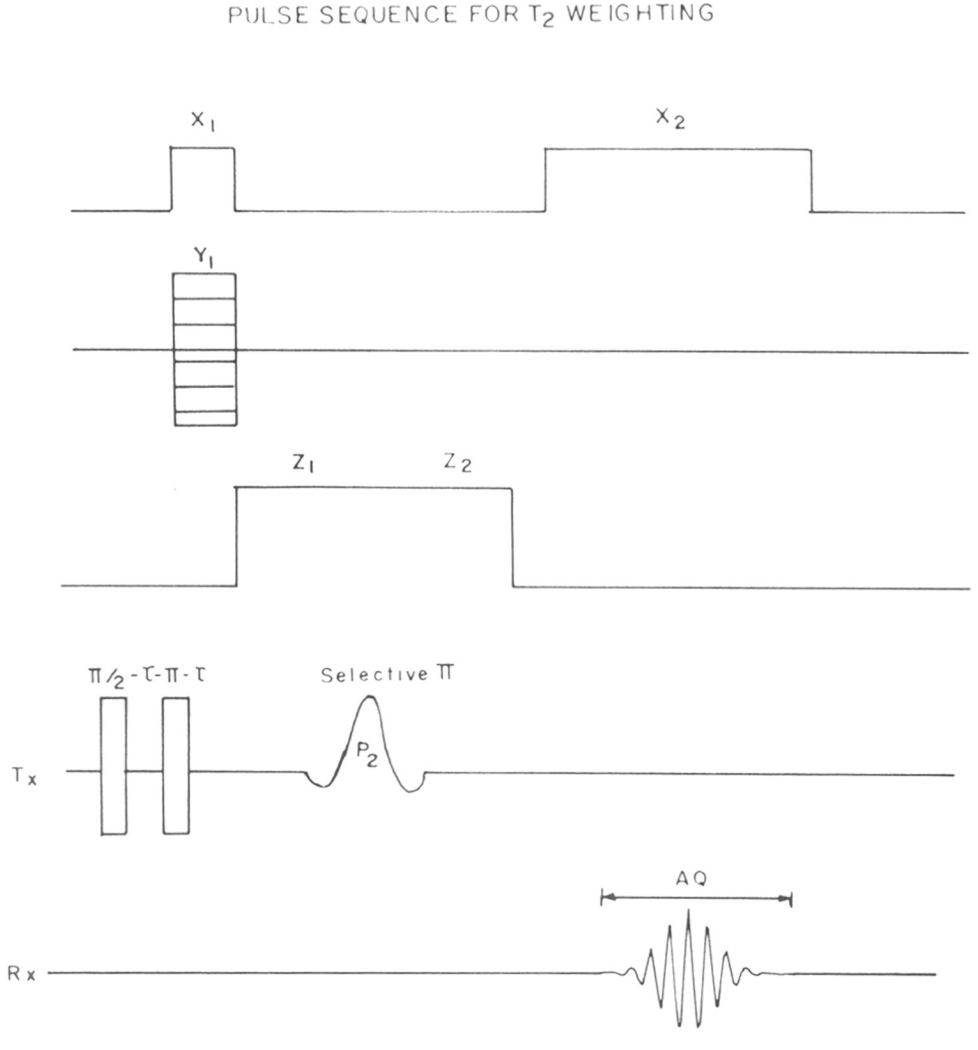

Figure 6.4: T_2 weighted single slice image pulse sequence obtained by incorporating the 90°- τ- 180° -τ (CPMG) pulse sequence into the single slice imaging sequence given in Figure 6.2.

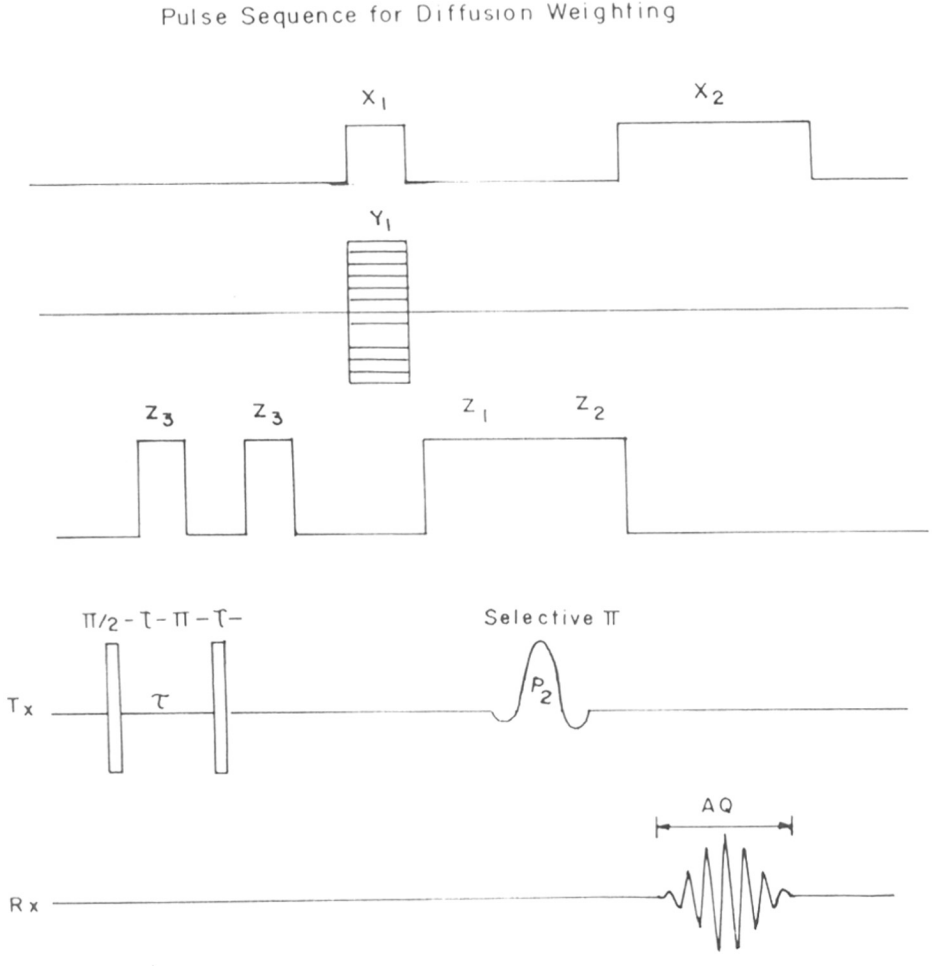

Figure 6.5: Pulse sequence for diffusion weighting single slice imaging.
Here, the PFGSE pulse sequence is combined with single slice image pulse sequence given in Figure 6.2.

Further insights into the state of water in the gel as well as the enhanced molecular mobility of polymer are provided in the relaxation (T_1), (T_2) and diffusion (D_{self}) weighted proton images presented in Figure 6.6. The enhanced polymer mobility is reflected in the detected proton spin density for the gel structure when a T_1 weighting is employed prior to image acquisition. The polymer contribution to the gel image is emphasized (Figure 6.7 A) by tailoring an inversion recovery scheme prior to the imaging sequence and adjusting the τ delay to put the water at its relaxation null. This may be compared with the image obtained in the absence of any T_1 preconditioning (Figure 6.6 A). For the water in the polymer, exchange is rapid among the bound and free states, characterized by their respective site populations P_b and P_f, and, further in the equilibrium swollen gel, $P_f >> P_b$.,The spin-lattice relaxation time, being a population weighted average of relaxation time for water in its bound (T_{1b}) and free (T_{1f}) states (Halle and Wenner sroms 1981, Ray *et al* 1998), approaches that of bulk water in the equilibrium swollen gel. Since we have reduced the proton spin density contribution from the water to a great extent by the T_1 weighting scheme, the proton image in Figure 6.6 (B) reveals a dominant contribution from the polymer protons to the gel image. It may be noted that the T_1 weighting has little effect on the polymer protons since their spin-lattice relaxation times lie in the hundreds of msec range which are an order of magnitude smaller than the T_1 of water in the equilibrium swollen gel. The observation further shows that in the equilibrium swollen gel the homonuclear proton-proton dipolar interactions are effectively removed by hydration induced polymer motions so that the proton resonances of the polymer are exited by the pulse scheme and detected in the imaging experiment. This is supported by the fine proton resolution observable in the water suppressed ^1H spectrum (Figure 6.6 **C**) as well in our earlier magic angle spinning (MAS) experiments of PNIPAm gel (Badiger *et al* 1991, Ganapathy *et al* 1994). The increased proton spectral resolution is also clearly seen in the 2-D separation experiment of PNIPAm gel presented and discussed in Chapter IV. The thermally induced collapse of the gel,

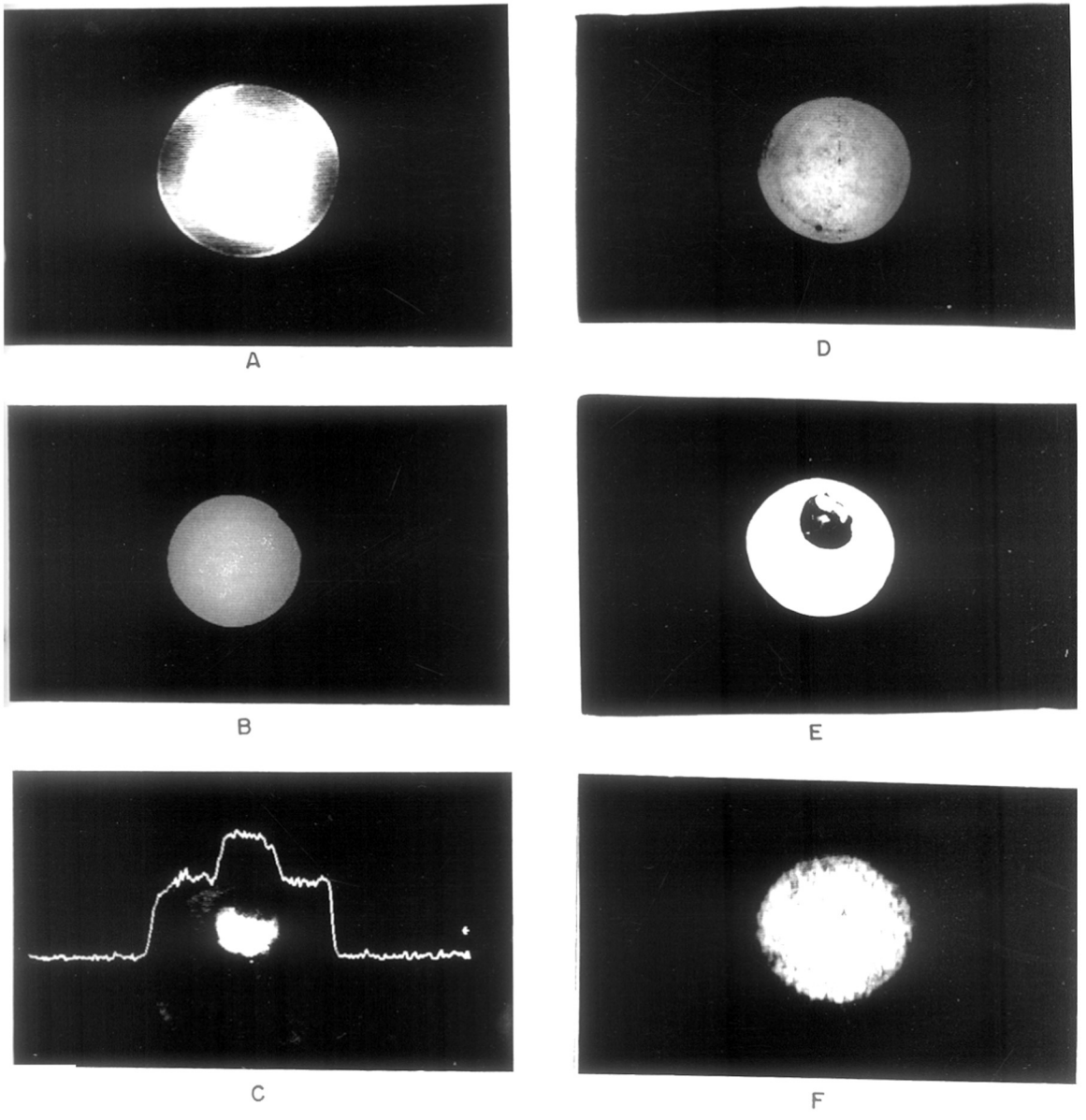

Figure 6.6: Planar (XY) images obtained on equilibrium swollen (A, B, D, F) and collapsed (C, E) gel of poly(*N*-isopropyl acrylamide) at 22 and 40°C, respectively. A, B, C: T_1 weighting; D, E: T_2 weighting and F: Diffusion weighting. The T_1 weighting was achieved by adjusting the recycle delay to 2 s (A) and 750 ms (C), while in (B) the T_1 weighting is done by using an inversion recovery sequence prior to the slice selection and adjusting the τ delay (1.68 s) to null the water magnetization. The T_2 weighting scheme (D, E) used a CPMG sequence (τ = 1 ms for D and 50 ms for E) prior to the 2-D imaging sequence. The diffusion weighting (F) was achieved by tailoring a PFG-SE sequence (δ = 5 ms; Δ = 15 ms; G_Z = 22 Gauss/cm) prior to the 2-D imaging sequence. The image in (E) is taken at a higher vertical scale due to poor S/N. The 1-D proton spin density profile of the row passing through the center of the collapsed gel is also shown in (C).

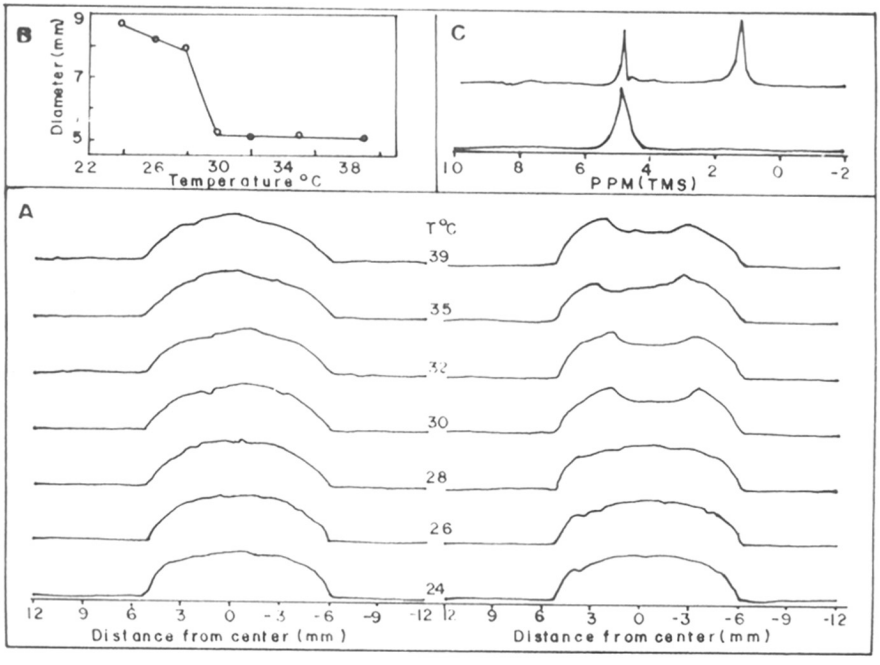

Figure 6.7: A) Proton spin density profiles of a slice (1 mm thickness) along the X-axis as a function of temperature in poly(*N*-isopropylacrylamide) gel, obtained with partial T_1 weighting (left, using fast recycle time of 750 msec) and with T_2 weighting (right). The pulse scheme consists of the usual CPMG sequence (τ delay of 50 ms), prior to the slice selection using a sinc shaped soft π pulse, with the phase encoding switched off during the 1-D imaging. The spin system is preconditioned with the decay of the transverse magnetization during the τ delay period to produce an effective T_2 weighting on the 1-D-image profiles. The 1-D image profiles were obtained by Fourier transformation of the echo, followed by magnitude calculation. B) A plot depicting the LCST transition from the T_2 weighted 1-D image profile data. C) Normal 1-D ^1H spectrum of the gel with (top) and without (bottom) water suppression. The water suppression was achieved by selectively dephasing the transverse magnetization of water through its fast self-diffusion (D_{self} = 2.2 x10^{-5} cm^2/sec) (Ray *et al* 1998). The enhanced signal resolution for the proton resonances in the repeat unit of the polymer may be seen in the bottom spectrum.

depicting the volume phase transition, is clearly seen in the proton image and 1-D profile shown in Figure 6.6 (C).

The T_2 weighted images of the equilibrium swollen and collapsed PNIPAm gel are shown in Figure 6.6 D and E, respectively. For the equilibrium swollen gel (Figure 6.6 D), the proton density of exterior water, gel water and polymer protons all contribute to the image intensity, due to the short dephasing delay (1 ms) we have used, compared to the spin-spin relaxation time of water (ca. 3 sec) and that of polymer protons (10-20 ms). The thermal collapse of the gel, past the volume phase transition is clearly depicted in the T_2 weighted image shown in Figure 6.6 (E). The dramatically enhanced contrast between the exterior water in the tube and the collapsed gel can be achieved when a longer T_2 dephasing delay (50 ms) was deliberately used. More importantly, the T_2 weighted image of the collapsed gel shows uneven proton spin density, implying a heterogeneity in water release, presumably due to thermal gradient across the gel. Interestingly, the same feature may also be noticed in the T_1 weighted image of the collapsed gel (Figure 6.6 C).

The diffusional weighting in a gel also influences image contrast as shown in Figure 6.6 (F). Here again, the exterior water that surrounds the gel has D_{self} of neat water and offers a benchmark for image comparison. In equilibrium swollen gel, D_{self} of water in the gel is governed by the diffusion of water in its bound and free states, appropriately weighted by their site populations and the associated self-diffusion coefficients (Ray *et al* 1998). In the equilibrium swollen state, where the free water content in the gel is high (P_f = 0.95), the difference in D_{self} of gel water and exterior water is not very large. Since polymer particles diffuse ever so slowly, a scheme, which allows diffusional dephasing of water in the gel, and exterior water alike, would emphasize the contribution from the polymer component to the gel image. However, since the T_2 values for polymer protons are short (10-20 ms), there is a partial loss of polymer signal intensity in the diffusion weighted experiment due to an unavoidable T_2 dephasing in the spin-echo experiment. This would account for the poor S/N in Figure 6.6 (F), quite in contrast to the T_1

weighting experiment in which the S/N for the polymer protons is inherently superior. We also tried to get a diffusion weighted image of the PNIPAm gel in its collapsed state (40^0C) under identical experimental conditions. We however do not see any image at all. It may be realized that while the water contribution to the image intensity is nearly removed by the diffusional dephasing of the water magnetization, the polymer contribution is altogether absent due to the predominance of proton-proton dipolar interactions ($\Delta\nu_{dipolar}$ = 8 kHz) in the collapsed state of the gel (Ganapathy *et al* 1994).

6.4 Concluding remarks

It has been shown that proton magnetic resonance imaging experiments are viable in studying the stimuli response of polymeric gels. This has been demonstrated in the LCST polymer PNIPAm. The microscopic differences in the motional state of the polymer and water components are used to bring in image contrast through appropriate relaxation and diffusion weighting. In view of the adequate signal resolution for the polymer and water components, chemical shift based imaging experiments would be useful.

6.5 References

Badiger, M.V., Kulkarni, M.G., Rajamohanan, P.R., Ganapathy, S. and Mashelkar, R.A. Macromolecules **24**, 106, (1991).

Blumer, P. and Blümich, B., Rubber Chem. Technol., **70**, 468, (1997).

Blumich, B. and Blumer, P., Makromol. Chem., **194**, 2133, (1993).

Callahan, P.T., Principles of Nuclear Magnetic Resonance Microscopy, Oxford University Press, Oxford, (1991).

Cohen Addad, J. P., Prog. NMR Spectroscopy, **25**, 1, (1993).

Gladden, L.F., Chem. Eng. Sci., **49**, 3339 (1994).

Ganapathy, S., Badiger, M.V., Rajamohanan, P.R., and Mashelkar, R.A. Macromolecules, ***25,*** 4255, (1992).

Ganapathy, S., Rajamohanan, P.R., Badiger, M.V. and Mashelkar, R.A. New Polymeric Materials, **2**, 205, (1990).

Ganapathy, S., Rajamohanan, P.R., Ray, S.S., Mandhare, A.B. and Mashelkar, R. A. Macromolecules**, 27**, 3432, (1994).

Halle, B. and Wennerstrom, H., J. Chem. Phys., **75,** 1928, (1981).

Hyde, T.M., Gladden, L.F., Mackley, M.R. and Gao, P., J. Polymer. Science Polymer Chem.Ed., **33**, 1795, (1995).

Hyde, T.M. and Gladden, L.F., Polymer, **39**, 811, (1998).

Koening, J.L., in Solid State NMR of Polymers, Mathias, L.J. (Ed.), Plenum Press, New York, p. 61, (1991).

Parker, D.D. and Koening, J.L., Current Trends in Polymer Science, **1**, 65, (1996).

Pop, I.E., Dhalluin, C.F., Deprez, B.P., Melnyk, P.C., Lippens, G.M. and Tartar, A.L., Tetrahedron, **52**, 12209, (1996).

Rajamohanan, P.R., Ganapathy, S., Ray, S.S., Badiger, M.V. and Mashelkar, R.A. Macromolecules, **28,** 2533, (1995).

Ray, S.S., Rajamohanan, P.R., Badiger, M.V., Devotta, I., Ganapathy, S. and Mashelkar, R.A., Chem. Eng. Sci, **53**, 869, (1998).

Tokuhiro, T., Amiya, T., Mamada, A., and Tanaka, T., Macromolecules, **24**, 2936, (1991).

Webb, A.G. and Hall, L.D., Polymer, 32, 2926, (1991).

Yokota, K., Abe, A., Hosaka, S., Sakai, I., and Saito, H., Macromolecules, **11**, 95, (1978).

Yasunaga, H., Kobayashi, M., Matsukawa, S., Kurosu, H., and Ando, I., Annual Reports in NMR Spectroscopy, **34,** 39, (1997).

Chapter VII

Summary and conslusions

In the present study the response of macromolecules to hydration has been followed with the help of NMR Spectroscopy and molecular modeling. A wide range of NMR Spectroscopic techniques have been employed to study the hydration induced dynamics of macromolecules which are in the gel state. Wide line Proton NMR spectroscopic technique has been used to follow the hydration events at earlier stages of hydration in many hydrophilic macromolecules. The proton line width showed a transition when plotted against hydration level. The transition is termed as "mobility transition".

We have demonstrated that the mobility transition occurring in the very early levels of hydration has been detected and demonstrated for the first time in many polymer-water systems. Molecular mobility is shown to occur through an isotropic averaging process for the proton-proton dipolar interactions. The static proton NMR line-width measurement studies in polymers possessing hydrophilic groups such as $-CONH_2$, $-COO^-$, -OH etc, hydrated by 99.8% D_2O, exhibit a mobility transition at very early levels of hydration (0.25-0.5 g/g). The mobility transition depends on the nature of hydrophilic groups present in the polymeric system. The presence of more polar functional groups shifts the mobility transition to a lower level of hydration. The hydration levels at which the mobility transition is seen corresponds most probably to the non-freezable bound water content in the systems studied. The mobility transitions are no way related to the phenomenon of macroscopic volume phase transitions of certain hydrogels. Our findings have implications in the use of such gels as reactive media, where molecular mobility and the amount of water are crucial in enhancing the reaction rates.

It is shown that macromolecular hydration can be conveniently studied by MAS based two-dimensional NMR. In these studies we have demonstrated that the 2-D NOESY experiments can be conducted on hydrogels with relative ease, taking advantage of enhanced spectral resolution obtained by sample rotation at the magic angle. The resulting data contain valuable information about the spin connectivity established by dipolar relaxation interactions in the mobile phase of the polymer gel. This technique is

established by dipolar relaxation interactions in the mobile phase of the polymer gel. This technique is potentially useful in unraveling the motional pathways in polymers, which readily respond to hydration. It appears that a common feature of the gel NOESY behavior is that the network is largely dominated by cross-relaxation mechanism in the "spin-diffusion" regime. The importance of dipolar relaxation interactions between the water of hydration and the polymer system is also revealed from these studies. The heteronuclear ^{13}C - ^{1}H separation spectroscopy is a useful technique to separate local dynamics at specific hydration sites in a polymeric gel. Further, the 2-D separation experiment provides dynamical insights in thermally collapsible gels that expel water while undergoing a volume phase transition. These experiments offer considerable scope to delineate dynamic details at an enhanced level of molecular inspection and further pave the way for studies of hydration in biopolymers such as collagen, DNA, etc.

Mobility transition demonstrated in PAM and PNIPAm-water systems was further studied by using the molecular modeling and molecular dynamics techniques. Molecular modeling and dynamics calculations for a linear polymer indicate the influence of water molecules on the single chain conformation of the polymer. The interaction of water with the single chains of these two polymers is maximum at the chain-turns and the interactions with linear region lead to distortion of the chains. These conformational changes of the polymer chains allow further uptake of the water into the polymer network. Thus the close relation between the single chain conformation and the orientation of water molecules around it are brought out by these studies and the mechanism of the water uptake is also revealed. The existence of similar mechanism is expected in the cross-linked polymer, which can also be studied using these techniques. The average distance of 3.5 Å between the carbonyl group of PAM and water bound to that, predicted by MD studies are in good agreement with that reported by earlier NMR studies. The average distance between carbonyl group of PNIPAm and water bound to it was calculated and found to 3.95Å. Our MD

We have shown that proton imaging experiments are viable in studying the stimuli response of polymeric gels. This has been demonstrated in the LCST polymer PNIPAm. The microscopic differences in the motional state of the polymer and water components are used to bring in image contrast through appropriate relaxation and diffusion weighting. In view of the adequate signal resolution for the polymer and water components, chemical shift based imaging experiments would be useful.